Aalto-yliopisto
Insinööritieteiden
korkeakoulu

Gowtham Radhakrishnan

Analysis of accidental iceberg impacts with large passenger vessels and FPSOs

Thesis submitted in partial fulfilment of the requirements for the degree of Master of Science in Technology

Espoo, 29.07.2018

Supervisor: Professor Pentti Kujala

Analysis of accidental iceberg impacts with large passenger vessels and FPSOs

Gowtham Radhakrishnan

Supervisors: Professor Jorgen Amdahl
Professor EKaterina Kim
Co Supervisor: Postdoc Zhaolong Yu

Professor Pentti Kujala
Department of Mechanical Engineering
Aalto University of Science and Technology

Norwegian University of Science and Technology
Department of Marine Technology

Espoo,
29, July 2018

ACKNOWLEDGEMENTS

First of all, I would like to give whole hearted thanks to the God, The Almighty for giving me this wonderful opportunity.

Nextly, my Father, Mother and Brother who gave me strong moral support throughout my Master studies.

My main supervisor from NTNU Professor Jorgen Amdahl, who spent more time with me thus giving valuable suggestion for my thesis. From him I learnt the art of how to infer the numerical simulations and possibilities of applying them in the physical scenarios. My main supervisor from Aalto University Professor Pentti Kujala who took time even during weekends and holidays and helped me with my thesis. His research materials on ice was really helpful. My additional supervisor from NTNU, Professor Ekaterina Kim, from her I learnt how to understand things deeply. And my co-supervisor PostDoc Zhaolong Yu, who cleared my doubts whenever I approached him.

I would also like to give thanks to Professor Kaj Riska and Claude Daley, who inspite of their busy schedules took time to give me some suggestions.

The following PhD and fellow Master students from NTNU who helped me a lot with their inputs at crucial times which turned out to be really valuable.

Chana Sinsabvarodom, Jita Priya Das, Jorge Rangel, Stian Hagen and Rui Dou

Aalto University
School of Engineering

Aalto University, P.O. BOX 11000, 00076 AALTO
www.aalto.fi
Abstract of the master's thesis

ABSTRACT

Author Gowtham Radhakrishnan

Analysis of accidental iceberg impacts with large passenger vessels and FPSOs

Degree programme in Mechanical Engineering

Major/minor: Maritime Engineering

Thesis supervisor Professor Pentti Kujala

Date 29.07.2018 **Number of pages** 157+35 **Language** English

Nowadays, on account of the rapid increase in the global warming, the extent and thickness of sea ice in the Arctic region is diminishing at a very fast pace. It has even been forecasted that the Arctic region will be ice free in the very near future. Owing to this fact, the Arctic waters are increasingly becoming attractive to different classes of society because of its immense reservoirs of oil and gas, short ship routes in the NE and NW region and attractive tourist places. These activities face the major hurdles from harsh environmental conditions like ice loads, insufficient infrastructure in the Arctic regions and the threats from impact of large ice features.

The ships or offshore structures need to be sufficiently strengthened to resist the extreme ice impacts. However, very few data or models do exist that can quantify the extreme ice actions, and in addition the reliability of those data is open to question. For instance, the ice going vessels or offshore structures are designed based on pressure-area curves, but most of the P-A curves are based on Ultimate Limit State (ULS) design whereas the P-A curves for Accidental Limit State (ALS) are very rare. The work carried out in this thesis aims to study the response of structures subjected to those accidental ice impacts.

The thesis work can be regarded as a continuation of work carried out by Ekaterina Kim in department of Marine technology, NTNU. In addition, considerable improvements and progress have been achieved in quantifying the accidental ice loads in terms of a novel numerical model. Both FEM and coupled FEM-SPH techniques have been efficiently applied in ice modelling and validated against existing Pressure-Area curves. In addition, computationally demanding spatial envelope curves have been plotted using which the existence and spatial variation of high pressure zones most commonly known as HPZs are effectively studied. Moreover, further step has been taken in applying the FEM-SPH ice modelling in large scale impact simulations. In order to resemble accidental ice impacts, the ice has been modelled significantly harder and successfully applied in collision simulations.

The pressures corresponding to the hardest ice surpassed the existing analytical curves by a huge margin.

For large scale simulations, FPSO and a large passenger vessel have been chosen. Certain structural scantlings are different between these two structures. The impacts using the modelled hard ice produced extensive deformation on these structures. Furthermore, the ice shape effect in accidental collisions is studied and it turned out that the tabular bergy pit produced massive deformations in structure and it can rightly be considered as the best shape for the analysis concerned with accidental ice impacts. Direct ice impacts seemed to produce more deformation on the structure when compared with oblique ice impacts. The impacts simulated using decoupled approach provides a conservative estimate of force levels and subsequent deformations.

Structures with lesser thickness deformed more during the ice impacts, however lower force levels are recorded. Similar trend has been observed in the simulations performed using lower steel grades. From the coupled collision simulations, it has been noted that the kinetic energy of ice plays a very important role in determining the maximum possible deformation experienced by the structure.

Finally, some simplified analytical formulas have been developed for estimating the crushing of ice and deformation of structures subjected to direct and oblique ice impacts. The developed formulas are successfully applied and validated using the collision data obtained from numerical simulations. In addition coupled FEM-DEM ice modelling in LS DYNA has been proposed and compared with that of FEM and FEM-SPH ice modelling.

SCOPE OF WORK

The objective of the project/master thesis work is to assess the resistance of an ice-strengthened passenger vessel and an FPSO to ice floe/bergy bits ice impacts.

The work is proposed being carried out in the following steps:

Discuss potential ice floes/ice berg shapes and select the geometries that will be used in numerical simulations. Conduct simulation with LS-DYNA of ice crushing against a rigid wall beside on a continuum mechanics modeling of ice, both with and without Smoothed Particle Hydrodynamics (SPH) included. Calculate and compare force-displacement curves and process – and spatial pressure-area curves. Compare also with typical design pressure-area curves. The ice feature may be a small iceberg (growler) and an ice floe. Discuss pros and cons for the use of SPH in further numerical studies of ice-structure interaction.

Perform integrated ice-structure analysis of ice impact against a stiffened panel. The panel should be designed such that significant interaction is expected. Calculate the force deformation curve and the process – and spatial pressure area curves. Compare with the results from crushing against a rigid wall.

Describe the various contributions from fluid forces (submersion, added mass etc.) for growlers and ice floes and how this can be modeled for integrated analysis in LS-DYNA. Perform numerical analysis of ice impacting a passenger fore ship using an existing finite element model. Potential fracturing of ship shell panels shall be considered. The ice should preferably be strong enough to interact significantly with the fore ship, but also rigid ice may be simulated for comparison. The impact should be made both normal to the ship side and oblique to the side, so that also "sliding" ice impact can be simulated. Compare results from numerical simulations with those based on simplified "external mechanics" approach. How much of the energy remains as kinetic energy after impact? Analysis of impacts outside the ice-strengthened region due to wave induced motions may also be considered

Create a finite element model of a panel representative for an ice strengthened FPSO. Perform numerical analysis of ice impact. The ice should preferably be strong enough to interact significantly with the fore ship. The impact should be made both normal to the FPSO side and oblique to the side, so that also "sliding" ice impact can be simulated. Compare results from numerical simulations with those based on simplified "external mechanics" approach. Analysis of impacts outside the ice-strengthened region due to wave induced motions may also be considered.

Propose models that may be used to estimate the deformation of ship side subjected to lateral

and sliding impacts. Previous work on ship grounding may be useful may be useful

Conclusions and recommendations for further work for the master thesis

Literature studies of specific topics relevant to the thesis work may be included.

The work scope may prove to be larger than initially anticipated. Subject to approval from the supervisors, topics may be deleted from the list above or reduced in extent.

In the thesis the candidate shall present his personal contribution to the resolution of problems within the scope of the thesis work.

Theories and conclusions should be based on mathematical derivations and/or logic reasoning identifying the various steps in the deduction.

The candidate should utilise the existing possibilities for obtaining relevant literature.

Thesis format

The thesis should be organised in a rational manner to give a clear exposition of results, assessments, and conclusions. The text should be brief and to the point, with a clear language. Telegraphic language should be avoided.

The thesis shall contain the following elements: A text defining the scope, preface, list of contents, summary, main body of thesis, conclusions with recommendations for further work, list of symbols and acronyms, references and (optional) appendices. All figures, tables and equations shall be numerated.

The supervisors may require that the candidate, in an early stage of the work, present a written plan for the completion of the work. The plan should include a budget for the use of computer and laboratory resources, which will be charged to the department. Overruns shall be reported to the supervisors.

The original contribution of the candidate and material taken from other sources shall be clearly defined. Work from other sources shall be properly referenced using an acknowledged referencing system.

PREFACE

The Master Thesis is submitted to the Norwegian University of Science and Technology (NTNU) and Aalto University of Science and Technology (Aalto) for the partial fulfilment of requirements for the degree of Master of Science. The thesis work has been performed at the Department of Marine Technology, NTNU, Trondheim, with Professor Jorgen Amdahl as main supervisor and Professor Ekaterina Kim as additional supervisor from NTNU and Professor Pentti Kujala as main supervisor from Aalto University The Primary funding for the thesis was through strategic university funds.

CONTENTS

LIST OF FIGURES

LIST OF TABLES

LIST OF SYMBOLS

P_{avg} – Average Pressure

P_0 – reference pressure

A – Contact area

C – coefficients

H_{ice}- Ice thickness

F_n- Normal Force

E – Modulus of Elasticity

σ_{ice}- Strength of ice

j_2 – invariant of deviatoric stress tensor

E_T-Tangent Modulus

m – mass of ice feature

V – Velocity of ice feature

E_{st} – dissipated strain energy

E_{fn} – dissipated sliding energy

E_{dm} – dissipated damping energy

E_{Int} – Internal energy

dl – deformation

V_R – Resultant velocity

ε_0 – initial strain

ε_f – failure strain

LIST OF ACRONYMS

FEM – Finite Element Method

DEM – Discrete Element Method

ULS – Ultimate Limit State

ALS – Accidental Limit State

NORSOK – Norwegian Petroleum Standards

P-A – Pressure-Area relationship curves

NLFEA – Non-Linear Finite Element Anaysis

KE – Kinetic Energy

IE – Indentation Energy

PE – Potential Energy

FPSO – Floating Production Storage and Offloading

SPH – Smoothed Particles Hydrodynamics

CAM – Constant Added Mass

FSI – Fluid Structure Interaction

IACS – International Association of Classification Societies

PC – Polar Class

PPF_i – Peak Pressure Factors

LSTC – Livermore Software Technology Corporation

DNV – Det Norske Veritas

EM – External Mechanics

IM- Internal Mechanics

SE -Strain Energy

HPZ – High pressure Zones

ALE – Arbitrary Eulerian Lagrangian

CFD – Computational Fluid Dynamics

AM – Added Mass

CEM – Cohesive Element Method

STRUCTURE OF THE MASTER THESIS

The Master thesis on the "Analysis of accidental ice berg impacts on large passenger vessels and FPSOs". Relevant literature reviews presented in the project thesis are included in the Master thesis. The structure of the thesis is as follows.

Chapter 1 deals with the theoretical explanation of the problems that arises owing to the ice structure interaction and the challenges faced by the engineers and scientific community in evaluating the interaction scenario. Moreover, elaborate discussion on the design of structures with respect to the ULS and ALS design criteria is made. Various existing models for quantifying the actions of ice on structures have been presented. In addition, the idea of evaluating the collision scenario by separating the internal mechanics and external dynamics has also been reviewed.

In Chapter 2, various empirical models for analysing the external mechanics of the collision process (estimation of the energy dissipation) have been put forward and compared.

In Chapter 3 introduction to the structural rules for the design of ice strengthened ship has been given along with the procedures for designing the various structural members in bow, mid ship and stern area. In addition, according to PC 1 rules, shell plating for the bow region of FPSO is designed.

Chapter 4 is concerned with the elaborate discussion on various available ice material models pressure area curves and fluid-ice-structure analysis. Secondly, the physical and mechanical properties of ice berg are presented with the experimental results. Moreover, the theories associated with the P-A relationship have been reviewed.

Chapter 5 deals with the strength design analysis, in which the chosen ice features are collided against the rigid plate. It begins with the procedures for modelling numerically efficient and accurate ice features. Then from the ice-structure interaction analysis using FEM and FEM-SPH ice models, the f-d, process P-A, spatial P-A and envelope curves are plotted and the results are compared with some analytical curves as well. Elaborate study on the pros and cons of FEM and FEM-SPH techniques in ice modelling has also been made.

In Chapter 6, integrated analysis has been conducted by colliding the ice features with a stiffened panel. The results are compared with that of the rigid plate analysis and suitable discussions are made. In addition, simulations representative of the strength, ductile and shared energy design are carried out.

Chapter 7 begins with the theory related to consideration of hydrodynamic effects while performing ship-ice collisions in LS DYNA followed with a brief explanation regarding FEM modelling of the FPSO side model. Collision based on both decoupled and coupled principles are performed. Using decoupled approach, impact assessment due to various ice shapes, different structural thickness, and collision outside ice strengthened region are carried out. And using coupled approach, the oblique impacts at different angles and friction effect have been analysed. In addition sliding of ice has also been simulated.

In Chapter 8, FEM model of a passenger vessel has been given and the simulations are conducted using that. The collision assessment on impact at ice strengthened region and outside that region and effect of different structural steel grades are analysed using decoupled approach. Whereas using coupled approach, the collision effect due to different floe velocities

and masses are simulated. In addition, ice sliding has also been simulated.

In Chapter 9, simplified analytical models are derived to estimate the deformation of ice and ships and compared with the numerical simulations

In Chapter 10, some simulations using FEM-DEM approach have been conducted and the results are presented.

Chapter 11 concludes the works performed in this project thesis and in addition recommendations for further work are outlined.

CHAPTER 1

1.1 OVERVIEW OF PROBLEMS IN ICE-STRUCTURE INTERACTION

Ice-Structure interaction is one of the major problems faced by the engineers in designing ships, offshore structures, subsea pipelines in sea ice-infested areas and bridges, piers in freshwater–ice infested areas. The problem of ice-structure interaction should be studied and modelled in detail, in order to have reliable structures that can withstand ice actions. The characteristics of sea ice and freshwater ice considerably vary and their physical and mechanical properties must be studied in detail to analyse the loads they exert on the structures (Tukhuri, Ice Mechanics - Bearing Capacity of Ice 2016). In this project, the action of sea ice on structures is taken into consideration. There are different types of sea ice in existence which vary in their size and strength significantly. From the point of view of engineers, while studying the ice loads on structures, the following types of ice are usually considered. They are level ice, rubbles, ridges, icebergs etc (Tukhuri, Ice Mechanics - Introduction 2016). The main aim of this project is to analyse the forces caused by these ice types on structures and extend the problem to an ice berg colliding with a ship.

Let us take the case of an ice floe hitting a structure. This complex problem can be solved by considering the following main components involved in the interaction scenario. They are ice floes, surrounding ice, formation of ice rubbles due to the fracture of ice floes, the surrounding water, the structure and its foundation. The structure will be subjected to plastic collapse if the rubbles contribute loads higher than the structure's yield strength or it may even result in fracture if the loads exceed beyond the ultimate strength of the structure. Moreover, the ice interaction with a structure also causes vibration leading to fatigue damage. In addition, the ice loads may even excite a structure nonlinearly which in turn depends on the foundation of the structure (Konuk 2011). Figure **1** is a simulation picture that shows the interaction of an ice floe with a conical structure.

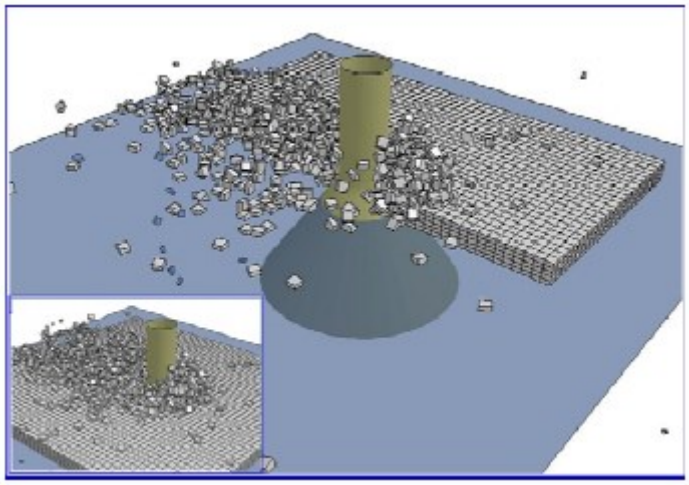

Figure 1 Numerical simulation of crushing of ice particles (Konuk 2011)

One of the most important factor which results in the nonlinear excitation of the structure is the hydrodynamic force caused due to the interaction of ice and structure with water (Konuk 2011). However, due to the complexity of this problem, as of now this hydrodynamic factor is not typically accounted while solving the ice-structure interaction scenarios.

Structures that are commonly used in sea-ice infested areas are ship shaped structures like LNG tankers, cruise vessels, icebreakers for transportation and sloping or conical shaped offshore structures for extracting the hydrocarbons. (Hamid Daiyan 2011)

The loads exerted on the offshore structure will mainly come in the form of energy dissipated from ice after it collides in front of the structure. In addition to it, clearing of ice rubbles around the structure also contributes some loads. Loads due to clearing will be because of the frictional resistance between ice and structure and its magnitude depends mainly on the fracture toughness of ice. Furthermore, clearing process also involves forcing the ice rubble to move under the water. Recent research shows that when the current induced flow pattern around the structure interacts with the ice rubbles, it could result in pressure variations around the structure which are really difficult to account in calculations because of its coupled nature (Konuk 2011) Furthermore, the non linearities inherent in the structure and in its foundation can affect the ice-structure interaction scenarios.

1.2 CHALLENGES

Collision between ship or structure and ice can lead to severe consequences like significant damage of the structures, environmental pollution owing to spillage of materials in case of cargo ships, and loss of crew. In order to have a safe design, versatile techniques are necessary to assess the collision scenario during the design phase of the structures. Till now, no reliable methods have been established that can predict the material strength and fracture propagation in structural panel in an impact scenario. The big responsibility of choosing an apt analysis method (model test / simulations) and to make a safer design lies with the designer. (Storheim 2016)

Figure 2 Ship with a damaged bow due to collision with ice berg (Amdahl 2017)

Till now, most of the design calculations to account for ice induced loads are based on empirical

and semi-empirical relations. Though they provide good estimation of the forces, these equations inherently have elements of uncertainty. The uncertainties come from varying ice conditions, complex geometry of structures which lead to complicated ice-structure interaction. Notwithstanding, there are some numerical tools based on the principles of FEM and FEM-DEM that simulate the ice-structure and ice-ice interaction scenarios. The disadvantages associated with these tools are that they cannot simulate perfectly the failure pattern of large volume of ice and these tools are used only by few specialized universities, industries and research institutions. The model scale tests are used as a reliable method to represent the actual ice-structure interaction scenario. However, they also possess some disadvantages when compared with full scale tests.

Moreover, the ice loads exhibit considerable variation with respect to time, as a result they should be represented using a stochastic model as that of waves (Kujala, Winter Navigation - Ice Induced Loads 2017). However, no accurate stochastic models exist till date to capture ice actions from different types of ice, since high degree of complexity is associated in predicting the return period of ice. However, researchers have modelled site specific ice conditions in probabilistic terms. In addition, the ice loads cannot be represented in a spectrum like that of the wave loads, this is due to the fact the time variation of ice loads is not zero.

1.3 REVIEW OF DESIGN PRINCIPLES OF ULS AND ALS

As per the limit state design, the structural design is assessed for various limit states in order to ensure that a sufficient safety margin is maintained between the maximum probabilistic loads and the weakest possible structural resistance.

The various types of limit states are

- Serviceability limit state
- Ultimate limit state
- Fatigue limit state
- Accidental limit state

In this section, the Ultimate limit state and Accidental limit state (progressive collapse limit state) are discussed briefly. (Bai 2003)

1.3.1 Ultimate Limit State

The Ultimate Design State (ULS) is a computational condition for safe design of a structure by limiting the stresses experienced by the materials and components of the structure. A structure should satisfy the ULS condition in order to maintain its structural integrity and stability under the ultimate design loads. (WikiPedia 2017)

ULS design principle uses Partial safety factors for both the load and resistance. These factors are estimated using statistics of structural failures and estimated probability of failure of the concerned structure. In addition to it, uncertainties inherent in material quality and construction procedures are also considered. The resistance safety factor varies with respect to different kinds of materials. (Designing Buildings Wiki 2017).

1.3.2 Accidental Limit State

Accidental limit state usually concerns with the design of structures against accidental loads. The accidental loads are defined as the unexpected loads that may result in severe damage to structures, environment, materials and human lives. In marine design, these loads are classified as ship collision, ship grounding, fire/explosion, freak waves, dropped objects, accidental objects, unintended pressure etc (Moan, Development of Accidental Collapse Limit State Criteria for Offshore Structures 2007).

The structural design for accidental loads involve determination of the loads in probabilistic terms, estimation of the structural response to these loads and selecting the risk based acceptance criteria. According to NORSOK, the accidental collapse limit state design check is introduced as a two step procedure.

- Damages should be estimated due to accidental actions with annual probability of 10^{-4}
- Survivability of damaged structures should be checked against relevant functional and environmental actions

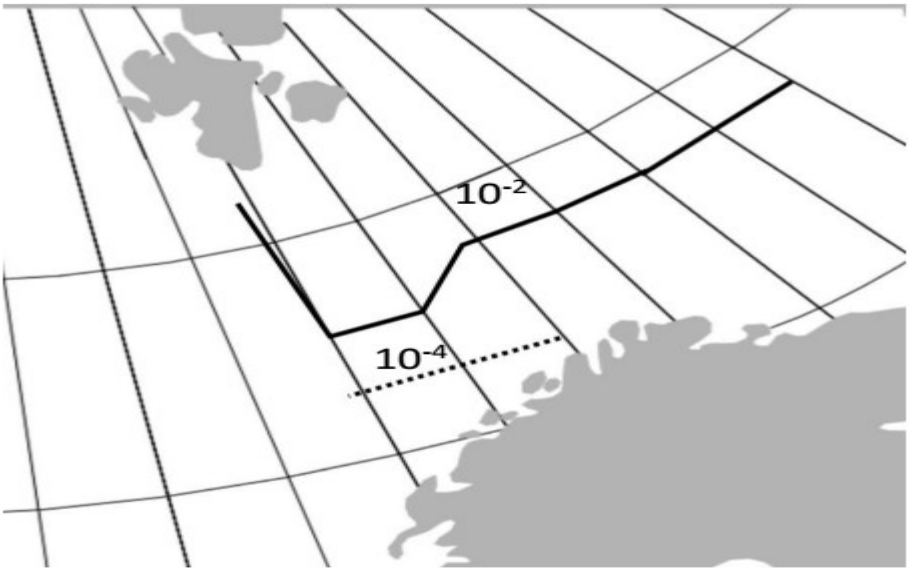

Figure 3 Pictorial representation of probabilistic limits of collision with ice berg (Amdahl 2017)

In this project, the accidental loads from ice bergs are taken into account. Ice bergs can impact both the structures on sea surface as well as the riser and pipeline structures. Their impact probability depends on iceberg aerial density, size of structure, average drift velocity and size of ice berg. Figure **3** shows the limits of collision with ice bergs in Barents sea. The solid line in the figure indicates the ice berg limits with a probability of exceedance 10^{-2} and dotted refers to 10^{-4} exceedance probability. One important fact that should be that the action of sea ice must also be taken in to account in addition to ice bergs in regions where the probability of occurrence of sea ice are more frequent than 10^{-4}. After that risk analysis must be carried out in order to determine the probability of failure of the structure subjected to the these loads. Figure **4** is probability density function diagram showing the applied load, resistance of the structure to these loads and the probability of failure.

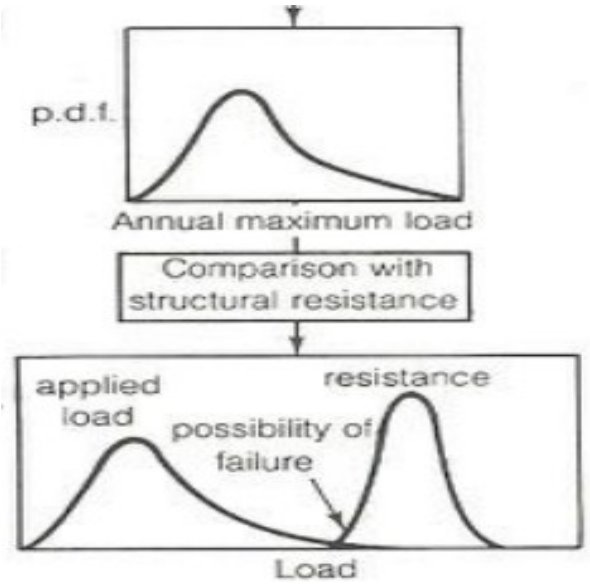

Figure 4 Probabilistic representation of interrelation between the applied load and structural resistance (Tukhuri, Ice Mechanics - Ice failure against structures 2016)

The general expression for the risk based design against accidental actions is given by

$$P_{FSYS}(i)=\sum_{j,k} P[FSYS \mid D].P\left[D\middle|A_{j,k}^{(i)}\right].P[A_{j,k}^{(i)}] \quad (1)$$

Where P[FSYS] is the probability of damaged system failure under relevant conditions, $P[A_{j,k}^{(i)}]$ is the probability of accidental action at location (j) and intensity (k) and P[D] is the probability of damage. (Moan, Development of Accidental Collapse Limit State Criteria for Offshore Structures 2007)

1.3.3 Comparison between ULS and ALS design for accidental loads:

As already stated, the ULS resistance of structure is based on the yield strength multiplied by a safety margin. The capacity of ULS is much limited when compared with ALS capacity (Amdahl 2017). This can be inferred from Figure **5 .** The figure shows the response of a plate subjected to ice patch load. A structure designed according to ALS can sustain large inelastic deformations.

The response of structures is traditionally predicted using plastic analytical formulas because the structure usually undergoes large plastic deformations by absorbing the energy from accidental loads. These empirical formulas provide a good estimate of the actual deformation and energy absorption. However, in recent times, the non-linear finite element analysis has been used to model the structural deformation as it gives an accurate estimation of the response and in addition, it can be used to perform coupled analysis for complex accident scenario. (Amdahl 2017)

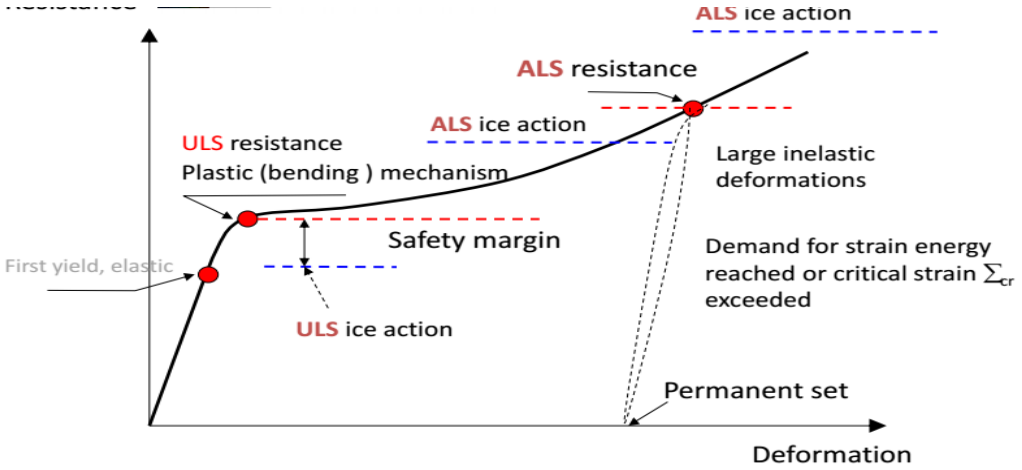

Figure 5 ULS and ALS design ranges (Amdahl 2017).

1.4 MODELS FOR ICE ACTIONS:

As of now, various types of ice features have been known to exist in Arctic, Antarctic and other ice-covered areas. The terminology used to describe the ice features have been standardised by the World Meteorological Organisation. They are frazil ice, grease ice, anchor ice, slush, shuga, ice rind, gray ice, young ice, pancake ice, first-year ice, brash ice, ice floe, fast ice, pack ice, hummock, rubbles, ridges, ice shelf, ice island, glaciers, ice bergs, bergy bit, growlers. In addition to this, the Russian Pomor people and Whalers have identified and termed some ice types such as stamukha, nilas, polynia, pancake ice, glass ice and frost smoke. However, there are many other ice types that have not been discovered and reported yet in the Antarctic region. (Tukhuri, Ice Mechanics-Occurence of Ice 2016)

From the point of view of engineering considerations, the ice types that are of interest are the level ice, rubbles, ridges, ice bergs etc. Figure **6** illustrates how the ice cover will be developed. The level ice, rubble, ridges are usually formed by a process called Rafting, which is a deformation process in which one ice over rides another ice.

Figure **6** shows the development of different types of ice cover through the deformation process. Both rafting and ridging process in ice is shown. The difference between rafting and ridging is not always clear. From the picture, it can be inferred that rafting process occurs in ice types of all thickness, starting from young ice to Multi-year ice. When young ice sheets undergo rafting process, level ice is formed. Similarly, rafting process in first-year ice gives rise rubbles and ridges. Figure **7** shows the flow chart that represents the different feature of ice that are commonly found in seas, along with their properties, limiting mechanisms and failure modes.

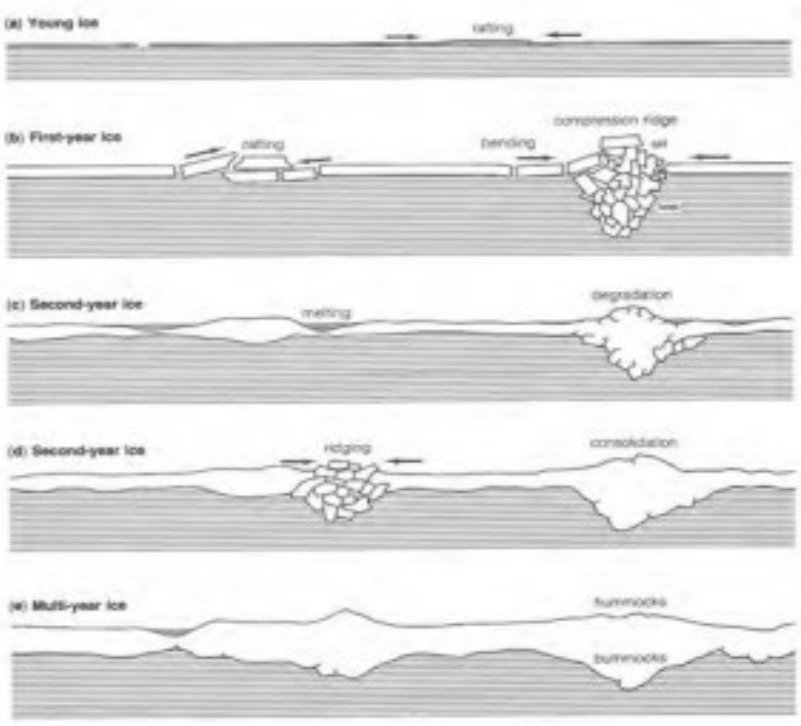

Figure 6 Development of Ice Cover (Tukhuri, Ice Mechanics-Occurence of Ice 2016)

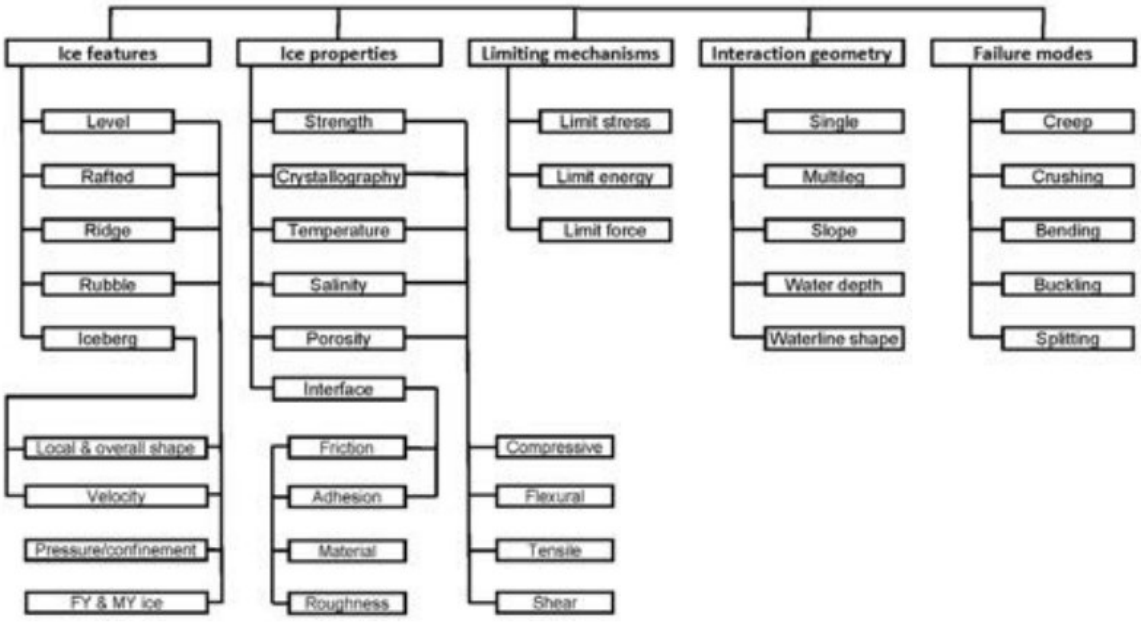

Figure 7 Flow chart showing the ice actions on offshore structures (Tukhuri, Ice Mechanics - Ice failure against structures 2016)

1.4.1 Calculation of resistance

Throughout the history of ice engineering research, the action of level ice against ships had been given a special consideration and various analytical formulas had been derived to evaluate the resistance of ships level ice.

The very first empirical expression for calculating the level ice was put forth by Robert Runeberg (1846 – 1918). It was published in the Streamers for winter ice breaking (1899).

$$\boldsymbol{R_i \sim \sqrt{B}, h^3, \mu, \varphi, \alpha} \quad (2)$$

Where B is the ship beam, φ, α are hull angles, μ is the hull-ice friction coefficient, h is the ice thickness. Through this formula, the mechanism by which the hull breaks the ice had been found out. The hull breaks the ice downwards.

$$\boldsymbol{R_i = K_1 \mu B \sigma h + K_2 \mu B \rho h^2 + K_3 \mu B^{k_4} h v^{k_5}} \quad (3)$$

Where B is the ship beam, v is ship's velocity, σ, h, ρ is the strength, thickness and density of ice respectively . Kashtelijan et al (1968) came out with another formula for the estimation of level ice resistance. It was developed based on the model and full scale tests of IB Yermak. (Tukhuri, Ice Mechanics - Introduction 2016)

In addition there were other formula for calculating the level ice resistance that were followed in different geographical areas throughout the years. As of now, the widely accepted empirical expression for calculating the resistance of ships in level ice is the Lindqvist's formula.

Total Resistance: $\boldsymbol{R_{ice} = (R_C + R_b).\left(1 + 1.4\frac{v}{\sqrt{gH_{ice}}}\right) + R_s(1 + 9.4.\frac{v}{\sqrt{gL}})}$ (4)

Where R_C is the crushing resistance, R_b is the bending resistance and R_s is the submerging resistance.

The above total resistance gives the level ice resistance of ships. Usually while calculating the resistance of an ice going ship or ice breakers, it is customary to compute the open water resistance of that particular ship and add it with the ice resistance. For determining the ships resistance in ice channels, Sandkvists analytical method is used. (Kujala, Winter Navigation-Ship resistance in ice 2016)

In order to study the ice actions on structures and rubble formation in detail, it is important to understand the two most important failure modes associated with ice-structure interaction. They are the crushing and bending failure of ice. Usually the failure of ice happens in the following sequence as illustrated in Figure **8,** first the ice starts to crush against the structure, which is followed by shear fractures. And then finally, the bending failure occurs. (Kujala, Winter Navigation-Ship resistance in ice 2016) These two failure modes contribute to the formation of ice rubbles and are discussed in detail in this section.

1.4.2 Ice crushing:

The ice forces acting on a ship or offshore structure are due to the relative movements of the structure and ice. During an ice-structure interaction scenario, firstly, the ice crushes locally and then the contact area and force increases until the force is high enough to cause ice failure and then the load decreases. To illustrate this fact better, Figure **8** shows the case of a ship breaking the ice. Initially, the ship's side crushes the ice locally and then the bending failure

occurs.

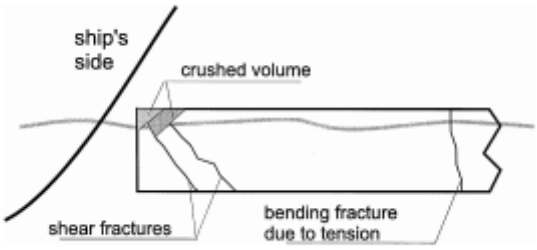

Figure 8 shows the crushing and bending patterns of ice after it hits a ship side (Tukhuri, Ice Mechanics-Crushing and Contact 2016)

Ice crushing also paves way to different crack growth mechanism in ice. The formation of different types of cracks during crushing are represented clearly in Figure **9**

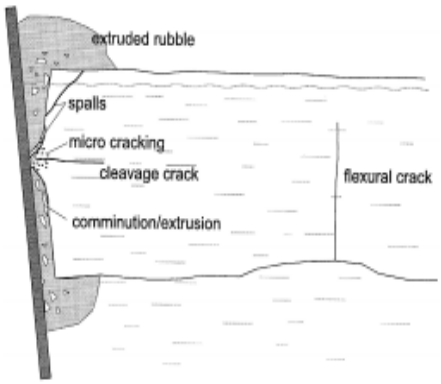

Figure 9 Shows the formation of different types of cracks when an ice is crushed against a structure (Tukhuri, Ice Mechanics-Crushing and Contact 2016)

The crushing failure mode occupies a most important place in the ice failure process, the reason being that crushing of ice contributes huge loads on structures, particularly on vertical structures. Moreover, if no other failure modes of ice get activated, the crushing load can be considered as the maximum load that a structure will encounter. Furthermore, the ice fails in compression at the contact between the structure and ice, so the local pressure acting on the structure can be estimated by studying the crushing process in detail. These local pressure forces, in turn can be considered for structural design.

From the point of view of engineering design, the crushing load is evaluated from the following formula

$$F = p_{av} h_{nom} l_{nom} \quad (5)$$

In addition to the analytical expressions, various model and full scale experiments have been conducted at different periods of ice engineering research for estimating the pressure on structure due to ice contact. Based on the results from the experiments, the famous Pressure-Area diagram was created which plays a crucial role in the evaluation of pressure force on structures. As of now, numerous P-A curves are used for the engineering design. A more

detailed explanation about P-A curves is explained afterwards.

The impact velocity of ice on structures influences the crushing process significantly. For example, if the velocity of impact is low, it may result in wider contact between ice and structure, therefore creeps and micro cracks are developed in ice at the point of contact. Figure **10** illustrates this phenomenon clearly. (Tukhuri, Ice Mechanics-Crushing and Contact 2016)

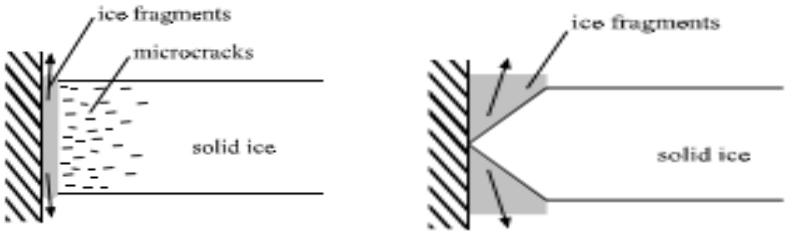

Figure 10 Left picture depicts the case of low velocity impact and the right picture illustrates the case of high velocity impact (Tukhuri, Ice Mechanics-Crushing and Contact 2016)

On the other hand, if the impact velocity is high, it may lead to narrow contact between ice and structure. Consequently, flaking of ice could be seen at the local contact area. Figure **10** shows the crushing pattern of ice during high velocity impact. In vertical offshore structures, the crushing of ice usually dominates. The ice loads on structures due to crushing can be evaluated using Korzhavin's equation and analytical expressions listed in ISO 19906. (Tukhuri, Ice Mechanics - Ice failure against structures 2016)

1.4.3 Bending failure of ice:

In ice infested areas, inclined structures are usually preferred, because it fails the ice in bending thereby the structure will be subjected to lower ice loads. On the other hand, crushing process dominates in vertical structures which lead to high local pressures on the structure. Figure **8** shows pictorially the bending failure of ice sheet. Bending failure is associated with the flexural strength of ice. Bending failure of ice is one of the important reasons for formation of ridges and rubbles. (Tukhuri, Ice Mechanics-Ridges and Rubble piles 2016).

It has already been mentioned that the ice acting against an inclined structure fails in bending and it contributes some loads. Croasdale et al(1980) and Ralston et al(1977) formulated analytical formulae for estimating the horizontal and vertical components of ice loads acting on the structure.

Croasdale's(1980) approach assumes elastic behaviour of ice and use flexural strength in the calculations. The drawback of this method is that since it is based on flexural strength of ice, it shows pronounced scale dependant behaviour. In other words, it yielded upper bound solutions for forces in full scale. On the other hand, Ralston's(1977) method considers the plastic behaviour of ice and uses the yield strength of ice in the calculations. The drawback of this method is that it does not account for non-simultaneous contact. (A. Polojarvi, Ice Loads on Inclined Structures-I 2017)

1.4.4 Ridges:

Ridge Profile:

A ridge is an elongated pile of ice block and they are formed when two ice sheets, driven by winds and currents break against each other. The concerned typical ridge profile has a keel, consolidated layer and a sail. Ridges in Baltic sea are difficult to break even for ice breakers. (Tukhuri, Ice Mechanics-Ridges and Rubble piles 2016) The picture of a typical ridge is shown in Figure **11** below

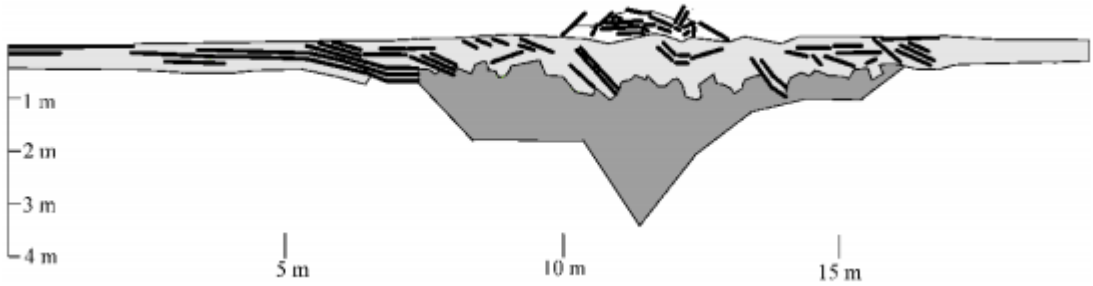

Figure 11 shows the sketch of a typical ridge profile with sail, consolidated layer and keel part of ridge. (Tukhuri, Ice Mechanics-Ridges and Rubble piles 2016)

There are two types of ridges, compression and shear ridges depending on their formation. The strength of ridges is usually measured by conducting full scale tests or by performing direct shear box tests on ridges. There are no reliable analytical models that exist for calculating ridge loads. However, one reasonable approximation that is currently in use is that the consolidated layer of ice is assumed as level ice and calculated accordingly, whereas the load caused due to sail part is neglected because of its insignificance. The estimation of loads from the keel part of the ridge is the most complicated assessment. Since some properties of the ridge keel resemble that of the soil, the Mohr-Coulomb failure criterion is applied in order to determine the keel loads. (A. Polojarvi, Ice Rubble and Ridging 2017)

1.4.5 Limit Mechanisms

ISO developed three limit mechanisms for evaluating the ice loads acting on the structures.

- Limit stress condition arises when the ice feature is driven against a structure with sufficient energy and make the ice to crush in front of the structure. In limit stress, the magnitude of ice loads on structure is governed by failure processes in ice like tensile, compressive, flexure, buckling, splitting etc. Limit stress mechanism gives rise to the highest ice forces on the structure.
- Limit energy condition arises when the ice feature moves with some velocity and collides against a structure. In this case, the ice actions on structures are purely due to the kinetic energy of the ice.
- Limit force condition arises when metocean parameters like wind, current, or pack ice ice drives the ice feature against the structure. Usually, limit force condition contributes low forces on structure.

1.4.6 Numerical simulation

Nowadays, the numerical modelling of ice is conveniently used to simulate the ice-structure and ice-ice interaction scenarios. The biggest advantage inherent in numerical simulation is that manifold simulation can be performed and the variation of results will not be significant. Moreover, the costs associated with numerical modelling are very low when compared with model and full scale tests. Though not widely used, the CFD techniques for determining the resistance of ships in ice are being used nowadays. (Kujala, Winter Navigation-Ship resistance in ice 2016) Figure **12** shows the CFD simulation of ship in ice. The disadvantages in numerical modelling is that it cannot model the ice features exactly as in real conditions, and thus there exist significant uncertainties in numerical techniques.

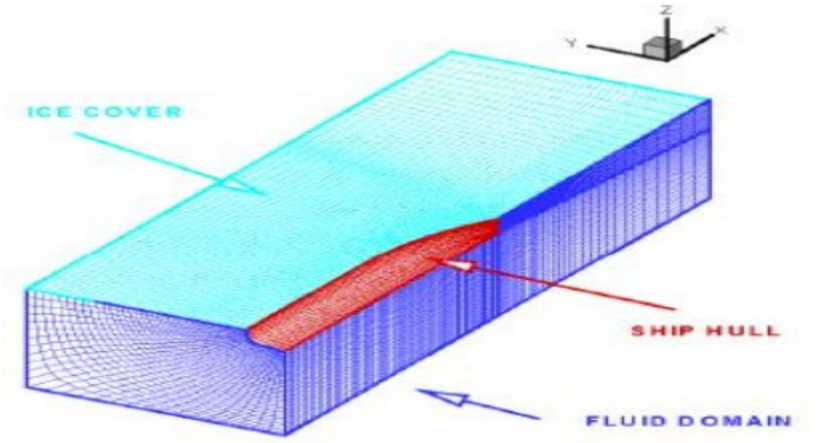

Figure 12 CFD simulation of ship in ice (Kujala, Winter Navigation-Ship resistance in ice 2016)

1.4.7 Model scale tests

Ice model tests are carried out in ice tanks, and there only handful number of such tanks around the world. Typical tests conducted in an ice tank are ship resistance tests in level ice and ice channels, propulsion tests, manoeuvring tests in ice, ice-structure collision tests & ice-ice interaction tests. In addition, flexural and indentation tests are conducted on ice beams in laboratories for measuring the physical and mechanical properties of ice. The main drawback inherent in ice model tests is that it is performed in a controlled environment which does not represent the actual environment exactly. Figure **13** shows the picture of a model ice resistance test. Though it comprises some uncertainty, it is far better in evaluating the ice actions on structures when compared with numerical simulation (Kujala, Winter Navigation-Ship Design Principles 2017)

Figure 13 Picture of ice model scale testing (Kujala, Winter Navigation-Introduction 2017)

1.4.8 Full scale tests

Usually full scale tests include in situ measurements on ice, ship trial runs in ice infested areas. Sea trials are conducted with ships in order to verify the integrity of the design, and also to check whether the results from model tests and numerical simulations matches with full scale trials (Kujala, Winter Navigation-Ship Design Principles 2017). Real world results in chaotic testing environment where the target ice conditions may not be found and there may be large variations between tests. Additionally there will be more variables in the full scale testing than in model scale and numerical testing. Figure **14** shows the in situ tests performed on ridges.

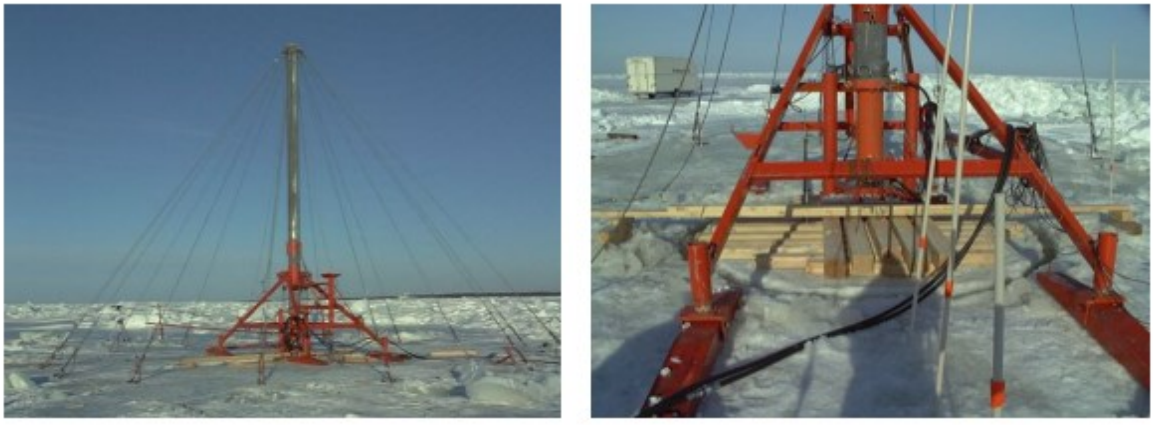

Figure 14 Picture showing the full scale tests on a ridge in Baltic sea (Tukhuri, Ice Mechanics-Ridges and Rubble piles 2016)

1.5 STRENGTH VS DUCTILE DESIGN

Usually, the ships and ocean structures are designed based on the principle of structural crashworthiness. A crashworthy ship structure should possess the capability to secure both humans and the materials present in it during collision or grounding, and it should remain watertight as well. As described in Standards Norway (2004), a structure can be designed in three ways taking into consideration the principle of crashworthiness. Figure **15** shows the design philosophies. One is the strength design, other being the ductile design and the third one is the shared energy design.

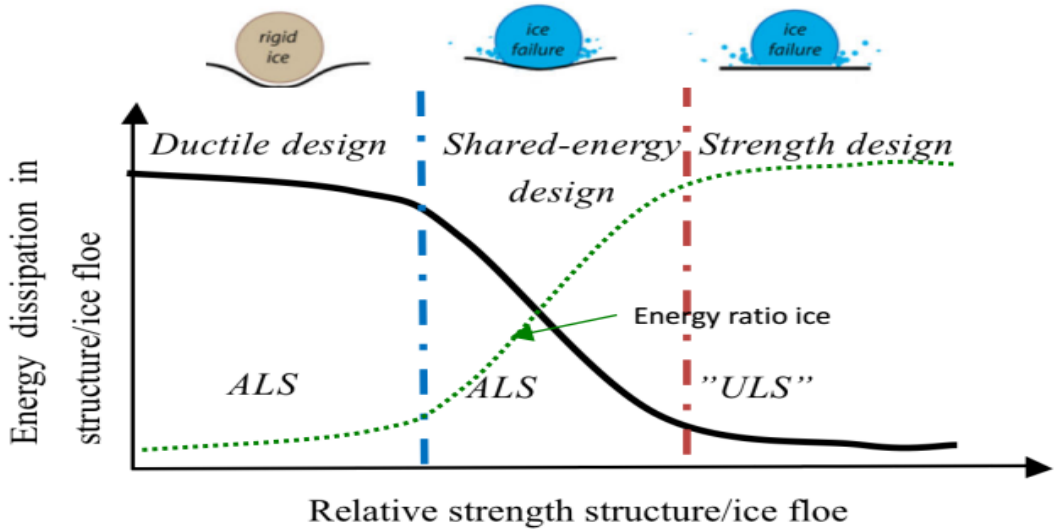

Figure 15 Graph showing the energy dissipation as a function of relative strength. Curves represent the interelation between different design philosophies (Amdahl 2017)

Strength design concept dictates that the struck ship structure should undergo minor deformation and deep penetration of ice berg is not allowed. Furthermore, in this design philosophy, the striking ice berg should absorb most of the energy dissipated. The studies carried out by Rubino et al. (2010) showed that the structures designed based on this strength concept exhibited inferior performance when compared with the well-known X- and Y- core structures.

The ULS design criteria is used with strength design philosophy, which means the ice actions corresponding to an exceedance probability of 10^{-2} is taken into consideration. The probability of collision limits with ice bergs have been discussed in section **1.3.2.** The ice loads on structures is usually calculated in terms of pressure-area curve. Figure **16** shows the P-A curve, highlighting the domains where different design concepts are valid. Also, in the picture two design curves can be seen which are plotted corresponding to the design ice load levels of 10^{-2} and 10^{-4}.

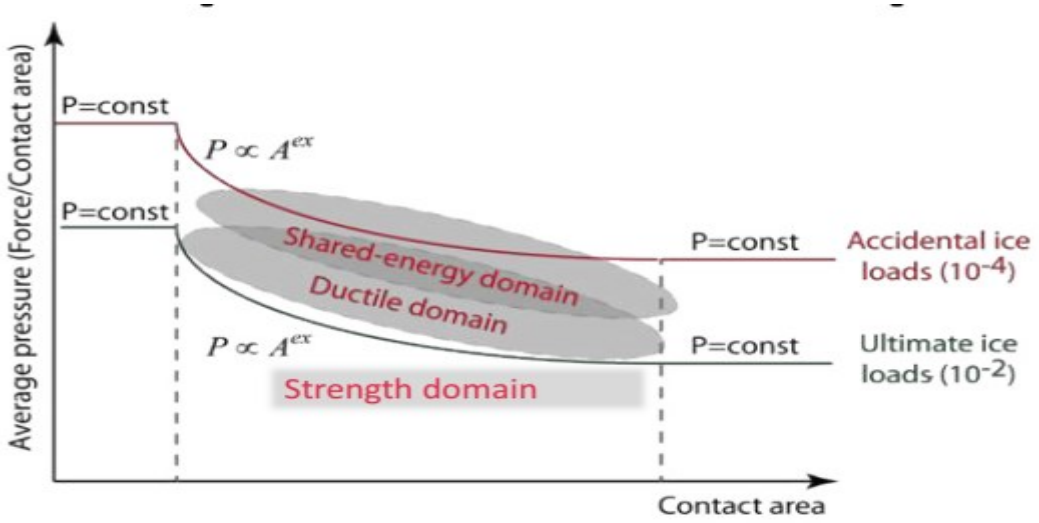

Figure 16 Pressure-Area curves for accidental and ultimate ice loads (Amdahl 2017)

On the other hand, ductile design philosophy states that the struck ship structure can undergo large scale deformation and can allow large intrusion of the striking iceberg as well. Moreover, in ductile design, as large deformation of structure, deep penetration of colliding iceberg and large contact area of ice berg on ship's side can be considered. By this way, the energy dissipated can be distributed to large parts of the ship structure. The ALS design criteria is followed in ductile design concept, so the ice actions corresponding to 10^{-4} probability is considered in ductile design. Ductile design is superior to the strength design in the sense that it accounts for the extreme ice load actions. Usually, double hull sided ship structure is preferred in ductile design concepts. The best double hull design has been proposed by Karlsson (2009), in which corrugated plate is used as the inner side shell and is intermittently welded to the web frames and the inner plates might get separated in the event of collision. Owing to this separation, the corrugated plates are free to unfold and much deeper penetration of ice and energy is required to damage the entire double hull side. Through this kind of design, the ship will be safe and water tightness is ensured as well. (Riley 2011)

Shared energy design introduces the fact that in an accident scenario, both the ship and the striking ice berg contributes to the energy dissipation. In most cases, the ductile and shared energy design are used, though in some cases strength design is carried out by minor increase in steel weight.

From calculation perspective, the strength or ductile design philosophy is often preferred, as the computation is easier to perform. For example, in ductile design, the struck ship is modelled as a softer object and the geometry of ice berg is modelled as rigid structure. In this way, the response of the ship can be estimated. In the case of shared design, the interaction problem is complex to solve, as the magnitude of the collision forces depends on both the ship and ice berg.

1.6 EXTERNAL DYNAMICS AND INTERNAL MECHANICS:

In realistic ship-ice collisions, the total kinetic energy is absorbed in several ways like strain energy dissipation, acceleration of structural and hydrodynamic added mass and hydrodynamic dissipation. While assessing the accidental limit state all these effects are taken into consideration. The collision problem is generally studied in terms of problem of external dynamics and internal mechanics. These two are coupled phenomenon, but in order to simplify the calculations, these two are decoupled and analysed separately. (Liu 2011)

External dynamics is mainly concerned with analysing the rigid body motions during and after the collision. The amount of energy dissipated in the collision process is determined from the external dynamics analysis. Traditionally, the external mechanics assessment are carried out with the help of simple analytical expressions put forward by Popov(1967), Stronge(2004), Daley(1999), Liu(2011) etc. In these methods, the dissipated strain energy is calculated by the conservation of energy and momentum conservation equations. These methods provide a good estimate of the energy dissipation. However, they did not account for the effects due to surrounding water, therefore they are used only as a preliminary analysis. Non linear finite element analysis (NLFEA) seem to provide better results. The estimated energy dissipation is the input for the internal mechanics analysis. (Liu 2011)

In internal mechanics evaluation, based on the dissipated energy from external mechanics, the extent of damage on the structure is determined. In other words, the depth of penetration and the consequent deformation can be known from force vs penetration curve. As far as method of analysis is concerned, it can be performed either with simple empirical models or using NLFEA. The analytical methods evaluate the deformation based on plastic method of analysis. Most of the rule books used for assessing the internal mechanics are based on analytical expression derived using plastic analysis. (Liu 2011)

A coupled analysis involves development of model which both the internal mechanics and externl dynamics can be integrated and evaluated together. This model can be simulated with the help of some FE numerical simulation tools and this approach facilitates exact simulation of the ship-ice collisions. However, this approach presents a considerable difficulty in modelling the extensive water domain, since simulation of the large water domain in FE software demands excessive memory time and paves way for additional problems. Notwithstanding, in recent times, some simplifications are taken into account while performing the coupled FE analysis.

CHAPTER 2

The structural response of ship hitting an ice berg can be determined either by the usage of analytical energy methods or resorting to 3D non-linear finite element analysis. ISO 19906 presents a simple 1D analytical expression equation for evaluating the kinetic energy dissipation when an ice feature strikes the offshore structure (Tukhuri, Ice Mechanics - Ice failure against structures 2016). In this section, various empirical models that are in existence for calculating the energy dissipated in a collision process are presented.

2.1 ESTIMATION OF ICE -STRUCTURE COLLISION FORCES

Ice actions on structures are mainly due to the collision between them. The resultant and magnitude of forces involved in the collision process are determined by some limit process. In a typical collision scenario, the maximum force on the structure is dictated either by the strength of ice or by the available kinetic energy. In the latter case, the available kinetic energy is dissipated into crushing (irrecoverable) and potential (recoverable) energy. Collision forces arise due to the impact between two objects, and in such cases, it is usually conceived that one object is moving whereas the other one is stationary. In this project, an ice berg hitting a FPSO is taken into consideration. So, from collision point of view, the ice berg is considered to be the impacting body and FPSO taken as the impacted body. Energy methods seem to be simple and effective in evaluating the forces involved in these impact cases. The important basis of the energy method is equating the available kinetic energy with the indentation (crushing) and potential energy and is given by the following equation (Daley, Energy based ice collision forces 1999)

$$\mathbf{KE = IE + PE} \tag{6}$$

Here, the effective kinetic energy has to be determined, which is the kinetic energy of both the objects after the impact. If the struck object has finite mass, its kinetic energy will increase after the impact, and in turn introduces further complexity in solving the problem. In order to make the problem simpler, it is assumed that the struck body is very large. On account of this simplification, it is considered that the motion of the objects will cease at the point of maximum force. This kind of analysis will be discussed in detail in section **2.2.1.**

The indentation/internal energy is calculated as the integral of the indentation force F_n on crushing displacement $d\zeta_c$. The indentation energy is expended in irrecoverable process and is given by

$$\mathbf{IE} = \int_0^{\zeta} \boldsymbol{F_n}\ \boldsymbol{d\zeta_c} \tag{7}$$

The potential energy dissipation can be due to the rigid body motions (pitch/heave in ramming) or elastic deformation of both the objects. The potential energy is estimated as the integral of the indentation force F_n, on the displacement $d\zeta_e$. Here, the potential energy is expended in recoverable process and is represent by

$$\mathbf{PE} = \int_0^{\zeta} \boldsymbol{F_n}\ \boldsymbol{d\zeta_e} \tag{8}$$

These equations constitute the general energy methods used for solving various types of simple impact cases. (Daley, Energy based ice collision forces 1999). Moreover, reference ice pressures are necessary to calculate the average pressure, which in turn is used to derive the Force-Indentation relationship. The reference ice-pressure can be evaluated from the Pressure-Area curves.

The average pressure P_{av} in the nominal contact area A, is given as

$$\boldsymbol{P_{av} = P_0 A^{ex}} \quad (9)$$

P_0 is the reference pressure at 1 sq.m taken from Pressure-Area curves and ex is a constant

The ice force F_i on the nominal contact area is given through the equation

$$\boldsymbol{F_i = P_{av} A = P_0 A^{1+ex}} \quad (10)$$

2.2 COLLISION TYPES

2.2.1 Initial Impact Collisions

In a normal impact case, the collision analysis is conducted at the point of impact. In other words, the analysis is performed with respect to the collision point of both objects. In this case, the potential energy dissipated in the collision process is assumed as zero and the bleaching, ice frictional effects are neglected as well. As a result, the total kinetic energy involved in the collision process will only be equated to the indentation energy. However, the added mass terms corresponding to 6-DOF motions of ships are considered. For ice bergs, surge, heave and pitch motions are considered if it is symmetrical collision. Suppose if it is an unsymmetrical collision, yaw motion of the ice berg will also be taken into account in addition to the three rigid body motions of ice. (Yu.N.Popov 1967) The normal impact case is also called as Popov impact and can be applied to both ship-ice and ice-structure collision scenarios. The picture of a head on impact case is displayed in Figure **17**

As already stated, the normal kinetic energy is equated to the indentation energy, KE = IE

$$\text{KE} = \frac{\boldsymbol{P_0}}{\boldsymbol{f_x}} \boldsymbol{f_a \zeta_n^{f_x}} \quad (11)$$

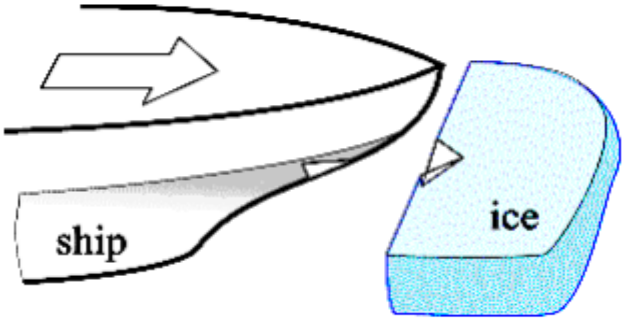

Figure 17 Head on normal impact of ship against ice (Daley, Energy based ice collision forces 1999)

The indentation force for the normal impact collisions is determined using the equation,

$$\boldsymbol{F_n = P_o \cdot f_a \left(\frac{KE_e \cdot f_x}{P_o \cdot f_a}\right)^{\frac{f_x - 1}{f_x}}} \quad (12)$$

Where f_a and f_x are the geometric functions. The values of f_a and f_x are given for different geometries in Daley(1999) and when those values are substituted in indentation force equation for normal impact, the indentation force F_n corresponding to those different indentation geometry cases can be derived. Through this way, the normal impact analysis can be carried out for ice-structure collision scenarios. (Daley, Energy based ice collision forces 1999)

2.2.2 Beaching impact type collisions

The collision incident, in reality, paves way to a phenomenon called beaching. The beaching impact analysis takes the ice beaching phenomenon into account, so the collision analysis becomes more complex than initial impact case as the beaching force and the potential energy dissipation have also been accounted for. However, this kind of analysis ignores the frictional effects between the ice and structure, like the normal impact case. In this case, the total kinetic energy is equal to the sum of ice crushing energy and potential energy, KE = IE +PE.

The kinetic energy is KE = ½ M$\boldsymbol{V^2}$ (13)

The potential energy is given by, PE = ½ $\frac{F_v^2}{K_b}$ (14)

The indentation force equation can be written as $\boldsymbol{F_n = K_{ice} \cdot \zeta_n^{f_x - 1}}$ (15)

Where $\boldsymbol{K_{ice} = P_0 \cdot f_a}$ (16)

The indentation energy equation can be written as

IE = $\frac{K_{ice}}{f_x} \boldsymbol{\zeta_n^{f_x}}$ **(Daley, Energy based ice collision forces 1999)** (17)

Like in normal impact case, the indentation force and energy dissipated, can be estimated for different indentation cases. The procedure involved in the beaching analysis can be applied to both the ship-ice and ice- offshore structure collisions.

In Figure **18,** the relative position of the ship and ice after the initial and beaching impact are shown. In addition, the force exerted on ship's structure corresponding to the impact scenarios considered are also shown.

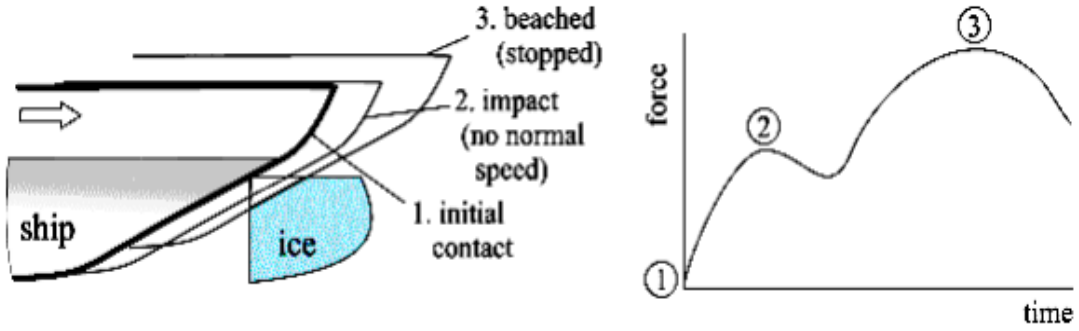

Figure 18 Picture on the left shows the ship-ice relative positions aftermath of different impact scenarios and the right figure shows the force vs time plot corresponding to the impact cases. (Daley, Energy based ice collision forces 1999)

2.2.3 Oblique collision

In ice-structure interaction, considerable amount of force may be produced due to the sticking of ice and frictional effects. So, a 3-dimensional approach is needed in order to evaluate the oblique collision.

Firstly, in this section detailed description of the Stronge's impact theory is presented. He proposed a solution for the analysis of 3D impact, widely known as Stronge's impact mechanics model. The basic assumptions underlying the derivation are given as follows:

- The impact duration is short and the impact force is large, therefore all other external mechanics forces are neglected.
- The deformations are confined to a small area within the contact surface (Liu 2011)

Taking into account these assumptions, Stronge derived the equations of motion in a local coordinate axis. Consider two bodies colliding against each other at some arbitrary point. The points of contact on each of the mass are denoted by C and C' respectively, as shown in Figure **19.**

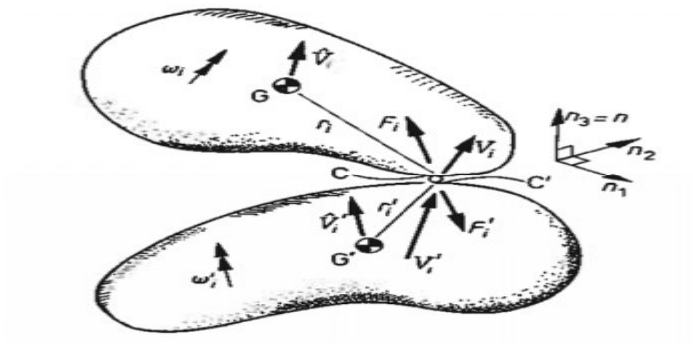

Figure 19 Free Body Diagram of two impacting bodies (Liu 2011)

Here, the prime symbol ($'$) is used to signify the second object involved in collision. It is also assumed that both the bodies have a common tangent plane and they have no displacement constraints. After that, a local coordinate system is established by defined set of mutually perpendicular vectors n_i in the tangent plane that can be seen in Figure **19.**

$\widehat{V_i}$ and $\widehat{V'_i}$ shown in figure indicates the translational velocities of the centre of mass of the objects and ω_i and ω'_i represent their angular velocities respectively. The translation velocities are defined with respect to the centre of mass, but in order to analyse the impact problem, the velocity at the point of impact is needed. These velocities at contact point can be derived using the relation

$$\boldsymbol{V_i = \widehat{V_i} + \epsilon_{ijk}\omega_j r_j} \quad (18)$$

$$\boldsymbol{V'_i = \widehat{V'_i} + \epsilon_{ijk}\omega'_j r'_j} \quad (19)$$

Where ϵ_{ijk} is the permutation tensor. If the indices i,j,k are in cyclic order, the value of tensor will be equal to 1 and it will be 0 if the indices are in anti-cyclic order. r_k and r'_k are the distance of contact points (C and C') of both the bodies from their respective COG's.

At the point of contact, the objects will be subjected to forces F_i and F'_i. Based on these forces, the impulse reactions of the two impacting bodies are calculated by the formula

$$\boldsymbol{dP_i = F_i dt} \quad (20)$$

And, $\boldsymbol{dP'_i = F'_i dt}$ (21)

The mass of the bodies are represented as M and M' and their moments of inertia are given as $\widehat{I_{ij}}$ and $\widehat{I'_{ij}}$. The equation of translational and rotational motion of the colliding objects are expressed and then the velocities at the contact points, the translational and rotational motions are derived. Using these, the relative velocity (v_i) and incremental impulse reaction (dp_j) can be calculated. The relative velocity and incremental impulse, in turn are used to formulate the inverse mass matrix (m_{ij}^{-1}) using the relation $dv_i = m_{ij}^{-1}\, dp_j$ in Liu(2011). This is the Stronge's(2004) impact mechanics formulation.

Using Stronge(2004) impact theory and Peder & Zhang's(1998) approach to collision, Liu et al formulated the expression for the dissipation of energy for the 3 dimensional collision case.

In Peder and Zhang's method, the hydrodynamic effects involved in the collision are quantified using the added mass factors. These factors are included in the mass and inertia matrices. Furthermore, there is a flexibility in this method in which the mass and inertia matrices can be reduced to diagonal matrices with reference to global coordinate systems.

Two types of coordinate systems are considered in this problem. First one being the global coordinate system, in which the X,Y,Z coordinates are defined at the centre of gravity of the ship. Figure **20** illustrates the global coordinate systems of the ship clearly. The local coordinate system (n_1, n_2, n_3), which is defined exactly in the same way as in Stronge's(2004) theory.

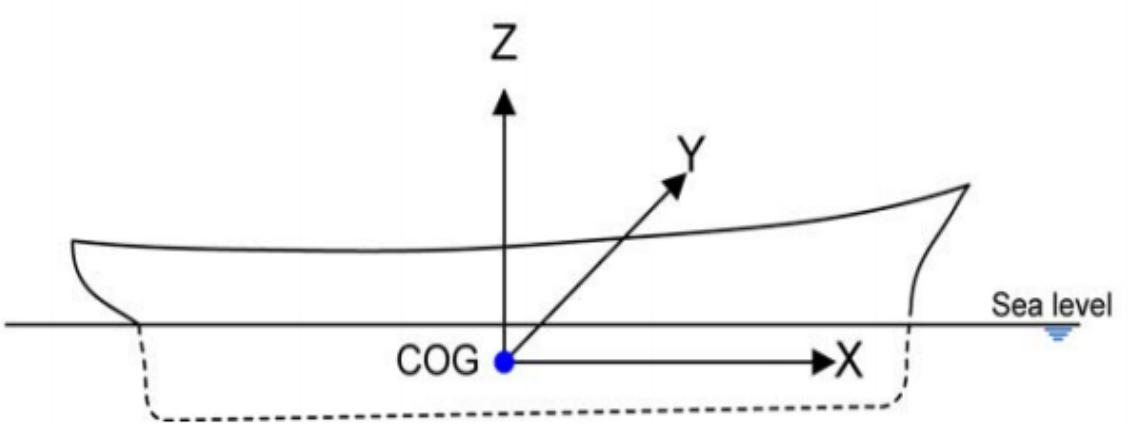

Figure 20 Global coordinate system axis of the ship (Liu 2011)

Now the mass $(\widehat{M_{ij}}, \widehat{M'_{ij}})$ and inertia $(\widehat{I_{ij}}, \widehat{I_{ij}}')$ matrices in the global coordinate system are known. In order to apply Stronge's(2004) impact theory, the equation of motions must be framed with respect to the local coordinate system. The transformation matrix can be used to represent the mass and inertia matrices in local coordinate system.

So, let us look into the procedure of forming a transformation matrix. The following hull angles are used to derive it. The pictorial representation of the angles is shown in Figure **21**

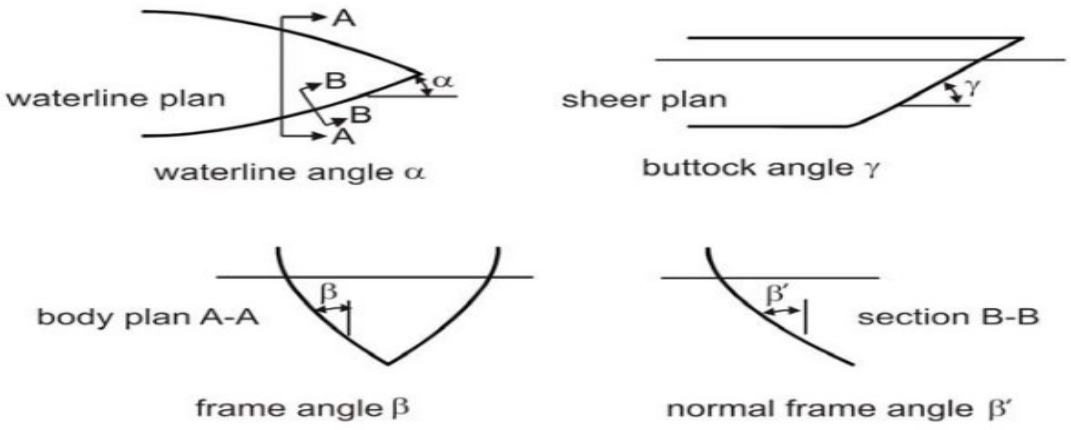

Figure 21 Hull Angles (Liu 2011)

α – Water line angle

β – frame angle

β' - normal frame angle

γ – sheer angle

Based on these angles, the transformation matrix can be written as

$$T_{ij} = \begin{bmatrix} cos\alpha & -sin\alpha & 0 \\ -sin\alpha sin\beta' & -cos\alpha sin\beta' & -cos\beta' \\ sin\alpha cos\beta' & cos\alpha cos\beta' & -sin\beta' \end{bmatrix} \quad (22)$$

Using this transformation technique, the mass (M_{ij}, M'_{ij}) and inertia (I_{ij}, I'_{ij}) matrices in local coordinate system are known

After this step, the inverse mass(m_{ij}^{-1}) matrix is estimated based on the procedure outlined in Stronge's(2004) theory. Then, the absolute value of the dissipated energy is determined using the formula

$$E_i = \frac{1}{2} abs(\overline{m_i} \Delta v^2) \quad (23)$$

Where $\overline{m_i}$ is the equivalent mass variable which is found by normalizing the inverse mass matrix with the force components in the i&j directions.

$$\overline{\boldsymbol{m_i}} = \boldsymbol{m_{ij}^{-1}} \frac{\boldsymbol{f_j}}{\boldsymbol{f_i}}. \quad (24)$$

Review: Having explained the procedure of Liu's method, now let us look into the pros and cons of this method. The equation **23** is a 1 –DOF equation that can be solved in each direction thereby finding the solution for complicated 6-DOF problem. It is derived by substituting proper boundary conditions for the relative velocity, and frictional effects. (Liu 2011)

The biggest advantage inherent in this method is that the 3D effects like sticking and sliding of ice can be evaluated. In addition, the versatility of this method lies in the fact that the impact taking place at any area along the ship can be analysed. Though this technique is good in many respects, there are uncertainties associated with this technique.

- It makes use of only a simplified model of the ice berg in the calculation.
- The ice berg model is assumed as strain independent but actually the ice depends on strain rate
- This model do not take into account the failed ice, thereby ignoring the force caused by the ice pieces.

Liu et al also derived a 2D formulation for collision problem by introducing some simplifications to the 3D equation by setting the normal frame angle (β') and the Z-axis components of the direction vectors(r_z, r'_z) to zero. (Liu 2011)

Conclusion: In this chapter, analysis of three types of impact scenarios have been presented. The impact scenarios are the direct normal impact, beaching impact and oblique impact. The energy equations of the first two cases (direct normal and beaching) were derived by Claude Daley(1999) and the equations for oblique analysis presented here was derived by Liu(2011). In short, the direct collision analysis ignores the beaching and frictional effects. On the other hand, the beaching impact analysis takes into account the beaching forces involved in the collision, but totally ignores the sliding and sticking effects of ice. Finally, the oblique collision analysis proposed by Liu(2011) considers the sliding and sticking effects as well. As a result, it can be concluded that the Liu's method can be used for full 3-dimensional collision analysis.

CHAPTER 3

Ice going ships must be sufficiently ice strengthened in order to withstand extreme ice actions during the transit. Their design should be carried out according to the widely accepted design rules. As of now, there are many design rules in practice that present the design and operational requirements for ice going ships. They are Russian rules, Finnish-Swedish rules etc **.** However, their main restriction is that these rules have been designed taking into consideration the local ice conditions, thus they cannot be applied for ships intended for polar operations. For example Finnish-Swedish rules, developed in 1971 hull, propeller, and propulsion machinery requirements with four ice classes 1A Super, 1A, 1B, and 1C (Kujala, Winter Navigation-Ice Strengthening Rules 2017). It can be applied to the design of ships whose intended operational area is around Baltic region. There is another set of rules, popularly known as Polar Class rules which defines the unified requirements for ships sailing in polar waters.

Polar class rules present a set of design requirements for the ice going ships. It consists of both the structural design and machinery requirements that must be followed while designing ice ships. The ice strengthened ships are designed using the IACS polar class rules. The structural design rules of ice going ships mentioned in PC are based on the plastic assessment of structural deformation of ships subjected to extreme ice events.

3.1 DESCRIPTION OF AN ICE STENGTHENED SHIP IN THE BOW AND MID SHIP AREA

The ships that are meant for sailing in ice infested waters and constructed in steel must comply with the unified requirements of polar class. In addition to the unified PC requirements, the ice going ships must also satisfy open water requirements. Other than conventional ships, there are completely different class of ships whose structures and machineries are designed for extreme operational cases, they are usually called as ‘Ice Breakers’. Their main functions are to escort the ships stuck in ice and to create ice channels for manoeuvring of ships, the ice breakers’ design must also have to comply with the general PC design rules and certain other rules as well. There are totally seven PC design rules (PC1-PC7) each should be used in accordance with the operational profile and time spent by ships in ice infested areas. Table **1** presents all the seven PC rules along with the ice descriptions in which the designed ships will operate. For example, PC1 should be used for ships that are intended to operate in polar waters throughout the year, likewise PC7 for vessels which operate in thin first year ice during summer/autumn. (International association of Classification Societies 2016)

Polar Class	Ice descriptions (based on WMO Sea Ice Nomenclature)
PC 1	Year-round operation in all polar waters
PC 2	Year-round operation in moderate multi-year ice conditions
PC 3	Year-round operation in second-year ice which may include multi-year ice inclusions.
PC 4	Year-round operation in thick first-year ice which may include old ice inclusions
PC 5	Year-round operation in medium first-year ice which may include old ice inclusions
PC 6	Summer/autumn operation in medium first-year ice which may include old ice inclusions
PC 7	Summer/autumn operation in thin first-year ice which may include old ice inclusions

Table 1 Summarizes different subdivisions within the PC rules for structural design of ice strengthened ships (International association of Classification Societies 2016)

3.1.1 Structural Requirements of Polar Class ships

In this project, more importance is devoted to the structural design of ice vessels and almost nil importance to the machinery design. The hull areas of an ice strengthened ships is divided into four parts longitudinally. Figure **22** shows the picture of the ice strengthened ship along with the subdivisions. B, BI, M, S in the picture refers the Bow, Bow intermediate, Middle and Stern part respectively. Further, each part (except bow) is subdivided into three regions in vertical direction like ice belt (i), lower(l) and bottom(b). The ice belt(i) and lower(l) regions can be clearly seen in Figure **22**, and the lower (l) and bottom(b) regions are visible in Figure **23.**

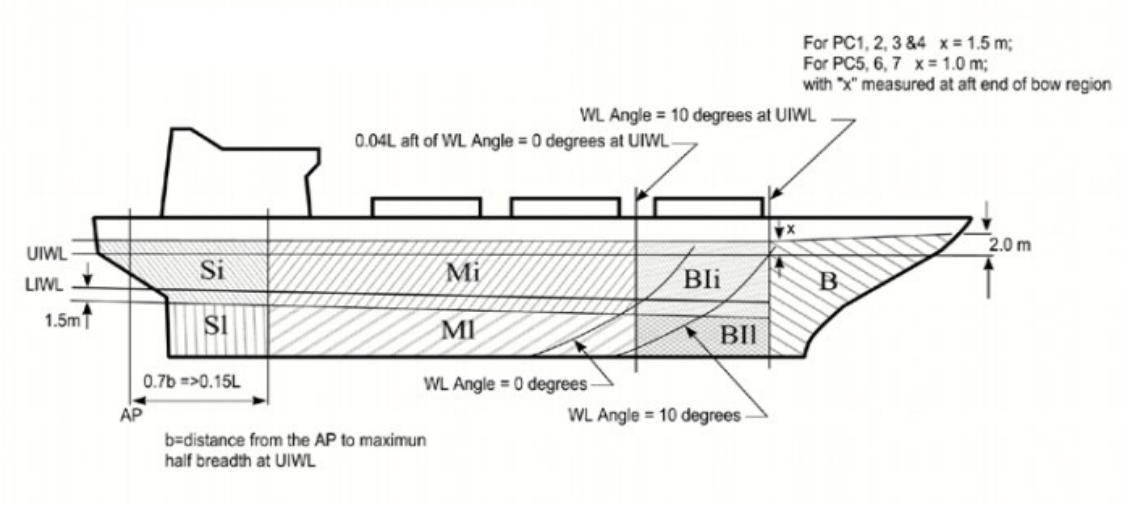

Figure 22 Different regions of an ice strengthened ship (International association of Classification Societies 2016)

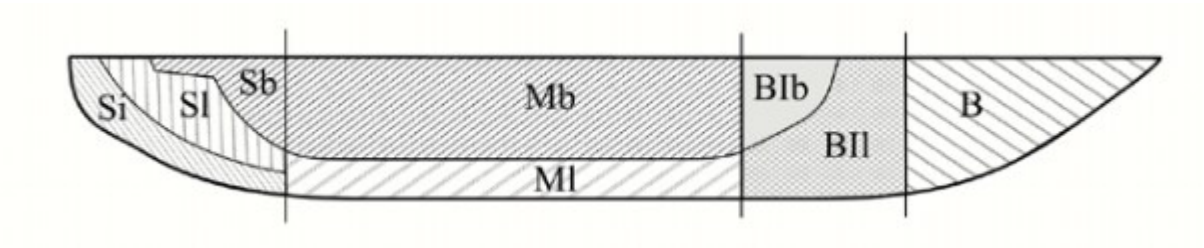

Figure 23 Regions of ice strenghened ship (International association of Classification Societies 2016)

Ice resistant structural members should be designed for these regions and in order to determine them, the loading scenario usually considered is the glancing impact on the ship. According to PC rules, the design ice loads must be quantified as average pressure (P_{avg}) , which is the uniform pressure acting over a patch of height(h) and width (b). In order to evaluate the average pressure, the following characteristics of loads like force(F), line load (Q) and pressure(P) must be estimated at bow regions ($F_{bow,}Q_{bow}$) and at regions other than bow ($F_{non\ bow,}Q_{non\ bow}$) of the ship.

Table **2** summarizes different structural members used in the ice strengthened regions and the corresponding design peak pressure factors (PPF). PPF's are used to represent the high local pressures in each region because of ice loading. From Table **2,** it can be figured that PPF's are always chosen higher than the allowable limit in order to have a conservative design.

Structural member		**Peak Pressure Factor (PPF_i)**
Plating	Transversely-framed	$PPF_p = (1.8 - s) \geq 1.2$
	Longitudinally-framed	$PPF_p = (2.2 - 1.2 \cdot s) \geq 1.5$
Frames in transverse framing systems	With load distributing stringers	$PPF_t = (1.6 - s) \geq 1.0$
	With no load distributing stringers	$PPF_t = (1.8 - s) \geq 1.2$
Frames in bottom structures		$PPF_s = 1.0$
Load carrying stringers Side longitudinals Web frames		$PPF_s = 1.0$, if $S_w \geq 0.5 \cdot w$ $PPF_s = 2.0 - 2.0 \cdot S_w / w$, if $S_w < (0.5 \cdot w)$
where: s = frame or longitudinal spacing [m] S_w = web frame spacing [m] w = ice load patch width [m]		

Table 2 Peak Pressure Factors for different structural members (International association of Classification Societies 2016)

In this section, a brief introduction and structural requirements of different members that will be used in a typical ice strengthened ship are outlined.

3.1.1.1 Shell Plating

Shell plating consists of stiffened plate elements that are in contact with the hull exposed to ice loading. From the perspective of stability considerations, these plates must be designed in such a way that it should withstand these ice loads. Furthermore, the thickness of plates and stiffeners that are in contact with the plates should be chosen in such a way that the degree of end fixity required for shell framing is ensured. Considering the above mentioned

requirements, the minimum shell plating thickness is given by,

$$t = t_{net} + t_s \text{ (mm)} \quad (25)$$

To account for corrosion/abrasion of plates in ice, an additional 1 mm should be included with the above estimated thickness. Figure **24** shows a typical shell plate used for ice strengthening in ships.

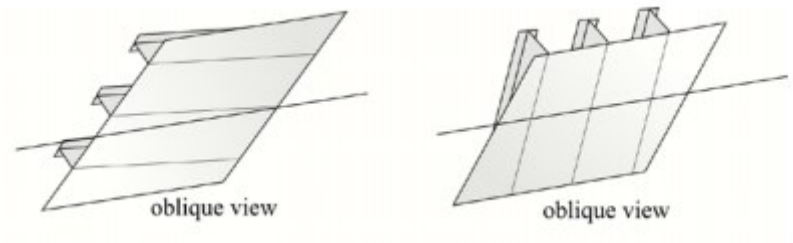

Figure 24 Oblique view of shell plates (Kujala, Winter Navigation-Ship Design Principles 2017)

3.1.1.2 Framing

In an ice strengthened ship hull, there are longitudinal and transverse frame members, web frames and load carrying stringers. The strength of a framing member depends on the fixity provided at the supports. The frames can either be continuous, simply supported or can be attached to another section through brackets. There exist specific design criteria for frames located in different parts of the hull, they are outlined below.

3.1.1.3 Bottom, longitudinal, transverse frames

While designing a vessel for ice strengthening, frames are usually placed at Bow intermediate bottom (BIb), Mid ship bottom (Mb) and Stern bottom (Sb). Here, the ice load is taken as the average pressure acting over a rectangular patch.

The transverse frames and longitudinal frames are placed in the side structures. They should be designed in such a way that the combined effects of shear and bending should not exceed the frame's plastic capacity. In order to determine the scantling requirements of longitudinal and transverse frames, the actual net effective shear area and plastic section modulus should be calculated for both the longitudinal and transverse frames. The corresponding analytical formula and the calculation procedure are elaborated in IACS (Req.2006/Rev.2.2016).

3.1.1.4 Web frames and stringers

The web frames and stringers must also be designed to withstand the combined effects of shear and bending. The scantlings of web frame and stringer members can be determined similar to other frame members and the procedure is given in IACS Req.2006/Rev.2.2016. Typical view of web frames is displayed in Figure **25.**

More importantly, all the frame members designed for ice strengthened vessel should be designed so as to resist buckling, as part of the structural stability consideration. For preventing buckling, the IACS Polar class dictates that the ratio of web height to net web thickness of any framing member should not exceed: $282/(\sigma_y)^{0.5}$ for flat bar sections

$805/(\sigma_y)^{0.5}$ for bulb, tee and angle sections

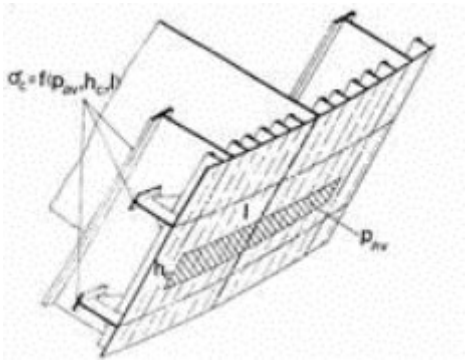

Figure 25 Web frame and stringers in an ice-strengthened ship (Kujala, Winter Navigation-Ship Design Principles 2017)

3.1.1.5 Structural steel

Special consideration should be given while choosing the steel grades for ice going ships. Polar class rules specified the materials classes for structural members, which is shown in Table **3** . Material classes for a range of thickness of structural members are listed in Table **4**.

Structural members	Material class
Shell plating within the bow and bow intermediate icebelt hull areas (B, B_{II})	II
All weather and sea exposed SECONDARY and PRIMARY, as defined in Table 1 of UR S6.1, structural members outside 0.4L amidships	I
Plating materials for stem and stern frames, rudder horn, rudder, propeller nozzle, shaft brackets, ice skeg, ice knife and other appendages subject to ice impact loads	II
All inboard framing members attached to the weather and sea-exposed plating, including any contiguous inboard member within 600 mm of the plating	I
Weather-exposed plating and attached framing in cargo holds of ships which by nature of their trade have their cargo hold hatches open during cold weather operations	I
All weather and sea exposed SPECIAL, as defined in Table 1 of UR S6.1, structural members within 0.2L from FP	II

Table 3 shows the material classes for different structural materials for its use in ice strengthened ship (International association of Classification Societies 2016)

Thickness, t [mm]	Material class I				Material class II				Material class III					
	PC1-5		PC6&7		PC1-5		PC6&7		PC1-3		PC4&5		PC6&7	
	MS	HT	MS	HT	MS	HT	MS	HT	MS	HT	MS	HT	MS	HT
t ≤ 10	B	AH	B	AH	B	AH	B	AH	E	EH	E	EH	B	AH
10 < t ≤ 15	B	AH	B	AH	D	DH	B	AH	E	EH	E	EH	D	DH
15 < t ≤ 20	D	DH	B	AH	D	DH	B	AH	E	EH	E	EH	D	DH
20 < t ≤ 25	D	DH	B	AH	D	DH	B	AH	E	EH	E	EH	D	DH
25 < t ≤ 30	D	DH	B	AH	E	EH[2)]	D	DH	E	EH	E	EH	E	EH
30 < t ≤ 35	D	DH	B	AH	E	EH	D	DH	E	EH	E	EH	E	EH
35 < t ≤ 40	D	DH	D	DH	E	EH	D	DH	F	FH	E	EH	E	EH
40 < t ≤ 45	E	EH	D	DH	E	EH	D	DH	F	FH	E	EH	E	EH
45 < t ≤ 50	E	EH	D	DH	E	EH	D	DH	F	FH	F	FH	E	EH

Table 4 Material classes with respect to the thickness of structural members

CHAPTER 4

4.1 ICE BERGS

Ice bergs are huge masses of floating ice found in the seas/oceans which are separated from the continental shelf or ice glaciers. The ice bergs have a free board of more than 5m and they have a greatly varying shape. Small ice berg pieces are termed as Bergy bits and pieces that are even more smaller than bergy bits are named as Growlers. The ice bergs cause serious hazards to Arctic ships and offshore structures (Tukhuri, Ice Mechanics-Occurence of Ice 2016). So, quantification of the ice berg properties becomes essential to evaluate their actions on Arctic structures. In the current section, the structure of ice berg and the physical, mechanical properties have been discussed.

Many research experiments were conducted on fresh water ice and sea ice in order to assess the properties of ice. On the other hand, for the case of ice bergs, only very few experiments had been carried out for measuring their properties.

4.1.1 Physical properties of Ice bergs

The physical properties of ice bergs include its structure, density, porosity, brine content. These properties are discussed in some detail below.

The structure of the ice berg can be separated into three layers. The upper layer of ice berg comprises compressed snow and its depth is very small compared to other two layers. The second layer which extends to some depth inside ice berg is called "firn". The density of second layer is about 400 kg per cubic meter (approx), and due to its low density both air and water may pass through the spaces in between the grains. The third layer extends to the bottom of the ice berg . This layer has a density of about 800 kg per cubic meter and because of its higher density it collapses the air channels present and contributes the formation of air bubbles inside the iceberg. (Britannica 2017)

R.E Gagnon & P.H Gammon(1983) from National research Council of Canada conducted a series of experiments on ice samples taken from ice bergs in Labrador, Canada and Greenland in order to study their properties. This was the first ever research experiment that was performed on ice bergs. The ice properties derived from those experiments are presented below and some discussions have also been made accordingly.

A thin plate of ice had been cut from each of the ice samples and certain ice characteristics like grain diameter, bubble diameter, bubble density, c-axis orientation were found out. The results of that analysis were listed in Table **5**.

As already mentioned, the deeper layers of ice berg are replete with air bubbles. Based on the experimental analysis, it had been found out that the bubbles were not present along the boundaries but were evenly distributed throughout the interior part of the ice. Moreover, the bubble diameter and bubble density were also measured and given in Table **5**. The term G, L used in Table **5** refers to the ice samples taken from Greenland and Labrador respectively and usage of terms 1P,1PP indicates the orientation of optical axis.

The mean grain diameter falls within the range of 8-20 mm.

The c-axis in ice is the optical axis . In the "Preferred c-axis orientation" column in Table **5** , terms like 'Moderate' and 'Strong' were used to describe the axis orientation. 'Moderate' means that 20% of the grains were aligned to extinction and 'Strong' means that 35 % of grains were aligned to extinction. (R.E Gagnon 1983)

Ice type and orientation	*Mean grain diameter*	*Standard deviation*	*Maximum observed grain diameter*	*Mean long and short bubble diameter*	*Standard deviation*	*Maximum observed bubble diameter*	*Bubble density*	*Preferred c-axis orientation**	*Grain elongation*
	mm	mm	mm	mm	mm	mm	# mm^{-3}		
G1	9.16	5.73	31.63	0.38	0.28	1.20	1.30	Moderate	Slight
G1P	3.96	1.77	10.75	0.33					
G1PP	12.95	5.17	25.64						
G2	16.55	6.07	37.94	0.34	0.23	1.20	0.49	Moderate	Slight
G2P	15.84	5.30	35.21	0.27					
G2PP	24.44	6.06	35.32						
G3	18.91	8.43	40.48	0.55	0.39	1.46	0.40	Moderate	Slight
G3P	23.40	8.62	61.25	0.39					
G3PP	23.30	10.38	57.55						
G4	16.43	7.73	42.97	0.30	0.14	0.69	3.02	Moderate	Moderate
G4P	17.92	9.59	49.52	0.23					
G4PP	18.06	9.86	51.30						
L04	9.69	4.53	22.83	0.32	0.21	1.09	2.66	Strong	Moderate
L04P	8.71	3.26	20.92	0.27					
L04PP	6.03	2.21	12.97						

Table 5 summarizes the results of experiments conducted on ice berg samples (R.E Gagnon 1983)

It has been said that the grain type of ice berg is somewhere in between granular and columnar, so it is postulated that the grains in an ice berg will be of granular type. Since no measurements were conducted to study the salinity of icebergs, the saline properties of granular sea ice is presented in Table **6**. Timco & Frederking used YSI conductivity meter for studying the salinity range of granular sea ice samples. From their experiments, they concluded that the salinity in ice samples varies both in horizontal and vertical directions and furthermore added that the upper layers of ice samples possessed higher salinity than the lower layers. Their findings are summarized in Table **6,** where the variation of salinity values with respect to the block depth are shown. The salinity values are given in percentage and totally six ice samples were tested (Garry Timco 1983).

Salinity of the ice (‰)

Block depth range (cm)	Sample					
	1	2	3	4	5	6
0– 5.0	–	–	–	–	–	–
5.0–11.5	7.0	5.9	6.7	6.1	5.6	5.6
11.5–18.0	5.2	4.6	4.7	4.6	4.8	5.0
18.0–24.5	4.8	5.5	5.0	5.0	5.1	4.9
24.5–31.0	4.9	4.1	4.3	4.4	4.5	4.6
31.0–37.5	–	–	–	–	–	–
37.5–44.0	4.1	3.6	4.4	4.2	4.1	3.8
44.0–50.5	4.3	3.9	4.6	4.5	4.5	4.1
50.5–57.0	4.2	3.7	3.7	4.1	3.8	3.8
57.0–63.5	4.7	4.8	3.6	4.7	4.8	4.3
63.5–70.0	2.8	4.2	–	3.8	4.8	4.5

Table 6 Saline Properties of granular sea ice (Garry Timco 1983)

Ice porosity is defined as the percentage of total volume of ice occupied by air bubbles. In that experiment, the ice porosity had been estimated from the volume and density of the ice berg samples. The values of porosity for each of the samples are mentioned in Table **7**

Sample type	*Number of measurements*	*Fractional porosity* %
G1	10	3.0 ± 0.35
G2	10	0.7 ± 0.20
G3	10	2.0 ± 0.26
G4	10	2.8 ± 0.23
L04	10	3.5 ± 0.38

Table 7 shows the measured fractional porosity of ice bergs (R.E Gagnon 1983)

4.1.2 Mechanical Properties of Ice bergs

The mechanical properties of ice bergs encompass

- Flexural Strength
- Compressive strength
- Fracture Toughness

The ice berg samples were cut into beams they were subjected to four point beam bending test in a loading frame. The flexural strength of the ice berg sample had been determined for a range of temperatures and strain rates (R.E Gagnon 1983). The results of those tests are presented below

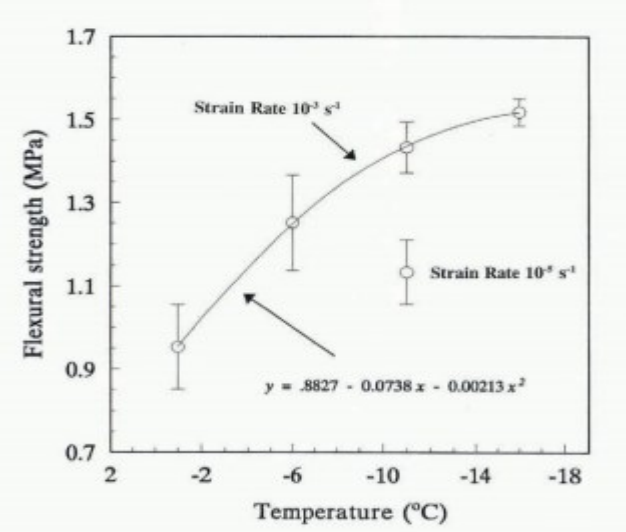

Figure 26 Flexural strength plots of ice as a function of temperature (R.E Gagnon 1983)

Figure **26** shows the plot of flexural strength as a function of temperature. Most of the measurements were taken with a constant strain rate of $10^{-3}s^{-1}$. From the graph, it was noticed that the flexural strength of ice berg samples increased when the temperature is decreased. This is usually the case for the flexural strength of all types of ice. Only test performed at a different strain rate at $10^{-5}s^{-1}$, which showed that the flexural strength changed significantly corresponding to the variation in strain rate. This confirmed the fact that the flexural strength is strain dependant.

Figure **27** shows the plot of flexural strength against bubble density. It was seen that the flexural strength of ice berg increased with the increase in air bubble density. This result led the concerned researchers to conclude that the ice bergs with numerous air bubbles possess considerable flexural strength (R.E Gagnon 1983).

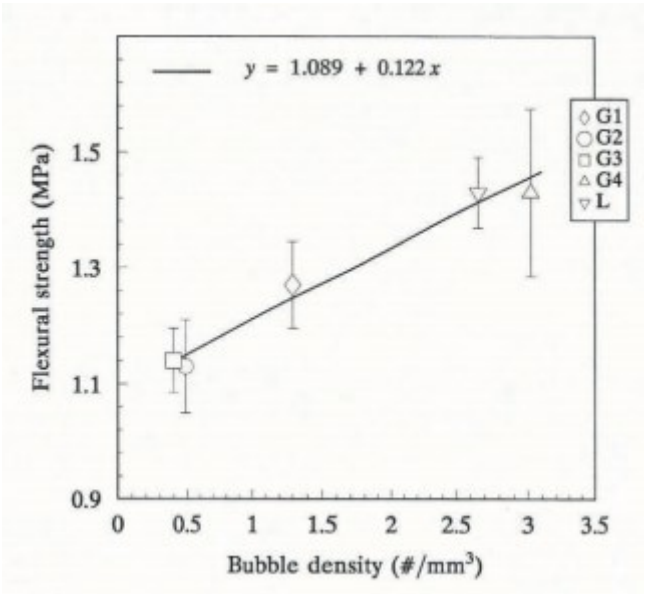

Figure 27 Flexural strength curve of ice bergs plotted against bubble density (R.E Gagnon 1983)

The study of the fracture properties of ice occupies a paramount importance in order to precisely predict the failure process of ice. However, till now there are no reliable experiments that had been conducted to evaluate the fracture toughness of ice berg due to the complexity involved. It is hypothesised that the ice berg internal structure corresponds to the granular sea ice. There are many literatures that present the fracture toughness of granular sea ice based on valid experiments. In this report, the fracture toughness values of granular freshwater and sea ice have been presented based on an assumption that they could be the same for ice bergs too. Usually laboratory fracture tests on ice are performed using four point loading apparatus. The results of that are shown in Figure **28** It can be seen that the granular sea ice possess higher fracture toughness in their deeper regions. So it can be inferred that the low fracture toughness of the upper part of the ice samples can be due to the presence of snow. More importantly, the low fracture toughness can also be attributed to the melting of ice samples in laboratory, so there is significant uncertainty associated with this experiment. (Garry Timco 1983)

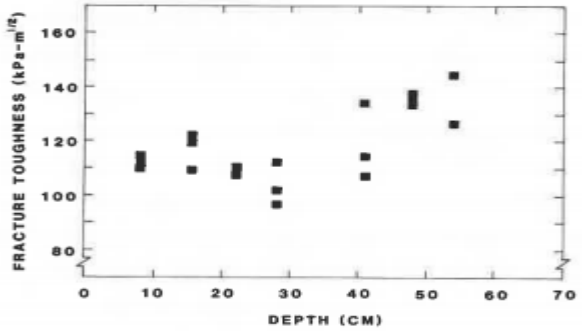

Figure 28 Fracture toughness of granular sea ice plotted as a function of depth (Garry Timco 1983)

Usually, the ice properties can be measured either in site or in laboratory. However, the sea ice exhibits long term variations, it would be really expensive to perform these experiments during different seasons. Moreover, there are some uncertainties associated with laboratory measurements like melting of sample, laboratory environment failing to replicate the full environment etc. So, C. Horvat & E.Tziperman(2015) developed a prognostic model for the sea-ice floe size and thick ness distribution. (C.Horvat 2015)

In this literature review, the main objective of describing the values of physical properties and mechanical properties of ice bergs based on the experiments by R.E Gagnon & P.H Gammon(1983) is to show the typical values of ice berg properties and how the measurements should be conducted. These values may represent only the ice bergs found in Labrador region and Greenland and in no way can be taken as representatives for all the ice bergs found in this world. This due to the fact that properties of ice bergs vary greatly with respect to the location. For example, the icebergs found in Antarctic region might possess different properties than the ones found in Arctic region. In addition, the ice bergs with different size and shape belonging to the same region may exhibit varying properties. Therefore, for design purpose, insitu or laboratory tests should be performed on ice bergs in the concerned area or statistical distributions involving data from manifold experiments must be used.

There are many varieties of ice bergs that exist throughout the world. These ice bergs vary in size, shape and texture. There are various classifications of ice bergs in terms of size and in addition also presents the characteristics of those ice bergs like their length, height above the sea surface and weight. For the design of ships and offshore structures subjected to ice berg impacts, only few ice berg and ice floe shapes that are commonly found in most places are

considered.

In this section, a brief discussion on few such ice bergs and ice floes along with the pictorial representation of their shapes have been carried out. As already mentioned, ice bergs can be classified according to shapes and size. Here, the ice berg varieties are discussed according to their shape, and some of these shapes have been considered for the numerical simulation

4.1.3 Shapes and Size of Ice Bergs and ice floes

According to size, the ice bergs are most commonly classified into growlers, bergy pits, Small, medium, large and very large ice bergs. The approximate dimensions of each of the above ice bergs are listed in Table **8.**

Ice features	Height (m)	Length (m)
Growler	< 1	< 5
Bergy Pit	1-5	5-15
Small ice bergs	5-15	15-60
Medium ice bergs	16-45	61-120
Large ice bergs	46-75	121-200
Very large ice bergs	>75	>200
Ice Floe	Varies	2m – 5 km (wide)

Table 8 Spatial dimensions of commonly found ice features (D.Diemand 2001)

4.1.3.1 Classification according to shapes

The characteristic features of each of the ice bergs are described in short and in addition their pictures are presented in Figure **29 (a,b,c,d,e,f)**

- **Tabular-** These type of bergs are rectangular in shape with a flat top and steep sides. The length:height must be greater than 5:1
- **Wedge-** These are triangular in shape with one side sloping gradually the hypotenuse of a triangle and the other side sloping steeply.
- **Drydock-** Drydocks have two massive peaks of ice separated by water filled channel.
- **Pinnacle-** These ice bergs do possess sharp peaks like a crown.
- **Dome**- Dome ice bergs have a spherical top. (D.Diemand 2001)
- **Ice Floes**- Ice floes exist in variety of sizes, their size ranges can be seen in Table **8.** 2 m wide smallest ice floe can be found in Montagu Island area, Weddel sea, South hemisphere. whereas the largest ice floes of almost 5km wide can be found in Kara sea, North hemisphere. (Marco Gherardi 2015). In this thesis, multi-year ice floes are taken into consideration. Multi-year ice features belong to the category of ice which has survived one summer. Multi-year ice features might have subjected to extreme freezing, as a result, most of their brine content might have got ejected from it, so they behave mostly like freshwater ice. (Tukhuri, Ice Mechanics-Occurence of Ice 2016) Based on these considerations, the same ice properties which are used for ice bergs in the numerical simulations also have been used for multi-year ice floes.

(a) Tabular

(b) Wedge

(c) Drydock

(d) Pinnacle

(e) Dome

(f) Ice Floes

Figure 29 (a,b,c,d,e,f) Ice features that are commonly found (D.Diemand 2001) (Patrick 2015)

4.2 MATERIAL MODELS USED TO SIMULATE THE CRUSHING OF ICE

Ice is strong in compression and weak in tension, so crushing of ice contributes extreme local pressure loads on the structure, thus studying the failure pattern of ice due to crushing is highly important to quantify the loads. Ice material exhibits variety of behaviours ranging from ductile to brittle. Figure **30** clearly shows the ductile and brittle transition of ice as a function of the strain rate. There are different material models in existence for modelling the crushing of ice. However, the choice of an apt model for a problem depends on the size of ice, its properties loading conditions etc. Some of the approaches that are generally used for ice modelling are listed discussed briefly in this section. In addition, more informative details regarding the user defined material model has been coded into LS DYNA for ice berg modelling.

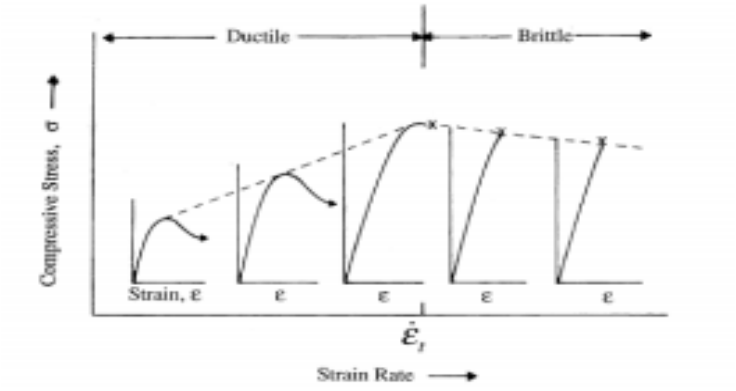

Figure 30 Ductile and brittle transition range of compressive strength of ice as a function of strain rate (Liu 2011)

4.2.1 Derradji-Aouat yield surface

A yield envelope for the ice berg had been put forward by Derradji-Aouat. It was represented in the form of an elliptical equation as

$$\left(\frac{\tau-\eta}{q_{max}}\right)^2+\left(\frac{P-\lambda}{P_c}\right)^2=1 \quad (26)$$

The terms τ is the octahedral stress, P is the hydrostatic pressure and $\eta, q_{max}, \lambda, P_c$ are constants. If $\eta = 0$ is substituted in the Derradji-Aouat condition, it will be similar to the Tsai-Wu yield condition.

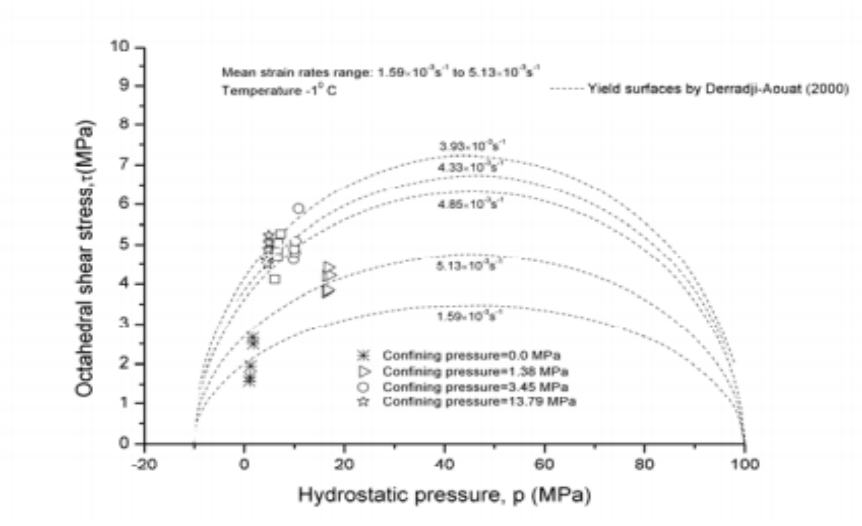

Figure 31 shows the yield surface of a Derradji-Aouat (Liu 2011)

Figure **31** shows the plot of octahedral shear stress as a function of hydrostatic pressure. The curves in the plot represents the yield surface of ice berg at temperature -1°C. (Liu 2011)

4.2.2 Tsai-wu yield surface

The Tsai-Wu yield surface for isotropic materials is formulated by

$$f(p,q) = q - \sqrt{a_0 + a_1 p + a_2 p^2} \tag{26}$$

Here, p is the hydrostatic pressure, q is the deviatoric stress and a_0, a_1, a_2 are constants taken from the tri-axial experiments conducted on polycrystalline ice under tri-axial stress state. The yield surface will be a function of p and q. For convenience, the deviatoric stress q is replaced by the second invariant of deviatoric stress J_2 while modelling the ice behaviour using tsai-Wu condition. (Liu 2011)

4.2.3 Mohr-coulomb criterion

After damage, the ice material shows some residual strength in a similar way like concrete, rock etc. This behaviour can be attributed to the existence of intergranular friction. A simple model that can represent this mechanism in ice is the Mohr-Coulomb criterion, in which the residual flow stress are considered as a linear function of pressure. It is given by

$$|\boldsymbol{\sigma}| = \boldsymbol{\sigma_f}(\boldsymbol{\sigma}, \boldsymbol{q}, \dot{\boldsymbol{\epsilon}}) + \boldsymbol{\mu}\mathbf{max}(\boldsymbol{P}, \mathbf{0}) \tag{27}$$

Where $|\sigma|$ is some norm of the stress, μ is the coefficient of friction and q is a vector representing the equivalent plastic strain. Schulson (2001) presented the reports showing that the ratio of confined to unconfined biaxial stress estimated using this criterion matched well will with the experiments. (Kelly S. Carney 2006)

4.2.4 Isotropic elastic-plastic material model

For modelling high velocity impact of ice using DYNA 3D, a simple isotropic elastic-plastic material model with failure is used. In this material model, the Jaumann stress rate σ^J has been used to handle large rotations which is given by

$$\sigma^J = \dot{\sigma} - \sigma\omega - \omega\sigma \tag{28}$$

Where $\dot{\sigma}$ is the material stress rate, and ω is the spin. In this modelling, the stress is represented in terms of two components – deviatoric and a pressure component. The final yield stress $\bar{\sigma}$ can be formulated assuming the J_2 flow rule theory and is written as

$$\bar{\boldsymbol{\sigma}} = \boldsymbol{\sigma_y} + \boldsymbol{h\bar{\varepsilon}^p} \quad (29)$$

Where, σ_y is the initial yield stress, $\bar{\varepsilon}^p$ is the plastic strain and h is the plastic hardening parameter.

Then through solving the pressure component, pressure in ice can be derived and is given as

$$P = K\left(\frac{\rho}{\rho_0} - 1\right) \quad (30)$$

K is the bulk modulus, ρ is the density and ρ_0 is the initial density. The failure model sets the deviatoric stress equal to zero and limits the pressure to be positive after $P < P_{fail}$, where P_{fail} is a material parameter. (Kelly S. Carney 2006)

This model, as of now, is used only in the aerospace industry for high velocity impact simulation. There are some uncertainties associated in it, like the yield stress is not a function of the strain rate or pressure and the hardening modulus is fixed randomly to match the test data.

4.2.5 Other Material models

kim et al.(2006) proposed that the ice can be modelled as a simple linear elastic-perfectly plastic material.

The works by Pralong et al.(2006) and Xiao & Jordan (1996) involved studying the ice behaviour by modelling the ice as visco-elastic material in combination with principles of damage mechanics. Similarly, Singh & Jordan(1999), modelled the ice as visco-elastic material and studied the ice crushing behaviour by considering the damage and porosity as state variables. It is said that the visco-elastic damage mechanics captures the actual ice crushing behaviour. (Storheim 2016)

4.3 USER DEFINED MATERIAL MODEL FOR ICE BERGS IN LSDYNA

Naturally, the ice berg is isotropic and well confined, the hydrostatic pressure governs the failure process to a large extent. The experiments conducted by Gammon(1995) also proved that the hydrostatic pressure plays a vital part in icebergs during the impact. In addition, the effect of friction in combination with hydrostatic pressure paves way for two most common failure mechanisms of ice under compression. They are coulombic faults and plastic faults. Coulombic faults appear due to shear forces at low confinement pressures, as a result, the ice elements will get eroded as soon as the shear forces acting on them reach a certain limit value. On the other hand, the plastic faults occur under relatively high confinement pressures, resulting in stiff behaviour of ice. (Liu 2011)

4.3.1 Liu's Ice model

From the above arguments, it can be said that the failure behaviour of natural ice bergs are highly dependent on hydrostatic pressure, so Liu brought forward a model that could replicate such behaviour. The ice model proposed by Liu(2011) is purely based on Tsai-Wu yield surface condition given in section **4.2.2.** This Liu's(2011) model constitutes an elliptical yield surface

which depends on pressure and a strain based failure criterion. The elliptical yield surface is dependent on stress components like the hydrostatic pressure (p) and the second invariant (J2) of the deviatoric stress component(q). The Yield surface is computed using the quadratic equation given below.

$$\boldsymbol{f(p,J_2) = J_2 - a_0 - a_1 p - a_2 p^2} \quad (31)$$

The Strain based failure criterion is based on the strain components. This model is an elastic perfectly plastic model and includes both the elastic(ε^{el}) and plastic(ε^{pl}) strain components. The plastic strain components are determined using a cutting plane algorithm which is given below inside the box no.2 of flow chart shown in figure **32**.

The 3rd box of the flow chart explains the erosion criteria followed in this model. The equivalent plastic strain is computed using the equation **33.**

$$\varepsilon^{pl}_{eq,j+1} = \varepsilon^{pl}_{eq} + \sqrt{\frac{2}{3}\Delta e^{pl}_{j+1} : \Delta e^{pl}_{j+1}} \quad (32)$$

and the failure strain proposed by Liu is given the equation **34.**

$$\varepsilon_f = \varepsilon_0 + \left(\frac{p}{p_2} - 0.5\right)^2 \quad (33)$$

Where ε_0 is the initial strain, p_2 is the largest root of the quadratic equation **32.**

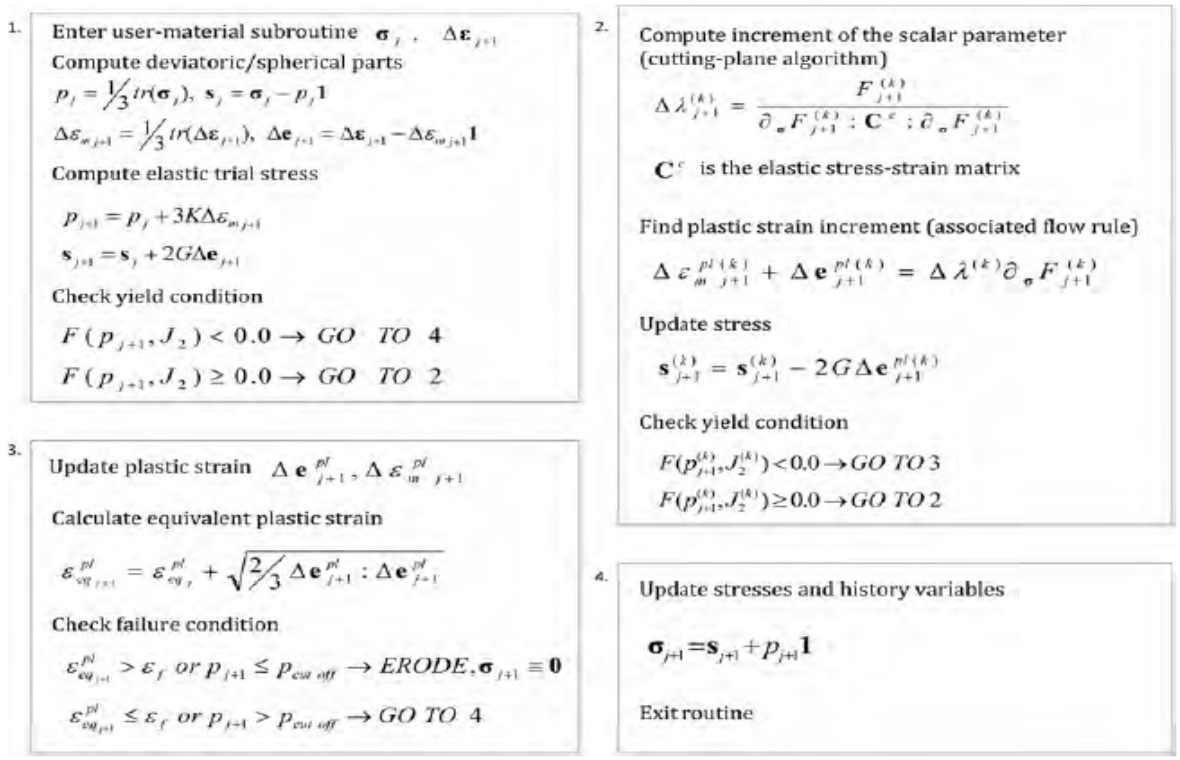

Figure 32 Flowchart showing the user defined algorithms for ice material model (Kim 2014)

It follows that if the plastic strain exceeds the failure strain of the material or if the hydrostatic pressure component falls below the tensile pressure cut off, the erosion occurs. In numerical simulations, the erosion of elements should be taken in the sense that the ice elements after

satisfying the failure criterion specified above will get deleted from the simulation. Through this way, the failure of ice is simulated according to Liu's model. It should be noted that, in nature, during ice-structure interaction scenario, the failure of ice is predominantly governed by fracture mechanics process, as different variety of cracks are formed and propagated throughout the ice when the ice is crushed. However, in this model, appearance and propagation of fractures cannot be simulated but the load effects due to fracture have been captured using erosion condition.

4.3.2 Kim's Ice model

The failure strain equation given forth by Liu(2011) incorporates only one parameter (ε_0), as a result it could not capture the complex failure pattern of the ice bergs and the Liu's equation is simple. So Kim(2014) introduced a general form of the above failure strain equation into the user material subroutine. The equation is shown below.

$$\varepsilon_f = \varepsilon_0 + \left(\frac{p}{M.p_2} - \frac{N}{M}\right)^2 \tag{34}$$

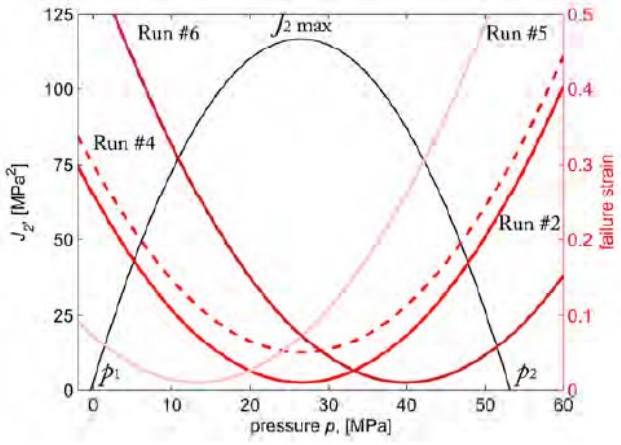

Figure 33 shows the shape of the failure curve of Kim's Ice model (Kim 2014)

Where M and N are the dimensionless parameters. The parameters M and N play a governing role on the behavior of failure strain of ice with respect to the pressure. (Kim 2014). Figure **33** presents the typical shape of the failure curves of this ice model. The curves are dependant on J_2 (second invariant of deviatoric stress component) and p (pressure). Kim's model can be regarded as further extension of the failure strain equation of Liu's(2011) model. The most important benefit of using kim's generalized failure strain equation is that ice of different strengths can be modelled by varying the dimensionless parameter N, which determines the failure strain of ice. In this thesis, all the simulations are carried out using kim's(2014) ice model.

4.4 SMOOTHED PARTICLE HYDRODYNAMICS

The movement of fluid particles in space can be represented by a method called Smoothed Particle hydrodynamics (SPH). SPH is popularly called as the particle method, is based on lagrangian formulation, in which the movement of particles at any time instant can be studied. Once the particle movements are known, it can then be used to represent the movement of fluid. This is the core idea underlying the SPH method (M.B. Liu 2009)

One of the unique features of SPH is that it does not use any mesh or grids and involves only particles. Owing to this feature, even objects that are not continuum (ice) can be modelled using it. The procedure for formulating the SPH can be the performed in two steps, they are discussed below.

4.3.1 Kernel Approximation

The concerned field variables like velocity etc in the governing PDE of fluid flow are continuous in nature. In the first step, initially, the continuous function and its derivatives are represented in an integral form. Secondly, these continuous functions are approximated using kernel smoothing functions or weight functions. So, the first step is also termed as kernel approximation. This concept is elaborately explained below

Let us consider that x be the positive vector and $f(x)$ be the continuous function, their integral representation is given by the following form

$$\boldsymbol{f(x) = \int_{\Omega} f(x')\delta(x - x')dx'} \quad (35)$$

Where Ω is the integral and $\delta(x - x')dx'$ is the dirac delta function. This dirac delta function signifies the continuity of the system, as a result the continuous integral cannot be discretized. In order to discretize the integral, the dirac delta function is replaced by a kernel function $(x - x', h)$. Now the continuous integral represented using kernel integrals can be written as

$$\boldsymbol{f(x) = \int_{\Omega} f(x')W(x - x', h)dx'} \quad (36)$$

Here h is the smoothing length.(The discretization will be performed in the particle approximation method). Figure **34** shows the support domain which is located inside the particle domain,

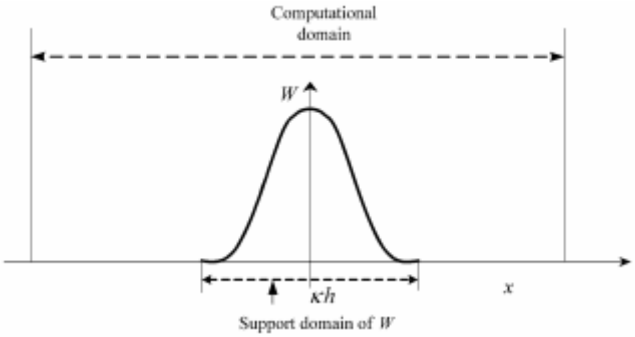

Figure 34 Support domain (M.B. Liu 2009)

In addition, the smoothing function defined here has to satisfy the normalized condition, delta function property and compact condition in order to be able to apply it in the integral. After satisfying these criteria, it is found that the approximation of the integral by kernel function has second order accuracy. (M.B. Liu 2009)

4.3.2 Particle Approximation

The second step in SPH is the particle approximation, in which the discrete particles are spread over the domain and the field variables are measured in each particle. The particles can be distributed in two ways, either as the centred particles or as the concentrated particles. After spreading the particles throughout the computational domain, the continuous function given in in equation **37** is now discretized and represented as

$$f(x) = \sum_{j=1}^{N} \frac{m_j}{\rho_j} f(x_j) W(x - x_j, h) \quad (37)$$

Where N is the total number of particles considered within the influential area of the particle at x. From equation **38,** the value of a function at a particle can be evaluated by taking the summation of the values of functions at all the particles within the support domain (effective area of the smoothing function at x) weighted by the smoothing function. This is the particle approximation of a function.

Similarly, the particle approximation of a derivative is carried out in the following way. The discretized form of the continuous derivative is given

$$(\nabla . f(x)) = \sum_{j=1}^{N} \frac{m_j}{\rho_j} f(x_j) \nabla W(x - x_j, h) \quad (38)$$

From equation **39,** the value of the gradient of the function at a particle is estimated by taking summation of gradient values of the functions at all the particles within the support domain weighted by the gradient of the support domain. In short, the particle approximation discretizes the continuous integral of the functions and its derivatives.

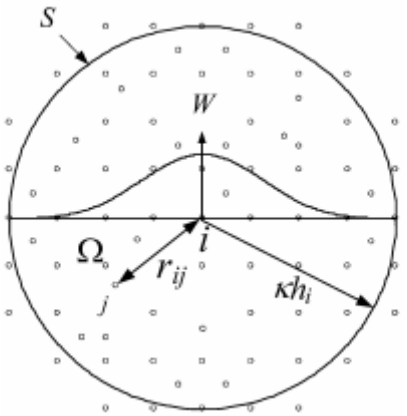

Figure 35 Particle approximation in a two dimensional problem domain (M.B. Liu 2009)

SPH methods can be applied to problems in solid and fluid dynamics. In certain cases, the particle approximation can lead to some unstable problems. This can be accounted for by considering more number of integration points than the actual number of particles within the concerned support domain. (M.B. Liu 2009)

4.5 THEORIES OF TEMPORAL AND SPATIAL DISTRIBUTION OF RANDOM CONTACT PRESSURE

The force transmitted to the structure owing to the contact between ice and structure can be represented using a pressure-area diagram. There exist several such diagrams based on the model scale and full scale experiments. The analytical expressions derived from these P-A curves can be used to perform design calculations. The pressure distribution on a structure when it comes in contact with ice can be of two types, spatial and temporal pressure distribution.

4.5.1 Pressure – Area Relationship

Spatial pressure distribution presents the pressure variation at the contact point at one instant in time. As already mentioned in section **1.4.2**, pressure in local contact area varies with respect to the velocity of impact. Figure **36** shows the peak pressure and average pressure distribution at the local contact area as well as the spatial pressure area plot. From Figure **36,** it can be seen that the higher pressure (P_1) acts on the smaller contact area whereas the average pressure (P_{avg}) acts over progressively larger area. As a result, the spatial pressure-area curve will always display an inverse relation between the pressure and area, the relationship is given by

$$\boldsymbol{P = CA^{-e}} \tag{39}$$

Where C represents the average pressure per unit area and has a range of 0.5 to 5 Mpa, and e is in the range of 0.25 to 0.7. (Daley, A study of the Process-Spatial link in Ice Pressure-Area Relationships 2004)

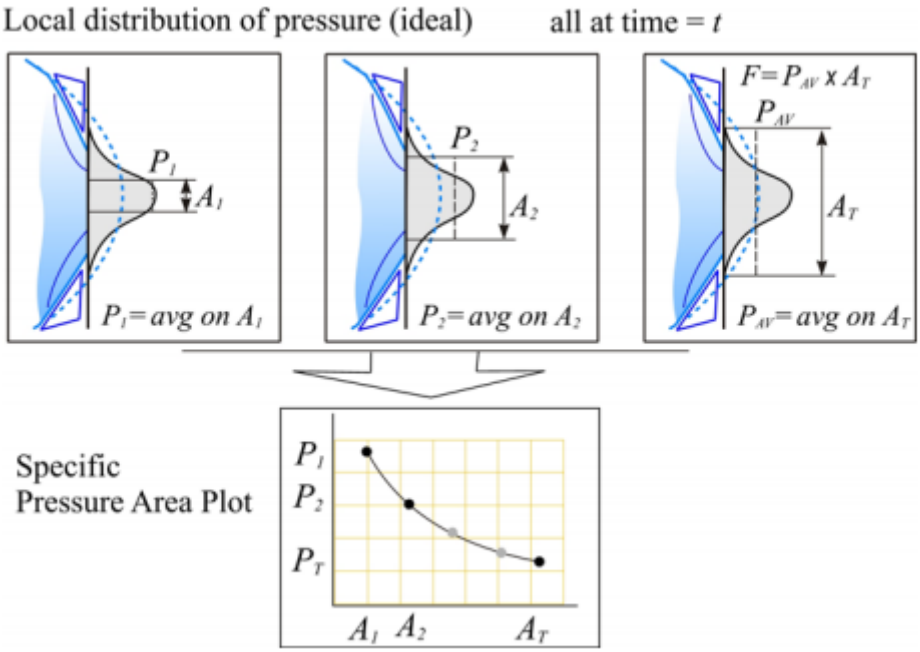

Figure 36 Spatial Pressure Area curves (Daley, A study of the Process-Spatial link in Ice Pressure-Area Relationships 2004)

The above equation gives a good initial estimate of the pressure distribution. However, fine spatial resolution of pressure distribution is hard to derive from this. To account of this, the general pressure is further refined into three types namely, nominal pressure, true pressure and measured pressure. Figure **37** illustrates pictorially how these pressures can be derived. First picture in Figure **37** corresponds to the nominal pressure which is the force divided by the nominal contact area. Though nominal pressure is a useful value, it cannot be used to estimate local pressure distribution. The middle picture shows the true pressure distribution which can be yielded by dividing the force with true area. This gives a high resolution spatial pressure distribution, but this an ideal case and is practically non existent. Third picture shows the measured pressures which is estimated with the help of pressure panels. This pressure is

measured on a coarse array, and it is the case that is quite often encountered in real scenario. Due to coarseness, there could be noise and some forms of errors present in the measured pressure signal. In order to account for these uncertainties, there are some pressure and aerial resolution limits that have to be considered. (Daley, A study of the Process-Spatial link in Ice Pressure-Area Relationships 2004)

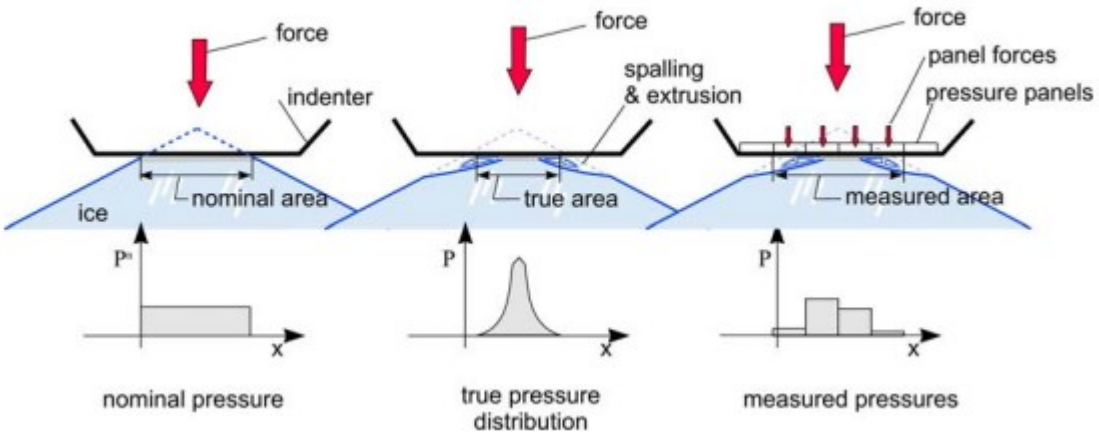

Figure 37 illustrates the procedure for detarmining the nominal, true and measured pressures and the respective pressure distribution plots (Daley, A study of the Process-Spatial link in Ice Pressure-Area Relationships 2004)

4.5.2 Process pressure distribution

In process/temporal pressure distribution, the average pressures are evaluated across the entire contact surface. The pressures are estimated using the pressure panels, and the process pressures are the average pressures over all the measured sensors. The force is calculated by multiplying the average pressure with total area. Figure **38** depicts the pressure distribution at different time intervals and s corresponding pressure-area plot is shown as well. From the Figure **38**, it can be seen that the process pressure distribution resembles the nominal pressure distribution.

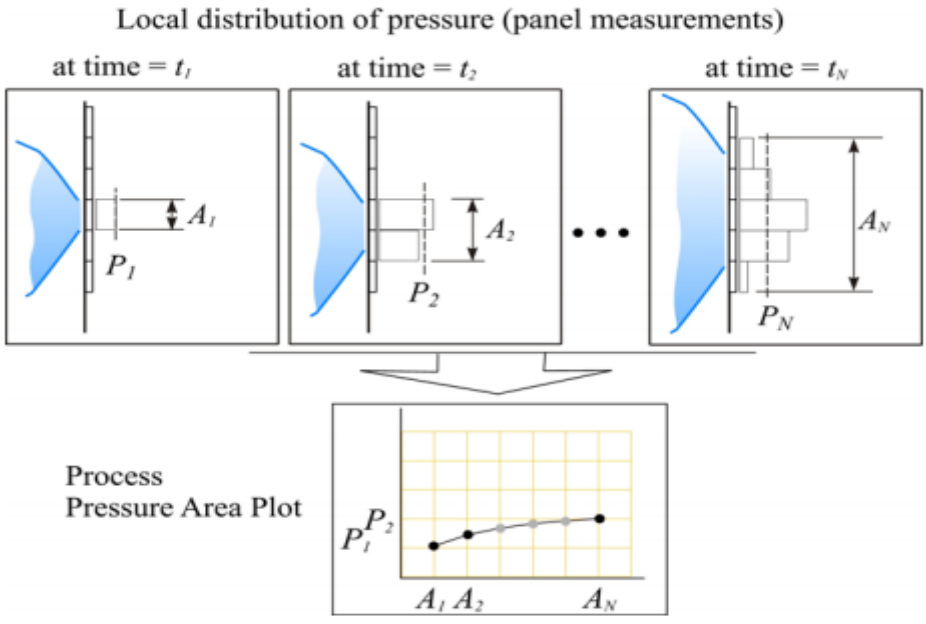

Figure 38 shows the process Pressure-Area Plots (Daley, A study of the Process-Spatial link in Ice Pressure-Area

Relationships 2004)

The difference between the spatial pressure and process pressure is that the spatial pressure presents the variation of local pressures across the contact area at different time instances. On the other hand, the process pressure is the averaged pressure of all the local pressures acting at different time instances. Most of the practical pressure measurements like the pressure exerted by ice on ship's side are carried out according to process/temporal measurement techniques by fitting pressure sensors to the side structure. As of now, the process pressures are widely for design purpose since these involves less computations, whereas the spatial pressures are more complicated to measure and in addition it involves huge computation. (Daley, A study of the Process-Spatial link in Ice Pressure-Area Relationships 2004)

There exists different pressure area relationship. Some of them are ISO P-A curves, Croasdale's P-A curves, Terry Fox curves (ice impact tests conducted on CCGS Terry Fox ice breaker) which are purely semi-empirical and obtained from experiments.

CHAPTER 5

5.1 SHAPES OF ICE FEATURES SELECTED FOR SIMULATION

In this section, numerical modelling of ice features is presented along with the modelling assumptions. As can be seen in section **4.1.3**, ice features exist in different sizes, shapes and characteristics. In addition, the shape and characteristics of a single ice berg are not uniform throughout its cross section. As far as numerical simulations are concerned, it is not possible to replicate the exact geometry and size of actual ice features. As a result, certain simplifications are introduced like maintaining a uniform surface without any irregular undulations so as to have better mesh quality and modelling only a part of the ice along with assigning the rest of the ice mass to an ice pusher attached at its end thereby increasing the computational efficiency. However, care should be taken to ensure that these modelled ice features behave more or less in the same way as original features. These cases are discussed in detail below.

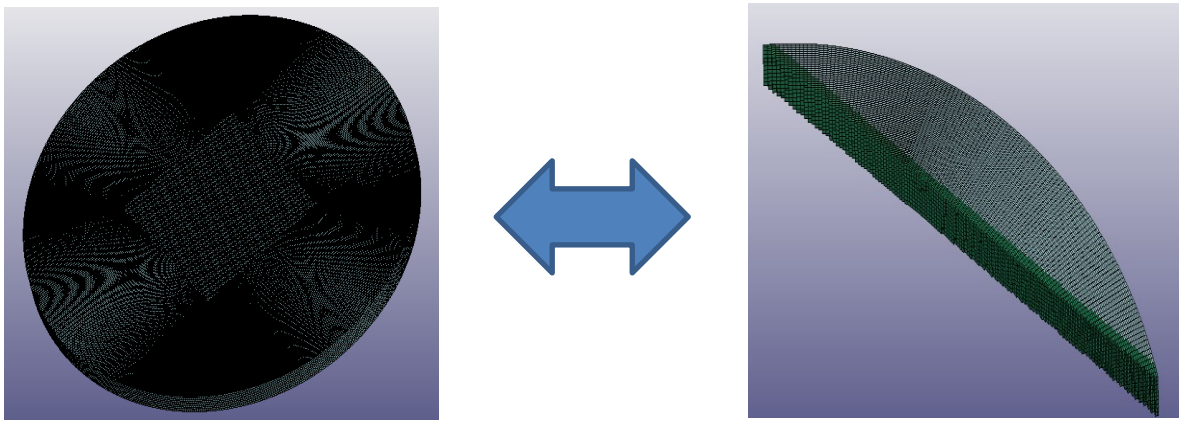

(a) Cylindrical Ice Floe

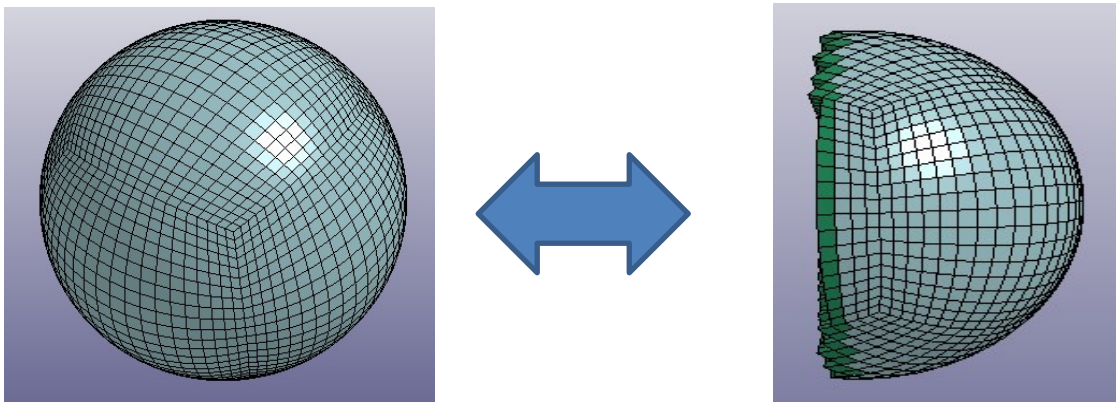

(b) Ice Growler

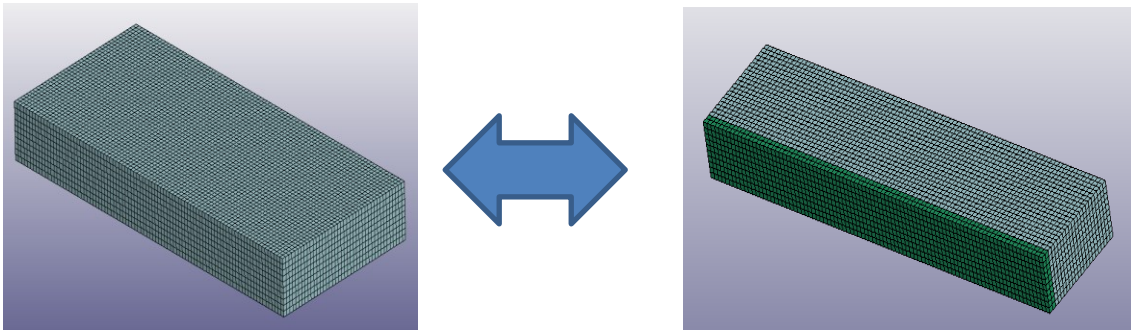

(c) Tabular Bergy Pit

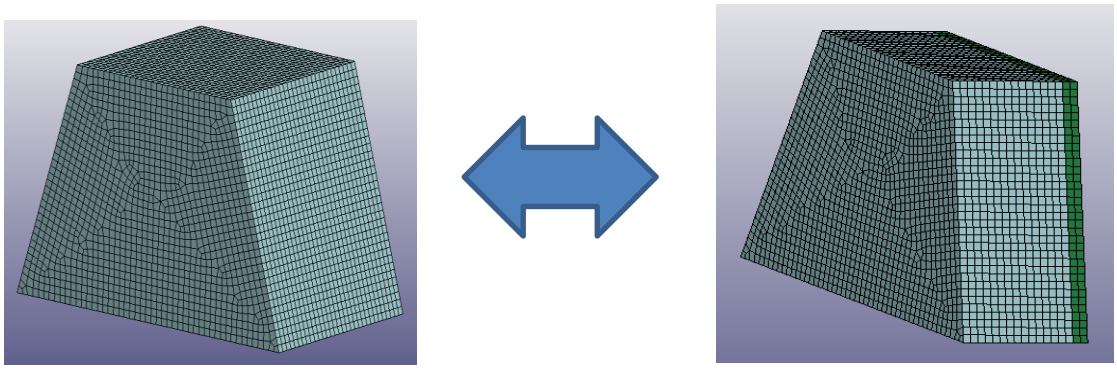

(d) Ice Blocky

Figure 39 (a,b,c,d) displays the numerical modelling of differect ice features on the left side and numerically equivalent minimized version of each ice feature are shown on the right side

Figure **39** shows different ice features that can be considred for the numerical simulations. In these models, the simplifications stated above are introduced. Figure **39 a** shows the image of an ice floe, this represents 20 m dia large ice floe, the model is cut 2 m from the outer edge and the rest of the mass is assigned to the ice pusher. The ice pusher can be modelled as a rigid material but the same physical properties should be assigned to both the ice and the pusher section. Figure **39 b** shows the 2m dia spherical growler, due to its symmetry, half of the growler is modelled as ice and the other half considered in the simulations in the form of ice pusher. Figure **39 c** depicts the tabular bergy pit. It has spatial dimensions of 4 m length, 9 m wide and 1m depth. Similar to the other models, half of the bergy pit is modelled as ice and an ice pusher which represents the other half. Figure **39 d** depicts the ice blocky of height 4m, top width 3m and bottom width 4m, it minimized version is shown on the right wherein one half is modelled as ice along with an ice pusher to represent the remaining mass.

5.1.1 Numerical ice modelling with respect to Coupled and Decoupled approach

Numerical simulation of ice collisions against ship structures can be carried out either by decoupled or coupled approach. In decoupled approach, the external dynamics and internal mechanics are evaluated separately. Furthermore, the internal mechanics analysis is carried out by pushing the ice against the structure at constant velocity. Thus, in this approach the kinetic energy remains constant throughout the simulation and is not physical, so the simulation gives the same results either when huge mass is assigned to the ice pusher or not. In other words, the ice pusher can be imparted either with huge mass or its default mass (mass based on its volume and ice density) for decoupled approach.

However, in the coupled simulations, the ice is pushed against the structure with an initial velocity and the velocity changes after the impact, so is its kinetic energy. Therefore, the kinetic energy obtained from the coupled simulations is physical. Thus, it is important to specify huge mass to the ice pusher. For example, for the case of 20 m dia ice floe, if its initial 2 m is modelled as ice, the rest of the mass of the ice that is not modelled should be assigned to the ice pusher. In this thesis, simulations based on both coupled and decoupled approaches have been performed, so in order to maintain uniformity, mass of the remaining ice feature that is not modelled is assigned to the ice pusher. This consideration does not affect the results of decoupled approach, since in decoupled case mass and subsequent kinetic energy is not important.

5.2 RIGID PLATE – ICE GROWLER COLLISION ANALYSIS

5.2.1 Modelling

Modelling of rigid Wall:

The rigid wall spans 2.5m in Y direction and 2.5m in Z direction. 4 Node shell elements were used to model the rigid wall. Thin shell elements were used to decrease the computational time. **Figure 40 a** shows the sketch of the rigid wall along with the dimensions and **b** displays the actual steel plate used for the simulations.

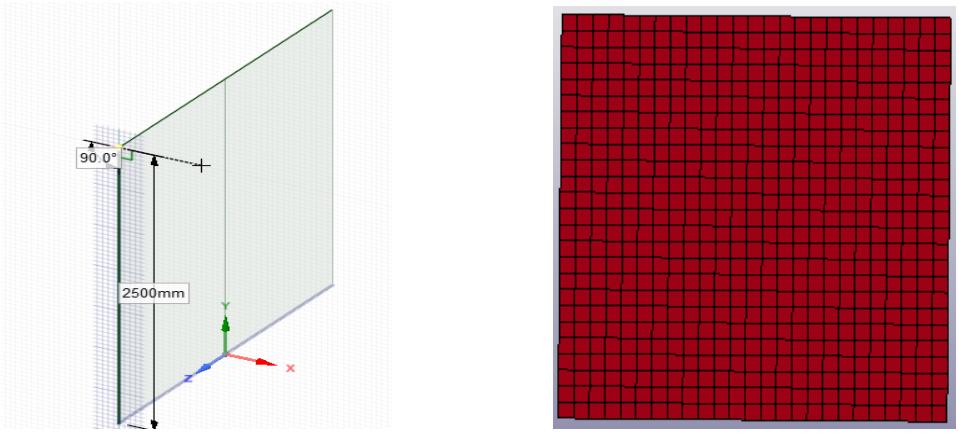

Figure 40 (a) sketch of the rigid wall and (b) Rigid wall model used in the colliison analysis

Modelling of ice:

Figure **41 a&b** shows the sketch of the ice growler and the growler that was actually used in the simulations. From the table **8,** it has been inferred that growlers have sizes <1m in height and <5m in length. Considering these, for collisions against rigid wall, a small spherical growler of 1 m diameter has been modelled. With respect to numerical considerations, initial 0.55 m of the growler is modelled as ice, and an ice pusher at the back imparted with rest of the mass.

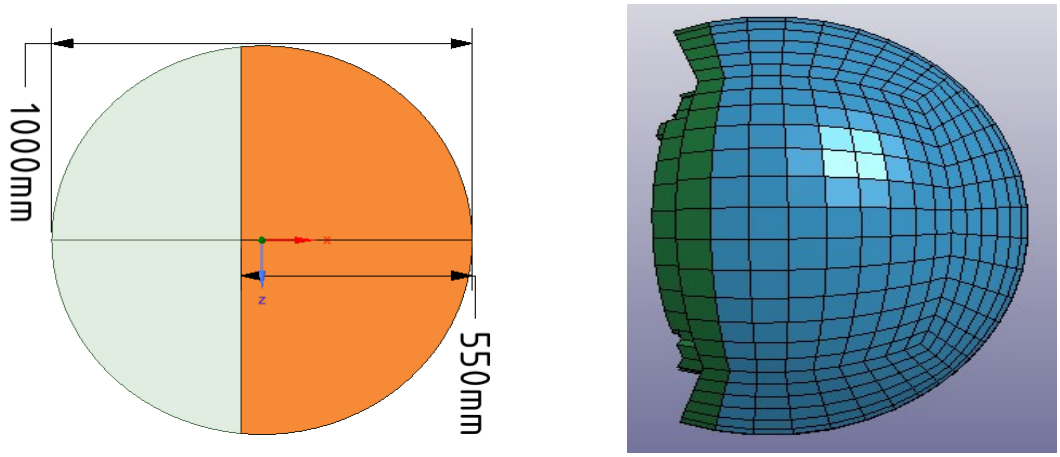

Figure 41 (a) sketch of the ice growler (b) ice model used in the crushing analysis in LS DYNA

In this collision analysis, two types of approaches were used for ice modelling. One is the finite element method (FEM). The FEM modelling of ice elements is based on the continuum approach, as per which the ice elements erodes after reaching the set failure criterion. The other technique is called FEM-SPH, finite element method coupled with smoothed particle hydrodynamics. The theory related to smoothed particle hydrodynamics(SPH) can be found in section **4.4.** According to FEM-SPH technique, the ice elements, after reaching the failure criterion will get converted to water like SPH particles. There are three subdivisions within FEM-SPH based on the number of SPH particles generated. Within FEM-SPH keyword, there is an option called NQ. Setting NQ=1 will generate 1 SPH particle after the failure of one ice element, NQ=2 generates 8 SPH particles whereas NQ=3 option produces 27 SPH particles when a single ice element erodes. All the above mentioned approaches were simulated and compared against each other and with the analytical curves as well.

5.2.1.1 Key Cards necessary for the collision analysis

In this section, the various keycards used in the analysis had been briefly explained. In LS DYNA, certain keycards were activated to input the physical parameters and the motions of the colliding objects. On the other hand, some keycards were activated just in order to achieve numerical stability in the simulation. So, in this section, the keycards necessary for the defining the motions and physical properties were grouped and explained firstly, and the keycards vital for imparting numerical stability were elaborated afterwards.

Boundary Conditions

For the case of ice crushing against rigid structure, the rigid wall had been constrained against movement and rotation in all direction. The rigid ice pusher was allowed to move freely only in X-direction and its movement and rotations in all other directions were prevented. Here, the ice pusher had been imparted with a constant velocity of 1 m/s. This was achieved using the keyword “PRESCRIBED_MOTION_RIGID” and in addition a load curve was generated and assigned to the PRESCRIBED_MOTION_RIGID keyword.

Contact

For the ice structure interaction, three contacts have been defined. The first one is the

ERODING_SINGLE_SURFACE- This contact is defined for ice alone. Since, in the collision process, the ice experiences considerable deformation and crushing, a self contact is mandatory, as a result this contact is used as a self contact for ice.

ERODING_SURFACE_TO_SURFACE: This contact is used to create the interaction between the ice and the structure. In this case, the ice is considered as slave part and the rigid wall as master part.

Furthermore, the static friction coefficient of ice is set as 0.15 for both of these contact keycards. And SOFT is set equal to 0 for Eroding Single Surface and 2 for Eroding Surface to Surface. SOFT option has a numerical significance which is detailed afterwards.

In addition to these keyword, an additional keycard named, "FORCE_TRANSDUCER_PENALTY" is activated. A transducer segment is created on the surface of the rigid structure, and assigned to this keyword. Through this way, the interface pressures on the surface of the rigid plate can be obtained.

Material Properties

Material properties of the interacting objects are defined under the MAT keyword.

The following keycards are used for the defining the material properties

MAT RIGID This keycard is widely used in strength design analysis. Using this keycard, a particular structure can be assigned with its natural properties and still it can be made rigid, for example the ice pusher is given ice properties but made rigid. In addition, this keycard consists of options which allows to introduce the necessary end conditions to the structure. (Livermore Software Technology Corporation 2011)

This analysis deals with the collision of ice against a rigid wall which is a strength design analysis. So the wall had been made rigid and assigned with the steel parameters. The ice pusher at the back of the ice was also made rigid and assigned with ice properties. Moreover, the end conditions were applied to these objects.

As already explained, the ice pusher can be modelled to resemble the huge ice mass behind the actual ice which is regarded as a convenience with respect to numerical simulations. Modelling of huge ice mass can be achieved by varying the density of the ice pusher or the mass can be increased directly by applying mass trimming option in LS DYNA. Both of the above options were tried in this thesis.

Properties	Steel	Ice Pusher
Density	7890 kg/m3	900kg/m3
Young's Modulus	210000 MPa	9500MPa
Poisson's Ratio	0.3	0.3

Table 9 Material properties of the rigid objects

MAT USER DEFINED (41) This keyword has been introduced by LS DYNA in order to facilitate the user to enter the material parameters of their choice. Kim coded her ice material subroutine under the MAT 41 section in the dyn21.f file. So, this keyword was used for ice modelling. Extensive details regarding the ice material model has already been put forth in section **4.3.** The ice properties entered as inputs is given below. (Bohlerengen 2013)

Density	900 kg/m3
Youngs Modulus	9500 MPa
Poisson ratio	0.3
Bulk Modulus	7916.6 Mpa
Shear modulus	3653.8 MPa
Initial Strain	0.01
Kierkegaard's ice constants	
a0	2.588 MPa^2
a1	8.63 MPa
a2	-0.163

Table 10 Material properties of the ice material model

Special Key Cards for FEM-SPH simulation

For FEM-SPH coupled simulation sin LS DYNA, in addition to the above mentioned keywords, the following additional keywords were also entered.

DEFINE_ADAPTIVE_SOLID_TO_SPH: FEM_SPH simulation mainly involves the conversion of solid elements to SPH particles which can be simulated using this keycard.

AUTOMATIC NODES TO SURFACE This keycard is used only for the FEM-SPH simulations in order to enable interaction between the generated SPH particles and the structure.

MAT_NULL: In FEM-SPH, the ice elements are converted to water like particles. The physical parameters of the SPH particles used were density=1350 kg/m3, pressure cut off = -1 MPa and dynamic viscosity coefficient, $\mu = 1 \times 10^{-3} Ns/m^2$

EOS_GRUNEISEN: The usage of water particles in LS DYNA requires an Equation of State, GRUNEISEN card was activated by entering the following parameters. c = 1489 m/s, $s_1 =$ 1.79 and $\gamma =$1.65

These parameters corresponding to MAT_NULL and EOS_GRUNEISEN were taken from Kim et al, 2014.

5.2.1.2 Considerations for achieving numerical stability

In this section, the parameters necessary for achieving the numerical stability in the system had been discussed. Even though these parameters did not contribute to any actual physical processes involved in the ice-structure interaction process, they turned out to be vital and governed the numerical stability of the system throughout the simulation.

SOFT option:

The SOFT option given in the contact card had been defined purely based on numerical reasons, in other words it contributed nothing to the physical behavior of ice during crushing but were crucial to achieve numerical stability during the ice-structure interaction. Three values given in the SOFT option were considered vital for the contact definition of ice and structure. SOFT = 0 was defined for the Eroding Singe Surface option, and either SOFT = 1 or 2 can be assigned for Eroding Surface to Surface contact as simulations were run using both options for Eroding Surface to Surface contact and both options yielded the same result. Even though, both of these options produced similar results, it is highly recommended to use **SOFT =2** for Eroding Surface to Surface contact between ice and structure, since it gave numerically better results in comparison with the SOFT = 1 option. Numerically better results in the sense, that SOFT=1 option produced negative volume errors in ice whereas SOFT = 2 option did not produce any such results.

However, SOFT = 1 option is recommended for AUTOMATIC_NODES_TO_SURFACE contact which was used for defining the contact between newly generated SPH particles and the structure. One important fact to be noted is the IGNORE option under the CONTROL-CONTACT card must be set to 1 while using the SOFT = 1, otherwise it would result in some inaccuracies.

ELFORM for Solids:

The element formulation for ice was assigned under SECTION_SOLID keycard. Element formulation (ELFORM) can be set either as 1 or 2. ELFORM=1 represents under integrated solid elements whereas ELFORM=2 represents fully integrated solid elements. Simulations were run using both options, and found that both produced the same results. The fully integrated solid elements(ELFORM=2) did not produce any hourglass modes (zero energy modes), however the fact that this option consumed more time than ELFORM=1. As a result, it has been concluded that the efficient formulation is to use ELFORM = 1 for ice along with hourglass control.

Hourglass Coefficients:

Hourglass type 4/5 can be chosen along with a hourglass coefficient of 0.1. In all the works carried out in this thesis, hourglass type 4 had been used as a measure for controlling hourglass. Hourglass parameters can be set in HOURGLASS keyword.

Mass Scaling:

In simulations based upon explicit time step procedure, the actual time step is governed by the smallest elements in the system. Thus, the simulation may run for longer time if the time step corresponding to the smallest element in the system is so small. Through mass scaling technique, a particular time step of the order of 10^-6 was specified and the mass of the smaller elements that require lesser time step was increased. However, it must be noted that the increased mass is purely numerical so it must be less than 5% of the actual physical mass. In LSDYNA, mass scaling was performed by specifying the time step in DT2MS.

5.2.2 Simulations

Crushing of an ice growler against a rigid structure after 0.15 seconds is shown in Figure **42.** The ice is crushed with a constant velocity of 1 m/s with prescribed displacement history. Figure **42 a** presents ice model constructed purely using Finite element method and it is based on Kim's technique. As already mentioned, kim's ice model is a revised version of Liu's model. Kim's model follows that ice elements which are subjected to considerable deformation will reach the failure criterion specified in Tsai-Wu yield surface. After satisfying the failure criterion, the ice elements are removed from the simulation. Figure **42 a** shows the crushing of ice against a rigid wall at 0.15 s, at this point of time, the initial 0.14 m of ice is crushed and the respective ice elements dis appeared from the numerical simulation.

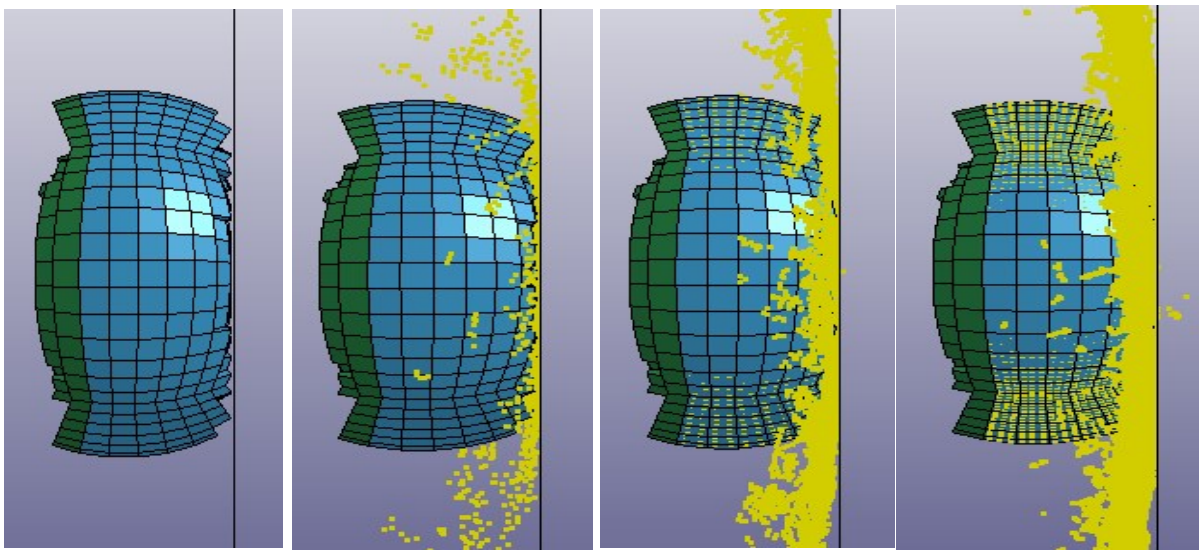

(a) FEM (b) FEM-SPH NQ1 (c) FEM-SPH NQ2 (d) FEM-SPH NQ3

Figure 42 (a.b,c,d) illustrates the crushing of ice growlers modelled using four methods

Kim developed a combined FEM-SPH approach in numerical ice modelling wherein the ice elements, after deforming to a critical limit set by the failure criterion, will get converted to SPH particles instead of getting removed from the simulation.

So, the same growler is also modelled using combined FEM-SPH approach and the simulation pictures are presented in Figure **42 b,c,d** and they correspond to FEM-SPH NQ1, NQ2, NQ3 respectively. Interestingly, in this case the ice elements have been converted to SPH particles instead of getting eroded. The number of SPH particles generated depends on the specified value of NQ.

5.2.3 Results and Discussions

5.2.3.1 Force-Deformation Curves

In this collision case, the spherical growler is driven against the rigid plate with a constant velocity of 1 m/s. Here, the curves in Figure **43** represent the force vs deformation relationship of ice only, as the structure is designed completely rigid. From the force vs time plot, the penetration depth of ice is computed from the simple formula (x=v*t). Initially, at the point of contact, force of almost 0.5 MN is recorded and then it gradually increases with the increase in the crushing distance.

It can be seen that the force increases more or less linearly with penetration depth, this trend can be attributed to the geometry of spherical growler in which larger part of the ice growler comes in contact with the rigid plate with respect to the amount of penetration. Along the crushing distance, the force curves exhibit rise and decrease of load levels (peaks and troughs), this is due to the crushing/erosion of ice elements. This behaviour can be compared with the real ice crushing scenario, as in natural scenarios there exists creep, micro cracks, radial cracks, circumferential cracks etc, that give rise to a load curve with peaks and troughs at regular intervals. In this model, exact fracturing of ice is not considered, but erosion technique is used to simulate the fracture effects. From this trend observed in the load plots, it can be supposed that this ice model represents the natural ice behaviour well. The magnitude of the force is dependent on the shape and size of the ice feature, level of confinement of ice, strength of ice and the structure. The more the ice elements crushed, the larger the forces transmitted to the structure. Velocity of ice plays an important part in coupled collision process, whereas in this case, the simulation has been performed based on decoupled approach so the ice velocity did not play a dominant role in the force levels.

In Figure **43**, four deformation curves from simulations are shown corresponding to FEM, FEM-SPH(NQ1), FEM-SPH(NQ2) and FEM-SPH(NQ3) ice models respectively. The lowest recorded forces belong to the FEM ice model. It can be noticed that FEM-SPH(NQ1) yields higher forces than FEM owing to the fact that the ice elements are replaced with SPH particles in the FEM-SPH technique instead of disappearing/eroding like in the case of FEM. These SPH particles further adds to the force levels. It is clearly evident that the FEM-SPH NQ1 ice growler model produced an average force of 0.48 MN which is around 2.4 times higher that of the average force (0.2 MN) from FEM ice model. Furthermore, the FEM-SPH NQ2 resulted in still more higher force levels, as 8 particles are generated after the failure of one ice element. Thus, the average force from FEM-SPH NQ2 is almost 0.79 MN. One strange behaviour noticed in the plots is the ice model based on FEM-SPH NQ2 and FEM-SPH NQ3 yielded more or less the same results. From logical point of view FEM-SPH NQ3 must produce higher force levels since 27 SPH particles are generated in place of erosion of one ice element, but the trend seen in this plot is illogical. The same simulation had been run twice, but ended up with the same results. So, here it is concluded that this could either be due to numerical errors and for the remaining simulations FEM-SPH NQ3 has not been used.

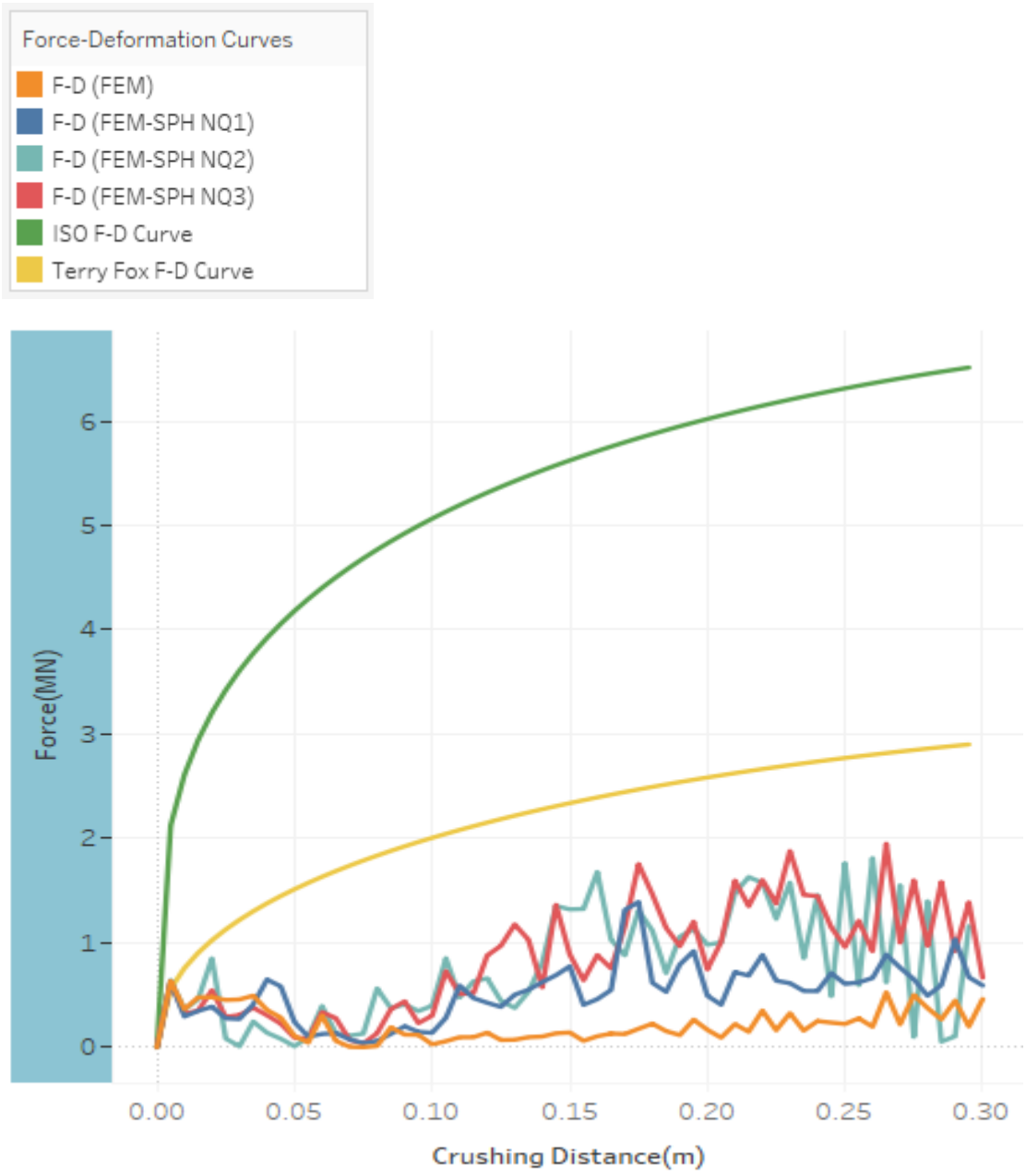

Figure 43 Force-Penetration curves of ice growler crushing against rigid wall

The simulation results are compared against the empirical curves and shown in the same plot. These empirical curves are actually based on P-A relationship and they are modified to represent the force-deformation relation. It can be inferred from the plot that the force levels from all the ice models fall below both the curves.

5.2.3.2 Process P-A Curves:

The process pressure area curve deals with the variation of pressure across the entire contact surface at all time instances in an ice-structure interaction.

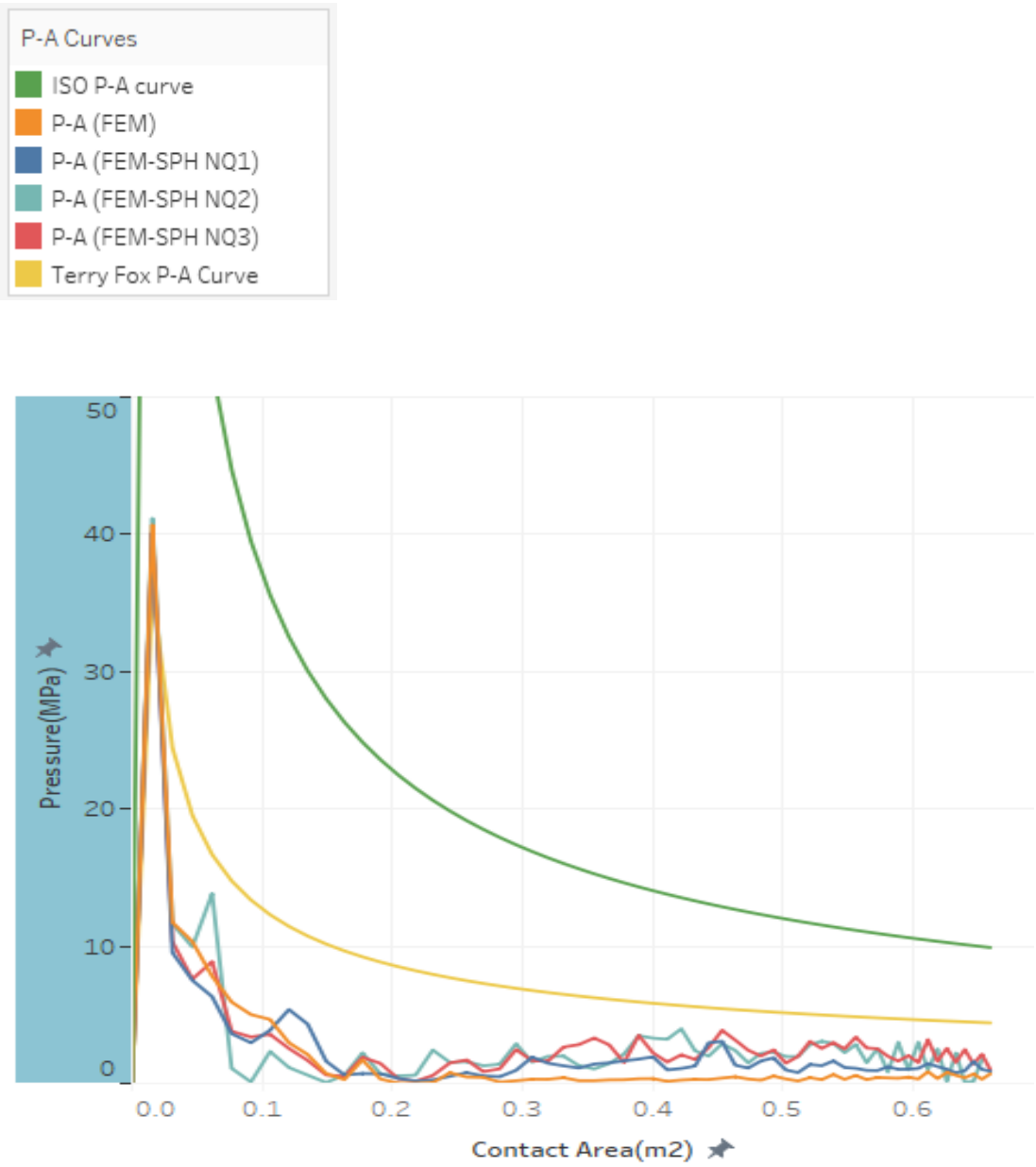

Figure 44 Process P-A curves for the rigid plate-ice growler interaction analysis

Figure **44** shows the process pressure area curves for the considered collision case. The Process P-A represents the average pressure over the entire contact surface. The contact surface is taken as the nominal contact area. The nominal contact area taken for spherical growlers is $x\pi(2r-x)$. As already mentioned, the ISO curves are based on local pressures so it can be considered as the empirical upper bound.

Since pressure and area has the following relation, P proportional to 1/root A, high pressures are initially recorded at the contact point and then the curve drops drastically. With the increase in the contact area the curve remains relatively constant in the domain of 1.5-2.5 MPa for all

the simulated cases, with FEM-SPH models having the higher limit. Appearance of relatively small peaks and troughs are visible in the P-A curves, which signify the pressure peak zones. High pressure zones (HPZ) consist of extreme pressure peaks acting in localized regions. They dictate the magnitude of load acting on a structure. The process P-A curve shown above consists of the averaged pressures of all the HPZs that arise in this ice-structure interaction. It can be seen that all the simulated P-A curves fall below the empirical pressure curves, since the latter corresponds to cases that are more extreme than the growler impacts. Process P-A can serve as a good model for determining the average pressures acting across the entire contact surface and hence it can be used for design considerations. However, one serious disadvantage related with process P-A is that it lacks the information regarding the location, magnitude and number of individual HPZs.

5.2.3.3 Spatial(Interface) Pressure animations:

The spatial pressure area curve tracks the pressure variation within sub or local areas at each and every time instance. The Spatial pressure area curve is vital for determining loads acting on the local components like stiffeners, frames and plates in ships and offshore structures (Hyunwook Kim 2014). In a typical ice-structure interaction, initially the load is transferred to these components, only after the failure of the local structures the main structures like outer plates start to deform. Experiments proved that the spatial pressures exhibited large variations over small areas (Andrew Palmer 2012). For these reasons, the evolution of the spatial pressures occupies paramount importance in the design of local and the global structures as well.

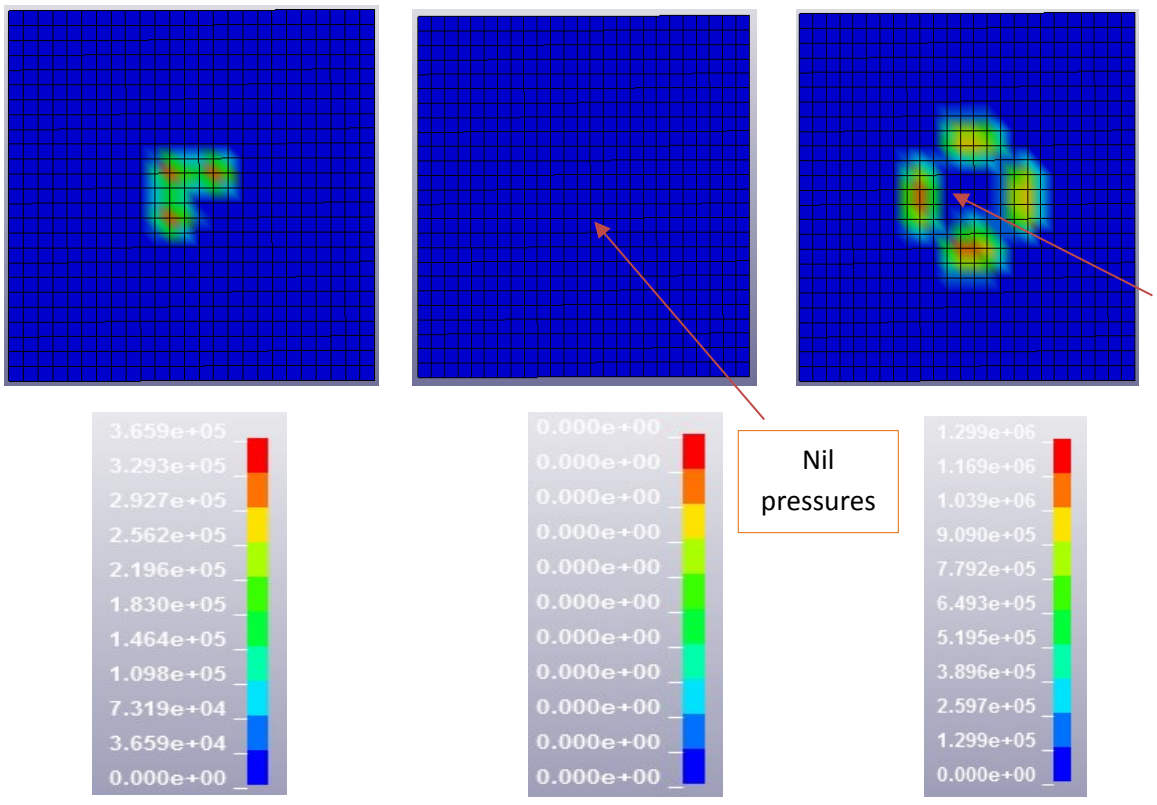

FEM (1a) 0.15 s (1b) 0.25s (1c) 0.3 s

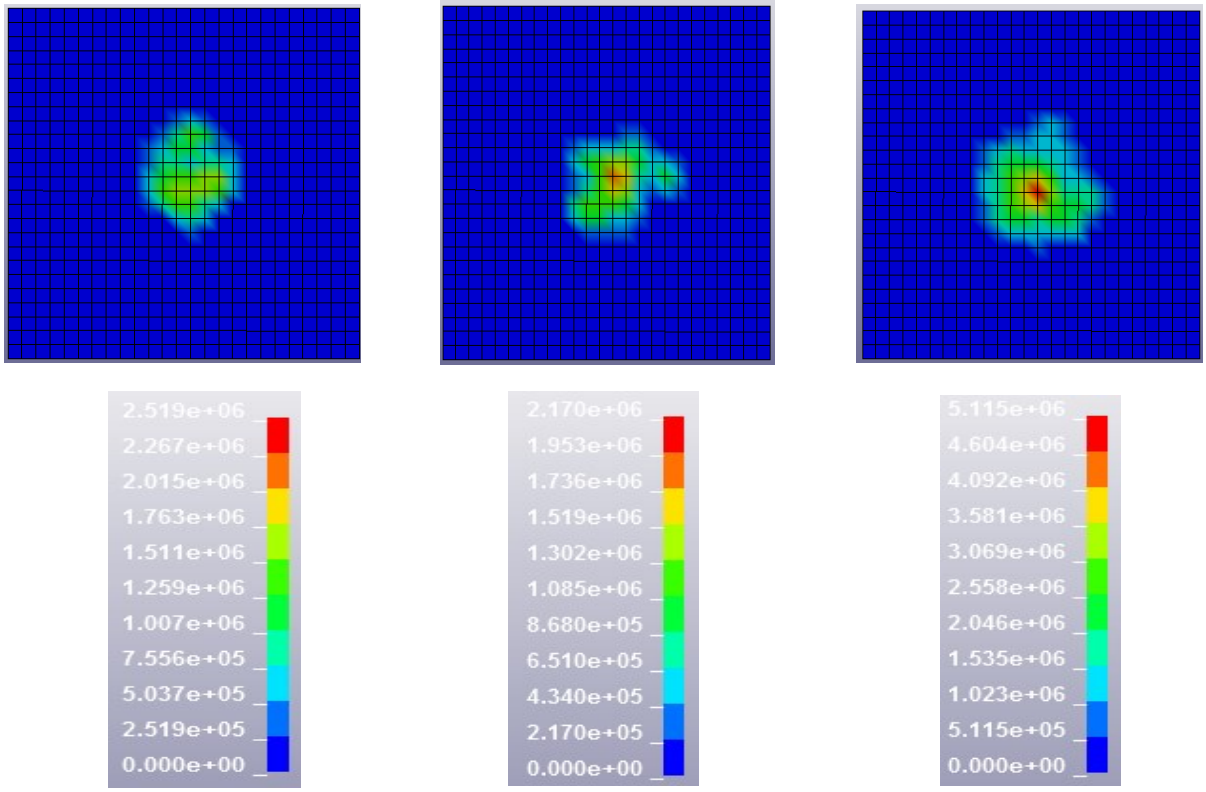

FEM-SPH NQ1 (2a) 0.15 s (2b) 0.25s (2c)0.3s

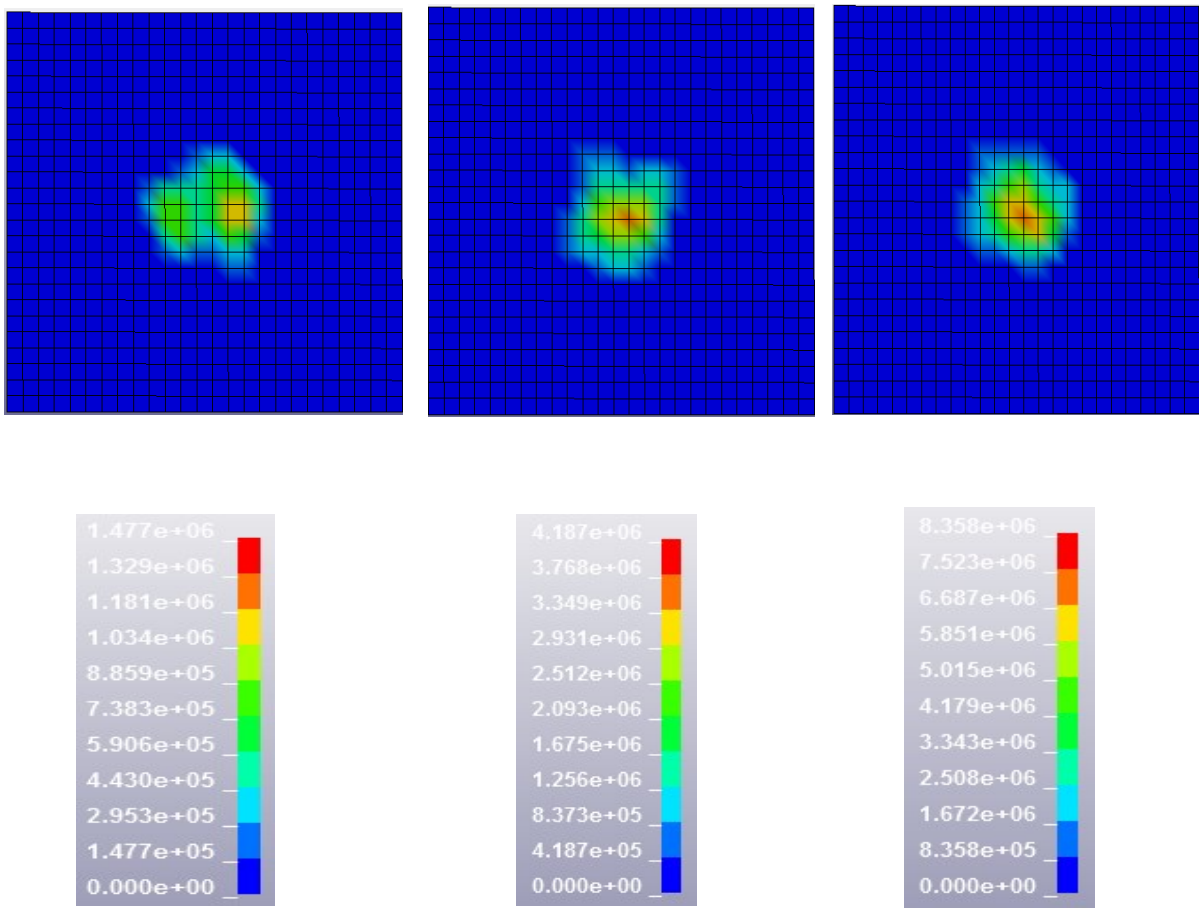

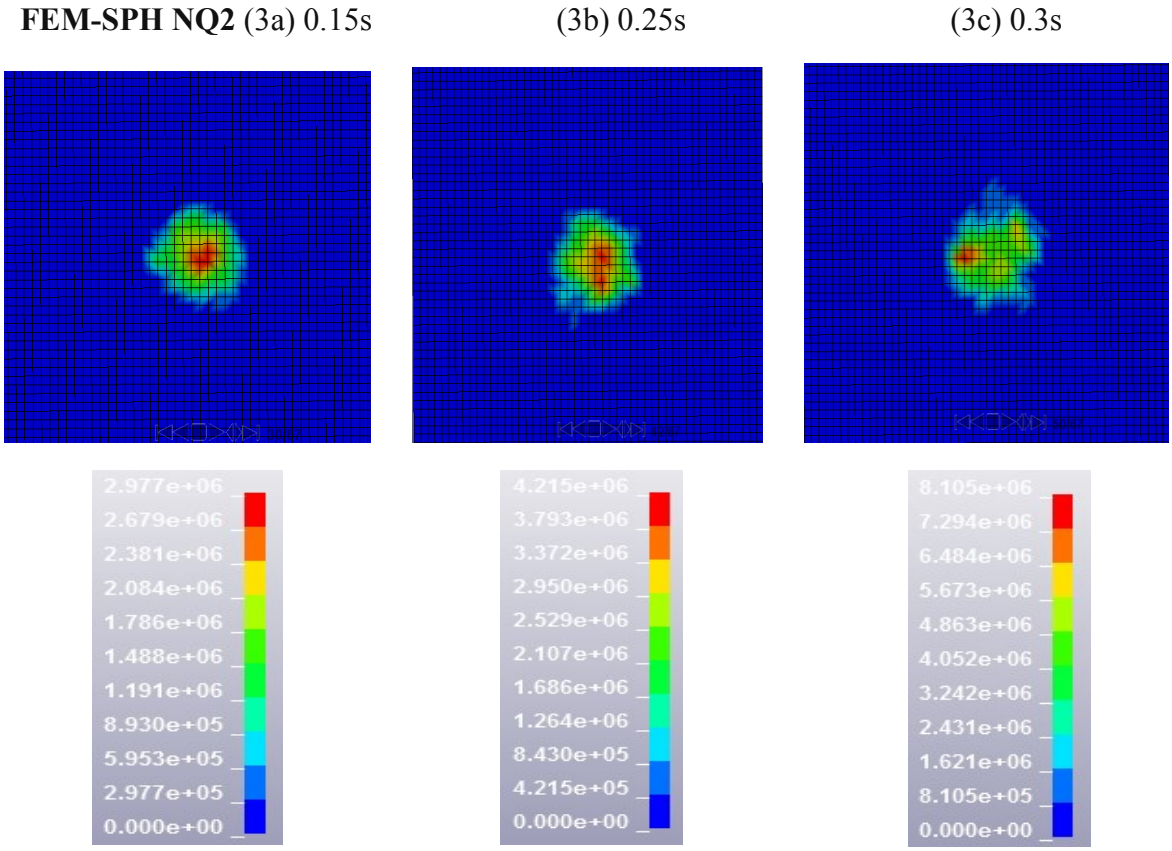

Figure 45 (1,2,3,4) Interface pressure patterns corresponding to FEM, FEM-SPHNQ1, FEM-SPH NQ2, FEM-SPHNQ3 ice models at three different time instances 0.15s, 0.25s and 0.3 s

In Figure **45** local ice pressures on the rigid plate at three different time instances are shown. There are 4 rows **1,2,3,&4** representing FEM, FEM-SPHNQ1,FEM-SPHNQ2 & FEM-SPHNQ3 respectively. In each row pressure patterns corresponding to 3 different time instances 0.15s, 0.25s, & 0.3s are shown. For FEM case, it could be seen that at 0.25 s, there is no visual pressure patterns on the plate even though significant portion of the growler is in contact with the structure at that instant. It is also noticed in the above pictures in 1st row that there exists pressure distribution on the wall before the time instant 0.25 s. In this case, there is no physical phenomena involved for this strange behaviour, the possible explanation for this behaviour in FE modelling is that the ice elements are removed when they reach a critical limit, as a result, at a particular time step the ice exerts zero contact pressures on the structure due to element erosion. This zero contact pressures on the structure have been observed not only at the time step 0.25s but also at few other instances throughout the entire simulation. In addition, at time instant 0.4s in FE ice model, there exists small zero pressure area at the centre of the plate which is purely unphysical. In other words, this type of behavior is completely opposite to what is observed in nature. In reality, spherical ice due to their shape and confinement exerts maximum pressure at the centre, but the FEM ice model does not replicate this physical behaviour. From these two examples, it could be deduced that the FEM ice model is inaccurate when it comes to capturing the distribution of local ice pressures.

FEM-SPH technique turns out to be a possible solution for the problems on interface pressures encountered in FEM model. Throughout the simulation, unlike the FEM case, no zero pressure

patterns existed at specific time instants or nil zero pressure circles present in the centre of the plate.

From Figure **45 1,2,3,4** it is seen that the spatial distribution of interface pressure increases with time with larger ice part coming in contact with the structure. The magnitude of pressure patterns vary excessively over small contact areas. For example, take the case of interface plots corresponding to FEM-SPH NQ2 at 0.3 s, the existence of maximum pressures upto 8 MPa could be witnessed over areas equal to 0.01 m2 at the centre, these represent the high pressure zones (HPZs), but, in the nearby areas, considerably less pressures could be observed. These pressure patterns which are highly varying over small areas dictate the magnitude of load acting on the structure. For ice growler impact, the HPZs are mostly concentrated around the centre. The central region of ice growler is subjected to maximum confinement and compression during the ice-structure interaction which is the cause for the existence of very high pressures.

5.2.3.4 Envelope of Spatial Curves:

Till now many researchers, developed various method for plotting the envelope of spatial curves like square averaging method(SAM), iterative search technique, contour averaging method etc. The first two techniques are important with respect to structural mechanics and the third technique CAM is useful when the study related to response of ice is important (Hyunwook Kim 2014) (people.brunel.ac.uk n.d.). The spatial curves envelope can be regarded as the graphical representation of local pressure patterns. Since in this chapter, more emphasis is placed on studying the ice response, CAM technique is used for plotting the spatial curve envelopes.

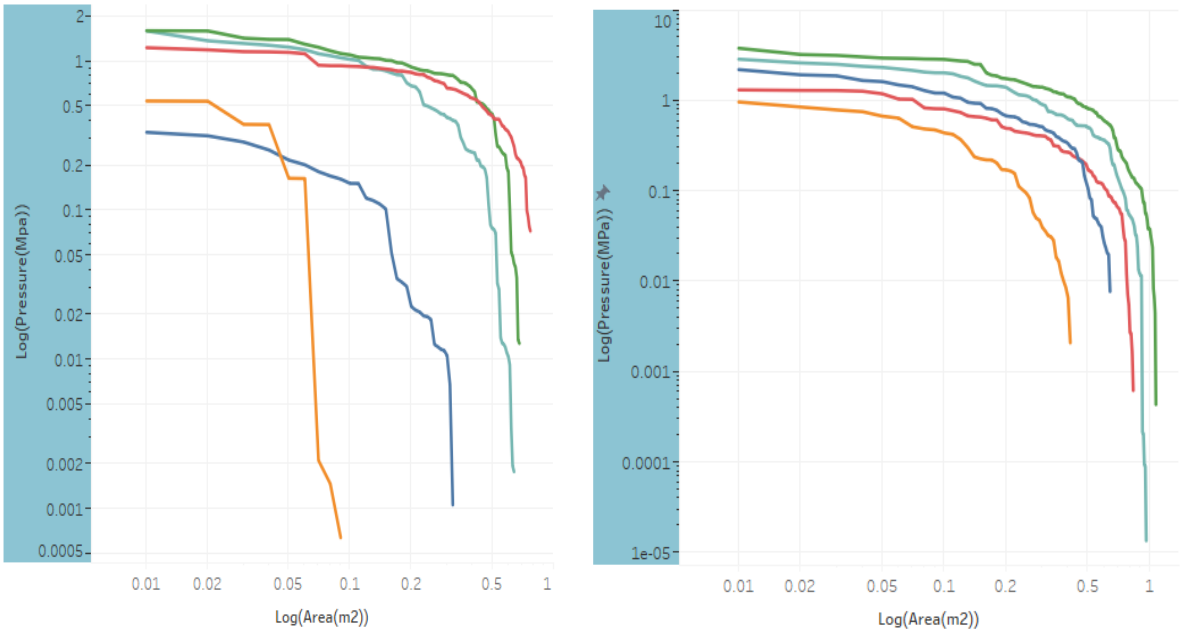

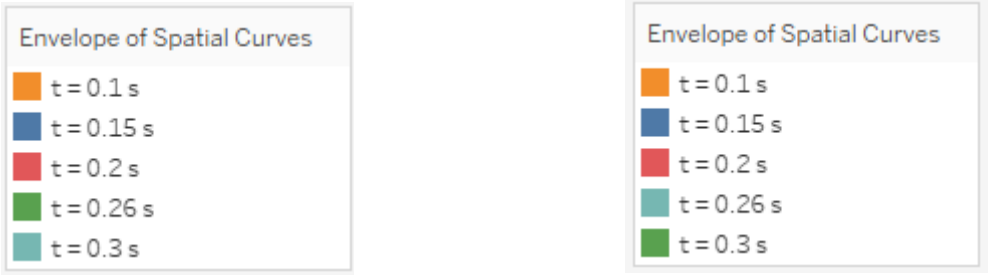

(a) FEM (b) FEM-SPH NQ1

Figure 46 Spatial curves envelope for (a) FEM ice model (b) FEM-SPH NQ1 ice model

The envelope of spatial curves is plotted based on CAM technique for five different time instances 0.1, 0.15, 0.2,0.26, and 0.3 s and presented in Figure **46 a & b.** Actually, interface pressures for 81 time realisations had been derived, but only five different time instances have been presented here, since it involved enormous computations. The left plot represents the FEM model and the other one represents the FEM-SPH ice model. According to CAM technique, the curves start from the highest pressures and it could be clearly seen from the spatial curves that the FEM-SPH ice model resulted in high interface pressures around 6 MPa on structure at 0.3 s time instant. This peak pressure of 6 MPA may exist anywhere within the area less than 0.01m2, as the exact location is not visible in envelope curves. However, from the animation pictures presented in previous section, it is evident that very high pressures existed at the centroid of the contact area. The CAM technique assumes that the local pressures gradually decreases for larger interface areas, which is evident from the gradual downfall of envelope curves shown. One important information that can be gained from this envelope of curves is that the difference between the slopes of curves corresponding to different timesteps suggest the magnitude of variation in local pressures at various time instances. From the trend of the curves shown in the above figures, it can be inferred that the slope of the curves belonging to FEM-SPH model do not vary much and in addition, the curves at different time steps are uniform, which indicate the fact that the pressures are distributed over the entire contact surface. On the other hand, considering the curves representing the FEM ice model, their slope vary abruptly at different time steps. This large difference in the slope of the curves can be attributed to the presence of zero pressure areas and un symmetric spatial distribution of pressure. These effects can be seen in interface animation plots shown in previous section. The spatial pressure curves of FEM-SPH follow more or less a smooth curvature path signifying that the pressure decreases in circular pattern from centre region till the outer most region.

5.3 RIGID PLATE-ICE FLOE COLLISION ANALYSIS

5.3.1 Modelling

Modelling Of Ice Floe:

In the case of cylindrical ice floes, their sizes may range from 2 m- 5 Km wide. Smallest of these ice floes was chosen for the crushing analysis i.e 2 m dia ice floe. Here, the rigid wall against which the ice has to collide has dimensions of 2.5m *2.5 m (the same wall used in previous analysis). and half of this was modelled as ice.

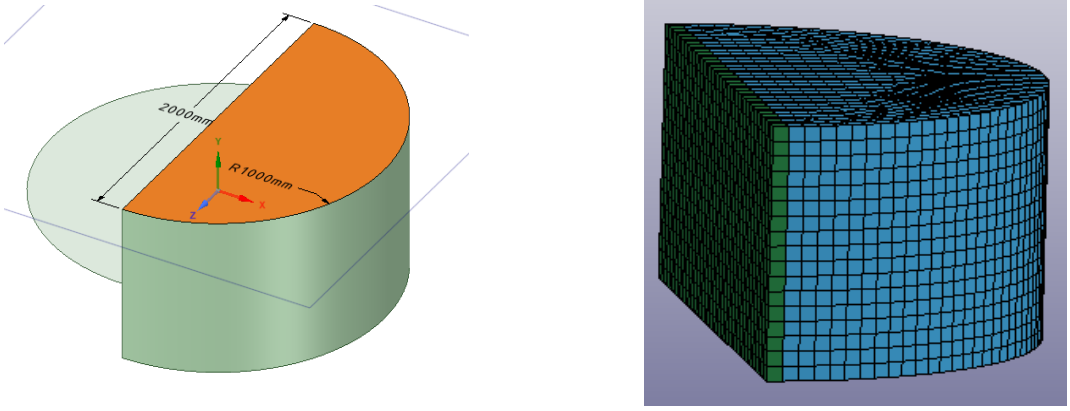

(a) (b)

Figure 47 (a) sketch of the small ice floe (b) model of the small ice floe used in NLFEA

Cylindrical ice of 2 m diameter with 0.8 m thickness was created. The sketch of the actual ice floe is shown in Figure **47 a.** When it comes to numerical modelling, an half cylinder was modelled as ice which is represented in blue colour in **Figure 47 b**, the mass of the rest of the ice floe had been assigned to the rigid ice pusher which is highlighted in green colour.

5.3.2 Simulations

Here three simulations have been conducted based on FEM, FEM-SPH NQ1 and FEM-SPH NQ2 and animation pictures are presented in Figure **48 a,b,c** respectively

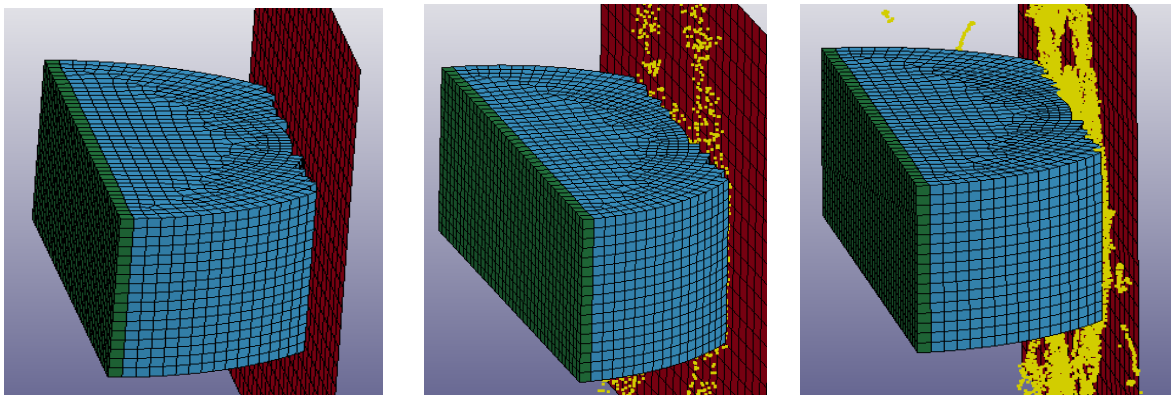

(a) FEM (b) FEM-SPH NQ1 (c) FEM-SPH NQ2

Figure 48 (a,b,c) Animation pictures of ice floe crushing against rigid plate modelled using three different methods

5.3.3 Results and Discussion

5.3.3.1 Energy Check

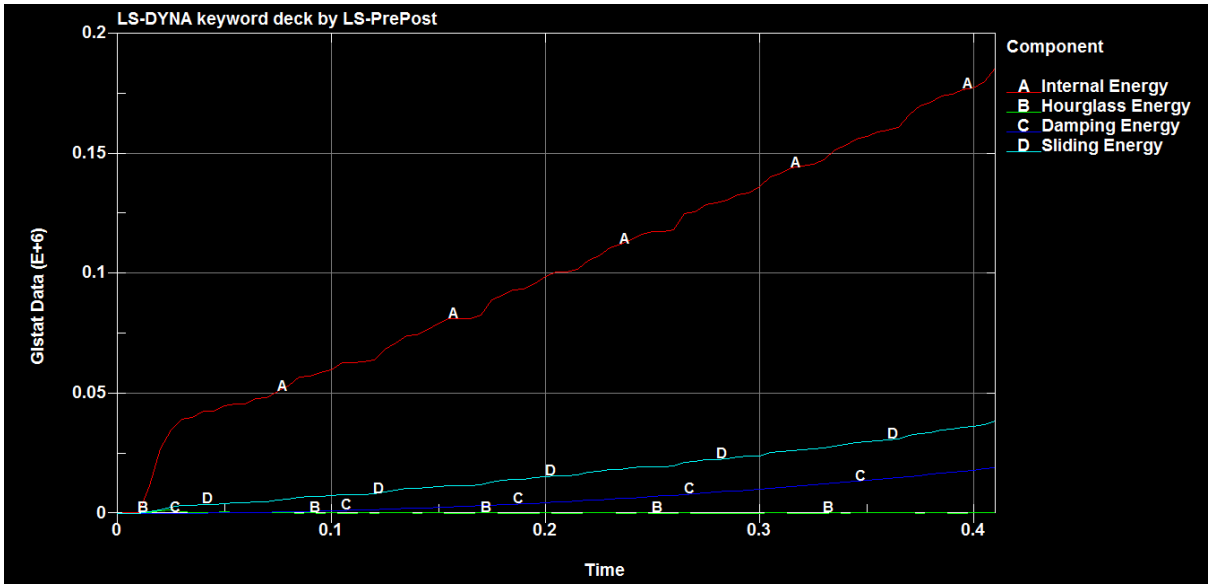

Figure 49 shows the different component sof energy dissipated for the rigid structure-ice floe interaction

Figure **49** shows the plots of internal energy, sliding energy, damping energy and hourglass energy of the system. This plot can also be used to verify the numerical accuracy of the simulation. As every numerically stable simulation requires that the hourglass energy should be less than 10% of the internal energy. The reason being hourglass energy are zero energy modes and are purely non physical. This simulation satisfies this criteria since the hourglass energy is almost negligible in comparison with the internal energy. Additional check for numerical stability is to verify whether the sliding energy remains positive throughout the simulation or not. Figure **49** suggests that the sliding energy is positive, these are proofs from which it can be concluded that the results are numerically stable.

Internal energy graph represents the strain energy released from the system. For the case of ice growler interaction with rigid plates, the ice is the only entity that is deforming so it is the strain energy of the ice that gets dissipated. Moreover, it can be noticed from Figure **49,** there are some minor energy contributions from sliding and damping. This is due to the fact that ice has a coefficient of friction equal to 0.15 that gives rise to sliding energy and damping is set active in the simulation. As a result, the total force has contributions from internal(strain), sliding, damping and hourglass energy. Apart from hourglass contribution which is almost negligible, the rest of the energies possess physical significance.

5.3.3.2 Force-Deformation Curves:

Figure **50** shows the force-deformation plot of the considered collision case. Here in this case also, the force levels increase linearly with the collision distance owing to the increase in contact area along the penetration distance. FEM results records slow linear variation in the force levels whereas the FEM-SPH results records larger linear increase on account of the force contribution from SPH particles. Like in the case of growler impacts, the peaks and troughs in the plots at regular intervals are due to the crushing of ice elements. Moreover, peaks and troughs are more finer in the FEM ice curves owing to the brittle nature of ice elements. Nevertheless, one cannot accurately point out that the brittleness of ice is the only cause for the finer peaks and troughs, as some numerical errors may also have some contribution towards these peaks. In this thesis, it is concluded that these fine peaks are mostly due to the brittle behaviour of ice as the simulation is verified and validated with some numerical stability checks.

From comparing the curves of FEM ice model with that of FEM-SPH, one can notice that the fine peaks are slightly blurred in the case of the FEM-SPH and this behaviour can be attributed to the additional force contribution from water like particles. FEM-SPH NQ1 yielded an average force of around 1.5 times higher than that of the FEM ice model.

Furthermore, it had also been noticed during the simulations that the FEM-SPH ice model, i.e the presence of SPH particles imparts some ductility to the ice. As during the simulations, a plastic upheaval, though smaller in size, had been formed on the surface of the ice floe. Initially it was thought of as hourglass formation, and various combinations of hourglass controls were provided. Then it was realized that this plastic upheaval might be the effect of ductile behaviour of ice. This formation of plastic upheaval had not been witnessed in the case of spherical growlers because of its shape and also due to the good level of ice confinement in spherical growlers.

From the plots shown above, the higher force levels associated with FEM-SPH ice model in comparison with FEM, may be due to the ductile behaviour of ice in FEM-SPH model in addition to force contributions from striking of SPH particles.

Though the formation and propagation of fractures are not considered in this ice model, the brittle and ductile behaviour of ice are accounted for in this model.

Actually, this change of ice phase from brittle to ductile and the subsequent formation of plastic upheavals can be equated to the coulombic faults and plastic faults related to the natural ice behaviour. Fault planes are associated to the fractures in natural ice. In this ice model exact fracture pattern of ice is not considered, however erosion technique is used to simulate the effects of fracture. Thus, it can be deduced that the plastic upheaval resembles closely to plastic faulting in natural ice, though not exactly as apparent in natural ice. This might be considered as another proof showing that this ice model represents natural ice to a considerable extent.

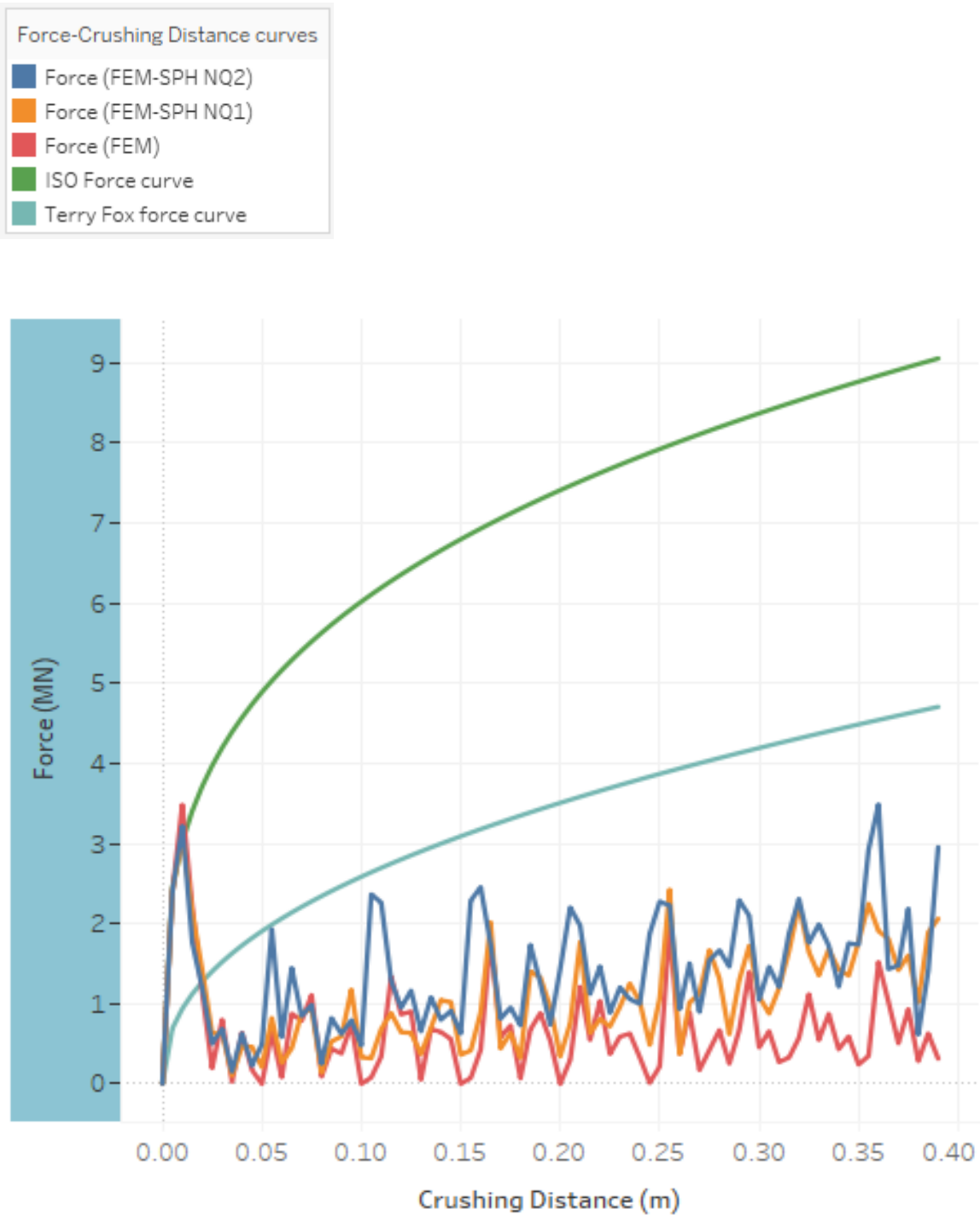

Figure 50 Force-Penetration curves for the rigid structure-ice floe interaction

5.3.3.3 Process P-A Curves:

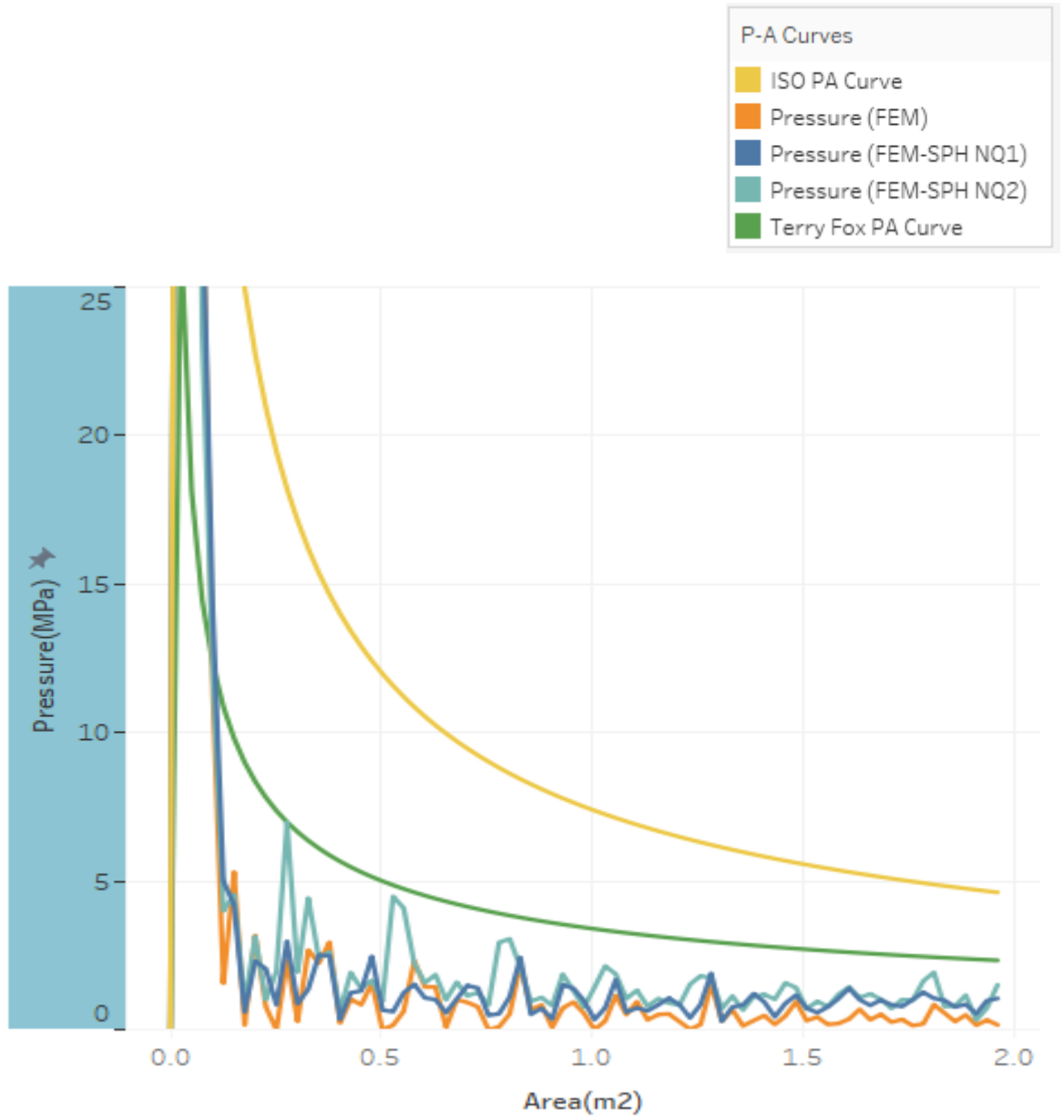

Figure 51 Process P-A curves for the considered ice-structure interaction scenario

Figure **51** shows the process P-A of this collision. P-A plots of FEM, FEM-SPH NQ=1, and NQ=2 are shown. The plots are calibrated against some empirical curves. ISO curves represent the empirical upper bound value as it is constructed based on local ice pressures. The nominal contact area for cylindrical ice floe is taken as $A = (2\pi r - 2\pi(r - x(t)))H = \mathbf{2\pi x(t)H}$. Pressure has inverse relationship with area so for areas less than 0.1 m2 very high pressures are recorded whereas when the whole contact area 0.6m2 is concerned, just less than 4 MPa of pressure acts across the entire contact surface considering all the ice models. Plots corresponding to FEM ice records the lowest pressure levels, as it signifies that the FEM model consists of lesser number of peak pressure zones. The average pressures corresponding to SPH(NQ1) and SPH (NQ2) are marginally higher than the FEM indicating that there might be higher number of HPZs owing to the generation of SPH particles. The number of HPZs, time instances at which

they occur and their exact locations on structure can be monitored only in interface(local) pressure plots. It must be noted that in addition to HPZ, the shape and strength of ice also contributes to the pressure magnitude.

5.3.3.3.1 Process Pressures – Comparison between Ice growler and small Ice Floe

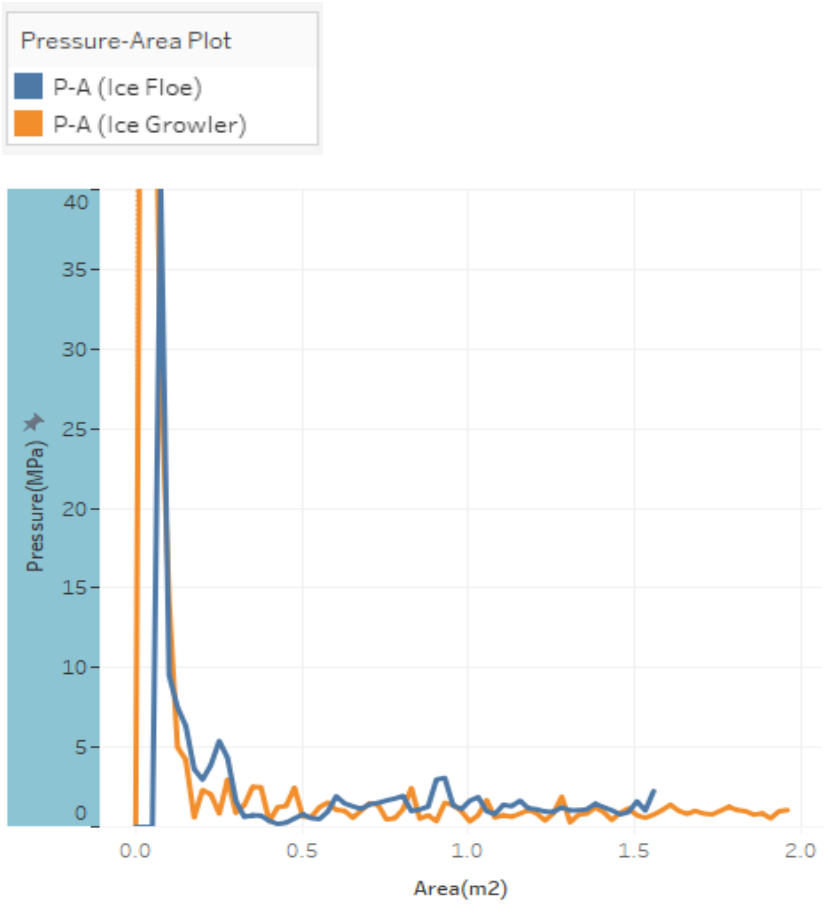

Figure 52 shows the comparison between the P-A curves of both ice grower and ice floe interaction with rigid structure

Here, a small comparison has been made to study the differences in the process P-A curves corresponding to two different ice features.

Figure **52** compares the process P-A curves of both the ice floe and ice growler during their interaction with rigid structure. With respect to their shapes, ice growler had a smaller contact area whereas the ice floe had a wider contact area during the simulations. Yet, it is apparent from the curves, that the growler produced marginally higher pressures over its impact area when compared with ice floe. This is because spherical growlers are well confined, so it can produce high magnitude pressure peaks at the centre of plate when it is compressed against the plate. However, the cylindrical ice floes resulted in higher average pressure acting across the entire contact surface owing to larger contact area.

5.3.3.4 Spatial Pressure Patterns:

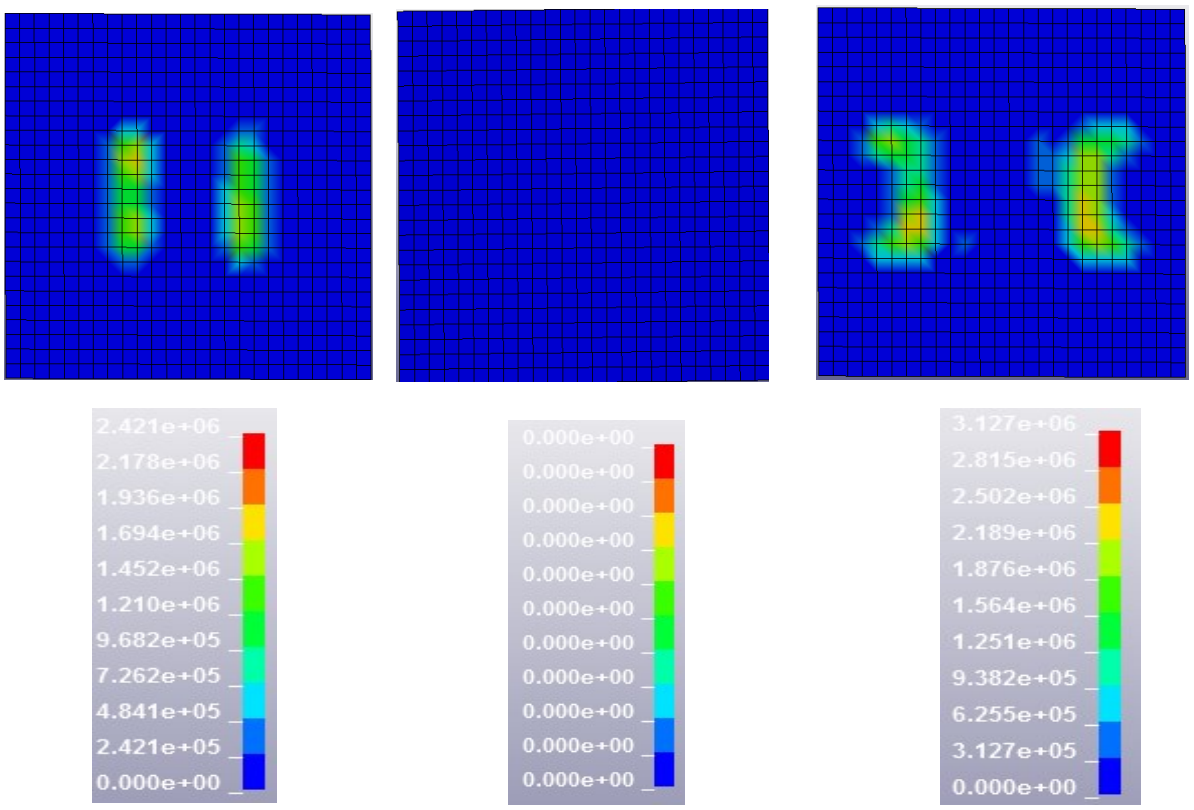

FEM (1a) 0.15s (1b) 0.21 s (1c) 0.3 s

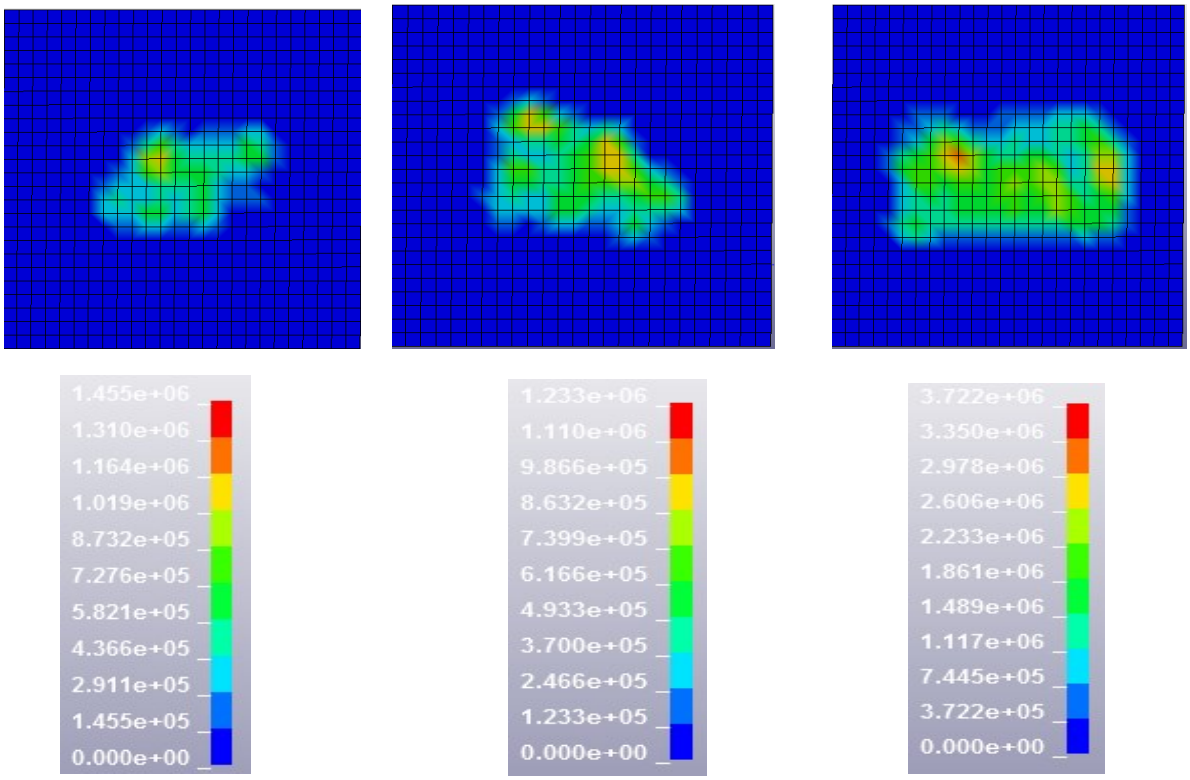

FEM-SPH NQ1: (2a) 0.15s (2b) 0.21s (2c) 0.4 s

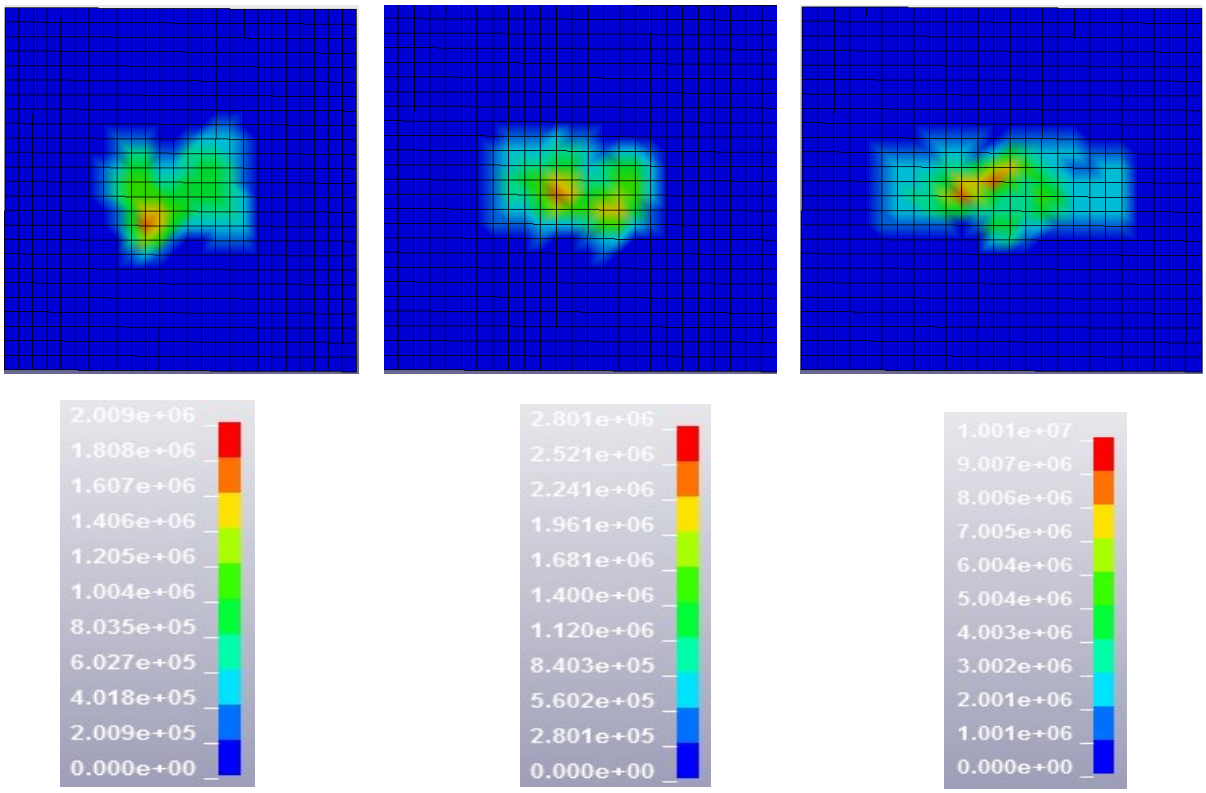

FEM-SPH NQ2:(3a) 0.15s (3b) 0.21 s (3c) 0.4 s

Figure 53 (1,2,3) Interface pressure patterns corresponding to FEM, FEM-SPH NQ1 and FEM-SPH NQ2 ice models at three different time instances

Figure **53** displays the local ice pressures at three different time instances for the considered collision case. Three rows **1,2,3** are shown each one represents the FEM, FEM-SPH NQ1 and FEM-SPH NQ2 respectively. Similar to ice growler impact, there exists zero pressure pattern on rigid plate at 0.21 s time instant and existence of zero pressure areas at the centre of the plate at other time instance can be seen which are purely unphysical. In addition, the spatial variation of interface(local) pressures produced from FEM ice model is highly different from that of FEM-SPH model. From these facts, it can be inferred that the FEM ice model is not a better choice when it comes to the analysis of interface pressures.

This erroneous behaviour is addressed in the FEM-SPH ice models where in spatial distribution of local pressures throughout the contact area can be observed. Spatial increase of contact pressure with respect to increase in time can be visibly seen. The magnitude of pressure peaks over small areas are highly unpredictable. For example, the average of process pressures over the entire contact surface is 3.9 MPa, for FEM-SPH NQ2 ice model, but the interface plots show maximum pressure of almost 10.01 MPa, acting over areas less than 0.01 m2. These represent the high pressure peaks, and they are concentrated close to the centre.

Another trend observed in the interface plots corresponding to FEM-SPH ice models is that the areas with high pressure magnitudes are present in the centre surrounded by areas with pressures of lesser magnitude. This is because that the ice might be subjected to high confinement and compression at the centre and lesser confinement along the outer edges during ice interaction with structure. This trend can be equated to pressure patterns observed in real ice-structure interaction wherein, the small regions of hard ice present at the centre of the ice feature exerts maximum pressure on the structure whereas the outer regions of ice features

usually surrounded by soft pulverized ice exerts pressures of lesser magnitude.

5.3.3.5 Envelope of Spatial Curves:

A brief explanation on how to construct the spatial curves has been presented first. From the interface pressure plots, the pressure patterns corresponding to one time instant during which the local pressures are distributed to a maximum extent along the plate surface must be chosen. Then, each small square segment should be selected in order to extract the spatial pressures acting at those segments in all time instances. One such picture is presented in Figure **54.**

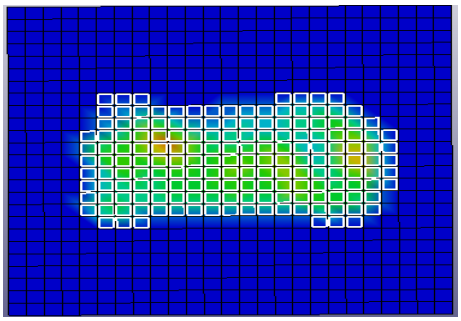

Figure 54 illustrates the local pressures acting over small segments

Then all the segment pressures for all time instances should be plotted in LS DYNA. A FORTRAN coding has been written to classify the data. Bird's eye view of the classified data is shown in Figure **55,** where each column consists of the interface pressure data from each segment for all time instances. For this case, there 220 columns representing 220 segments and 82 rows representing the time realizations. So a matrix of 82*220 is generated. From 82 time realizations, pressure corresponding to 5 time steps (0.1,0.2,0.3, 0.35,0.4s) are chosen. CAM requires that the curves should start from the highest pressures, so the pressure data has been arranged in such a way that the highest pressures act over small areas and the low pressures act over large contact areas. After the arrangement, the spatial curves are plotted using Tableau Software.

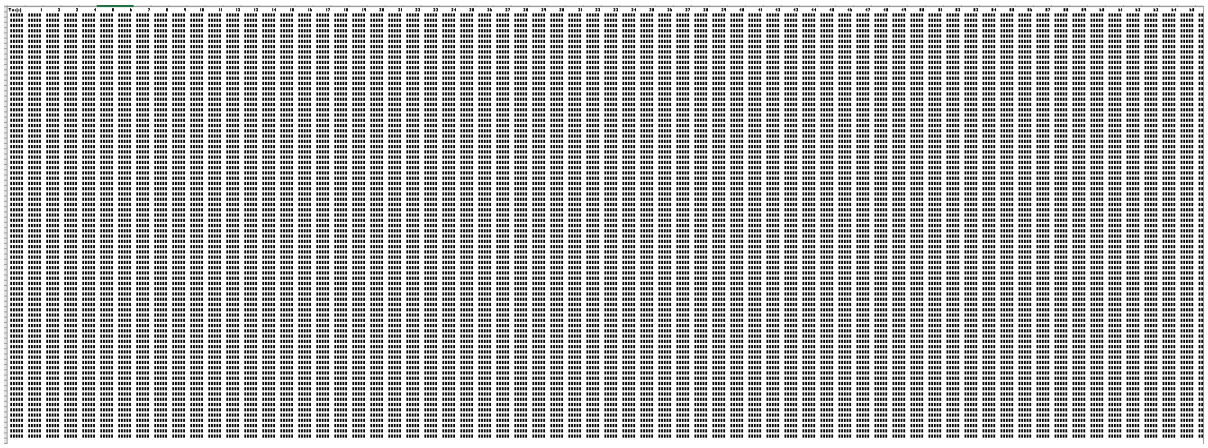

Figure 55 Birds eye view of the classified interface pressure data

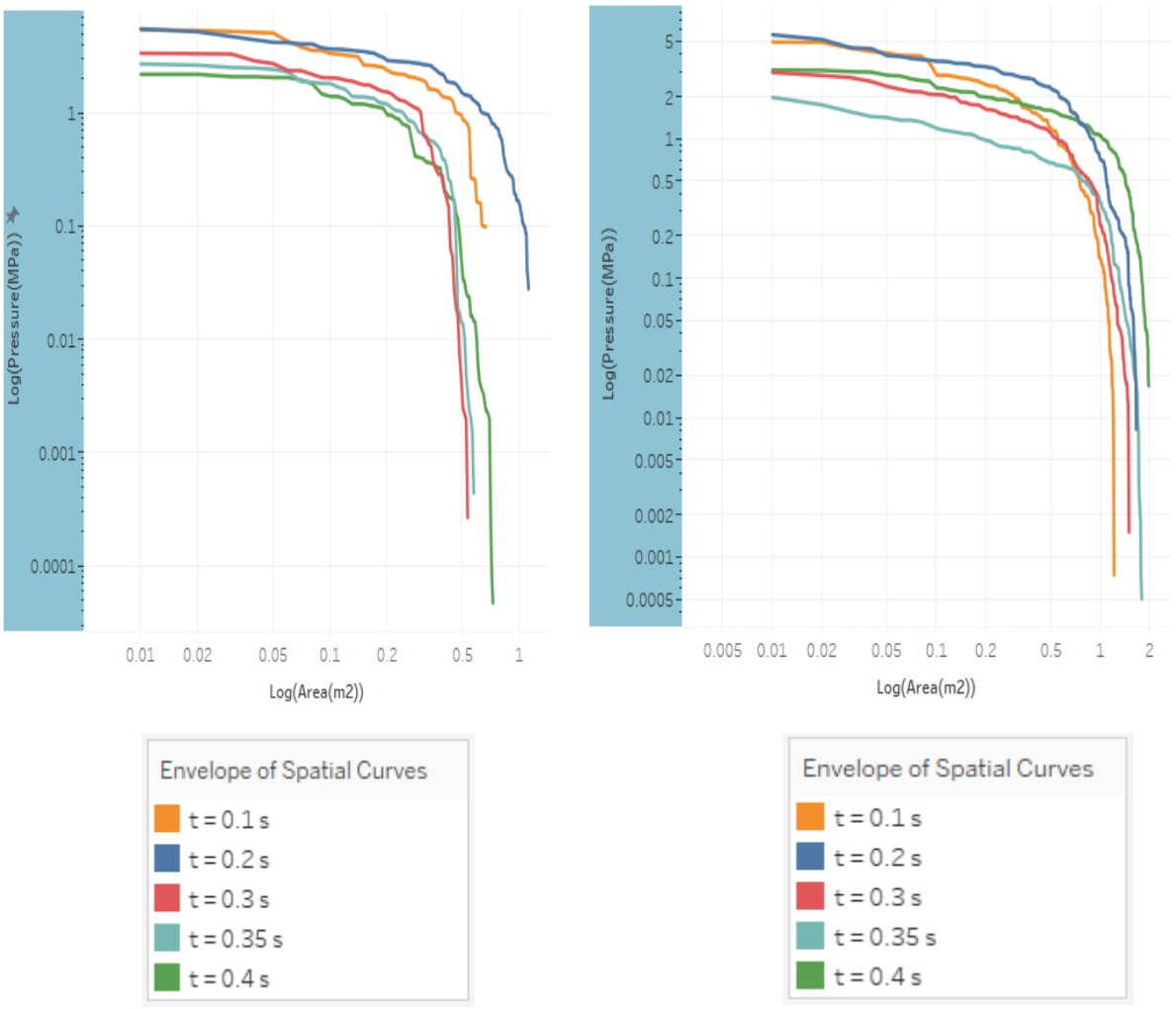

(a) FEM (b) FEM-SPH NQ1

Figure 56 Spatial envelope curves for (a) FEM ice model (b) FEM-SPH NQ1 ice model

Figure **56 a &b** shows two plots which represents the envelope of spatial curves from the ice floe-structure interaction performed using FEM and FEM-SPH NQ1 model respectively. Curves from five different time instances are presented. The spatial curves have been constructed based on CAM technique wherein the information on pressures acting over small areas are presented first followed by information on pressure acting over large surfaces. All the curves following a gradually decreasing trend signifying that the pressure magnitude is high in smaller contact areas and it decreases considerably over large interface areas.

In all time instance that are presented, FEM-SPH NQ 1 shows higher values of interface pressures than FEM because of the contributions from SPH particles. In addition, all the curves belonging to FEM-SPH NQ 1 appear to be more uniform because there are no unrealistic zero pressure areas related to FEM-SPH models.

5.3.3.6 Analysis using Coupled collision approach:

The collision cases described earlier have been performed using the decoupled approach, i.e crushing the ice with constant velocity. Here, one collision case is simulated using coupled collision process, i.e driving the ice floe against the structure with initial velocity of 1 m/s. In order to have large kinetic energy, huge mass is assigned to the ice pusher. As a result, this ice floe has mass equivalent to that of 20 m dia ice floe. Figure **57** shows the force-deformation curves for the coupled approach. The force levels did not increase along the penetration depth. This trend is because of the fact that the ice is driven with a low velocity of 1m/s. Furthermore, the velocity decreases with increase in the penetration distance and thus driving kinetic energy decreases correspondingly.

It can also be noticed that the F-D curve of coupled collision case displays some variation in the load peaks and troughs along the crushing distance, this might be due to the vibrations caused due to the change in velocity.

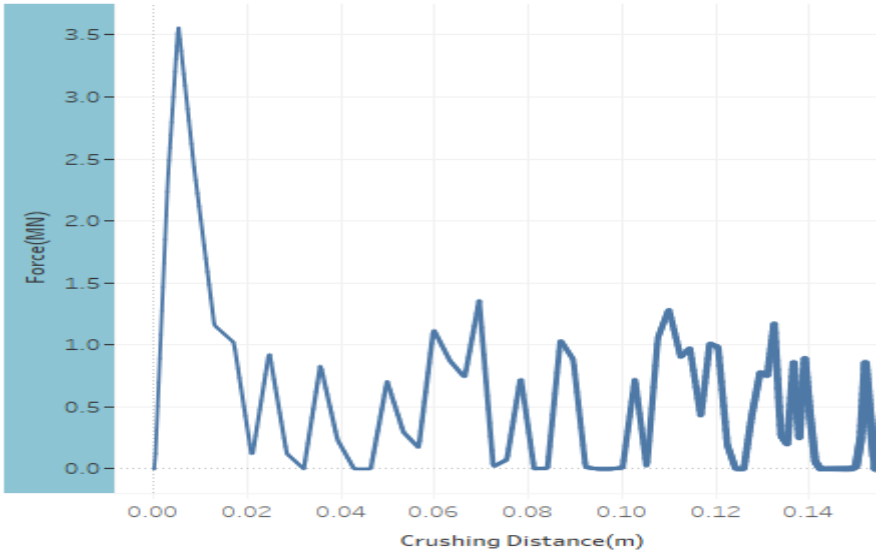

Figure 57 Force-penetration curve of the rigid structure-ice floe interaction for the coupled collision case

Since the ice is driven with an initial velocity in coupled approach, the simulated data can be compared using limit momentum mechanism and it is explained here.

Limit momentum approach presents a simplified formula based on the energy balance. According to this approach, the change in the kinetic energy of the ice feature can be equated to the work done.

$$E_{kin}^{Ini} - E_{kin}^{fin} = W \tag{40}$$

Where E_{kin}^{Ini} is the initial kinetic energy of the ice feature

E_{kin}^{fin} is the final kinetic energy of the ice feature

W is the work done.

Here, it is assumed that the ice is completely stopped after the impact. So, the final kinetic energy is zero. Thus, the initial kinetic energy can directly be equated to the workdone and is written as

$$\boldsymbol{E_{kin}^{Ini} = W} \quad (41)$$

Workdone, in relation to the crushing load can be written as

$$\boldsymbol{W = \int_0^x F\, dx}, \quad (42)$$

F is the crushing force and x is the penetration depth. By substituting this equation in equation **42**, we get

$$E_{Initial}^{Kin} = \int_0^x F\, dx$$

$$\frac{1}{2}mV^2 = \int_0^x F\, dx$$

In the simulations, the ice is crushed almost 0.16m, and in order to the calculate the force using the limit momentum approach, the penetration depth x=0.16 m is used in the above relation, it becomes.

$$\frac{1}{2}m1^2 = \int_0^{0.16} F\, dx$$

Here mass corresponding to 20 m dia ice floe with a thickness of 0.8 m has been assigned to the ice for this simulation. The same values are used here. The domain is from 0 to 0.16 m, so the average crushing force in that domain is calculated as

Crushing Force, $F = 706858$ N

F = 0.71 MN

NLFEA	Limit momentum approach
Average Force = 0.59 MN	Average Force = 0.71 MN

From the above comparison, the limit momentum approach produces almost 0.12 MN higher than the NLFEA. The reason being that in limit momentum approach it is assumed that the ice is completely stopped after the impact, so all the kinetic energy is transferred as strain energy, however, in the NLFEA the ice moved back with some residual kinetic energy.

5.4 ADVANTAGES AND DISADVANTAGES OF FEM-SPH COUPLING

The general theoretical view of smoothed particle hydrodynamics (SPH) has been discussed in detail in section **4.4.** In this section, the pros and cons of numerical modelling of ice using FEM-SPH technique have been discussed.

As can be seen from the results of crushing of ice against a rigid structure, the FEM-SPH produced better results than the traditional continuum model of ice, especially for local pressure patterns. The results from FEM-SPH appears to be more logical and reasonable in comparison with FEM model. In other words, the FEM model produced nil pressures at certain time instances which is unrealistic in an ice-structure interaction, whereas the FEM-SPH did not give any zero local pressures on rigid structure at any instance. Thus, it is concluded that for the analysis of design of local components (stiffeners, frames, brackets etc) in ships or offshore structures, it is strongly recommended to conduct analysis using ice modelled with FEM-SPH. Apart from local pressures, both FEM and FEM-SPH yielded reasonable results for force-deformation and average pressures.

The FEM modelling does not actually represent the crushing and failure mechanism of ice. As in real ice, the crushed ice is converted to discrete ice particles and the particles in turn impart some loading on the structure. In FEM-SPH, the ice elements are converted to SPH water particles instead of getting eroded. Moreover, in the outer regions of natural ice where spalling occurs during ice-structure interaction, the soft ice in those regions is converted to water. Thus, from this fact it can be concluded that the FEM-SPH model, though not completely, resembles the real ice crushing to some extent.

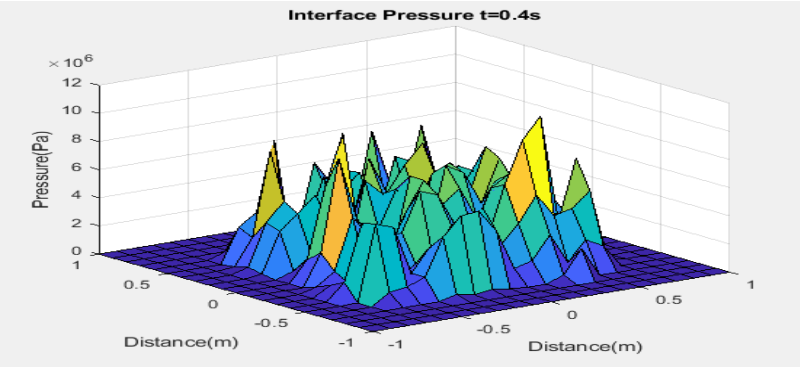

Figure 58 Local pressure pattern with visible peaks for rigid structure-ice floe interaction

In previous sections, lot has been mentioned regarding the HPZ's. However, the extremity of each peaks is not quite visible from the LS DYNA animation plots. So the data has been exported from LS DYNA and a contour plot has been created using MATLAB. Figure **58** shows a contour plot where the magnitude of each pressure peak is clearly visible. This plot corresponds to the rigid structure – square ice interaction.

Now, the disadvantages associated with the FEM-SPH ice model are discussed. Mesh uniformity poses great restriction when it comes to FEM-SPH modelling of ice. In other words, FEM-SPH coupled simulations in LS DYNA demand a uniform square meshes in order to produce numerically stable results, otherwise the presence of irregular meshes introduces instability in the system. For example, the presence of triangular and quadrilateral mesh elements in the simulations results in shooting off of ice elements from the system. As a result, great care must be exercised in forming even sized square meshes all throughout the ice model

which requires precise modelling. Initially, the FEM-SPH coupled simulations were undertaken with uneven meshes concentrated at certain parts of the model. During these simulations, one peculiar thing noted is that the unstable removal of elements from the system closely resembled the physical behaviour of ice when crushed against a structure. However, this un stability resembled real ice crushing just pictorially and it cannot be relied when it comes to the load or pressure curves.

The above uniform mesh restriction only applies to (NQ=1) in SPH keyword, that is conversion of one ice element to SPH element. NQ=2(8 SPH elements) and NQ=3(27 SPH elements) works well even with tetrahedral elements in addition to uniform square meshes. As a result, it is advisable to use NQ=2 or 3, if it is not possible or hard to generate uniform meshes for the ice part.

One serious disadvantage lies in using the SPH NQ=2, NQ=3 is that they consume massive amount of simulation time. The details of the CPU time consumption for each of the ice model is given in Table **11.** The simulations are run using laptop with the following configurations: i5 intel processor, 8GB RAM capacity.

S.No	Ice Models	CPU computational time
1	FEM	15 minutes
2	FEM-SPH NQ1	40 minutes
3	FEM-SPH NQ2	9 hours (approx.)
4	FEM-SPH NQ3	30 hours (approx.)

Table 11 CPU time consumption for each ice model

The CPU consumption time presented in the above table is based on the rigid structure-ice growler (1 m dia). The simulation has been run for 0.305 s with a constant velocity of 1m/s. The simulation time may decrease when the constant velocity is increased.

It can be seen from table **11,** that FEM-SPH NQ 3 consumed almost 30 hours just for the penetration of 0.3 m distance. So for very large models, usage of NQ=2 and NQ=3 in FEM-SPH is strictly not advisable if computational time is a constraint. From the F-D curves, it is evident that the SPH NQ=2 , NQ=3 do not show large variation in comparison with SPH NQ=1. As a result, it may be inferred that wise choice is to have NQ=1 with uniform meshes for FEM-SPH ice modelling. The choice regarding the number of generated particles is case specific. From the point of view of computational efficiency, FEM ice berg model is far better than that of the FEM-SPH NQ 1 coupled model as the former requires $1/4^{th}$ of the computational time in comparison with the latter.

5.5 CONCLUSION POINTERS

In this chapter, the behaviour of ice features when they are crushed against a rigid plate has been effectively studied with the help of force-deformation, process P-A, spatial P-A and envelope of spatial P-A plots. The ice features used are a small growler and an ice floe. The crucial points from the analysis, results and discussion are again briefly outlined below.

- The disadvantage associated with FEM ice modelling is that the ice elements disappear from the calculation after reaching the failure strain. This behaviour is quite untypical when compared with natural ice crushing. However, in FEM-SPH modelling, the ice elements are converted to SPH particles, thereby resembling to some extent the natural ice crushing scenarios. FEM-SPH model is more stronger as SPH particles add some ductility to the ice, this phenomenon is visible during the ice floe crushing.
- FEM-SPH is highly recommended for analysis concerned with interface pressure patterns, as this technique produced realistic local/interface pressure plots, in terms of the location of HPZs and the spatial variation of pressures
- The f-d curves and process P-A curves are calibrated against the analytical curves and in addition compared with analytical formulas as well. The simulated curves fall below the empirical curves, since the latter is a conservative estimate.
- Envelope of spatial curves, which involved huge computations have been plotted for various cases. Lot of information can be inferred from the behaviour of the curves. An important uncertainty is that only five curves are presented, so the worst pressure peaks occurring at some other time instance cannot be visualized in the envelope. Still some smart algorithm must be coded which could trace the time instance at which the high pressure peaks occur. Anyhow, all the worst pressure peaks can be seen in the interface animation plots from LS DYNA which are also presented in this chapter.
- The dissipated energy has four components, strain energy which occupies the dominant part, sliding energy due to friction, damping energy and hourglass energy. Since hourglass energy is negligible and purely non-physical, it can be ignored.

CHAPTER 6

In this chapter, integrated collisions have been simulated using the stiffened panel and ice features. This case is representative of shared energy design analysis

6.1 STIFFENED PANEL-ICE GROWLER INTERACTION ANALYSIS

6.1.1 Modelling

Modelling of Stiffened Panel

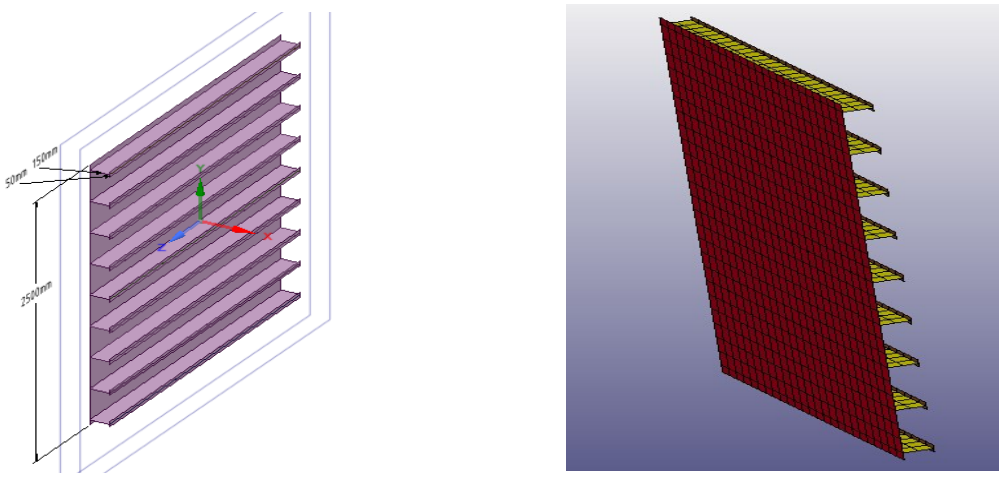

(a) (b)

Figure 59 (a) sketch of the stiffened panel (b) stiffened panel used in NLFEA

The stiffened panel consists of a square plate of dimension 2.5*2.5 m and T-shaped stiffeners that are spaced at a centre to centre distance of 300 mm. The web height of stiffeners is 150 mm and flange height is 50 mm. The thickness details are listed below.

Structural components	Thickness
Plate	15 mm
Stiffener web	14 mm
Stiffener flange	22 mm

Boundary Condition:

The outer edges of the plate were fixed and in addition the far axial ends of the stiffeners web and flanges were also fixed.

6.1.1.1 Keycards necessary for collision analysis

For strength design analysis, the steel plate had been modelled as a rigid structure. However, in the case of shared energy design analysis, both the ice and structure should deform. To account for the deformation in steel structure, the following MAT and CONTACT keycard have been used in addition to the cards used in the strength design analysis

LS DYNA includes a material called POWER_LAW_PLASTICITY which captures the plastic deformation of structures precisely. This MAT card also accounts for the material non-linearity. Steel properties have been assigned using this keycard and they are listed in below.

Density	7890 kg/m3
Youngs Modulus	210000 MPa
Poisson Ratio	0.3
Strength Coefficient	670 MPa
Hardening Exponent	0.24
Yield Stress	235 MPa
Critical Strain	0.3

Table 12 Steel Material Properties

AUTOMATIC SINGLE SURFACE

Unlike the rigid plate, the stiffened panel deforms when it interacts with ice, as a result, the plates interact with the stiffeners during the deformation. Thus, a self contact must be established for the deforming structure. This AUTOMATIC SINGLE SURFACE was used in creating the self contact for the stiffened panel. The static frictional coefficient was entered as 0.3

6.1.2 Results and Discussion

6.1.2.1 Force-Deformation Curves

Figure **60** shows the force-deformation curves for both the ice crushing against rigid plate and stiffened panel. The positive x-axis represents the ice deformation and the corresponding negative axis signifies the stiffened panel deformation. The representation of panel deformations in negative values do not have any physical significance, it is just an initiative to present the deformation of panel and ice separately.

Case 1	Stiffened Panel-Ice	FEM
Case 2	Stiffened Panel-Ice	FEM-SPH NQ1
Case 3	Stiffened Panel-Ice	FEM-SPH NQ2
Case 4	Rigid Structure-Ice	FEM
Case 5	Rigid Structure-Ice	FEM-SPH NQ1
Case 6	Rigid Structure-Ice	FEM-SPH NQ2

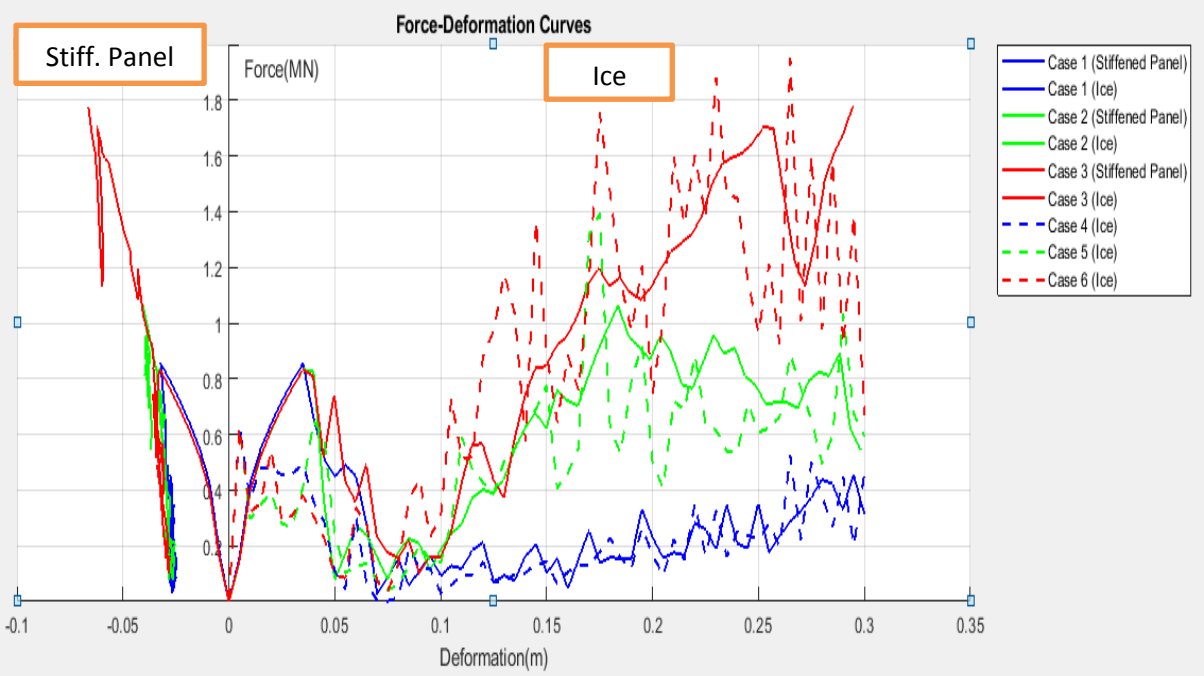

Figure 60 Force-Deformation curves for the case Stiffened Panel-Ice growler collision

Simulation results from FEM, FEM-SPH NQ1 and FEM-SPH NQ2 are presented. Here, FEM-SPH NQ3 is not used for ice interaction with stiffened panels because it requires massive computational time. As already mentioned in previous chapters FEM model records lower force values as there is no additional force contribution from SPH particles whereas FEM-SPH 1NQ(green line) and FEM-SPH 2NQ (red line) shows increasing force levels with respect to the amount of SPH particles generated. The analysis with ice colliding against stiffened panel is representative of shared energy analysis and it is an Accidental Limit State (ALS) based design condition. In other words, both objects deform during the collision process. Here, ice is crushed upto a distance of 0.3 m, whereas the recorded panel deformation is close to 0.08 m which is for the case of FEM-SPH NQ2. The failure modes including plastic bending, buckling of stiffeners and deformation of plates could be seen in the simulations. These failure modes are mild for the case of collisions with FEM ice model, but for the FEM-SPH NQ2 ice model, both the plate deformation and stiffener buckling are considerable. These effects are shown using illustrative pictures using pointer arrows in Figure **61.** The deformation in plates occurred only after the buckling of T stiffeners. However, buckling of stiffeners and plate deformation are minimum and not really massive. As a result, it can be concluded that the 1m dia ice growler implemented with ice properties and failure strain parameters M=1 and N=0.5 do not possess enough strength to cause significant damage on the structure.

The results from this collision analysis are compared with those of ice-rigid plate analysis (shown in dotted lines). In general, the more the ice is crushed, the more force it exerts on the structure. In the case of ice crushing with rigid structure, the ice deforms and dissipates all the energy and consequently more force is exerted on the structure. However, from the F-D curves corresponding to FEM and FEM-SPH NQ1, it can be seen that force levels from rigid structure analysis and stiffened panel analysis are almost the same with marginal variations. This is due to the fact that the panel displays minimal deformation close to 0.03m and subsequently the energy dissipated by panel is considerably less in comparison with the ice, thus the panel is

behaving more or less rigid. However, FEM-SPH NQ2 ice model seems to be somewhat stronger than the other two ice models, as a result it deforms the panel slightly more. Therefore, the force levels recorded from stiffened panel analysis (FEM-SPH NQ2) are apparently lower than the rigid structure analysis for the same ice model.

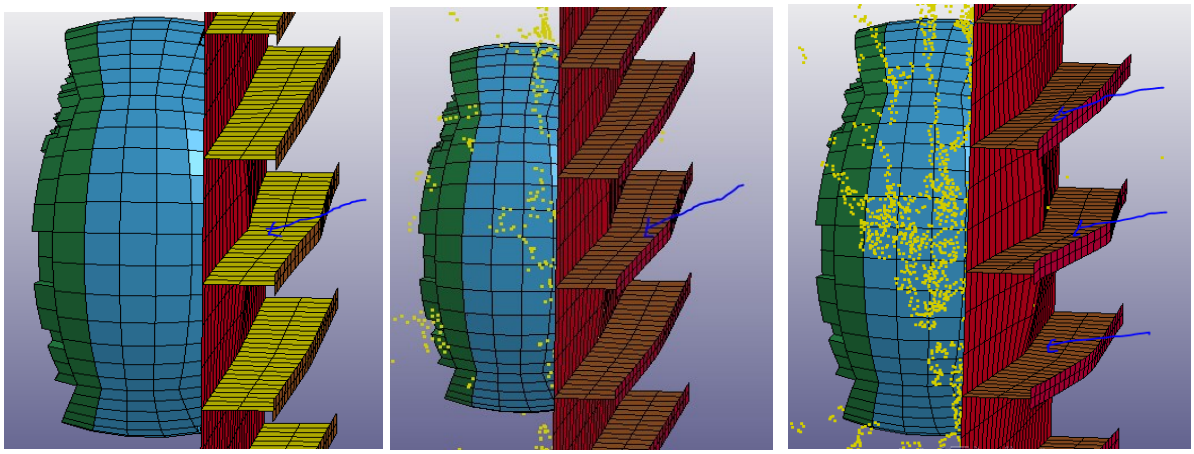

(a) (b) (c)

Figure 61 (a,b,c) shows the deformation modes of the stiffened panel corresponding to FEM, FEM-SPH NQ1 and FEM-SPH NQ2 respectively

Figure **61** shows the damage extent of the stiffened panels subjected to impacts from growlers modelled using FEM, FEM-SPH NQ1 and FEM-SPH NQ2 technique.

6.1.2.2 Process P-A Curves:

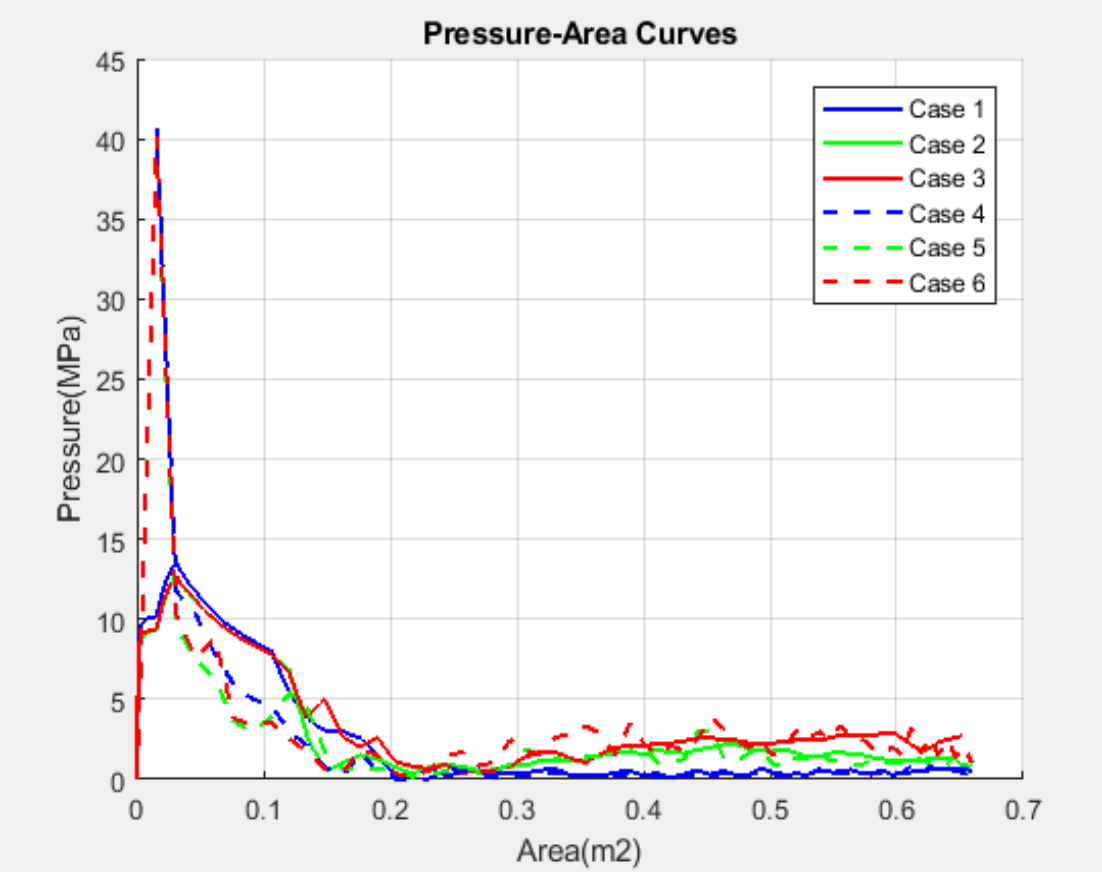

Figure 62 Process P-A curves for the case of rigid structure-ice growler interaction

Figure **62** shows the P-A relationship of FEM, FEM-SPH NQ1 and FEM-SPH NQ2 ice models. The results from ice crushing against stiffened panels cannot be verified using empirical checks as the existing analytical formulas are based upon ice-rigid structure interaction scenarios. So the results are compared with that of the strength design analysis (Ice-rigid structure analysis) which is presented in dotted lines. Initially at the contact point between the ice and structure, i.e at contact areas less than 0.03 m2, rigid structure analysis shows pressure peak of almost 40 MPa, on the other hand, stiffened panel records pressure levels just around 14 MPa. This variation of pressure at the initial contact point can be attributed to the fact that the ice starts to get crushed as soon as it interacts with the rigid structure whereas the stiffened panels deforms to some extent before the ice starts to get crushed.

Apart from the initial contact point, the pressure variation between strength design analysis and shared energy analysis is not significant throughout the entire contact surface owing to the reason that the ice is not strong enough to produce considerable deformations in the stiffened panel, thereby the pressure levels of ice-stiffened panel analysis do not differ much in comparison with the ice-rigid structure analysis. For example, from analysis using FEM-SPH 2NQ ice model, the average pressures from strength design simulation is 2.96 Mpa and that of shared energy simulation is 2.85 MPa. The minor difference of 0.11 MPa is due to the above mentioned reasons.

6.1.2.3 Spatial Pressure Patterns:

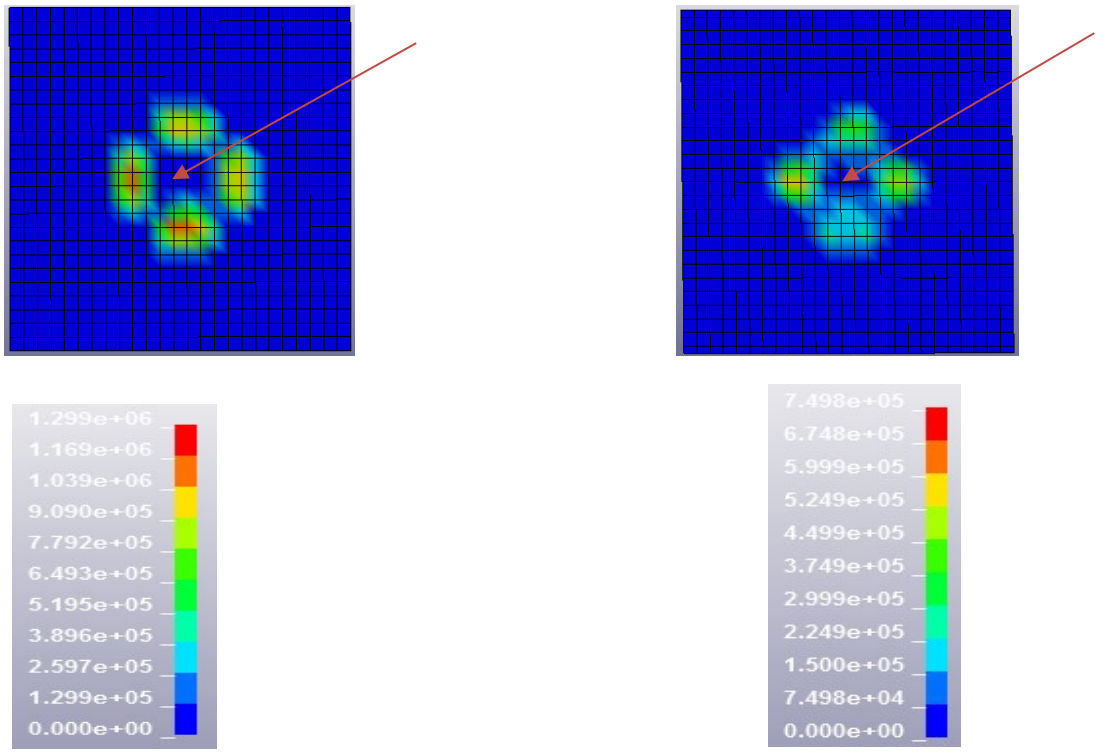

FEM (1a) 0.3s [Rigidstructure-Ice] (1b) 0.3 s [Stiffened Panel-Ice]

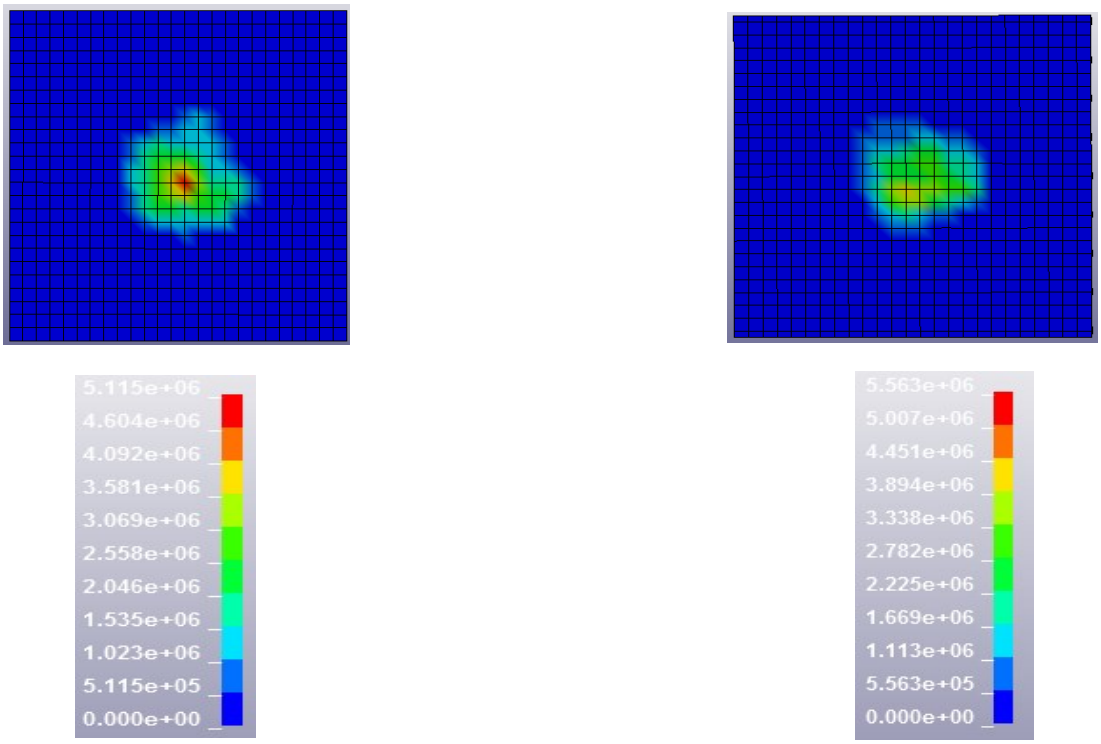

FEM-SPH NQ1 (2a) 0.3 s **[**Rigidstructure-Ice] (2b) 0.3s [Stiffened Panel-Ice]

Figure 63 (1,2) shows the comparison of interface pressure plots bwteen rigid structure and stiffened panel collision analysis at time instant 0.3 s

Figure **63** shows the interface pressure patterns at time instant 0.3s for the ice modelled using FEM and FEM-SPH NQ1 technique. The figures to left of the reader belong to the strength design analysis and figures to the right represent the shared energy analysis. There are two rows **1,2** representing FEM, FEM-SPH ice models. As mentioned in previous chapters, FEM ice model produces poor quality local pressure distribution, in the sense that zero pressure small circe is present at the centre of the panel. This phenomenon does not represent the mechanics of ice structure interaction as the spherical growlers due to its shape and confinement exerts maximum pressure at the centre. The information regarding local pressure patterns are highly important while designing local structural components.

For FEM-SPH NQ1 analysis, the maximum pressure peak corresponding to area less than 0.01 m2 is around 5 MPa, however, the average pressures is only around 2.85 MPa. This confirms the fact that there exists high pressure peaks in small areas which are unpredictable and exibit maximum variation.

By principle, the structures designed based on shared energy concept must be exerted with lower pressure levels as both the structure and ice deforms in the collision process. The difference in the local pressure levels exerted on rigid structure and stiffened panel are not really significant. Remember, it has already been mentioned that the stiffened panel did not deform considerably and it behaves more or less rigid .

6.1.2.4 Envelope of Spatial curves:

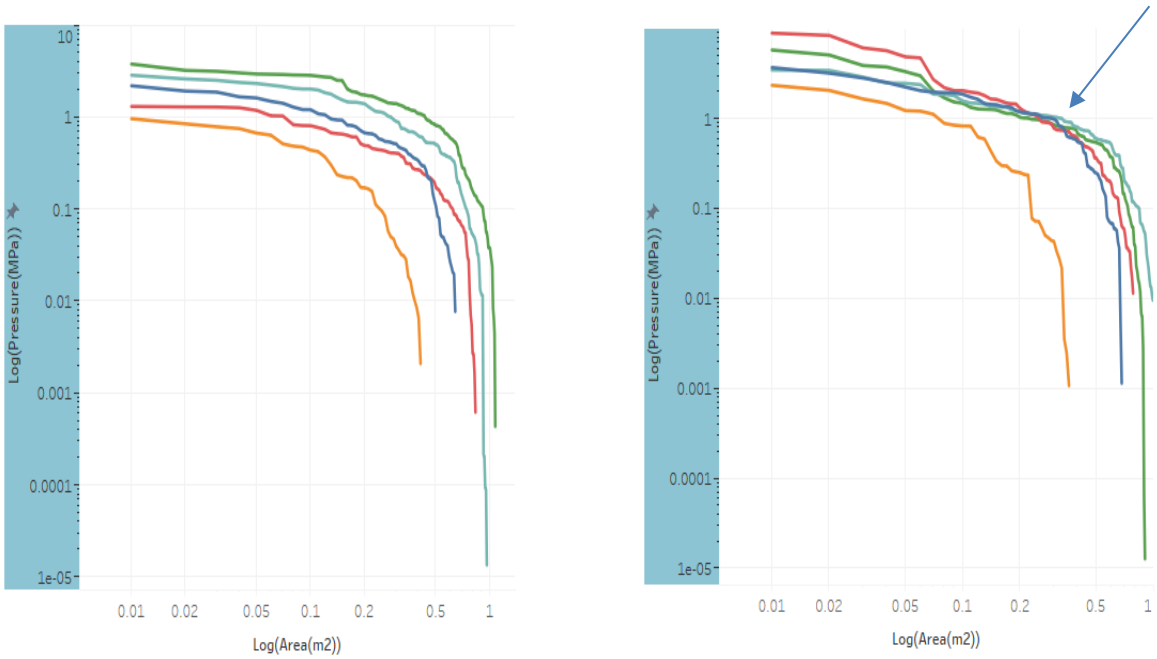

(a)Rigid structure analysis(FEM-SPH) (b)Stiffened panel analysis(FEM-SPH)

Figure 64 Spatial envelope curves-comparison between (a) Rigid Structure analysis (b) Stiffened Panel analysis

Figure **64** presents the log-log plot of envelope of spatial curves for ice-structure interaction using FEM-SPH NQ1 ice model. Curves in figure **64 a** represents the ice action against rigid structures and that in figure **64 b** represents the ice-stiffened panel collision. The curves are constructued using contour averaging method (CAM) technique, informative details regarding the construction of such curves can be referred in section **5.3.3.5.** As already mentioned, the most important characteristics of CAM curves are that they start from the highest pressures and gradually decrease. For the case of ice-stiffened panel analysis, one can notice the spatial curves in the region between 0.075 m2 and 0.5 m2, instead of following a smooth curvature as in the case of rigid structure analysis, gets bundled with each other. This peculiar behaviour might be attributed to the deformation of stiffened panel, as a result, low recorded pressures in that domain in comparisoin with the rigid structure analysis. This postulation seems to be reasonable, since the spherical growler has 1 m dia and good interaction between ice and structure is possible when the ice contact area with the structure is in between 0.075 m2 and 0.5 m2. Thus, the structural response can also be inferred from the behaviour of spatial curves.

6.2 COMPARISON BETWEEN STRENGTH, DUCTILE AND SHARED ENERGY DESIGN

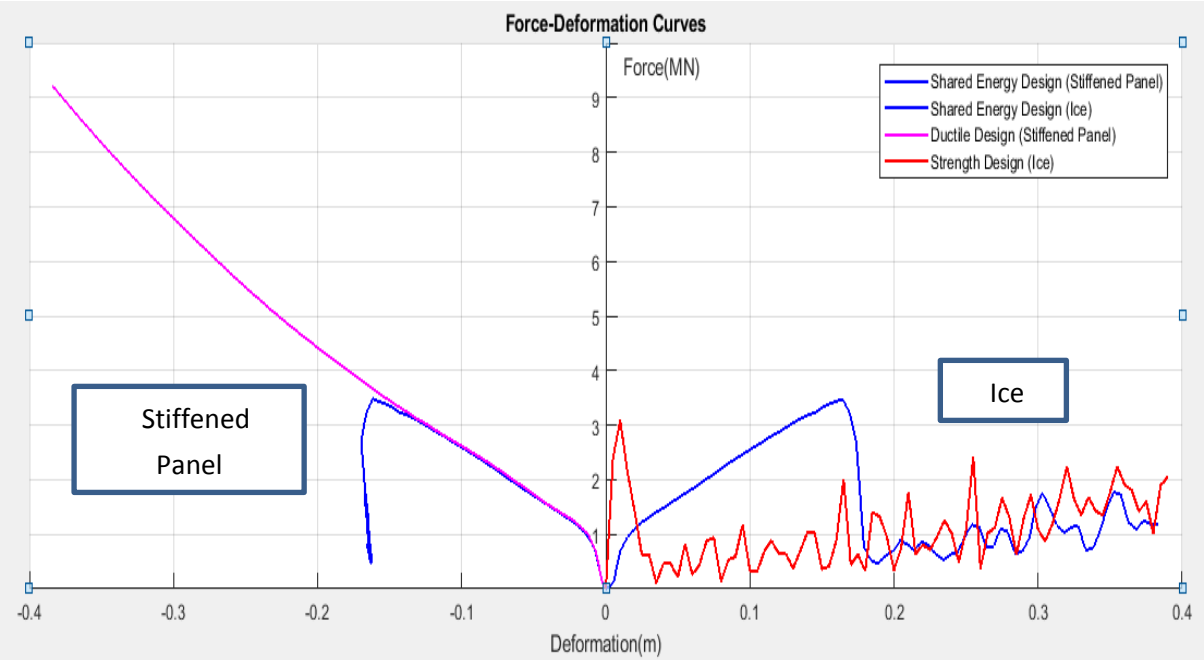

Figure 65 Comparison between strength, ductile and shared energy design for stiffened panel-ice floe collision

There exists three types of design conditions for analysing the collision scenarios. They are the strength design, ductile design and shared energy design analysis. Elaborate overview of these design conditions can be found in earlier sections**.** Here, the small ice floe used for strength design anlysis in chapter **5** is used here again for collisions with stiffened panels. The ice is modelled using FEM-SPH NQ1 technique and the ice is driven upto a distance of 0.4m.

In strength design, as discussed in previous chapter, the plate is made rigid and the ice is modelled as deformable, so only the ice is being crushed upto 0.4 m which can be seen in Figure **65.** In ductile design analysis, the stiffened panel is made deformable and on the other hand ice is modelled as rigid part. As a consequence, panel is the only entity that deformed and dissipated all the energy. From the plots it is seen that rigid ice deformed the panel to an extent of 0.4 m and the force is linearly increasing until the termination time.

For the analysis based on shared energy, both the ice and stiffened panel has been modelled as deformable such that both the objects deformed and dissipated energy in the collision process. This analysis resembles the real ice collision scenarios. Pictorial representations of all these three design conditions are given in Figure **66 a,b,c** respectively.

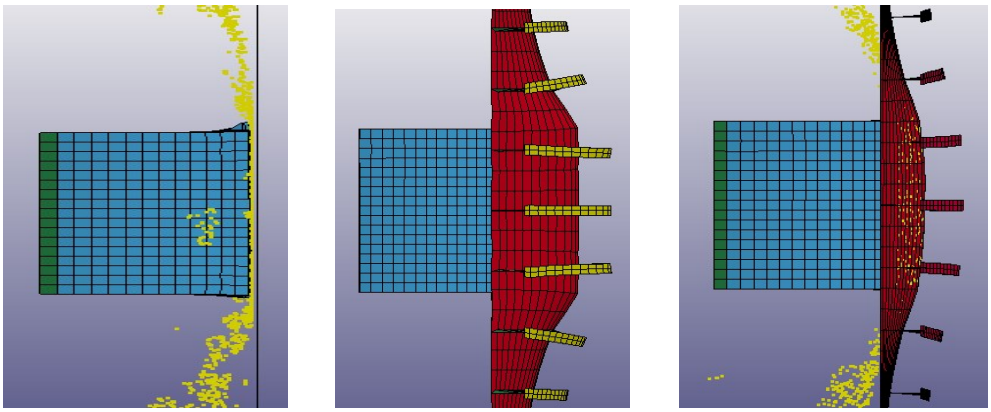

(a) Strength design (b) Ductile design (c)Shared Energy design

Figure 66 (a,b,c) shows the animation clicks corresponding to strength, ductile and shared energy design respectively

6.3 CONCLUSION POINTERS

The important facts from the analysis, results and discussions made in this chapter are briefly reitrated here.

- From the comparisons between strength design and shared energy energy analysis, it has been concluded that more force is exerted on the structure when more of the ice is crushed.
- The shared energy analysis yielded lower force levels since both objects are deformable. However, the difference between the force levels from strength analysis and shared energy analysis are not quite significant, since the stiffened panel did not deform significantly.
- The ice with failure strain parameters M=1 and N=0.5, is not strong enough to make sigificant impact on the stiffened panel. So the ice should be modelled much harder to cause extensive deformations.
- Variation of pressure levels during panel deformation can be clearly read from the behaviour of spatial curves
- Axial stiffness plays an important role in the deformation of the stiffened panel.

CHAPTER 7

This chapter begins with introducing two different proven techniques for the consideration of hydrodynamic effects in ice-structure interaction. The integrated analysis of ice-structure interaction has been conducted using different ice features against a FPSO side panel based on both coupled and decoupled approach. In addition, in this chapter, computation of external mechanics is performed through Liu's external mechanics codes, which is a matlab function file that was provided. The matlab input file for that Liu's code has been created and included in the Appendix section.

7.1 FINITE ELEMENT MODELLING CONSIDERATIONS FOR -ICE-STRUCTURE INTERACTION SCENARIOS

As stated earlier, the ship-ice or ice-offshore structure collision scenarios cause considerable structural damage to ships and platforms. So, there is a dire need to establish a method that can accurately predict the energy absorbed in the collision process. One of the most challenging work inherent in simulating the scenarios of this kind is to quantify the hydrodynamic effects triggered by the surrounding water. These hydrodynamic effects might induce some movements and motions to the floating structure before the actual impact which directly affects the response of the structure during ice collision and introduces some complexity.

In addition, some research observations were conducted by installing ice trackers on the surface of the ice bergs to monitor the drifting behaviour of the same. From this research, it was concluded that the ice bergs were rotating around its vertical axis on account of wind drag and unsteady water flow (Marchenko 2014). In this section, more emphasis has been laid regarding the inclusion of hydrodynamic effects in NLFEA performed in LS DYNA.

As of now, these hydrodynamic effects in a collision process are being captured by two methods known as the constant added mass method (CAM) and fluid-structure interaction method (FSI). In this section, the methodologies involved in these two methods and their relative merits and demerits have been discussed.

7.1.1 CAM method

In CAM method, surrounding water is modelled as constant added mass. As a result, the hydrodynamic effects can be evaluated using added mass coefficients. Minorsky(1959) derived a force-acceleration relationship for the case of ship collisions and proposed some added mass coefficients for the struck object. This value can be used for the ship-ice collisions as well. On the other hand, Wang et al(2002) and Zang & Suzuki(2006) used a coupled FEM analysis for determining the constant added mass in ship collisions (E. k. Ming Song 2016).

There are several limitations inherent with the CAM model that places the integrity of the fluid-body interaction analysis in question. M. Song et al(2016), in their research paper concluded that the added mass coefficients of the struck body changes with respect to the acceleration of that object. This acceleration in turn depends on the collision force level, a function that varies with time. This implies that the constant added mass value proposed by Minorsky(1959) holds good only for a collision process with shorter duration and will not give reasonable estimation for collisions with longer durations owing to the time varying nature of the coefficients. In addition, this method completely ignores the free surface wave effects, so it is not possible to

capture the instantaneous wetted surface of the bodies subjected to collision. Moreover, the motions of the striking object involved in the collision scenario is not taken into account, thus, the relative motion between the colliding objects cannot be simulated in CAM method. (E. k. Ming Song 2016)

7.1.2 Fluid structure interaction method

In the Fluid Structure Interaction method (FSI), the surrounding water contributing to the hydrodynamic effects in the collision process is modelled explicitly. Furthermore, in this analysis, the motions of the objects are also considered. There are many numerical methods that can be used in a FSI method for modelling the fluid, they are arbitrary lagrangian eulerian method (ALE), smoothed particle hydrodynamics (SPH), computational fluid dynamics (CFD) etc. FSI approach proved to be better and superior than the CAM method. (E. k. Ming Song 2016)

Even though many works dealing with ship-ice collisions had been carried out using FSI technique, those literatures lacked proper validation of their results. However, the research work on fluid-ice-structure interaction performed by S. Ming et al(2016) includes verification of the results with the experiments. Here, a brief outline of their work is presented, in order to have a clear picture of how FSI technique can be incorporated into a simulation software for the fluid-structure-interaction analysis. LS DYNA had been used for the simulations. The water and air were modelled using ALE procedure, the fluid characteristics were described using constitutive equations and equation of state (EOS). The lagrangian technique was used in modelling the ice and structure. In addition, a coupling algorithm was included which determines the coupling forces at the interface between fluid and structure. These coupling forces, in turn were added to the fluid and structural nodal forces computed using finite element method. The simulated results correlated well that of the experimental values. (E. k. Ming Song 2016)

Some important conclusions derived from this work were that the hydrodynamic effects influences the acceleration and oscillation period of the structure considerably. The motion of the structure and the contact force change significantly corresponding to the element size, whereas the viscosity does not affect the forces and motions predominantly. From these conclusions, it can be derived that that the modelling of hydrodynamic effects is mandatory in order to predict response similar to real ship-ice collisions. Moreover, the size of the elements must be chosen carefully while meshing the fluid, structure and ice in order to have precise calculation of the forces and motions. (E. k. Ming Song 2016)

Though ALE technique considered to be good for modelling fluid in many respects, it does not account for the drag effects and unsteady flow. As a result, the vertical rotation of the ice bergs due to unsteady flow and wind drag cannot be simulated in LS DYNA using ALE technique. Furthermore, this technique demands huge computational capacity and time.

7.1.3 Added mass considerations for decoupled and coupled collision approaches

In this thesis, for simulating ship-ice collisions, constant added mass (CAM) method has been used since the FSI technique is computationally more demanding. Collisions based on both decoupled and coupled procedures have been carried out. For decoupled approach, no added mass is considered since mass is not important in that case, whereas for the coupled collision simulations, it is mandatory to assign constant added mass to the ice. However, in the CAM method stated above, Minorsky(1959) proposed added mass coefficients only for the struck

object and not for the striking object. In all the collision cases considered in this thesis, the ice is the striking object. So, a constant added mass of 2% of the mass of the ice feature is assigned to it while performing coupled collision simulations. Same value of added mass is used for both the direct and oblique impacts. The reason for using the same added mass value is that the ice (striking object) is not oriented to any angles during the direct and oblique impact, only the ship(struck object) is inclined to certain angle during the oblique impacts.

7.2 FPSO-ICE COLLISION ANALYSIS

The concerned FPSO is called Sea Rose FPSO which operates in White Rose field. The details of the FPSO are listed below**.** (Wikipedia 2010)

Vessel details:

- Length – 258 m
- Beam - 46 m
- Draught – 18.043 m
- Displacement – 187100 tonnes

The FEM model of the FPSO side had been created as part of this thesis. The Sectional drawings of the FPSO were given, using which the side panel close to bow was modelled. The length modelled was 9.6 m and the vertical height is 19.6 m.

7.2.1 Modelling

As part of modelling, paper drawings were given. In order to make the finite element model with exact curvature as given in the plans, the Space claim software had been used. Firstly, the sectional curves were drawn using the space claim software by measuring the dimensions from the plans**.** Nextly, the coordinates were extracted from the Space Claim and transferred to GENIE to make the finite element model. The sectional curves are shown in Figure **67**

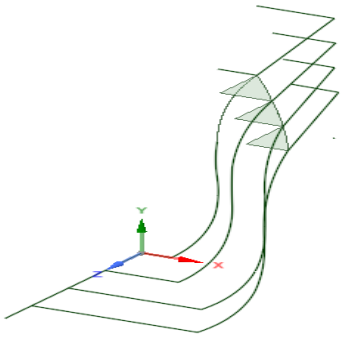

Figure 67 Sectional curves of the side model

In comparison with the original drawings, following simplifications are considered in the finite element model. These simplifications are detailed here

- The frames in the non-ice strengthened region were actually designed as Bulb profiles in the plans. The FE model is constructed using thin shell elements, so it is hard to create bulbs using thin shell elements. So instead of bulb profile, L-shaped frames have been created in the non-ice strengthened region.

The GENIE model is transferred to LS DYNA for the analysis. Figure **68** shows the different views of the model in LS Prepost version.

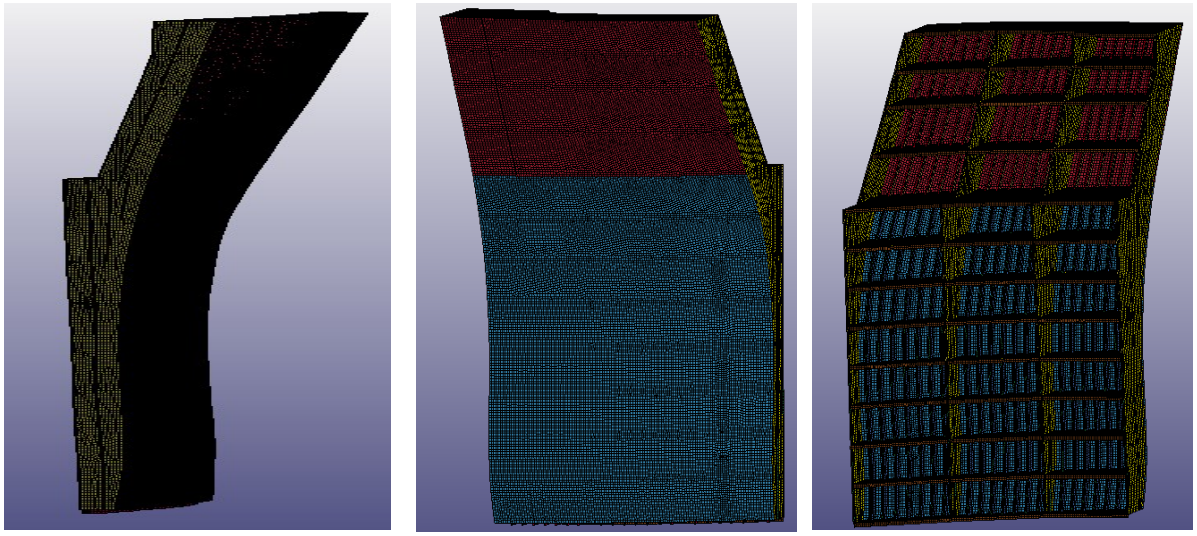

(a) (b) (c)

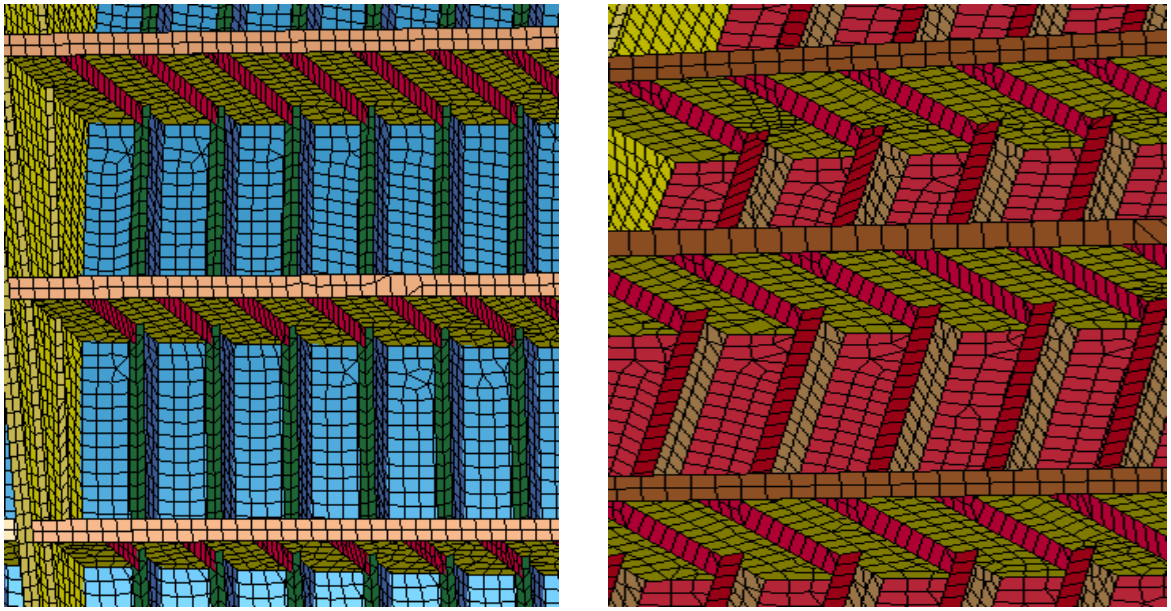

(d) (e)

Figure 68 (a,b,c,d,e) shows different views of the FPSO side FEM model

Using the above FEM model, side panels of two different strengths had been created by varying the thickness of its structural members. Table **13** shows the thickness of each of the structural members. Strength 1 column presents the default thickness of the panel members, i.e the thickness as given in the plan drawings. Strength 2 column shows the reduced thickness of certain members.

Ice Strengthened Region	**Strength 1**	**Strength 2**
Outer Plate	35 mm	22 mm
Frames :		
Web	18 mm	16 mm
Flange	11 mm	10 mm
Frame spacing	400 mm c/c	400 mm c/c
Girders	12.5 mm	11 mm
Girder Stiffeners	16 mm	16 mm
Girder Flanges	25 mm	25 mm
Stingers	12.5 mm	11 mm
Stringer Stiffeners	14 mm	14 mm
Above Ice Strengthened Region		
Outer Plate	31.5 mm	18 mm
Frames:		
Web	17 mm	14 mm
Flange	11 mm	9 mm
Frame Spacing	400 mm c/c	400 mm c/c
Girders	12.5 mm	11 mm
Stiffeners in Girders	16 mm	16 mm
Stringers	12.5 mm	11 mm
Stiffeners in Stringers	12.5 mm	12.5 mm

Table 13 Thickness of the structural members of FPSO

7.2.2 Decoupled Collision Approach

In this section, the decoupled approach has been used extensively for simulating the collision scenarios. Based on the principles of decoupled approach, the integrated analysis of the FPSO and ice berg can be carried out by separating the analysis in two different parts (external and internal mechanics). Decoupled approach works in the following way. Firstly, the external mechanics can be evaluated through Liu's(2011) simplified external mechanics codes. The results from the external mechanics represent the demand for energy dissipation. The demand for energy dissipation represents the maximum extent of deformation that can be expected in a structure.

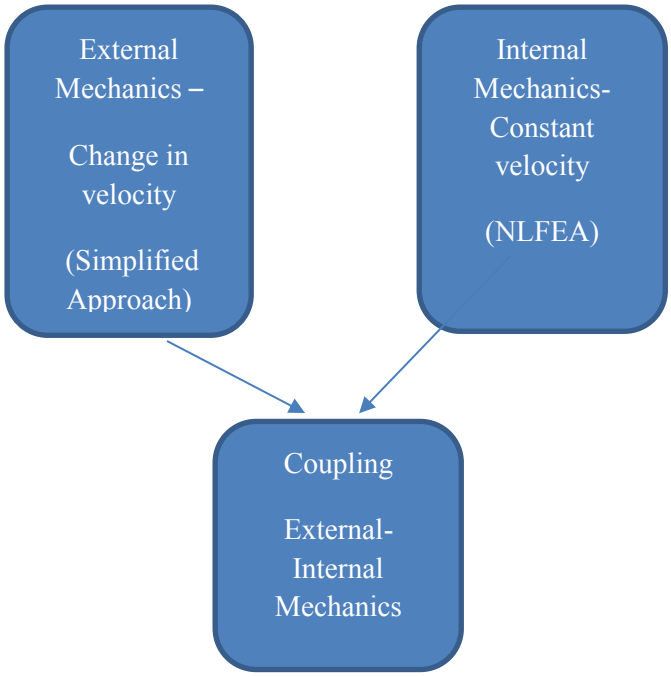

Figure 69 Flowchart showing the procedure followed in decoupled approach

On the other hand, the internal mechanics can be simulated through NLFEA approach in LS DYNA. It is performed by driving the ice with constant velocity against the structure and the deformation extent of the structure can be studied until termination time.

After analysing each of them separately, the strain energy output from the external mechanics which represents the maximum expected deformation is coupled with the internal mechanics analysis. Figure **69** shows the flow chart of the procedure followed in decoupled approach, here the coupling between the external and internal mechanics is carried out manually.

7.2.2.1 Results and Discussion

7.2.2.1.1 Modelling of hard ice:

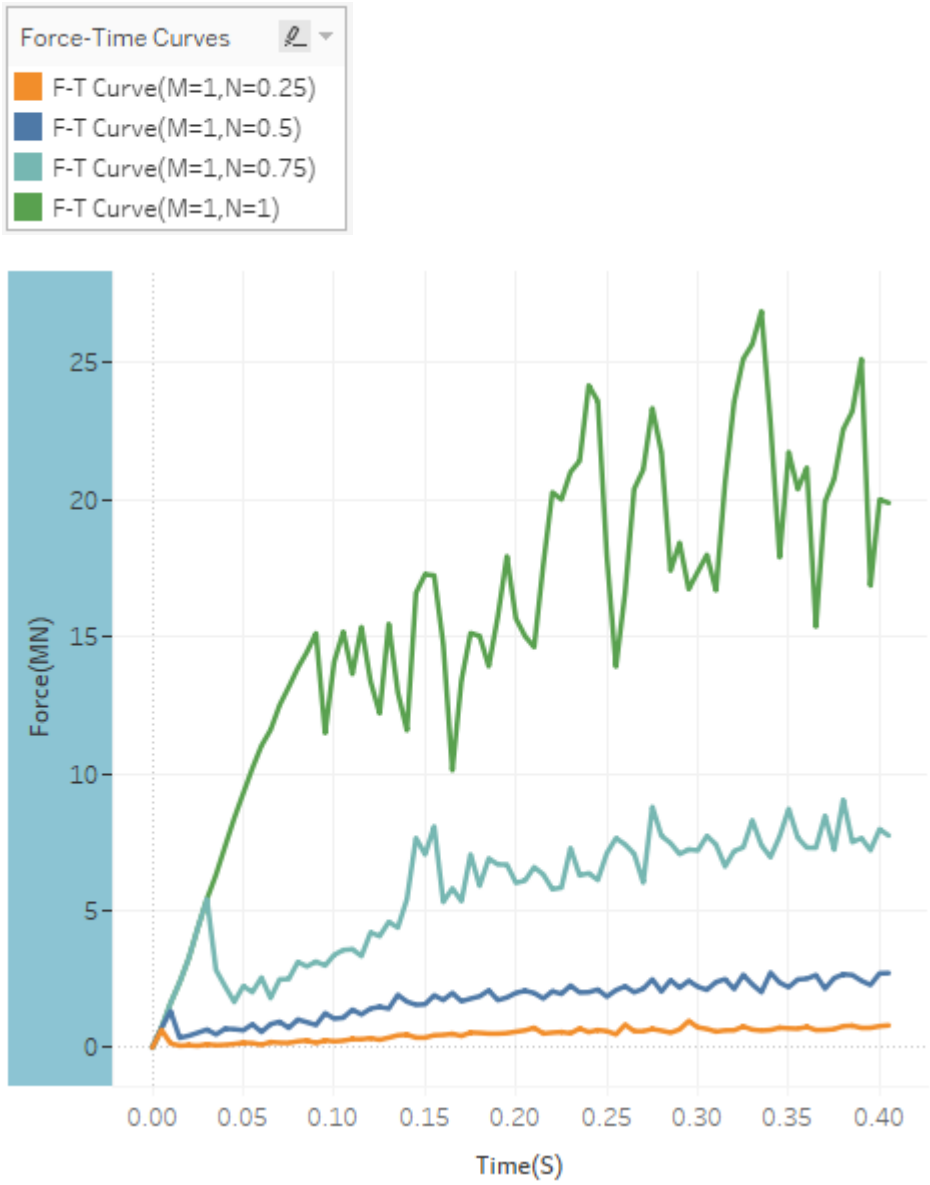

Figure 70 Force-Time curves correspomding to ice models of different strength

From the analysis performed on stiffened panels in the previous section, it is evident that the ice model with ice properties and parameters related to kim's failure strain equation (M=1 and N=0.5) lack strength to cause considerable deformation on the stiffened panel. Since, in this section, the FPSO panel is analysed against accidental loads, it becomes mandatory to use an ice model that can cause significant damage to ship structures. Kim(2014) suggested that the ice can be modelled by varying the values of anyone of the failure strain equation parameters(M or N). In other words, either the N values can be increased or values of M can be decreased. In

this current study, the former approach is used, four different runs has been simulated by varying the values of N (0.25,0.5,0.75,1) and on the other hand setting a constant value to M=1. The failure criterion of this elastic-plastic ice model states that when the equivalent plastic strain of ice elements reaches the value of failure strain, erosion/failure of elements occur. So the main idea of this hard ice modelling approach is that by increasing N, the failure strain of ice gets increased, therby the range of the plastic limit of ice also increases. In other words, the distance in between the elastic limit and the failure point which is the plastic domain increases. As a result, the ice elements behaves more plastic(ductile) before reaching the failure strain and exerts more forces on the structure. In addition, the ice can also be made hard by manipulating the values of initial strain but it is strongly not recommended to do so, as it might lead to numerical instability.

Four simulations are conducted by colliding the ice floe against the FPSO panel with a constant velocity of 2m/s until the termination time of 0.4 s.

Four different Force-Time curves are presented in Figure **70,** each curve corresponding to different values on N and M=1. The force exerted on the structure during ice interaction mainly depends upon the strength of ice and crushing distance. N=0.25 yielded negligible deformation of side panel and recorded minimal force levels. It can be termed as soft ice and it is unfit for usage in accidental design analysis. N=0.5 which had already been used in previous chapters produced around 0.04 m deformation in ship side and it yielded marginally higher forces than the initial run.

Deformation of plates were clearly visible in the case of N=0.75 and it produced force levels upto 8 MN. Finally, the run using M=1 and N=1, resulted in initial 0.2 m deformation of side panel and then the ice started to crush thus recording maximum force peaks upto 25 MN, which can be seen in Figure **70.** For accidental load analysis, the ice must be modelled in such a way that it must produce maximum deformation on the ship structure and in addition the ice must also crush during its interaction with the structure. Since the ice model with parameters (M=1 and N=1) satisfies the above criteria, it is chosen as the hard ice that can be used in the analysis of response of ships against accidental ice loads.

Before commencing the simulations, the pressure area relationship of this hard ice is compared with analytical curves in order to study the extent of pressure that is distributed on the structure. For this analysis, a rigid plate of 10*10 m is designed and the ice floe is collided against it. The rigid plate is discretized with elements of size 0.1 m, the model setup is shown in Figure **71.**

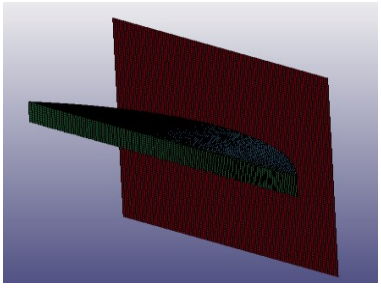

Figure 71 Model setup for verifying the hard ice model

Figure **72** compares the P-A curve corresponding to the hard ice with that of the ISO pressure curves. In Chapter 5, all the ice models with failure strain parameters (M=1,N=0.5) yileded

pressures considerably lesser than the ISO curve, since the latter is considered as the most conservative design estimate till now as far as strength design is concerned. However, the pressures corresponding to the hardest ice surpasses the ISO curve by a significant margin. In addition, the probability of ALS ice action is around 10^-4 and ULS ice action is 10^-2 (Amdahl 2017), and this hard ice P-A curve seems to represent very well the ALS ice action probability(10^-4) and the corresponding ALS P-A curve shown in a previously mentioned figure for ALS ice actions (please refer Figure **16**). Moreover, it is evident from the plots that there could be many high pressure peaks, since the process P-A is the average of all those pressure peaks. Thus, it can be approximated that the hard ice (M=1,N=1) could be the apt choice for accidental collision analysis.

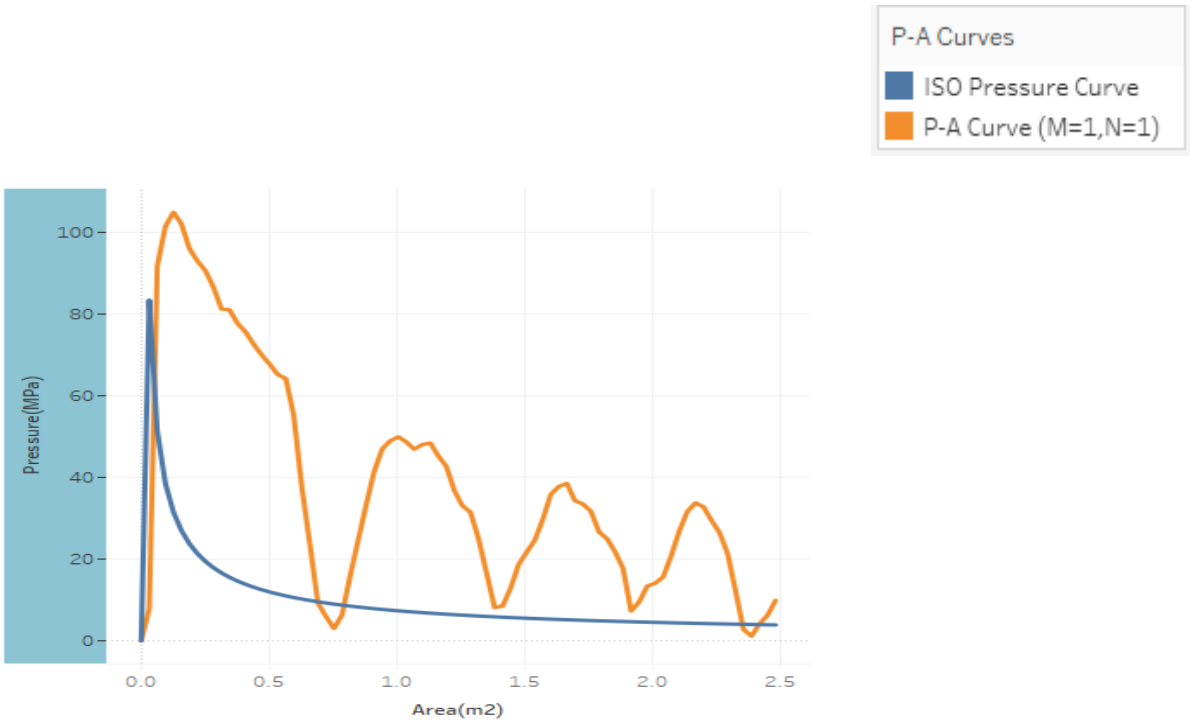

Figure 72 Process P-A relationship for the hard ice(M=1,N=1)

7.2.2.1.2 Impact assesment using different ice features:

In all the simulations conducted here, the ice had been modelled using FEM-SPH NQ 1 technique, so after the erosion of each ice element, one SPH particle will be generated. The impact location is at the ice-strengthened region.

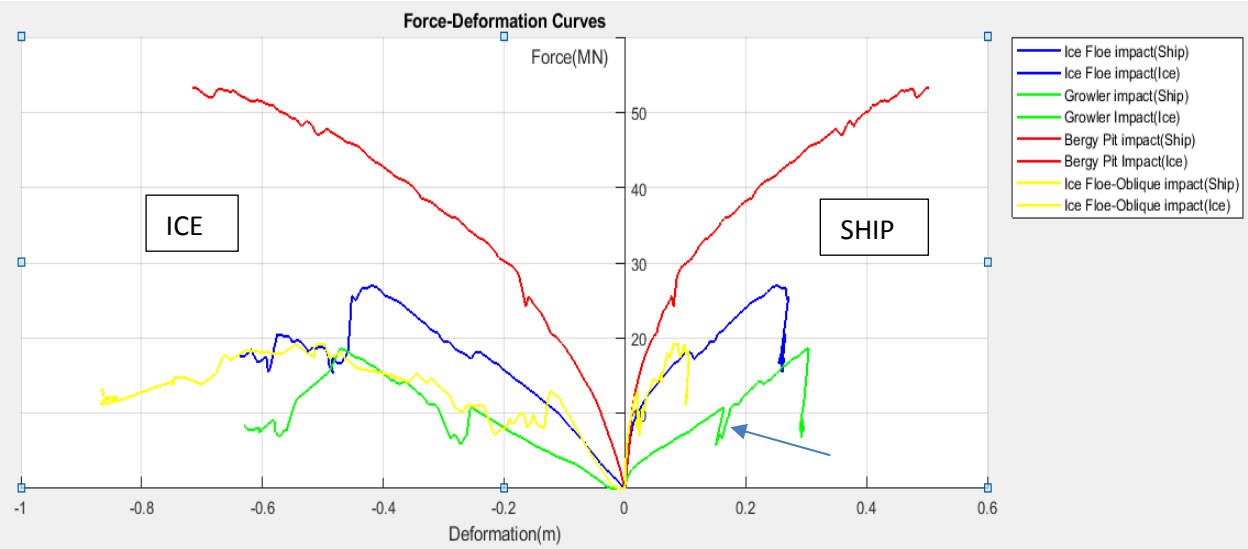

Figure 73 Force-Deformation curves corresponding to different ice features and impact cases

Using decoupled approach, four different runs have been simulated and displayed in Figure **73**. First three runs correspond to different ice types and the fourth run represents the oblique impact performed using ice floe. Positive X-axis shows the ship deformation and the negative X-axis presents the deformation of ice. Here, the internal mechanics (deformation of both ice and structure) is analysed first. Then finally, the force-deformation curves are limited based on the strain energy output from simplified external mechanics.

Damage extent for both ice and the ship panel for the case of ice floe impact is displayed in blue line. The simulations were run for 0.4s with a contant velocity of 2m/s. Within that time span, around 0.62m of ice floe is crushed and the panel attained a deformation of 0.28 m. The contact area of ice floe on structure increases with increase in the crushing distance. Green line in the above figure represents the 2m dia growler impact. Growlers, though smaller in size when compared with the ice floe, produced significant localized deformation on the ship structure due to its better confinement, geometry and narrow impact area. It is apparent from the plots that the growler impact resulted in higher deformation on ship side in comparison with ice floe impact. However, the force levels are lower because of its localized impact on the structure. In addition, it can be seen in the plots that there is a sudden drop in force after reaching deformation of around 0.08 m signifying that the side panel is exerting some resistance and then load increases again immediately. This phenomenon is an attribute of the material non linearity, since the material model used for steel in LS DYNA is POWER LAW PLASTICITY which do accounts for the isotropic hardening. Let us discuss the condition of isotropic hardening briefly and analyse its behaviour in this case. The materials, after attaining a certain limit of plastic deformation consists of many dislocations at micromechanical level. These dislocations start to interact with each other, thereby the material is hardened and thus larger stresses are required (people.brunel.ac.uk n.d.) for further plastic deformation of the material. More specifically, for the case of isotropic hardening uniform expansion of yield

surface in all directions in stress space can be witnessed (Emayavaramban E 2015). By virtue of isotropic hardening behaviour, steel after deforming to a certain limit, attains hardening and demands more stress for further deformation. The increase of force immediately after the drop in force signifies that the steel material started to crush the ice again, as the steel material attained more strength due to hardening. In the plots, this hardening behaviour is shown using pointer arrows. As per the principle of material non linearity, this sudden drop and consequent increase of force occurs till the material fractures. Not only the grolwer impact, but all the simulation cases exhibited isotropic hardening behaviour as well, which is evident from the curves.

The oblique impact using ice floe is performed by orienting the ship side to an angle of 70 degree. The oblique impact did not cause much deformations to ship side in comparison with the direct impact which can be seen from the yellow line in Figure **73.** A valid reason is that the contact area of ice that interacted with the structure is less because of orienting the ship structure. One peculiar thing noted in oblique impacts is that more ice elements are crushed though the contact area is smaller. One valid postulation is that in oblique impact frictional forces come into play. In this ice model, it is supposed that the frictional force increases the pressure, thereby the failure strain of ice elements gets reduced, as the U-shaped failure curve is a function of N.p2. Consequently, more ice elements are eroded due to the reduction in the failure strain.

Of all the ice types that have been used for the simulations, tabular bergy pit rendered maximum deformations (0.5m) on the ship side. On account of its wide and uniform rectangular contact area, it induced maximum compression on the structure. Tabular bergy pit impact recorded a maximum force upto 55 MN at the termination time. This is quite high and it is concluded that tabular shaped ice might be considered as a good choice for the analysis related to accidental ice impacts.

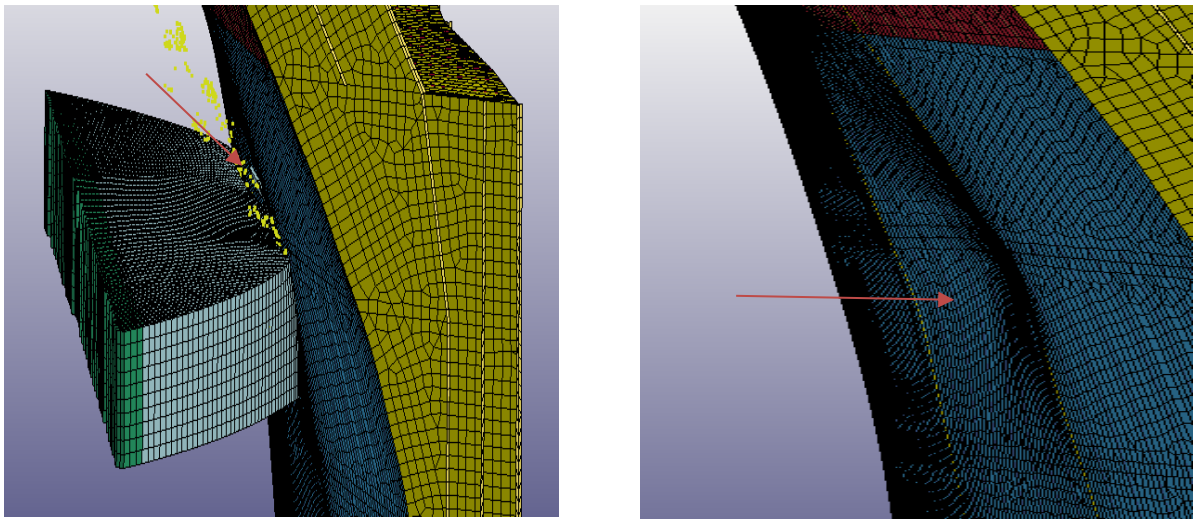

(a) Ice floe impact (b) Frontside damage

Figure **74 (a,b.c)** Shows series of figures representing the damage extent caused by ice floe impact on the front and backside of the structure. It is visible from the pictures that the strong ice deforms the outer shell plating considerably and the ice is being crushed and SPH particles generated as well. The ice floe impact activates different failure modes of the steel structure which can be seen in figure **74 c** that shows the damage on the backside.

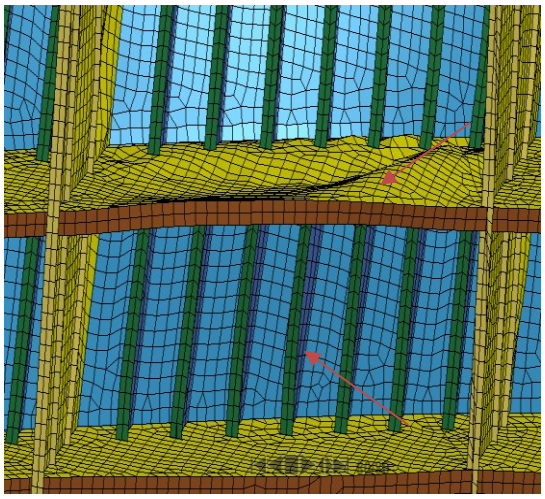

(c)Impact extent on backside

Figure 74 (a,b,c) presents the animation clicks of the ice floe impact along with the front side and backside damage extent

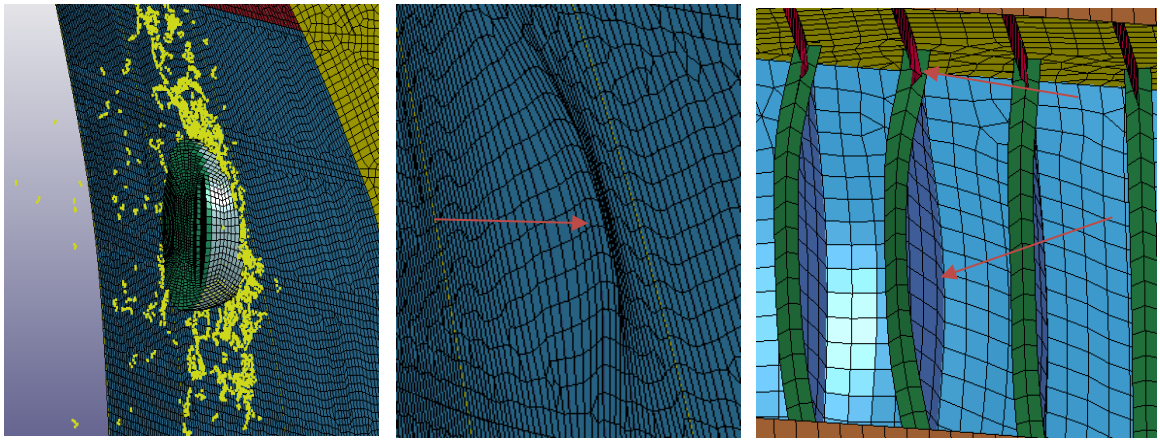

(a)Growler collision (b) Frontside damage (c) Backside damage

Figure 75 (a,b,c) shows the grolwer impact along with the frontside and backside damage

Figure **75 a,b,&c** displays series of figures showing the structural damage caused due to growler collision. Spherical growler, though smaller in size, created significant localized displacement on the outer shell plate. From the backside damage picture, tripping of T-shaped frames and buckling of stiffeners beneath the girder plates are visible. The extent of tripping of frames seemed to be high in the case of growler impact than that of ice floe collision, owing to the spherical impact geometry of spherical growler.

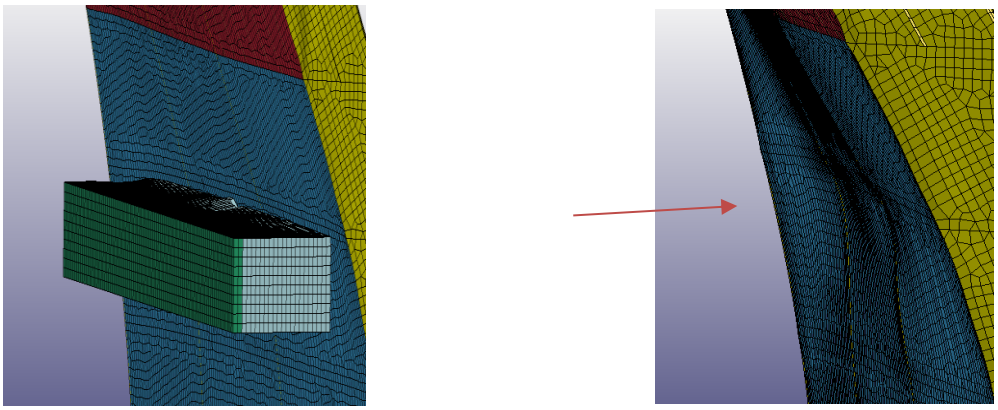

(a) Bergy pit collision (b) Frontside damage

Figure 76 (a,b) illustrates the bergy pit collision scenario along with the front side damage extent

Figure **76 a&b** presents the tabular bergy pit impact and the consequent frontside damage on the structure. As previously mentioned, tabular bergy pit caused the maximum deformation of the outer shell in comparison with the impacts made using other ice features.

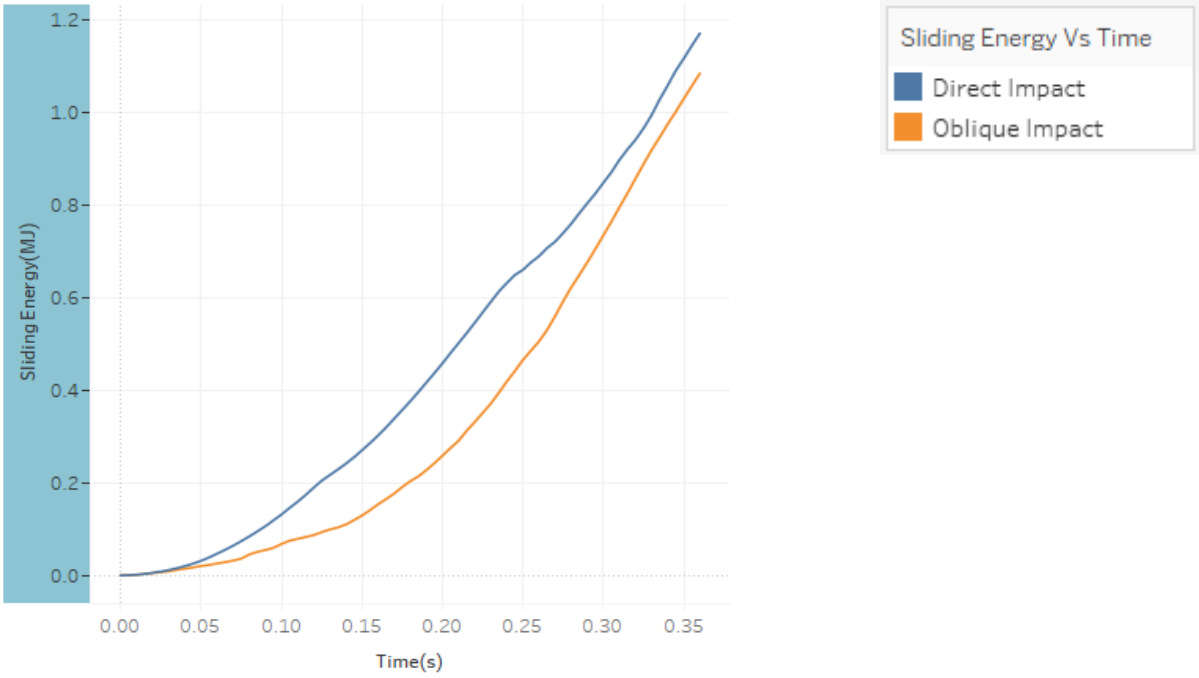

Figure 77 Plot showing the siding energy as a function of time for direct and oblique ice floe impacts

The main intention for conducting the oblique ice collision by orienting the structure is to simulate the sliding of ice. However, the ice did not actually slide in the simulations. It is even more apparent from the sliding energy plots shown in Figure **77.** The sliding energy dissipated from the oblique ice impact is lesser than that of the direct impact. The low sliding energy for the case of oblique impact is quite unrealistic as in actual sliding impact scenario more energy is dissipated in the form of sliding energy in comparison with direct impacts. However, the trend is opposite in the plots shown above, because the ice is pushed with a constant velocity and, as a result it gets crushed instead of sliding. Thus, it is deduced that the decoupled approach, though a better technique in analysing the structural response during accidental

loads, must not be used to simulate sliding of objects.

Till now, detailed analysis of both the ice and structural response have been studied just by considering the internal mechanics alone. In decoupled method, the ice is imparted with a constant velocity of 2m/s and driven against the structure until the termination time of 0.41s . However, in reality, the ice features do not collide against a structure with constant velocity, the velocity of the striking object reduces after the impact in real collision scenarios. The external mechanics code developed by Liu assumes that the ice is stopped after the impact. Thus, it is necessary to couple the output from external mechanics with the simulated internal mechanics to give the force-deformation relationship that could represent the actual ice collision events. The external mechanics code gives one value of strain energy which signifies the total energy dissipated in ice collision, the force and deformation corresponding to this value of strain energy is read from LS DYNA (NLFEA) and then the f-d curves are limited. Figure **78 a, b & c** show the f-d curves limited using the strain energy output from Liu's external mechanics codes for the cases of direct ice floe impact, growler impact and oblique ice floe impact respectively.

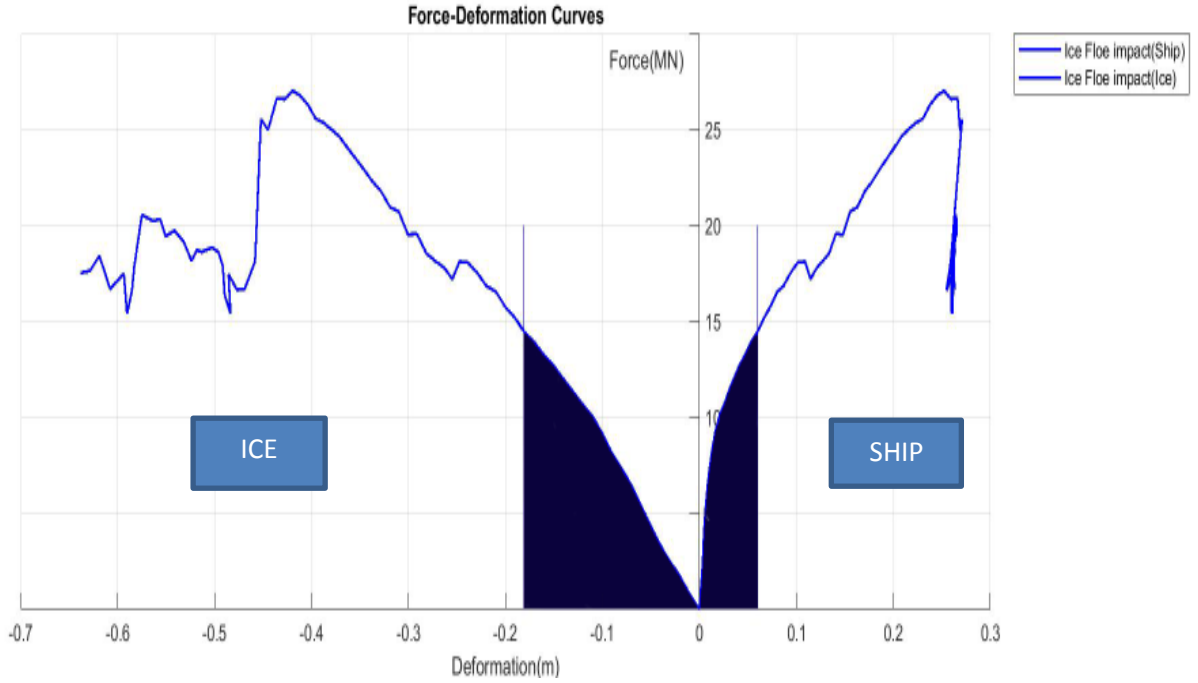

(a) Limited F-D curves based on EM output for the ice floe impact case

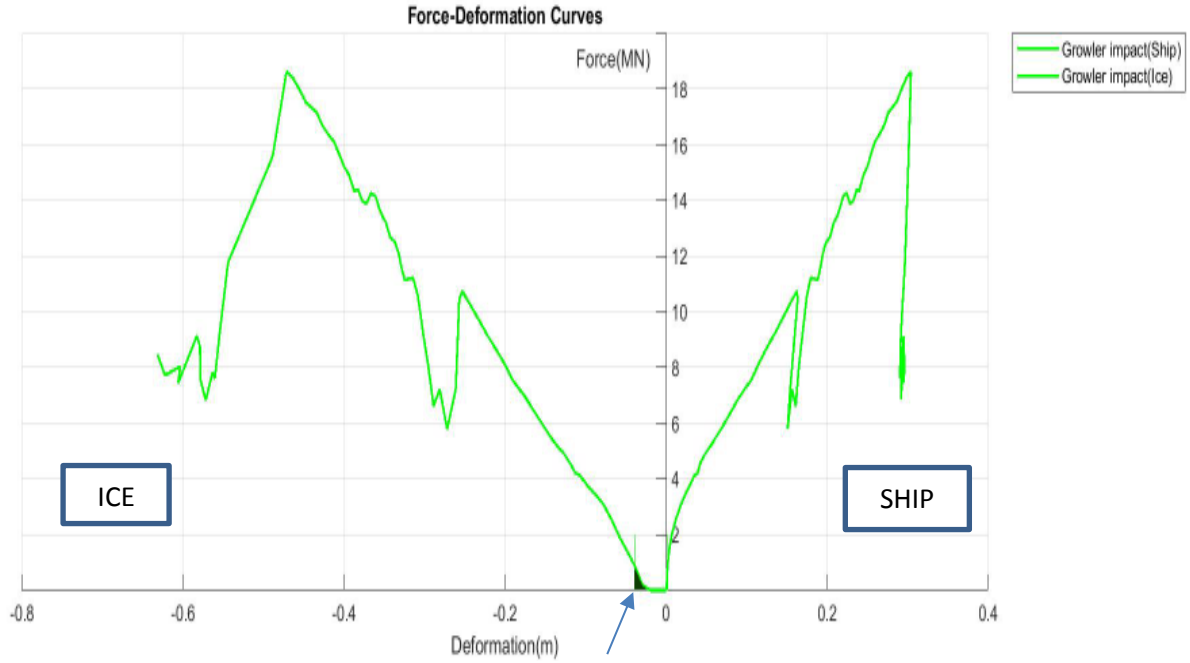

(b) Limited F-D curves based on EM output for the growler impact case

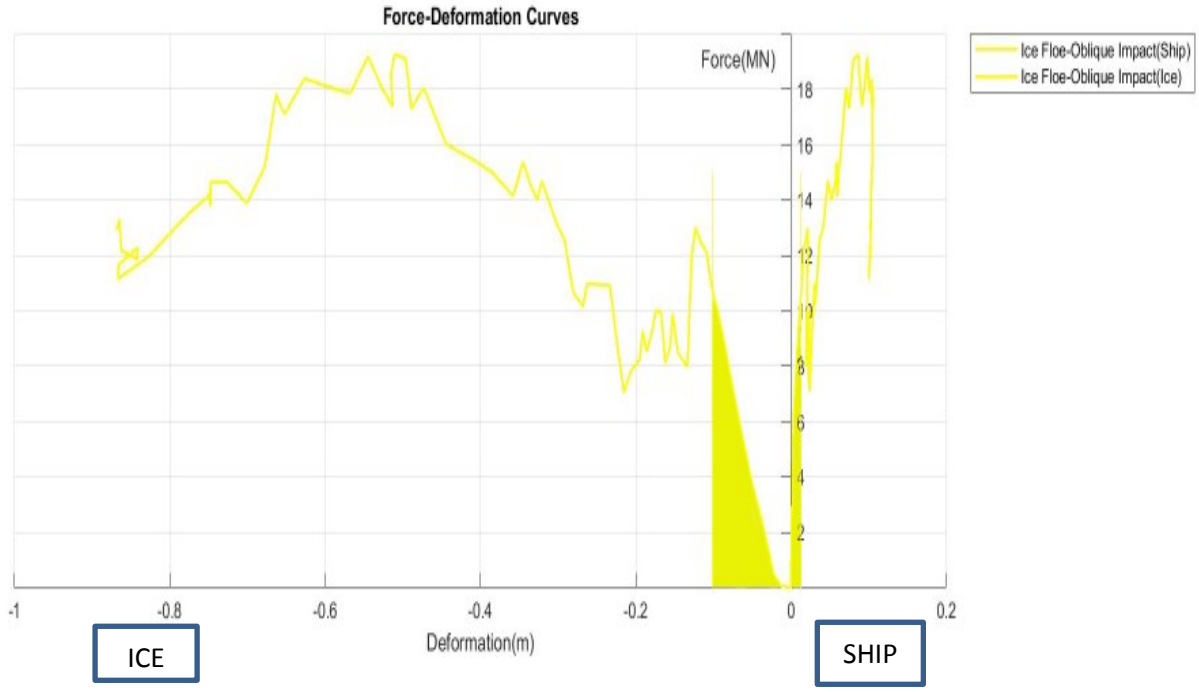

(c) Limited F-D curves based on EM output for the ice floe-oblique impact case

Figure 78 (a,b,c) presents the F-D curves limited using the strain energy output from external mechanics

The ship panel displacement and crushed distance of ice are shown separately. The area under the highlighted force-deformation curves in both the ship side and ice gives the amount of energy dissipated in the collision. Since the f-d curves are limited using the output from external mechanics, it follows that the dissipated energy from the highlighted area represents that the ice is completely stopped after the collision and the impact is purely plastic. The energy dissipation can be computed using the formula

$$E = F*x1 \text{ (Ship Panel)} + F*x2 \text{ (Ice)} \quad \text{[energy from limited f-d curves]}$$

Where E is the energy dissipated, x1 is the ship side panel displacement and x2 represents the ice deformation.

Using the equation stated above, the actual energy dissipated from the ice floe collision with a velocity of 2m/s is around 1.445 MJ. Similarly for growler impact, dissipated energy is around 0.012 MJ. The collision using 2 m dia growler caused a negligible amount of energy dissipation which is shown using pointer arrows in Figure **78 (b)**. For oblique ice floe collision, around 0.654 MJ of energy is dissipated. This value represents the total dissipated energy. In addition, the force and deformation magnitude inside the highlighted area represents the actual force levels exerted when an ice feature moving with a velocity of 2 m/s makes a purely plastic impact with the structure and is stopped after the collision. The deformation under the highlighted area denotes the maximum expected deformation, since they are based on the external mechanics output.

Previously, from the strength design analysis performed in chapter **5**, it has been concluded that ice in addition to dissipating strain energy, also dissipates sliding, damping and hourglass energies. However, the major contribution to the force value comes from the strain energy dissipation whereas the other energies (Sliding & damping) contribute relatively minor share

to the force levels. Furthermore, hourglass energy contributes negligible amount to the total share. Therefore, it can be concluded that the total dissipated energy consists of strain, sliding and damping energy components. Here, the contribution from hourglass energy can be ignored due its negligible value and more importantly it does not have any physical significance.

The f-d curves belonging to tabular bergy pit impact has not been limited using external mechanics output, because the simplified code assumes that the ice object is circular shaped and more importantly the added mass coefficients and gyration radius for a rectangular shaped object could not be found.

7.2.2.1.3 Thickness effect in collisions:

As already stated, FPSO side panels of two different strengths have been created one with the default thickness and another with reducing the thickness of certain structural members, the details of which can be seen in Table **13.** The intention is to study the role of thickness in accidental collisions. Using the three ice features (ice floe, growler and bergy pit), direct collisions against the strength 2 FPSO panel have been simulated and compared with the collisions against strength 1 side panel. Figure **79** shows the F-D curves of six cases mentioned in Table **14** below

Figure **79 (a)**	Case 1	Strength 1 Side panel	Ice Floe Impact
	Case 2	Strength 2 Side Panel	Ice Floe Impact
Figure **79 (b)**	Case 3	Strength 1 Side panel	Growler Impact
	Case 4	Strength 2 Side panel	Growler Impact
Figure **79 (c)**	Case 5	Strength 1 Side panel	Bergy Pit Impact
	Case 6	Strength 2 Side panel	Bergy Pit Impact

Table 14 Simulation cases

Internal mechanics study deals with the analysis of deformation of both ship and ice. Since in this section, the main motive is to study the extent of deformation with respect to thickness. Only the internal mechanics have been analysed.

Figure **79** has three plots **a,b,c** each representing the collision simulations using ice floe, growler and bergy pit respectively. The continuous lines represent the strength 1 panel and dashed lines represent the other. From all the three plots presented above, one common trend observed is that the panel of strength 2 (weaker panel) yields lower force levels in comparison with that of strength 1. In addition, the panel corresponding to strength 2 seems to have larger displacement and comparatively the ice is crushed less for all the three cases.

The same trend was seen from the animations in LS DYNA that the strength 2 panel deformed more and thereby the ice was crushed less in comparison with what was observed from the animations corresponding to strength 1 panel.

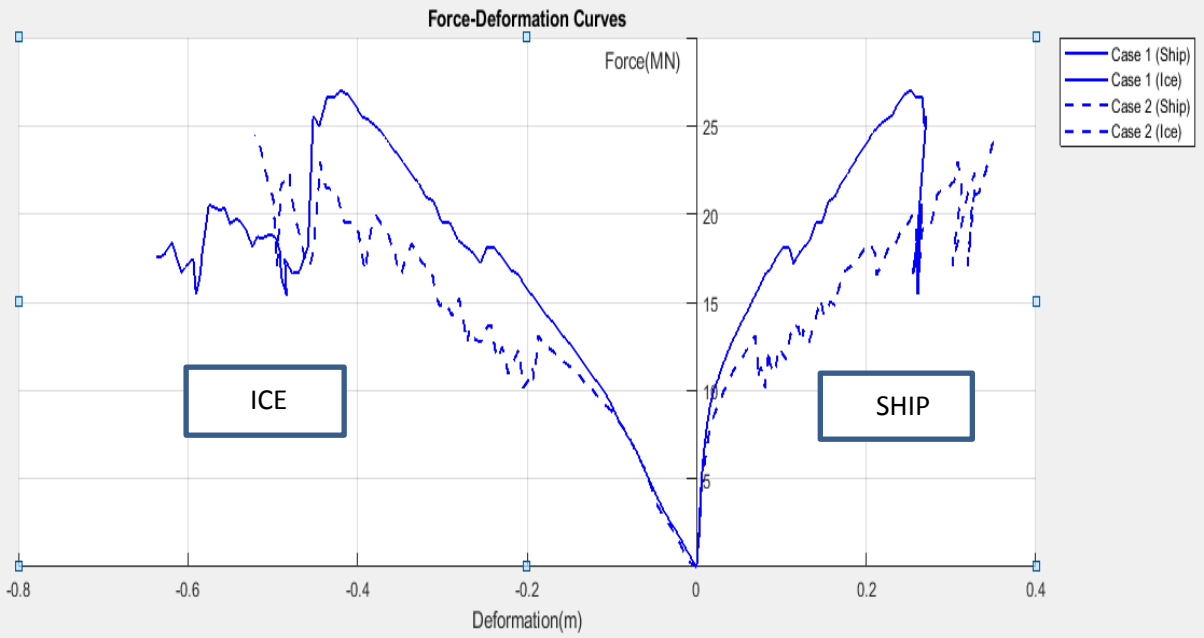

(a) Force-Deformation curves of the ice floe impact against strength 1 and strength2 side panels

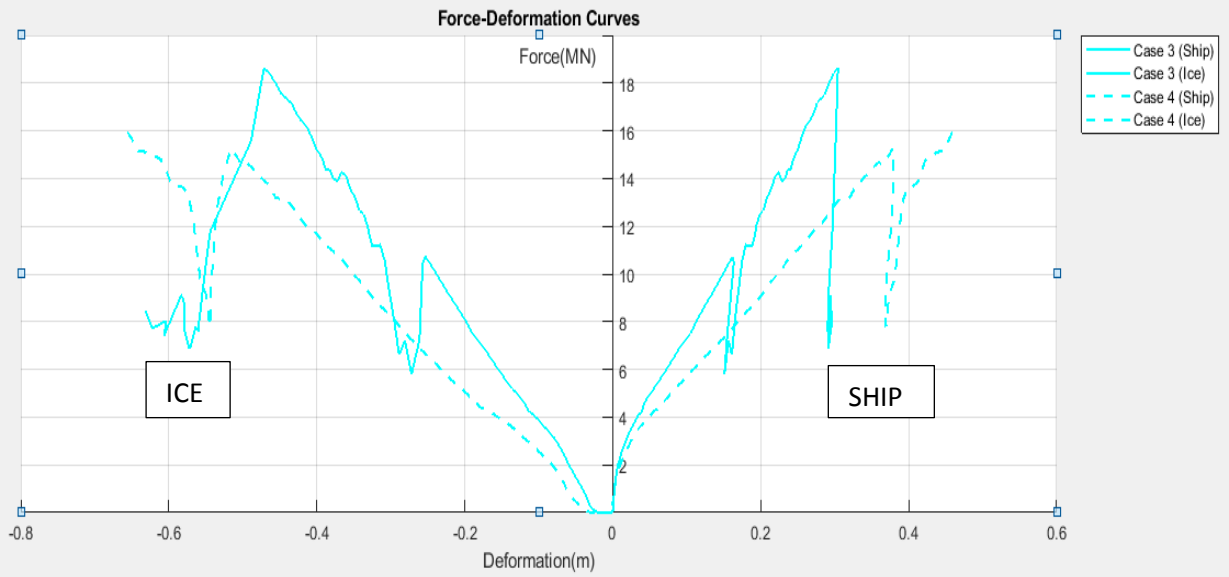

(b) Force-Deformation curves of the ice growler impact against strength 1 and strength2 side panels

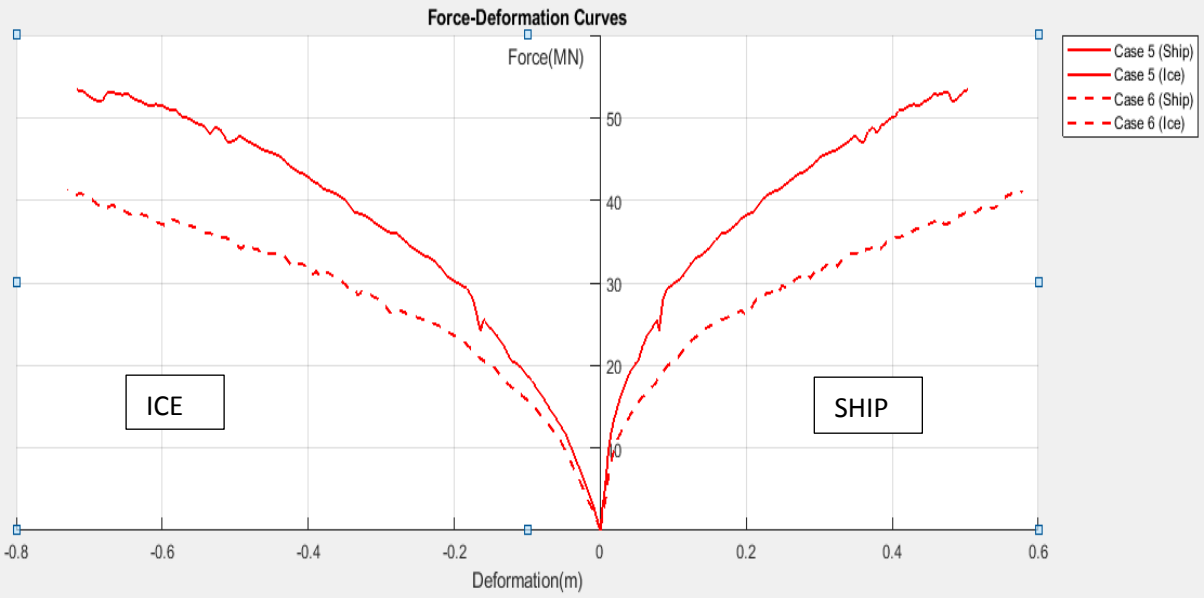

(c) Force-Deformation curves of the tabular bergy impact against strength 1 and strength2 side panels

Figure 79 (a,b,c) Force-Deformation curves for the impact cases of three ice features against side panels of different strengths

In general, the force exerted on the structure depends on structural strength, strength of ice and crushing distance. In other words, for a specific ice strength, the more the ice is crushed, the more force it exerts on the structure owing to failure of ice elements and in addition wider part of ice comes in contact with the structure thus contributing to more force. The weaker panel crushed the ice slightly less when compared with the stronger panel which could be the reason for exertion of lower force levels in weaker panel. For example, take the case of growler impacts shown in Figure **79 (b),** panel deformed to a limit of 0.45 m which is 0.15 m higher than the strength 1 panel, and the force levels on strength 2 panel are lower. In strength 1panel, slightly more ice is crushed and furthermore the contact area of growler increases with the crushing distance owing to its spherical geometry, thereby producing higher forces on structure. In the case of strength 2(weaker) panel, the side panel deformed more and lesser quantity of ice is crushed, so the contact area is not large as in the strength 1 case to produce high force levels and in addition lower force contribution from less quantity of crushed ice elements. The peaks and troughs in the load curve represents the crushing of ice elements, it can be inferred from the graph that there are relatively few peaks and troughs for the case of ice impact with weaker panel when compared with the stronger panel. These are the valid reasons for the lower force levels and higher displacement of side panel for the case of Strength 2 analysis. To summarize, the structure with reduced thickness yielded 16% lower force levels than the stronger structure.

The impact activated different failure modes in the weaker panel. Of all the deformation modes, it has been noticed that the tripping of frames happened to be extensive in the weaker panel. It could be due to the following reasons. In T-shaped frames the flange is located far from the plastic neutral axis and moreover, in this structure the ratio of web length to web height is high so the frames are subjected to maximum shearing and finally ended up in tripping. It can also be seen from the plots that the structure exhibited isotropic hardening behaviour in all the collision cases.

From the plots it can be inferred that reducing the thickness of the structures will yield lower force levels during accidental ice impacts. Therefore, one cannot come to a conclusion that reducing the thickness is a better design perspective, since the sections with reduced thickness are more prone to fracture which is explained using the following figures.

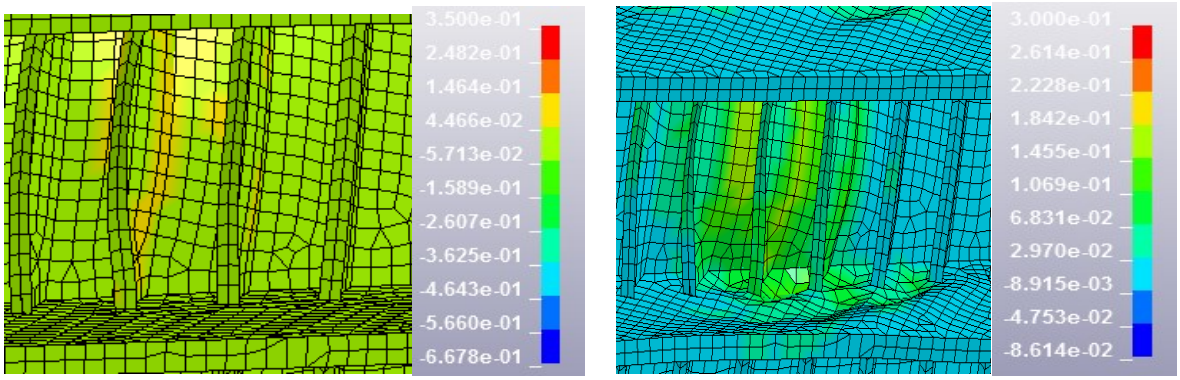

(a) Strength 1 side panel (b) Strength 2 Side Panel

Figure 80 Effective plastic strain animation plots for ice growler impact (a) Strength 1 side panel (b)Strength 2 side panel

Figure **80 a, b** presents the effective plastic strain levels of the two panels with different strengths. The maximum plastic strain level of strength 1 panel at the termination time (0.4 s) is around 0.15, whereas the maximum plastic strain level of strength 2 panel at termination time is around 0.22 since the panel deformed considerably. Here, the mild steel is used and the fracture strain is set as 0.3, the strength 2 panel has more possibilities to reach the fracture strain earlier. Thus, it can be deduced that the reducing the thickness of members, though may be advantageous in terms of yielding low force levels, also do possess the risk of development of fractures sooner. So it is concluded that the choice of thickness is case specific.

7.2.2.1.4 Impacts outside the ice strengthened region:

Usually, the non ice-strengthened areas are characterized as region with structural members of lesser strength than that of the ice-strengthened region. This is due to the fact that these regions have less exposure to ice loads. However, on account of the waves, there is every chance that an incoming ice feature may hit the regions outside the ice strengthened area. Therefore, the effect of impacts of ice features above the ice strengthened region have been analysed and described in this section. Collision analysis have been performed using the three ice features.

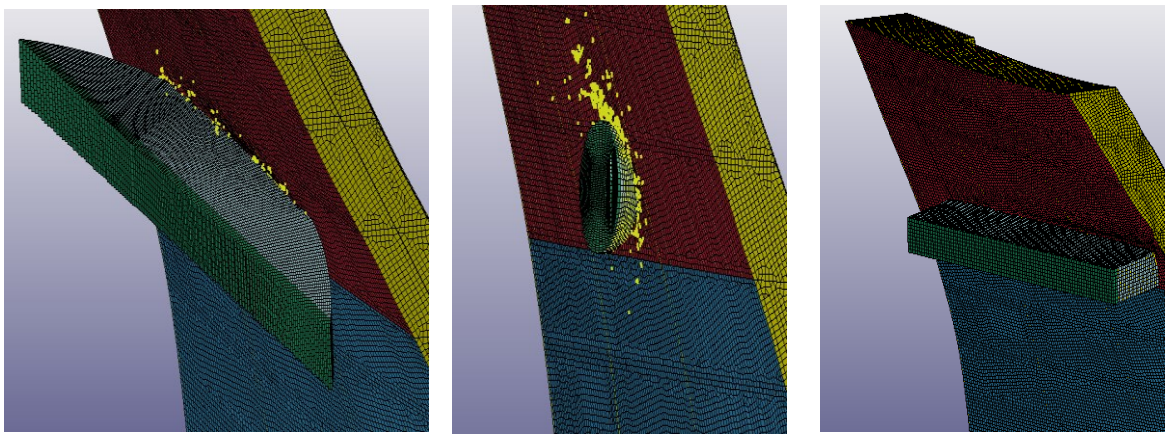

(a) Ice Floe Impact (b) Growler impact (c) Bergy pit impact

Figure 81 (a,b,c) shows the impact scenarios of three different ice features outside the ice-strengthened region

Figure **81 a,b,c** presents the animation pictures of the collision using three ice features. In the first two pictures, both the deformation of the structure, crushing of ice along with the generation of SPH particles are visible but in the third case, only few ice elements have been crushed thereby considerable SPH particles have not been generated.

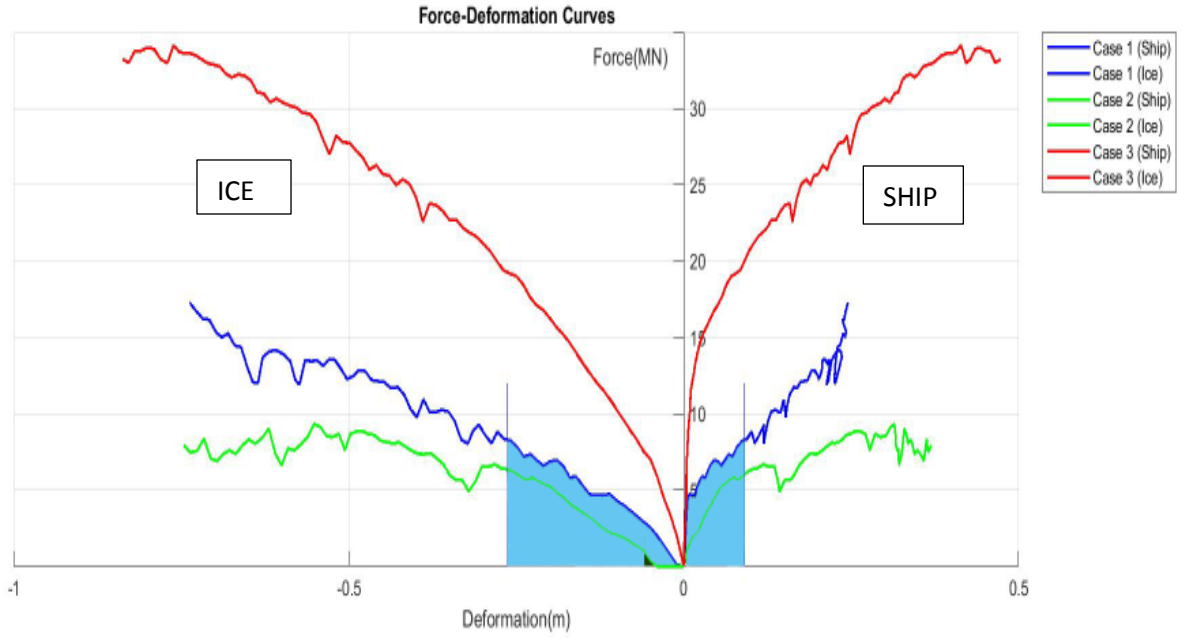

Figure 82 Force- Deformaion curves corresponding to three ice features colliding the FPSO outside the ice-strengthened region

Figure **82** shows the force-deformation relationship of both the ship side and ice for all the cases. The impact behaviour of these features is quite the same in terms of what is observed in previous cases. In other words, the bergy pit produced maximum deformation in the structure with less crushing of ice, growler impact resulted in strong localized impact and ice floe with increasing contact yielded wider deformation in ship side. Frames carried the loads through combination of shear, plastic bending and membrane action, whereas the outer plate carried the loads through membrane action. In all the cases except the tabular bergy pit impact, the outer

plates and the frames sustained massive deformation. However, for the case of bergy pit impact, in addition to outer plates and frames, stringer plates also experienced considerable deformation.

This analysis has been performed based on the decoupled approach, so using the strain energy output from the external mechanics, the force and deformation has been limited and represented in highlighted areas in Figure **82.** The total dissipated energy computed from the coloured domain corresponding to ice floe impact above the ice-strengthened region is 1.47 MJ and for ice growler impact is 0.0129 MJ.

7.2.3 Coupled Collision Approach:

Unlike decoupled approach, the procedure followed in coupled collision is simple and straight forward. The ice feature is imparted with some initial velocity and collided with the ship structure.

7.2.3.1 Results and Discussion

7.2.3.1.1 Comparison between coupled and decoupled collision:

Using coupled approach, 2.9MT of ice floe is collided against the FPSO side at an initial velocity of 2 m/s. The impact is not that heavy since the ice has been imparted with a velocity of 2 m/s. So only a small quantity of deformation is visible both on the ice and structure. Ice floe, after deforming to certain limit rebounded and moved back with some velocity. The results obtained from the NLFEA time domain analysis are compared with those from the simplified external mechanics codes. The external mechanics approach gives only the strain energy, therefore the dissipated strain energy from the NLFEA analysis is compared against the strain energy from the external mechanics codes and shown below

Strain energy from NLFEA	Strain energy from External Mechanics
0.45 MJ	1.14 MJ

Table 15 Comparison of strain energy dissipation between NLFEA and simplified codes

It can be seen from the above comparison**,** the simplified code gives higher dissipated strain energy than the NLFEA analysis. As previously said, the strain energy from the simplified codes represents a fully plastic impact which means that the ice is completely stopped and all the initial kinetic energy is converted to strain energy, and the external mechanics codes gives the maximum expected energy dissipation. These are the reasons for the high value of strain energy from simplified approach and this strain energy can be regarded as the demand for energy dissipation. However, in the case of NLFEA coupled analysis, the ice is moving back with some velocity after the impact, as a consequence, not all the energy is dissipated, some amount of energy is still left as kinetic energy. This is the cause for lower strain energy dissipation from NLFEA analysis. The strain energy from NLFEA represents the required energy dissipation. Therefore, from Table **15,** it can be inferred that the required energy dissipation is only 37.5% of the demand for energy dissipation. This value is quite closer to Liu's results (30%) who developed this code (Liu 2011). The strain energy from external mechanics can be taken as the empirical upper bound of the NLFEA analysis.

Strain energies from NLFEA and simplified approach has been compared above. However, previously it has been mentioned that the forces from the ice structure interaction in LS DYNA, consists of contributions from damping, sliding and hourglass energies as well in addition to strain energy. So it is equally accurate if the force-deformation plot of coupled NLFEA analysis is compared against that of the decoupled approach plot limited by the results from simplified EM technique.

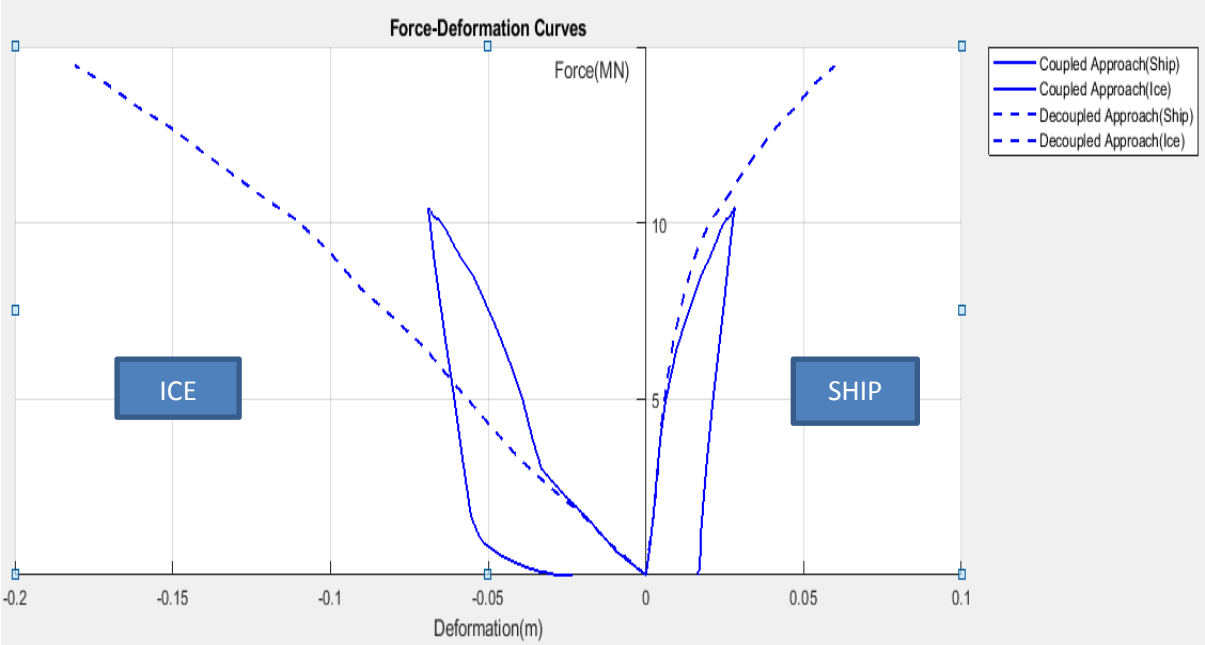

Figure 83 Comparison of the Force-Deformation relationship between coupled and decoupled collision approach

Figure **83** illustrates the comparison between the coupled analysis and the decoupled analysis limited by the values from external mechanics. The decoupled analysis limited by output from EM represents a fully plastic impact and the ice is stopped after the collision, thus the decoupled analysis produces large deformations (maximum expected deformation) on structure and crushes the ice more. On the other hand, the ship structure and ice have attained deformations less than 0.02 m and 0.06 m respectively in coupled approach.

From the area under the curve, the total energy dissipated is computed as

Coupled Approach	Decoupled approach (limited by EM output)
0.545 MJ	1.445 MJ

Energy dissipation from coupled approach is just 37.7% of that from the decoupled case. So, decoupled collision data can be taken as the conservative estimate for use in the design for accidental loads. Remember that the total energy from f-d curves consists of strain, sliding and damping energy components.

Usually, the allowable deformation of the outer plates is 1-3 times the thickness of the outer plate. If the deformation values exceed beyond this limit, it is mandatory to perform repairs. The thickness of the outer shell plate at the ice strengthened region is 0.035 m. For the case of coupled approach, the ship panels deformed almost 0.02 m which is just 0.57 times the thickness of the outer plate. In case of decoupled approach which is regarded as the conservative estimate, the ship side attained deformation of 0.06 m, thus the deformation is 1.7 times higher than the thickness of the plate. Both the analysis based on coupled and decoupled approach resulted in allowable deformation (1-3t) of ship side, as a result there is no need to facilitate immediate repairs, if a 20 m dia ice floe moving with a velocity of 2 m/s hits the ship structure.

7.2.3.1.2 Oblique Impacts:

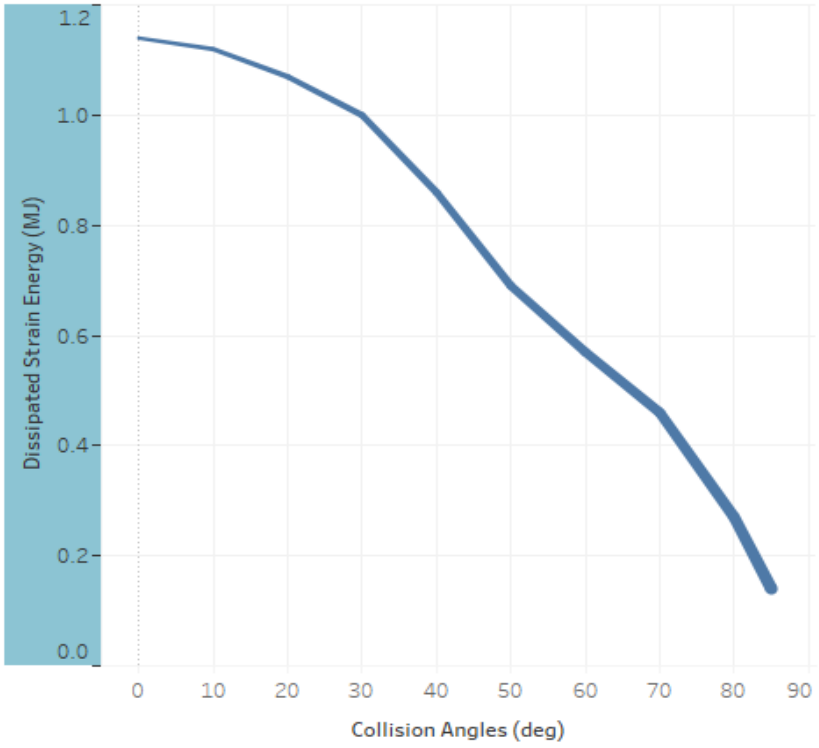

Figure 84 Plot of energy dissipation as a function of time computed from simplified external mechanics approach

Using the simplified codes meant for computing the external mechanics, the energy dissipated during ice-FPSO collision for each collision angles are calculated and shown in Figure **84.** From the plots, it can be inferred that the dissipated energy decreases with the increase in the collision point angle. This is due to the fact that the simplified external mechanics approach assumes that during oblique impacts, considerable amount of energy is dissipated due to sliding and the deformations of both the ice and the structure are less in comparison with the direct impacts. So, this happens to be the reason for the decrease in strain energy with increasing collision angles. This fact is based upon the simplified external mechanics approach and the applicability of this fact in NLFEA methods is conducted in the following sections.

Oblique impacts are essentially simulated in LS DYNA with the intention of making the ice floe to slide along the surface of the ship structure. So, impacts at different angles and with different combinations of friction coefficients are conducted in the following report. Sliding of natural ice directly depends upon its friction. Therefore, the coefficient of friction is changed for the ice model used in this thesis in order to check whether the ice floe slides during the simulation. To establish significant interaction between the ship and ice during oblique collisions, out of the 20 m dia ice floe, initial 5 m is modelled as ice and the remaining mass is assigned to the ice pusher. The kinetic energy of ice remains the same corresponding to the 20 m dia ice floe.

Table **16** lists the collision angles and the corresponding coefficient of friction that has been used in the NLFEA simulations.

Simulation runs	Impact angle (°)	Coefficient of friction
Run 1	40	0.15
Run 2	40	0.5
Run 3	70	0.15
Run 4	70	0.5

Table 16 Simulatoin runs corresponding to different impact angles and ice frictional coefficient

Figure **85** illustrates the force-deformation curves of all the impacts scenarios listed in Table **16.** Simulations have been conducted using two impact angles, 40° and 70°. It can be seen from the plots that with the increase in the collision angles, less deformations attained on the ship side due to the fact that the contact area becomes lesser. The contact area is lesser for 70 ° impact in comparison with the 40° impact. It should be noted that the ice did not slide in any of the simulated oblique impact cases.

Additionally, the effect of friction has been studied in this section. The coefficient of friction for ice has been changed to 0.5 in both the 40° and 70 ° oblique collision scenarios and their effect on the ship side and ice are discussed. In natural ice, increasing the friction will result in increase in the force levels. However, in this simulation, the trend is exactly the opposite. Slightly lower forces levels are recorded for the collision case with $\mu = 0.5$ when compared with that of the case with $\mu = 0.15$ and more ice elements are eroded. This behaviour might be due to the fact that the failure strain of ice would have decreased with higher values of coefficient of friction. Since, as already stated, in this ice model the failure strain of ice directly depends upon the relation N.p2 (N is the dimensionless parameter in failure strain equation and p2 is the largest root of the quadratic equation $F(J_2, p)$) and the failure curve reaches low values of failure strain with the increase in pressure(please refer Figure **33**). Thus, it can be related that higher values of frictional coefficient increases the pressure, consequently, there happens to be a reduction in the failure strain of ice.

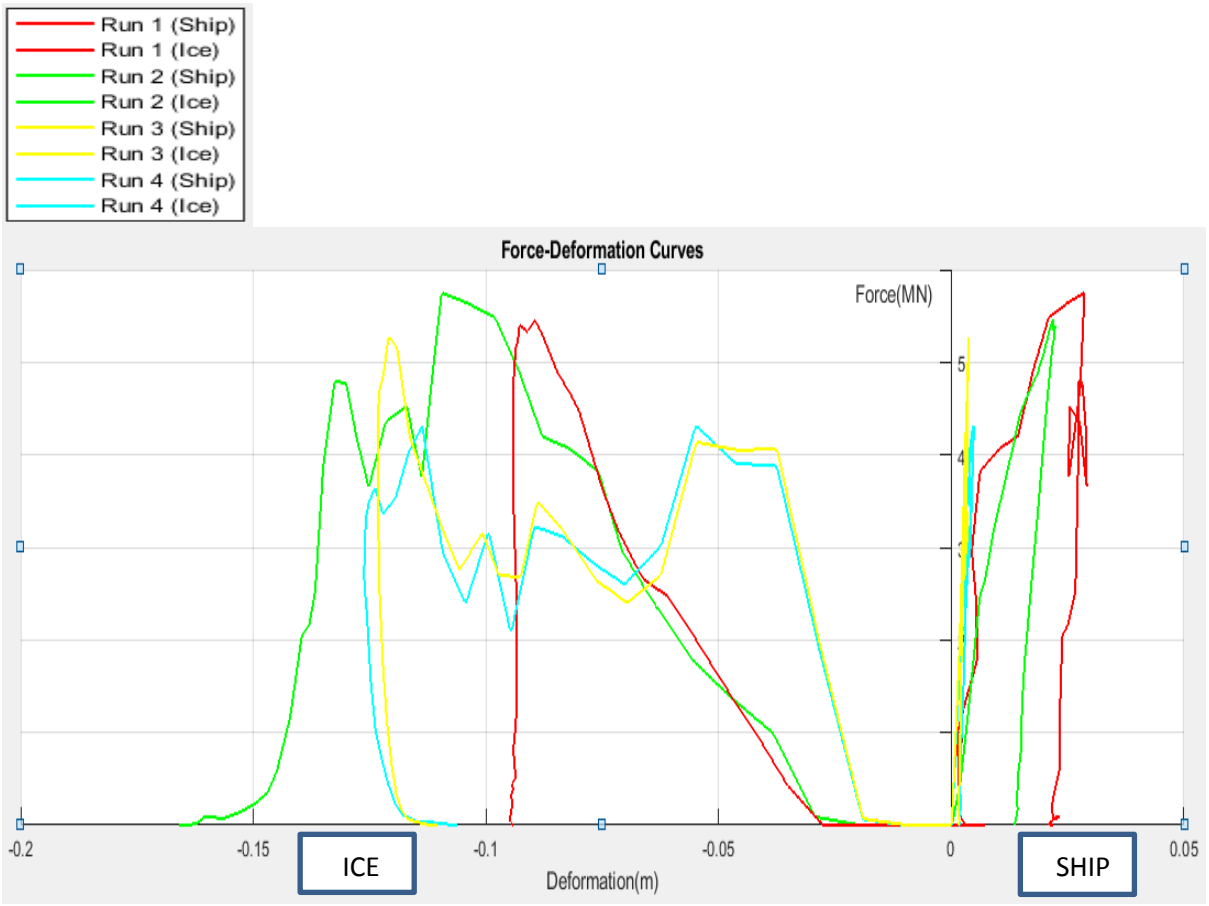

Figure 85 Force-deformation curves for different impact angles and frictional coefficient

One uncertain behaviour that can be observed in the plots shown above is that for 40° impact, there is a significant difference in the amount of crushed ice between the two frictional coefficient values (Run 1 and Run 2). However, for the 70 ° collision scenario, negligible difference in ice crushing can be witnessed between cases corresponding to two frictional coefficients (Run 3 and Run 4). It is hard to grasp the real reason for this behaviour. In addition, the ice did not slide with the change in frictional coefficients.

Therefore, it is concluded that in this ice model, higher value of frictional coefficient (0.5) resulted in unphysical behaviour in terms of reduction in force levels and moreover it contributes nothing to the ice sliding. Thus, it is not recommended to use frictional coefficient values higher that 0.15 while using this ice model.

Impact angle	Frictional Coefficient	S.E from NLFEA	S.E from EM
40°	0.15	0.326 MJ (38%)	0.86 MJ
70°	0.15	0.305 MJ (66.3%)	0.46 MJ

Table 17 Comparison of strain energy dissipation between NLFEA and simplified codes

In order to verify the accuracy of the simulations, the strain energy from simplified external mechanics codes is compared against the same from the NLFEA approach. The strain energy

values of 40° and 70 ° collision scenarios for the case of $\mu = 0.15$ is listed and compared above. In addition, the percentage values shown in brackets represents the S.E dissipation from NLFEA in relation to the S.E dissipation EM codes. In the direct impact (0°) case, it is concluded that the required energy dissipation (from NLFEA) is just 37% of the demand for energy dissipation (from EM), however from Table **17,** it could be seen that this percentage value increases with higher impact angles indicating the minimization of difference in the strain energy dissipation between the NLFEA and simplified approach. The fact is that the demand for energy dissipation from simplified approach assumes that for higher impact angles, considerable amount of energy is dissipated in the form of frictional energy due to ice sliding, so there will be lesser strain energy dissipation. More informative explanation along with illustrative plots on strain energy vs collision angle computed from simplified external mechanics is given at the start of this section. On the other hand, in the NLFEA simulations, the ice did not slide, therefore lesser amount of sliding energy is expended and strain energy still occupies the dominant part in total energy dissipation due to structural deformation and crushing of ice elements. This seems to be the valid reason for this trend in strain energy dissipation shown in Table **17.**

7.2.3.1.3 Sliding of Ice:

From the oblique impacts performed based on principles of decoupled approach and coupled approach, it could be seen that ice did not slide. So in this section, new method has been tried to simulate sliding of ice along the ship surface. This method is based on the coupled collision approach wherein the ice floe is imparted with velocity components in two directions both lateral and sideways. Figure **86** shows the top view of the ice floe along with the directional arrows indicating the direction of the velocity components.

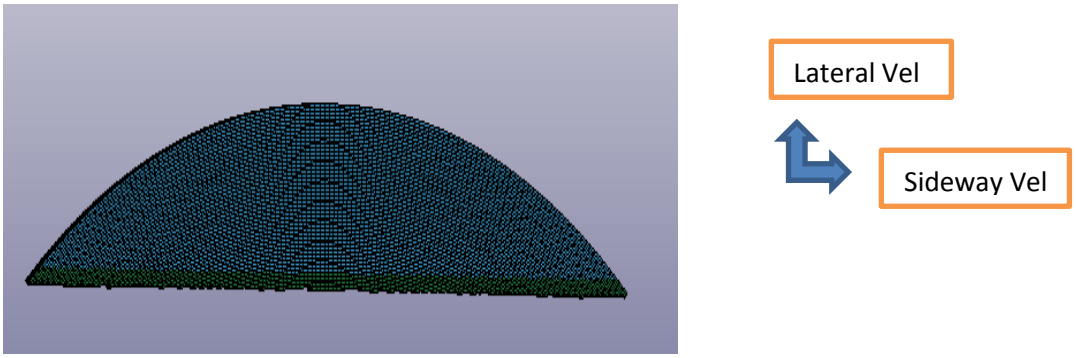

Figure 86 shows the picture of the ice floe imparted with two velocity components

Two simulations have been carried out, one with the velocity components 8m/s(lateral) &3m/s(sideways) and the other with the velocity 5m/s and 1.5 m/s in lateral and sideway directions respectively. Figure **87** & **88** present the illustrative pictures of the simulations corresponding to both cases. Direct impact has been made against the side panel. In both the cases, initially the ice moved laterally and crushed, then it started moving sideways to a certain distance and it rebounded back with some kinetic energy.

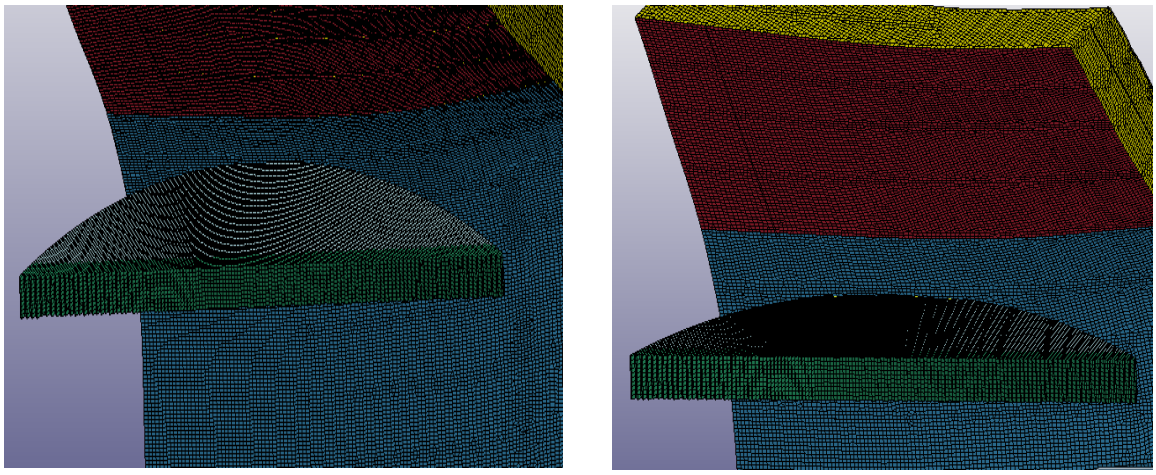

(a) Before the start of sliding (b) After sliding

Figure 87 (a,b) presents two animation pictures before the start of sliding and after the sliding for case 1

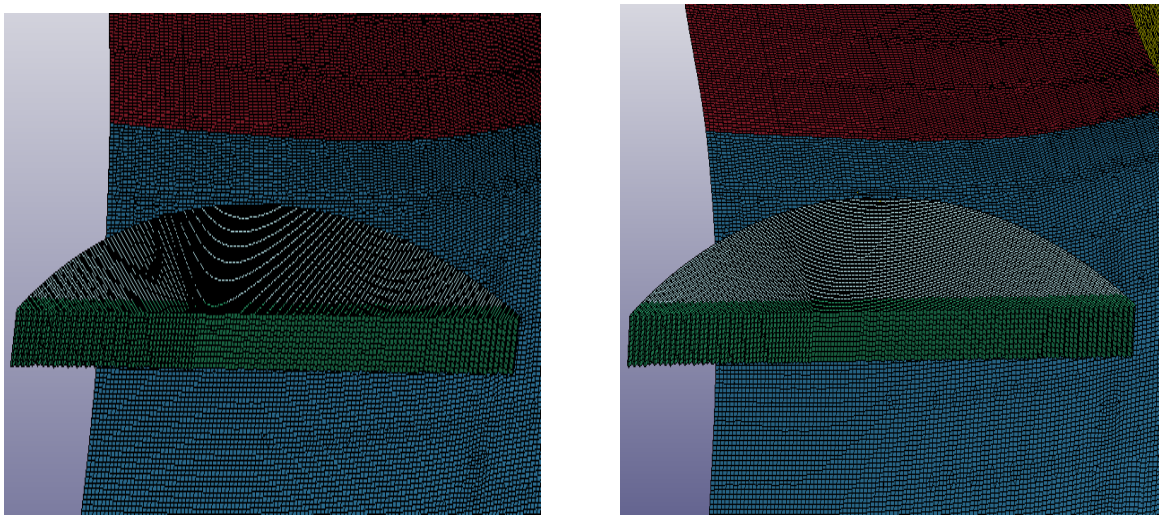

(a) Before the start of sliding (b) After sliding

Figure 88 (a,b) presents two animation pictures before the start of sliding and after the sliding for case 2

In the first case, the ice slided to a distance of 0.3 m to its right and in the second case, the sliding occurred for a distance of 0.17m. The distance the ice slided in the first case is 1.7 times that of the second case. The extent of sliding is more in the first case because of higher side way velocity, thus higher kinetic energy in ice. Figure **89** compares the sliding energy plots of the two cases presented here. Furthermore, two more sliding energy curves are also plotted which corresponds to the direct impact collisions with one velocity component in lateral direction.

The Collision cases performed are listed in Table **18.**

Simulation cases	Lateral Velocity component	Sideway velocity component
Case 1	8m/s	3 m/s
Case 2	5 m/s	1.5 m/s
Case 3	8 m/s	-

Case 4	5 m/s	-

Table 18 Shows the list of all simulated cases

In all the curves in Figure **89**, the sliding energy increases linearly until 0.1 s and then the curve becomes flat. The flat curve indicates that the ice rebounded and moving back with residual velocity.

For the case of impact with two velocity components (8m/s and 3m/s) around 0.95 MJ of energy expended in sliding which is 1.7 times larger that of the sliding energy dissipated (0.55 MJ) in the case with velocities (5 m/s and 1.5m/s). It has been mentioned previously that the distance the ice slided in the first case is also 1.7 times higher that of the second case. From this resemblance between the dissipated sliding energy and the ice sliding distance, it is concluded that the sliding energy increases in the same proportion corresponding to the increase in sliding distance. Third and fourth cases have low sliding energy values since the ice did not slide in these cases, they are plotted to make comparisons on the magnitude of dissipated sliding energy between the sliding and non sliding ice collision scenarios. In short, imparting two velocity components to the ice floe can actually make the ice slide. However, the maximum distance that the ice slided is just 0.3m, but still improvements are needed to make the ice to slide for longer distances.

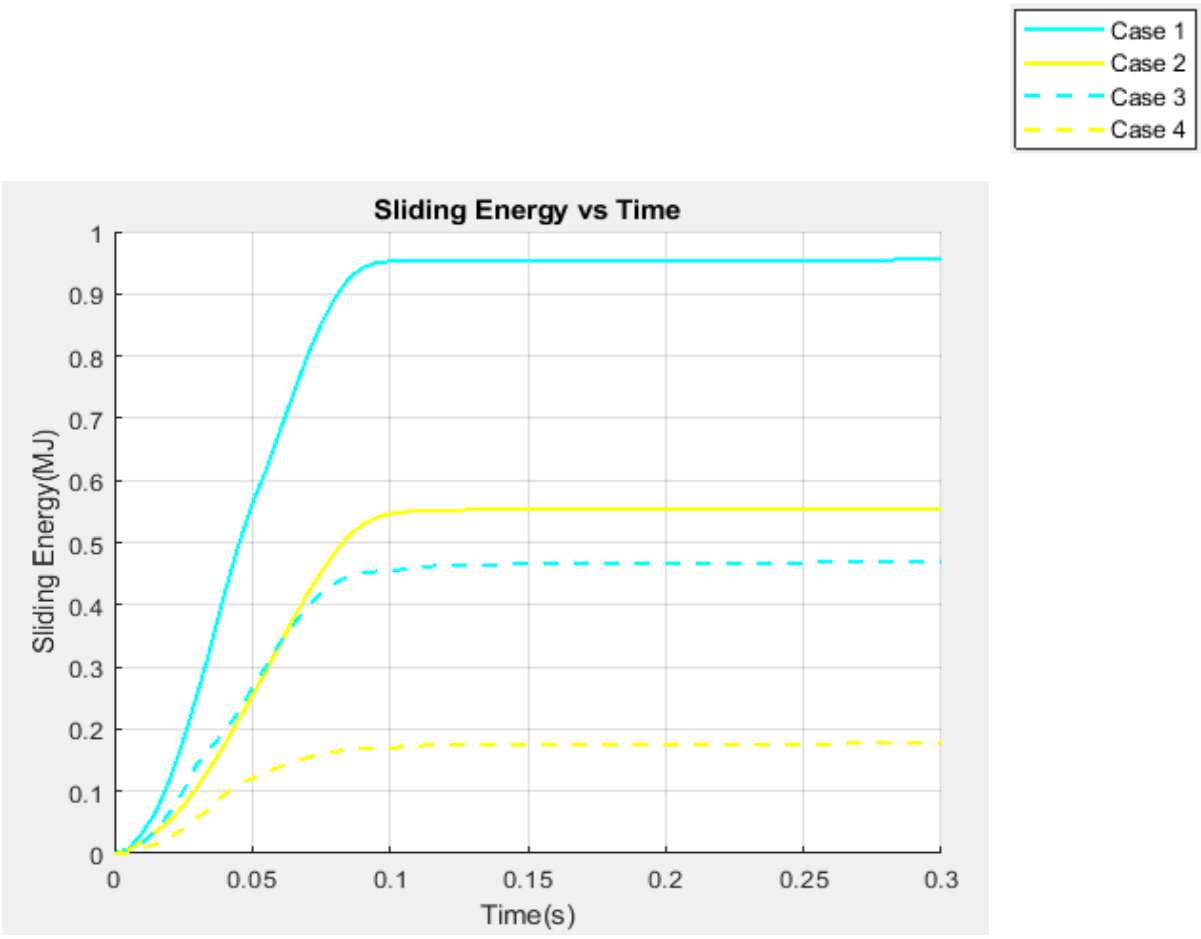

Figure 89 Plots showing sliding energy curves for all simulated cases as a function of time

7.3 CONCLUSION POINTERS

The points outlined here briefly recaps the analysis, results and discussions made in this chapter.

- Finite element model of the side panel of Sea rose FPSO has been created based on the drawings and the collision analysis has been performed following the principles of both decoupled and coupled approaches. FEM-SPH technique has been used for ice modelling.
- Many simulations have been carried out by varying the failure strain parameters (M,N) and it has been concluded that by setting M=1 & N=1 resulted in increase in the failure strain of ice, thus stronger ice. Consequently, it produced considerable deformations on the ship structure.
- Firstly, based on decoupled approach, the FPSO model is collided using ice floe, growler and bergy pit and the internal mechanics of both the structure and ice have been analysed. It has been found that the tabular bergy pit produced maximum deformation on the structure because of its wider uniform contact surface. The f-d curves from internal mechanics are limited using the strain energy computed from Liu's external mechanics codes. As a result, the area under the limited curves represent the actual dissipated energy considering that the ice is stopped after the impact and the impact is plastic.
- Collision have been conducted against side panel with default thickness(stronger panel) and reduced thickness(weaker panel). The weaker panel deformed more and crushed marginally less ice when compared with the stronger panel. Since less ice has been crushed by the weaker panel, low force levels have been recorded. This is in conjuction with the fact that if ice is crushed less, the transmitted forces will also be less.
- Collision results based on coupled approach resulted in less structural deformation when compared with decoupled approach. Moreover, the energy dissipated from coupled approach is just around 37% of the energy dissipated from decoupled approach limited by dissipated energy output from simplified external mechanics . The reason being that in coupled approach, the ice floe moved back with some kinetic energy energy after the impact, whereas in the decoupled case, ice is completely stopped resulting in purely plastic impact. So decoupled approach can be considered as a conservative collision analysis technique.
- Simulation runs made using different frictional coefficient values indicated that the higher values of frictional coefficient resulted in weaker ice, since coefficient of 0.5 decreases the failure strain of ice. This trend is quite opposite to the natural ice behaviour, so it is recommended not to increase the frictional coefficient values higher than 0.15 while performing analysis using this ice model.
- Sliding of ice never occurred for simulation runs carried out with single velocity component. Ice floe imparted with two velocity components in lateral and sideways direction resulted in ice sliding to a certain extent, though not considerably.

CHAPTER 8

8.1 PASSENGER VESSEL-ICE FLOE COLLISION ANALYSIS

In this chapter, ice floe collisions against the side model of passenger vessel has been effectively studied. A brief explanation about the vessel and and its details is dexcribed here.The passesnger vessel, taken into consideration is a cruise ferry called MS Color magic operated by Color Line which is a Norwegian based shipping company. Here, in this chapter, simulations based on decoupled and coupled approach have been performed. In this chapter, in addition to analysing the impacts at ice strengthened region and outside it, the effect of steel grades have been analysed using decoupled approach and the effect of ice mass and velocities are analysed using coupled approach.

8.1.1 Modelling

Passenger Model-Vessel Characteristics

Length – 224 m

Beam – 35 m

Draught – 6.8 m

Propulsion – 4* Wartsilla 8L46B (Wikipedia 2007)

The FEM model of this vessel had been given. So, in this thesis, only the ice floe is modelled and collided with the side model of this passenger ship. Figure **90** shows different views of the FEM model.

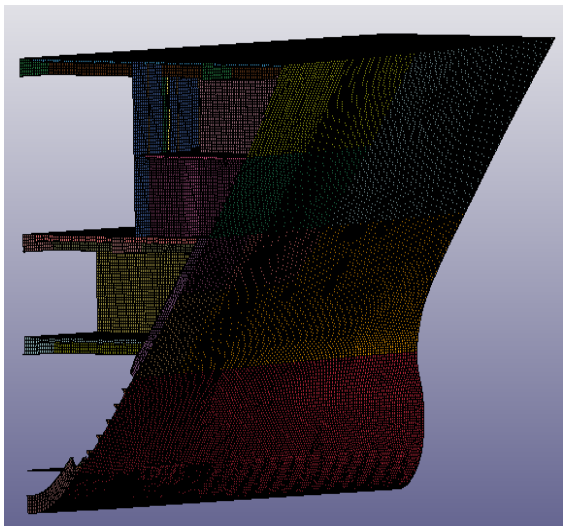

(a)

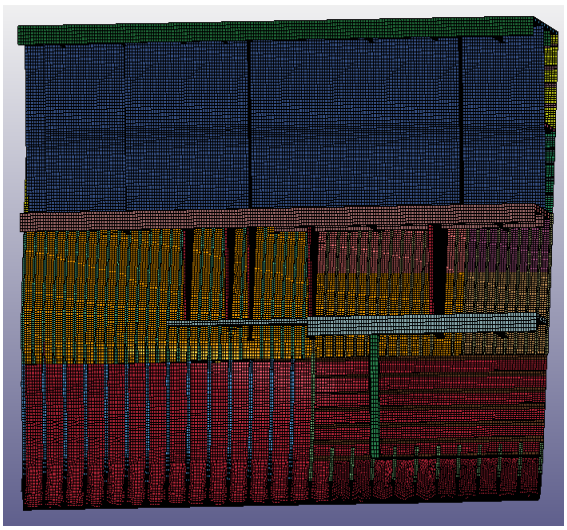

(b)

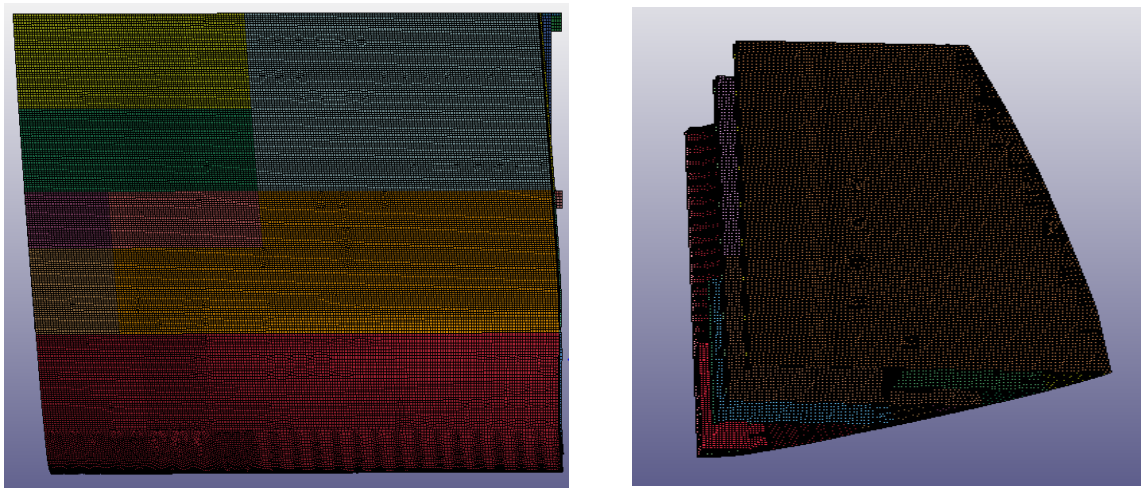

(c) (d)

Figure 90(a,b,c,d,e) presents different views of the FEM model of the passenger vessel

Ice Model

The ice floe is modelled based on continuum approach (i.e) FEM technique. The reasons for not using FEM-SPH technique for ice modelling, is that in this analysis main emphasis is placed on the force-deformation of both the ship and ice and not the interface pressure patterns. The other reason is that already FEM-SPH technique has been applied for ice collisions against FPSO in the previous chapter, so here efforts are made to study the force-deformation curves arising from hard ice impacting the side ship structure.

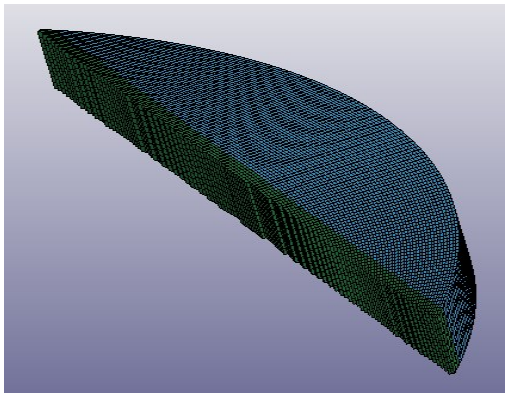

Figure 91 Ice floe model used in the simulations

Previoulsy, the ice has been modelled hard by varying the failure strain parameters(M=1, N=1) of ice. The same values are used here in this analysis for strengthening the ice.

8.1.2 Decoupled Collison Approach

8.1.2.1 Results and Discussion

8.1.2.1.1 Impact assessment at ice-strengthened and outside the ice strengthened region

In this section, the simulation of ice floe collision against side model of passenger vessel is carried using NLFEA decoupled approach. Ice floe is driven with a constant velocity of **5m/s** and the termination time is set as **0.3 s**. On account of the wave motions, there exists many possibilities that the ice may hit the ship structure above the ice-strengthened region. In order to study those effects, two simulation cases have been performed by colliding the ice both at the ice-strengthened region and non ice-strengthened region as shown in Figure **92.** Here, collisions at non ice-strengthened region must be taken in the sense that the impact has been carried out above the water line. In this section, the internal mechanics is detailed first and then the F-D curves are limited using the output from simplified external mechanics.

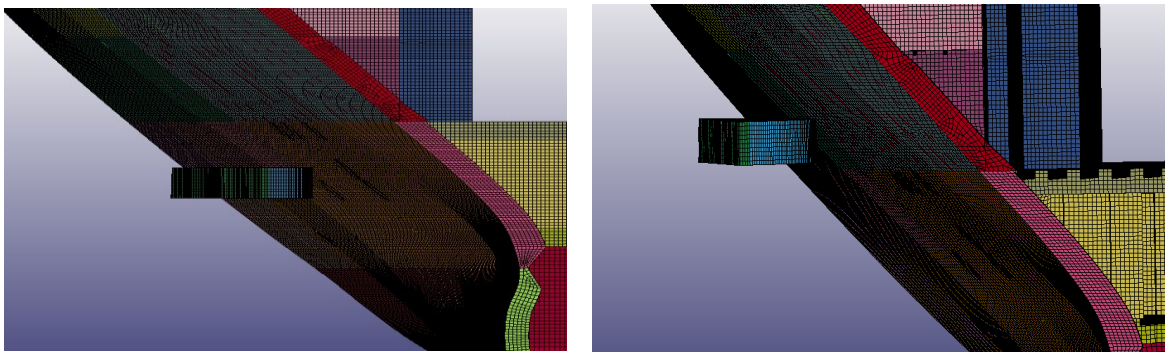

(a) Impact at ice-strengthened region (b) Impact outside ice-strengthened region

Figure 92 (a,b) shows the impact locations for the two simulated cases

Case 1	Impact at the ice-strengthened region
Case 2	Impact above ice-strengthened region

From structural design perspective, the basic difference between the ice-strengthened and non ice strengthened region is that the thickness of certain structural members are less in the non ice-strengthened area, moreover the frames are not closely spaced in comparison with those belonging to ice-strengthened region. Figure **93** compares the results of the NLFEA simulation at both the impact locations. It is stated above that from the structural strength point of view, the non-icestrengthened region is inferior to the ice-strengthened region since the former is not strong enough to crush the ice as the latter. As a result, non-icestrengthened area experience larger structual deformations upto 0.6 m at the end of termination time which can be seen from the light blue line in the plot. One advantageous fact inherent in large structural deformations in ice-structure interaction is that less force is transferred to the structure owing to the reason that slightly less quantity of ice is crushed. Thus when less amount of ice floe is crushed, larger part of the ice floe will not come in contact with the structure and lower force contributions from less quantity of ice crushing, thereby less forces are induced on the structure. This can be

seen from the ice f-d plot on the negative X-axis, that the number of peaks and troughs, which represent the failure/crushing of ice elements, are comparatively lower in the case of ice impacting at non-ice-strengthened region than the other curve.

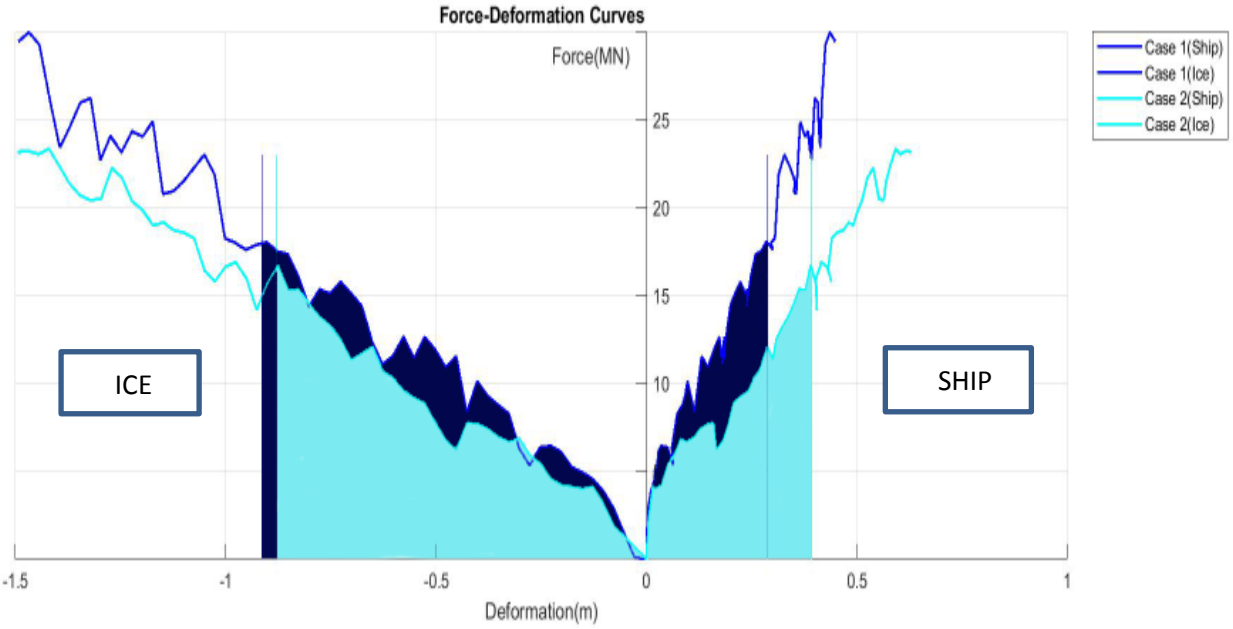

Figure 93 Force vs Deformation curves for the impacts made at ice-strengthened and non-ice strengthened regions

However, there is also an inherent disadvantage in the case of large deformations, if the plastic strain levels exceed beyond the failure strain of the steel material, fracture occurs. So, it can be concluded that the non-ice strengthened region in this passenger vessel, on account of experiencing higher diplacements during accidental impacts, might be subjected to fracturing more easily and sooner than the ice-strengthened region.

Figure **94** shows the damage extent both at the front side and backside of the structure for ice floe impact at ice strengthened region. Moreover, Figure **95** displays the outer plate deformation at the non-ice strengthened region. It can be seen that the dominant failure modes observed are excessive plastic deformation of the outer plate and the plastic bending and local tripping of the web frames. These deformation modes are illustrated clearly in the pictures using pointer arrows. Let us analyse more in detail regarding the development of failure modes after the ice impact. The load after the impact is uniformly distributed over the frames. At the initial contact point between ice and ship, large pressures existed since the contact area is small. As a result, initially, the frames deformed only due to shear. After sustaining more deformation, shear hinges are formed on the frames. On account of this, membrane stresses are developed in the frames and then the load has been carried by a combination of shear, membrane stress and plastic bending in frames.

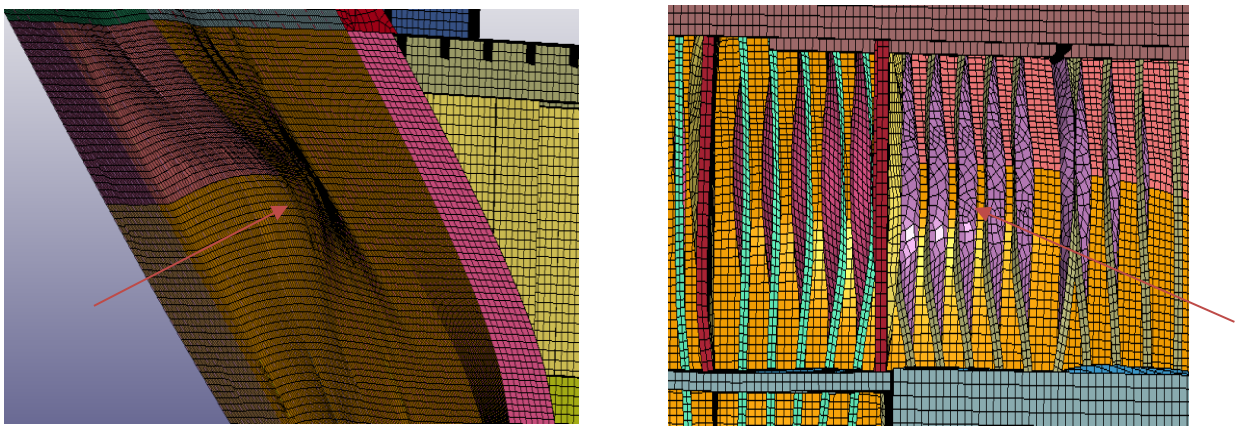

(a) Frontside damage (b) Backside damage

Figure 94 (a,b) presents the damage extent at the ice strengthened region both front and back of the FEM model

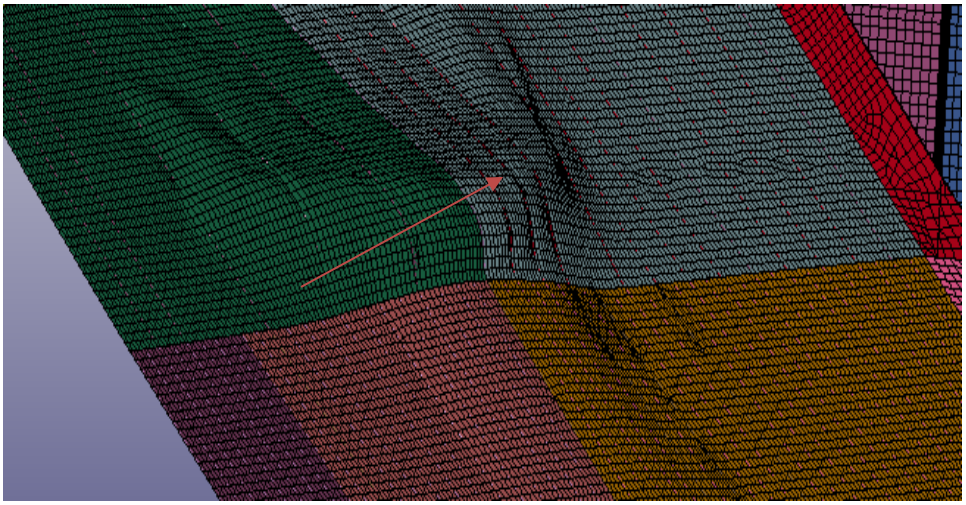

95 shows the damage caused by ice floe impact at the non ice strengthened region

In outer plate, the load is carried predominantly by membrane stress. In general, failure of the outer plates (fractures) will occur very sooner at the spacing inbetween the frames, if the frames had not deformed. However, in this considered collision case, the frames deformed through shear, membrane and plastic bending, as a result the outer plates also deformed to some extent thereby early fracturing has been prevented. So from the point of view of prevention of early fracturing of outer plate, it is necessary that the frames must be deformable.

Similarly, as in the case of FPSO collision simulation, in order to represent the actual collision scenarios, the decoupled collision data corresponding to impacts at ice-strengthened region and outside it have been limited using the strain energy output from external mechanics. The magnitude of force inside the coloured domain and the total dissipated energy computed from the coloured area represents the actual force and dissipated energy levels respectively when an ice floe hits the ship at a velocity of 5 m/s and is stopped after the impact. The force and deformation inside the coloured domain represent the maximum expected values.

The total dissipated energy calculated from the coloured domain is presented below. The dissipated energy for the impact at the ice strengthened region is slightly higher on account of the fact that more amount of ice is crushed in Case 1.

Total energy dissipated for Case 1	Total energy dissipated for Case 2
8.79 MJ	8.46 MJ

8.1.2.1.2 Effect of structural steel grades in accidental collisions:

Previously in chapter **7,** thickness effect in accidental collisions have been analysed by reducing the thickness of the FPSO side panel and driving the ice features against it. In this section, the effect of steel grades in accidental ice load impacts have been studied using NLFEA decoupled method. Using the passenger vessel FEM model, four simulation runs have been conducted by varying the steel grades (S235,S275,S355,S460) along with the respective strength parameters for each steel grade. The ice floe is collided against the structure with a constant velocity of **2 m/s** with a prescribed termination time of **0.41s.**

Simulation Runs	**Steel Grades**	**Constant Velocity**
Run 1	S235	2m/s
Run 2	S275	2m/s
Run 3	S355	2m/s
Run 4	S460	2m/s

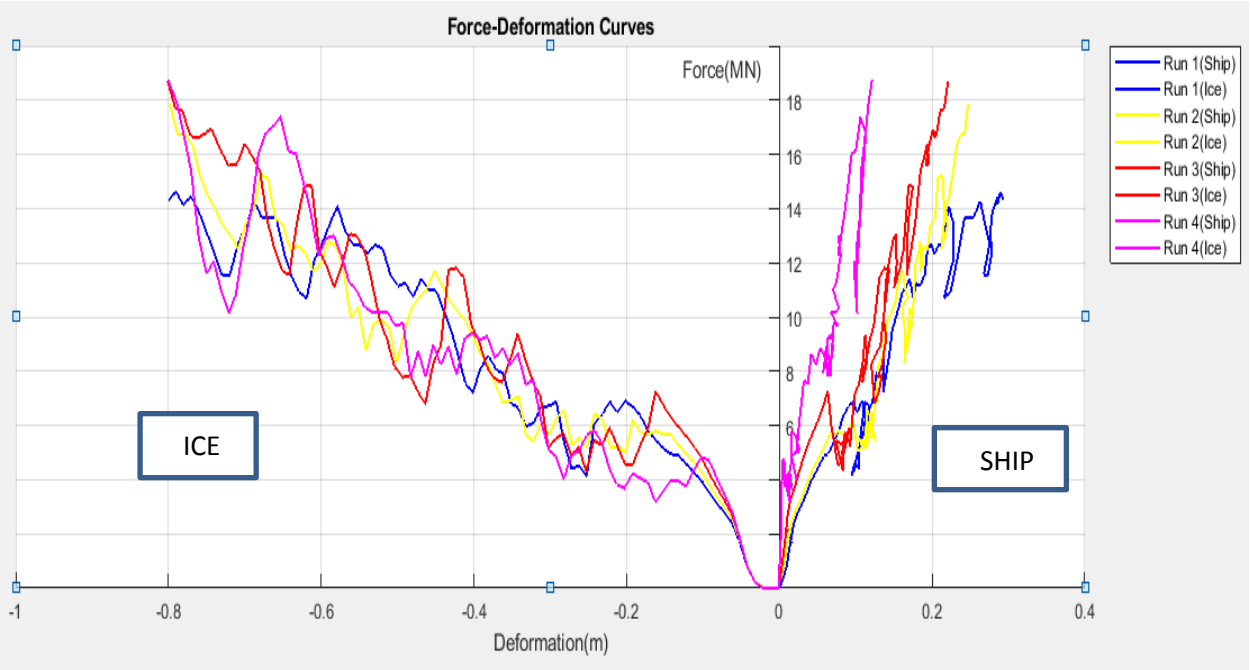

Figure 96 Force-Deformation relationship between different structural steel grades

Since the force-deformation study is important in this case, only the internal mechanics have been analysed. In other words, the external mechanics has not been applied to limit the F-D curves.

Figure **96** illustrates the force-deformation curves of both the ship structure and ice. From the plots, it is evident that with the increase in the steel grade, the structure deformed less but the force levels increased slightly. As previously stated, in ice collisions, if the structure is strong, more ice is crushed and consequently more force is transferred to the structure on account of larger part of ice coming in contact with structure. Since POWER LAW PLASTICITY material model has been used, the structure exhibits isotropic hardening behaviour which can be clearly inferred from the sudden drop and increase of force in the plots.

Let us analyse in detail the cases of S235 and S460. From the plots, structure with S235 attained a displacement of almost 0.3 m and the recorded maximum force is 14 MN at the end of the termination time(0.41s). However, for the case of S460, the structure attained deformation close to just 0.1 m and the maximum force level is 18 MN at termination time. The difference in the recorded maximum force level between S235 and S460 is 4MN which is not really significant. This small force variation might be due to the fact that there is only a marginal difference in the crushing of ice between these two cases. However, the deformation between these two steel grades is extensive. It has been observed that the structural members assigned with steel grade 235 deformed extensively. The risks due to large structural deformation associated with S235 is illustrated in Figure **97** along with a brief explanation.

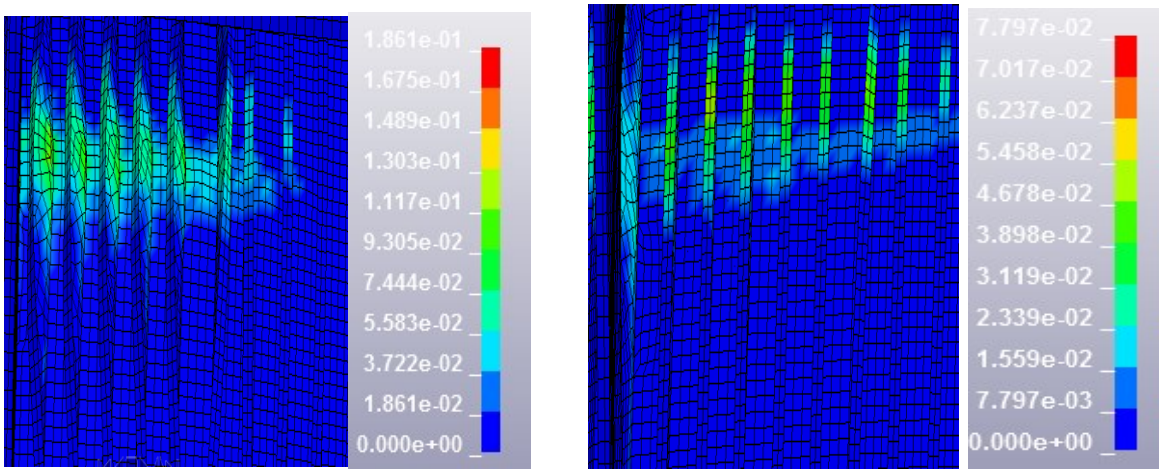

(a) Steel Grade 235 (b) Steel Grade 460

Figure 97 (a,b) shows effective plastic strain distribution for two steel grades S235 and S460

Figure **97 a,b** displays the effective plastic strain levels of the structure with S235 and S460 respectively. The fracture strain of S235 is set as 0.3 and S460 has been assigned with 0.55. At 0.41s, S235 shows maximum plastic strain levels upto 0.13, whereas the S460 shows plastic strain levels upto just 0.062. Therefore, it can be inferred that the structure with S235 have more possibilities of sustaining fractures during accidental ice impacts.

In short, the deformation of structure with steel grade 460 is considerably less in comparison with that of steel grade 235, moreover there is no huge variation in the ice induced force levels between these two cases and in addition the risk of development of fractures during accidental collision is less for S460. Considering these, S460 seems to be a better alternative for design of structures against accidental ice collisions. However, one fact should be noted that higher steel grades are more prone to fatigue. So, the choice of suitable steel grades for ice-strengthened vessels are entirely case specific and is at the sole discretion of the designers.

8.1.2.1.3 Consideration of fractures in ship side

In previous simulations, collisions had been carried out using the principle of decoupled approach thus pushing the ice with a constant velocity and displacing the structure to a certain limit. Here, in this section, the simulations had been run a little longer with a constant velocity of 5 m/s until a termination time of 0.6 s and the fracture strain is set as 0.3 for the S235 grade steel.

Even then it has been noticed that the hard ice model is not strong enough to produce fractures in the model. Therefore, it can be deduced that this ice model, though modelled harder, do not have the capability to fracture the steel panel.

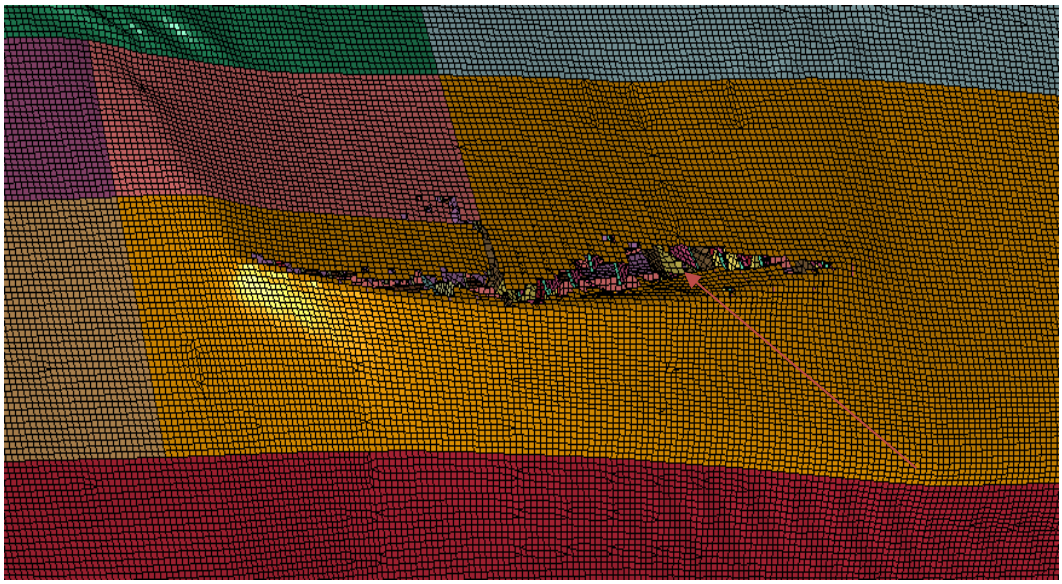

Figure 98 Fractured ship panels after being collided with rigid ice

Since fracturing of ship panels cannot be simulated using the ice model. One simulation has been conducted by modelling rigid ice and pushing it against the structure with constant velocity of 5m/s until the termination time of 0.8 s. Rigid Ice is created using MAT RIGID in LS DYNA but endowed with ice properties. Eventually, it turned out that the rigid ice does have the potential to create fractures and fail the steel ship panel. Figure **98** shows the fractured ship panel collided using the rigid ice floe. However, one fact should be remembered that the ice present in nature do not behave as rigid, no matter how hard the natural ice may seem to be, some part of it gets crushed during the ice-structure interaction.

Thus, there is a need to model the ice much harder by varying the numerical parameters in such a way that it can fracture the ship panel.

8.1.3 Coupled Collision Approach (Time Domain Simulations)

8.1.3.1 Results and Discussion

8.1.3.1.1 Comparison between coupled and decoupled collisions

In this section, using the ice floe, direct impact has been performed against the side panel of passenger vessel at the ice strengthened area. The ice floe has been assigned with an initial velocity of 5 m/s. During the simulations, considerable deformation on the ship structure has been observed. In addition, some quantity of ice at the frontal part has been crushed and the ice moved back with some velocity. Figure **99 (a)** shows picture of ice floe hitting the structure and **(b)** displays the ice floe moving back with some remaining velocity after the impact.

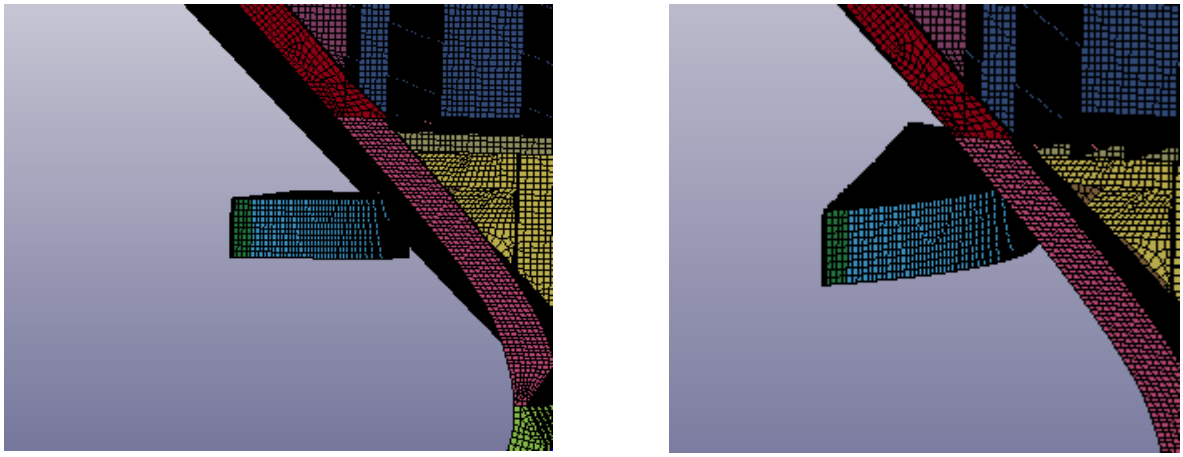

(a) Ice floe, during the impact (b) Ice floe moving back after the impact

Figure 99 (a,b) Location of the ice floe before and after the impact in a coupled collision simulation

While conducting the coupled collision simulations on FPSO panel using the same ice floe with initial velocity of 2m/s, less structural deformations had been observed and in addition, the ice elements just deformed and not crushed. However, in this simulation with ice floe-passenger vessel interaction, significant amount of ice elements had been crushed. This indicates the fact that the velocity of ice plays a crucial role in accidental ice impacts. Furthermore, the effect of velocity will be discussed in the coming sections.

The extent of deformation attained on both the ship and ice is presented in red line in Figure **100,** and this f-d curve has been compared with that simulated from the principles of decoupled approach and presented in red dashed line in the same figure. The collision data from the decoupled approach has been limited based on the strain energy values from simplified external mechanics codes. Therefore, the f-d curves from the decoupled approach represents fully plastic central impact, which denotes maximum expected deformation. So, the ship side panel deformed more and larger part of ice has been crushed as well when compared with that of the simulation corresponding to coupled approach. (see Figure **100**)

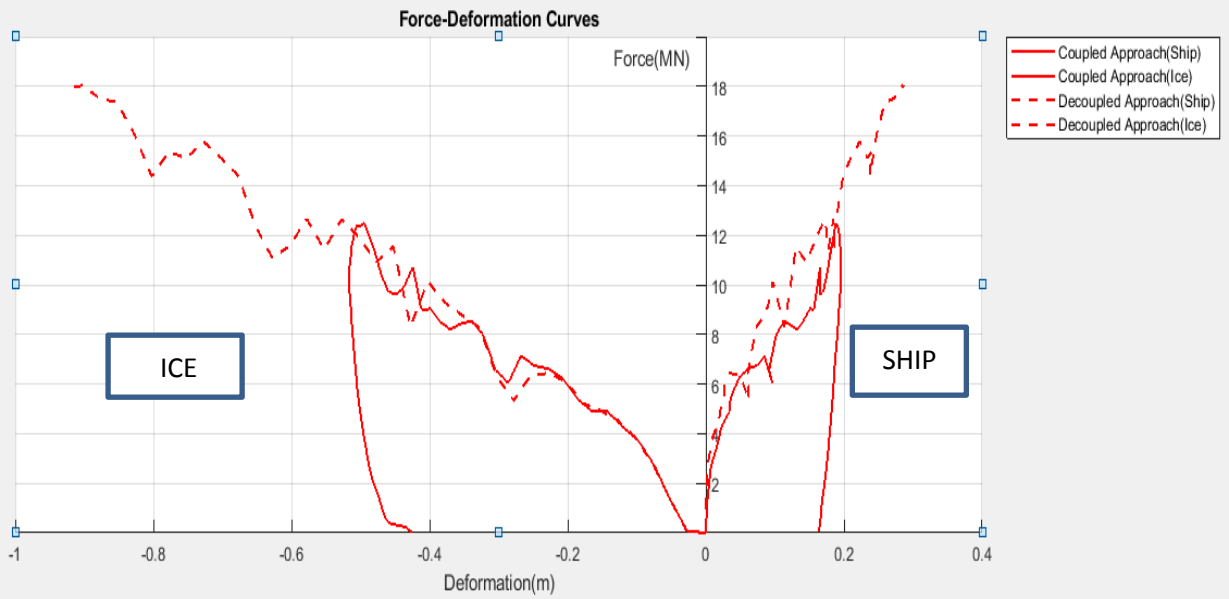

Figure 100 Force-Deformation curves corresponding to coupled and decoupled approach limited with external mechanics output

This is evident from the plots, that there exists a difference in the deformation of around 0.1 m in the ship side and almost 0.4 m in ice between the two approaches. Thus, it can be inferred that decoupled approach presents the conservative estimate (high values) and can very well be considered for the design. However, one fact should be remembered that the ship deformation resulting from coupled approach resembles more or less the actual deformations in real ice collision scenarios, since in this approach, the external and internal mechanics are coupled.

The area under the force-deformation curves give the actual amount of dissipated energies during the collision. As previously stated, strain, sliding and damping energies are part of the NLFEA collision and moreover, the negligible hourglass energy which is purely unphysical can be ignored. The energies (strain, sliding & damping) expended from the decoupled approach is around 8.79 MJ, and it can be taken as the demanded energy dissipation during the collision. On the other hand, around 3.29 MJ of energies (strain, sliding & damping) have been dissipated from the collision based on coupled approach and it is considered as the required energy dissipation during the collision. The lower range of energy dissipation from coupled approach is because of the fact that some amount of kinetic energy is still left since the ice is moving back, the impact is not fully plastic thereby less quantity of ice is crushed in coupled approach and moreover the external mechanics computation is based on simplified analytical approach so inherently there exists some small variations.

The decoupled data limited with external mechanics strain energy represents the maximum expected energy dissipation and hence can be considered as the upper bound value.

In this case, the required energy dissipation is just around 37.4% of the demand for energy dissipation. This required energy dissipation range is quite similar to what is observed from the ice floe collision against FPSO panel and closer to Liu's results as well. The amount of residual kinetic energy that the ice possessed after the impact is shown in Figure **101.**

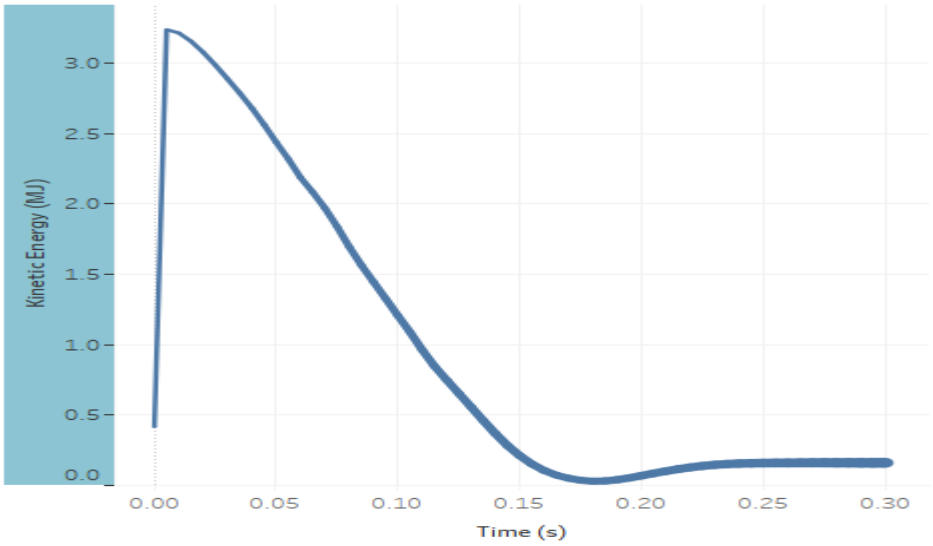

Figure 101 shows the kinetic energy plot as a function of time for the coupled collision approach

From Figure **101,** it could be seen that the ice moved with an initial kinetic energy of 3.5 MJ, but after the impact with the passenger vessel, it moved back only with a residual kinetic of 0.161 MJ.

The allowable limit for the deformation of outer plate without any need for repairs is 1-3 times the thickness of the outer plate. The thickness of the outer plate is 28.5 mm (0.0285m). For the case of coupled collision, the outer plate deformed almost 0.2 m which is around 7 times the thickness of the plate. In case of decoupled collision approach wherein fully plastic impact is considered, the plate deformed around 0.28 m which is close to 9.8 times the thickness of the plate. As a result, immediate repairs are needed if a 20 m dia ice floe collides the vessel at a velocity of 5 m/s. The extent of damage is larger in case of higher velocities. More detailed study on the intensity of structural damage with respect to different ice floe velocities is carried out in the following section.

8.1.3.1.2 Accidental impact assessment for different ice floe velocities:

From the previous simulations based on coupled approach, it has been noticed that kinetic energy of ice plays the dominant role in the collision process. In other words, the deformation of both the ship structure and ice depends upon the momentum of the ice floes. The damage extent is higher with the increase in the kinetic energy. The kinetic energy of ice is directly connected with these two parameters, mass and velocity of ice, and it increases proportionally with increase in these parameters.

So, in this section, a dedicated study has been carried out to analyze the effect of ice floe velocities on the deformation extent in both the ship and ice. As of now, there are not enough literatures that accurately describe the velocities of multiyear ice floes. Since the exact velocities of multi-year ice floes are not known, five collisions have been carried out by varying the ice velocities from 1-5 m/s using NLFEA.

Simulation Runs	Velocity
Run 1	1 m/s
Run 2	2 m/s
Run 3	3 m/s

Run 4	4 m/s
Run 5	5 m/s

Figure **102** shows the force-deformation plots corresponding to the ice velocities 1,2,3,4,5 m/s. It is evident from the plots that higher the kinetic energy, larger the deformations of ship panels and considerable amount of ice is crushed as well. A linearly increasing trend in the force-deformation curves with respect to the velocities can also be witnessed from the plots. The lowest ship panel displacement of less than 0.05 m is attained from the floe colliding with a velocity of 1m/s. In addition, none of ice elements have been crushed. As a result, the deformation patterns of the striking and struck object cannot be effectively studied with this velocity. Therefore, it is concluded that in a coupled approach, assigning the ice features with an initial velocity of 1 m/s, is a poor choice especially for analysis concerned with accidental impacts. Ice floes with 2m/s produced slightly higher deformations in ship than the former, whereas in collision simulations with floe velocities 3, 4m/s, occurrence of plastic bending in some of the structural members can be witnessed. Finally, floe colliding with a velocity of 5m/s activated failure modes like tripping in some of the web frames, buckling in some stiffeners and large plastic deformations in outer plate. For higher floe velocities(3,4,5 m/s), the ship side model exhibited some resistance(isotropic hardening) after sustaining deformations, which could be seen from the plots. Thus, it can be mentioned that in a coupled collision approach, the force and the deformation levels in the structure depend on the strength of ice, structural strength and kinetic energy of the ice feature.

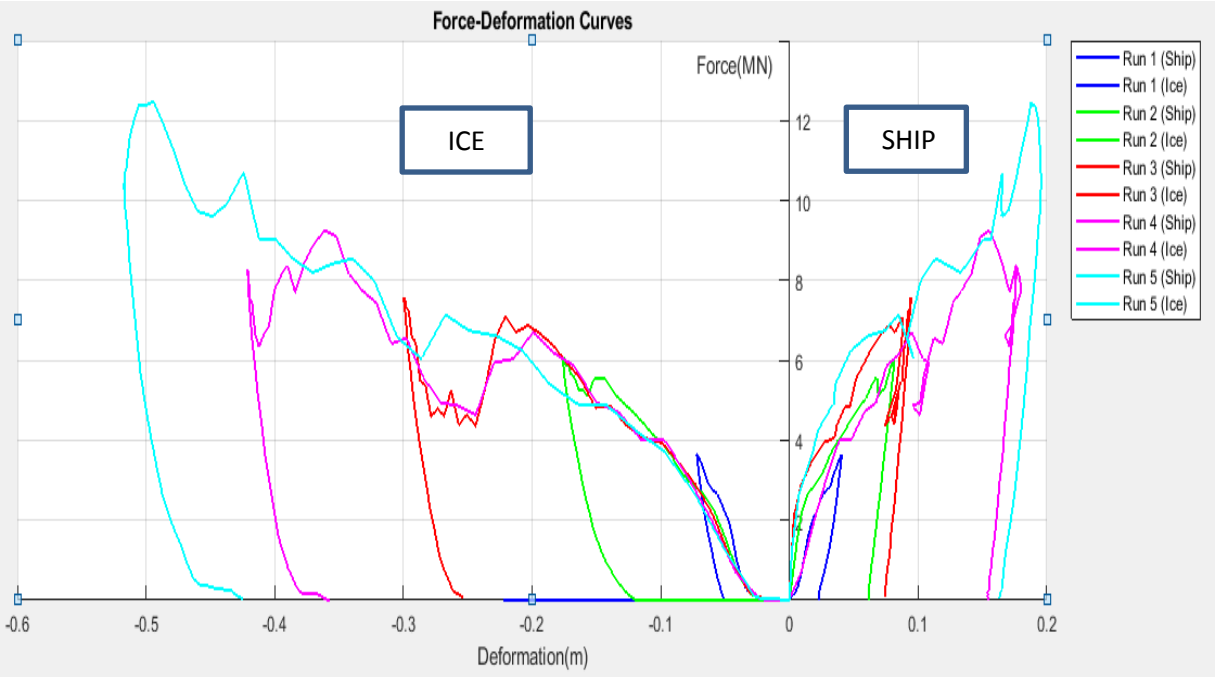

Figure 102 Force-Deformaion curves for five different ice floe velocities

Furthermore, significant amount of ice is crushed as well, thus resulting in larger contact area. This is the reason for high force levels and consequently high average pressures as well.

The reader can clearly see the effects of different velocities on the ship structure from the stress distribution pictures presented in Figure **103 a,b,c,d,e,** corresponding to different velocity cases. In addition, the stress ranges are also shown to the right. One can clearly notice the huge variation in the distribution of stress levels across the structure when the collision cases with

floe velocities 1m/s and 5m/s are considered. There exists a difference of almost 179.4 MN/m2 in the maximum stress levels between these two cases (1m/s and 5m/s), which is quite high.

Considering these facts, it is deduced that collisions with floe velocity of 5 m/s seems to be a better choice for analyzing the ice and structural response in accidental collisions.

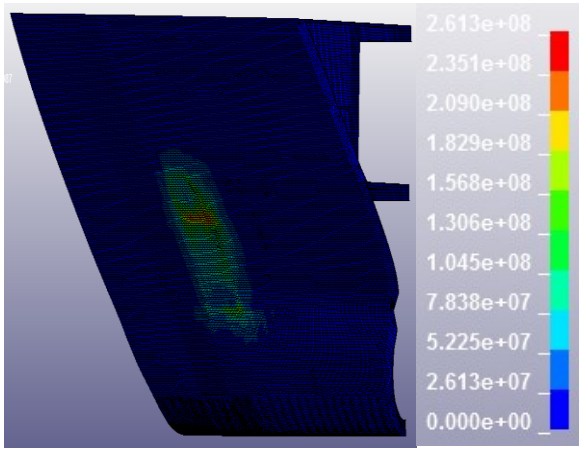

a) 1m/s floe velocity

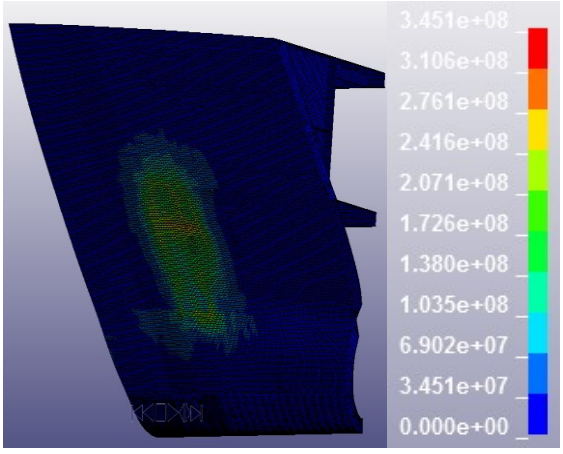

b) 2m/s floe velocity

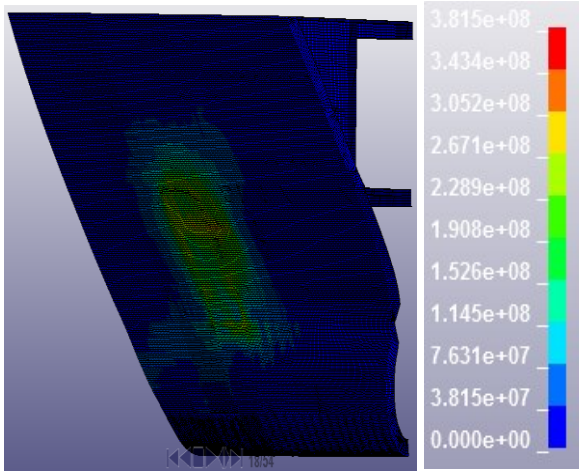

c) 3 m/s floe velocity

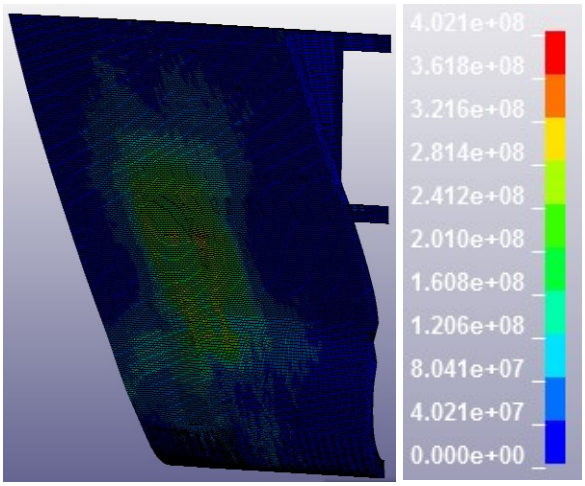

d) 4m/s floe velocity

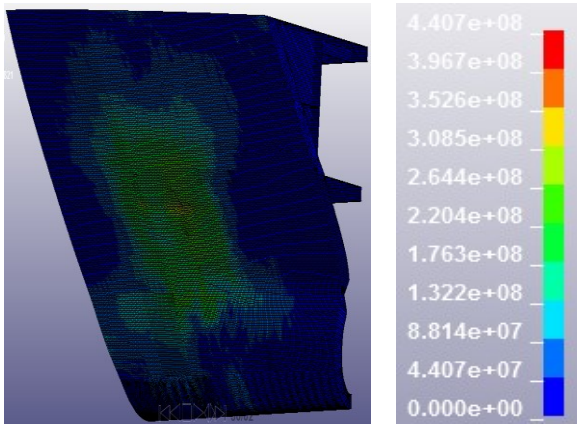

(e) 5m/s floe velocity

Figure 103 (a,b,c,d,e) Stress distribution on the ship side due to collision with ice floes with different velocities

Ice Floe velocities	Strain energy from LS DYNA	Strain energy from simplified approach
1 m/s	0.103 MJ (36.79%)	0.28 MJ
2 m/s	0.428 MJ (37.88%)	1.13 MJ
3 m/s	0.968 MJ (37.9%)	2.55 MJ
4 m/s	1.7 MJ (37.53%)	4.53 MJ
5 m/s	2.67 MJ (37.77%)	7.07 MJ

Table 19 Comparison between the NLFEA and simplified EM

In order to check the validity of the numerical simulations, the strain energy dissipated from the NLFEA approach is compared with that computed using simplified external mechanics approach for all the cases. The results are lised in Table **19.** The percentage of required energy dissipation in relation to the demand for energy dissipation is also shown in the column corresponding to the strain energy from NLFEA (LS DYNA) simulation. It can be seen the required energy dissipation (actual) is almost 37% of the demand for energy dissipation (expected deformation), which is equivalent to the previous cases and also close to what is stated in Liu's thesis. Thus, it can be deduced that the numerical simulations yielded reasonable results.

Here strain energy from NLFEA is listed and not the energy from the area under the F-D curves, since the latter consists of contributions from sliding and damping energies as well, however simplified approach assumes that the energy is dissipated only as strain energy. So the above comparison shown in Table **19** is sensible.

If one wants to compare the energy(strain,sliding,damping) from the arear under the F-D curves, it is manadatory to perform the internal mechanics analysis for all velocity cases using decoupled approach and limit the F-D curves based on the output from simplified external mechanics and then should compare it with the simulation data from coupled approach. This case is shown in section **8.1.3.1.1.**

8.1.3.1.3 Analysis of ice mass effect in accidental impacts:

As stated in previous section, the mass of the ice features is the another parameter that is directly connected with the kinetic energy of ice. So in this section, both the ice and structural response have been studied by varying the mass of ice. There exists many multi year ice floes with different shapes and sizes, so it is almost impossible to estimate the mass of ice floes. Therefore, four different ice masses (288, 500, 1000, 1500 tonnes) have been assumed. Four different NLFEA runs shown in Table **20** have been conducted by assigning these masses to the same ice floe, and with the initial velocity of 5 m/s. The mass of the ice floe is increased by imparting additional mass to the ice pusher located at the back of the ice. Since the kinetic energy is proportional to mass, larger kinetic energy can be achieved with the increase in mass.

Simulation Runs	Ice Mass
Run 1	288 tonnes
Run 2	500 tonnes
Run 3	1000 tonnes
Run 4	1500 tonnes

Table 20 NLFEA simulations runs conducted

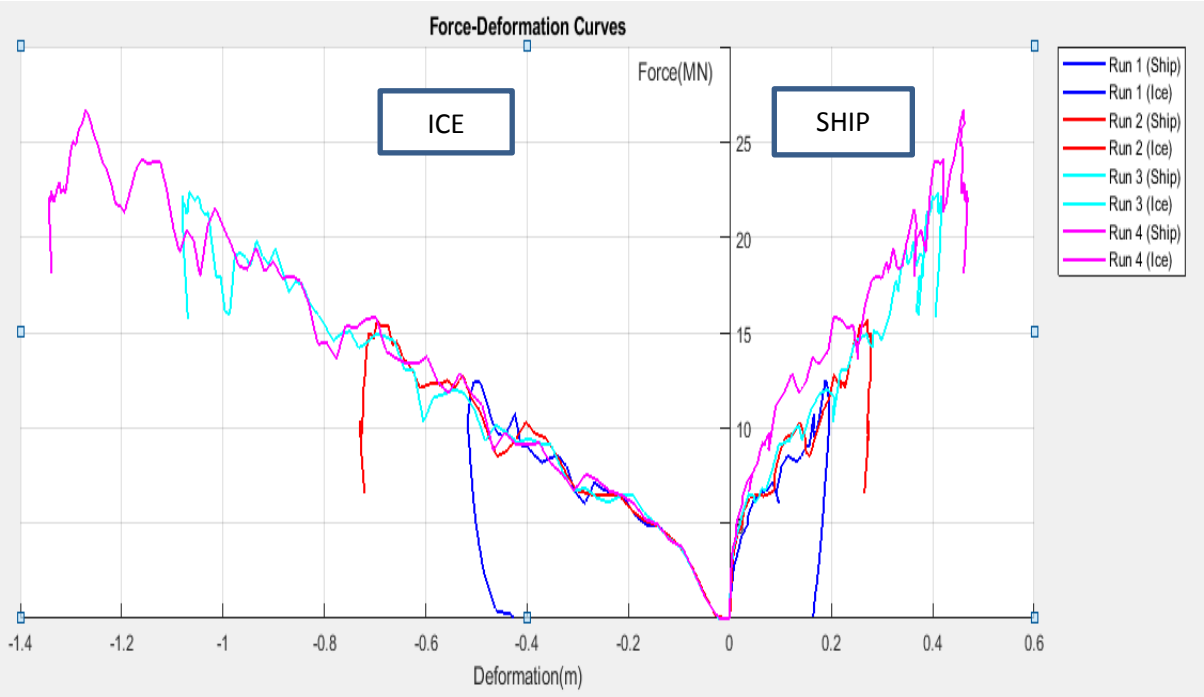

Figure 104 Force-Deformation curves corresponding to impacts with various ice masses

Figure **104** shows the F-D plots wherein each curve belongs to the respective ice masses which are clearly illustrated in the same figure. Since the coupled NLFEA approach is based upon the principles of momentum, kinetic energy plays the dominant role in the collision process. This fact is clearly evident from the plots that 1500 ton ice berg yielded huge deformations in ship panels and crushed larger quantity of ice than the other cases on account of the massive kinetic energy of ice. The F-D plots shows a linearly increasing trend since around 500 tonnes is added to the floe in each successive simulation. The ice floes with largest kinetic energy contributed more to the damage potential, as the 1500 ton ice floe induced maximum force and deformation on the structure in comparison with the other simulated cases. It has been found from the simulations that the ship outer plate and transverse frames seems to absorb most of the energies in the collision process, as these members deformed extensively when 1500 ton ice floe collided against it. The collision with 1500 ton ice feature moving with a velocity of 5m/s yielded energy dissipation (strain,sliding & damping) of around 17.5 MJ which is quite large and it denotes the fact that massive ice feature can cause significant damage to structures. Hence this value can very well be considered for ALS design. This value is more than that of the collision between platforms and supply vessels. For example, the energy dissipated in a collision between platforms and supply vessels in North sea is around 14 MJ (Liu 2011). This comparison indicates the massive damage potential inherent in large ice features with significant kinetic energy.

In short, the kinetic energy is the dominant factor in coupled collision process. As during collision process, this kinetic energy is transferred from the striking object to struck object and converted into strain energy owing to the deformation of both the objects.

8.1.3.1.4 Sliding of Ice Floe:

In the previous chapter, after many iterations, it had been concluded that the ice slided, if it had been assigned with velocities both laterally and sideways. Using the similar approach, in this section, the ice floe is imparted with velocity components both in the lateral direction and in the sideways. In the previous simulation using FPSO model, the ship side is kept perpendicular to the ice, however in this analysis the passenger ship model is oriented 70 ° with respect to the ice floe. To make good interaction between the ship and ice during oblique collisions, out of the 20 m dia ice floe, initial 5 m is modelled as ice and the remaining mass is assigned to the ice pusher. The kinetic energy of ice will be similar corresponding to the 20 m diameter ice floe.

Three different simulations have been conducted and are listed below

Simulation Runs	Lateral Velocity	Sideway velocity	FS parameters
Run 1	5 m/s	1.25 m/s	M=1, N=1
Run 2	5 m/s	3 m/s	M=1, N=1
Run 3	5m/s	3 m/s	M=1, N=0.25

Figure **105, 106 & 107** shows the stress distribution pics of the ice sliding at two time instances, one during the initial contact and other time corresponds to the instant where the ice has completed sliding and rebounded backwards with some residual kinetic energy.

Firstly, let us consider the first two simulations (Run 1 and Run 2). Sliding of ice happened in both the simulations, however the magnitude and extent of sliding is slightly higher in the second case with velocities (5 & 3 m/s). In the 1st case, sliding occurred almost 0.32 m whereas in the other case, the ice has slided almost 0.8 m to its right. Extent of sliding is 2.5 times higher than that in the first case because of higher sideway velocity, therefore larger kinetic energy. This in fact is more clearly illustrated in Figure **105 & 106**

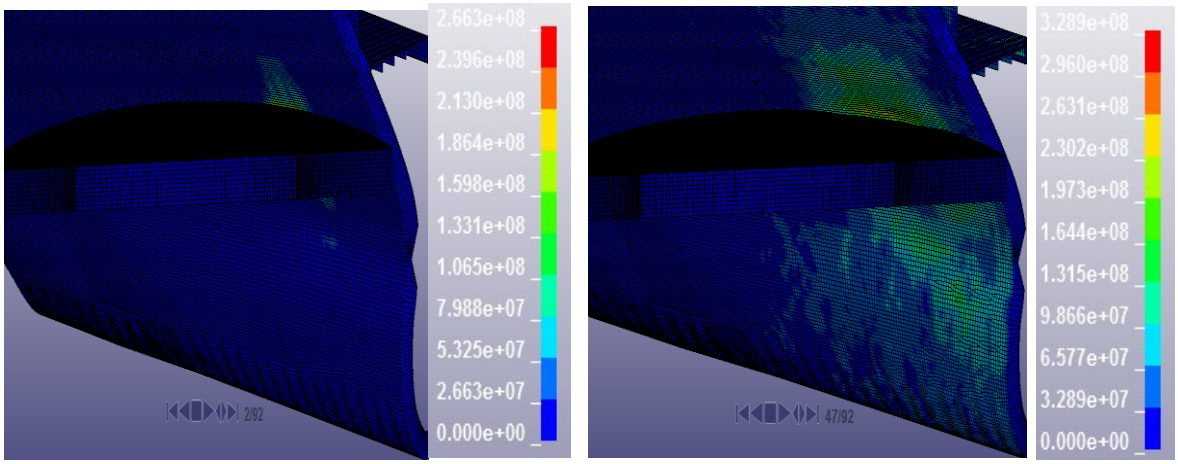

(a) Before the start of sliding (b) After Sliding

Figure 105 (a,b) Sliding of ice for Run 1

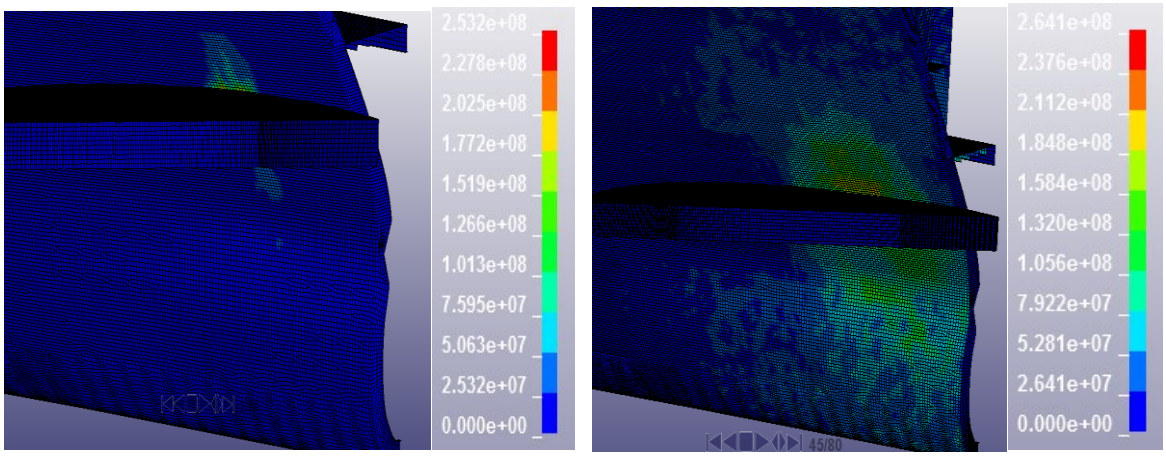

(a) Before the start of sliding (b) After Sliding

Figure 106 (a,b) Sliding of ice for Run 2

It is visible from the stress distribution pictures that the ice slides to its right. The reason for making the ice to move to its right (approaching the fore part of the ship side), is that the ice, by default moved to its right after the impact. So, by assigning the sideway velocity component to the right side of the ice resulted in considerably more sliding. This conclusion is based on the conducted trial runs.

In this analysis, by orienting the ship model almost 70 ° and imparting the ice floe with velocity components in two directions, maximum of 0.8 m sliding has been achieved when the first two simulation runs are taken into consideration. Though in the pictures presented above, it is hard to notice the sliding of ice, it can be clearly seen in the LS DYNA animations. The sliding of ice is considerably higher than what had been witnessed in FPSO simulations. The reason being the usage of oblique impact angles and different velocity components.

Run 3 is somewhat different from the first two simulations. The last simulation has been conducted from the point of view of natural ice sliding. In nature, based on ice strength, the ice is classified as brittle ice and ductile ice. The contact friction is higher in the case of brittle (weaker ice), so it has good sliding capabilities. On the other hand, ductile (stronger) ice has frictionless contact due to its plastic nature, so it does not slide. Applying this principle in the collision simulation, it has been found that the first two simulations have been conducted using harder ice (M=1,N=1), so the ice did not slide considerably.

For Run 3, the ice has been modelled more brittle using the failure strain parameters M=1 and N=0.25 which corresponds to the soft ice. Finally it turned out that the ice has slided for longer distance almost 1.5 m. The ice sliding corresponding to Run 3 in presented in Figure **107 a&b.**

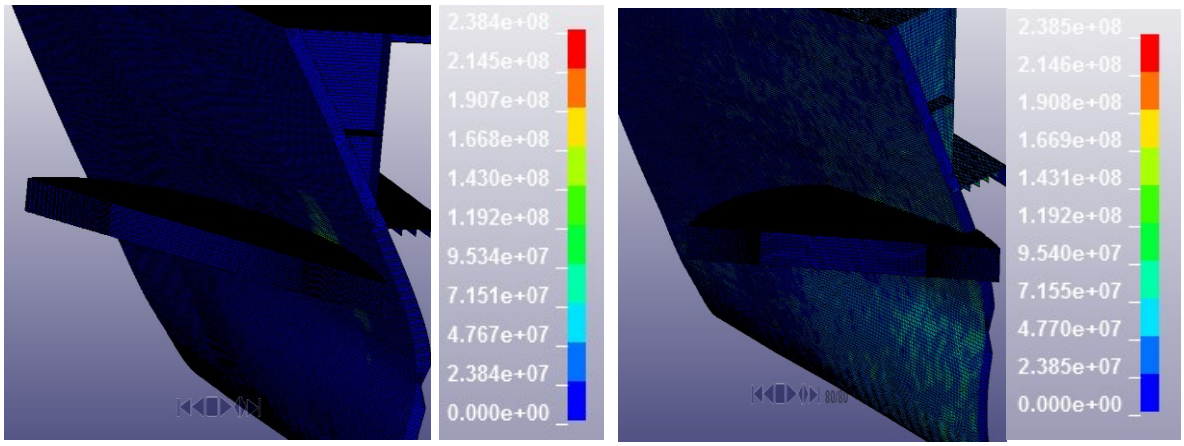

(a) Before the start of sliding (b) After Sliding

Figure 107 (a,b) Sliding of ice for Run 3

So, from this section, it is concluded that in the simulations, brittle/weaker ice is sliding for longer distances thus coinciding with the behaviour of natural brittle ice. Still, with the choice of better combination of impact angles and velocity components, the ice can be made to slide for longer distances along the ship surface. However, there is no direct method to choose the suitable impact angles and ice velocities, as the ice sliding in NLFEA is completely different from the sliding in simplified external mechanics approach and they cannot be compared particularly for ice sliding. As a result, numerous iterations should be conducted to find the impact angles and velocity components that can make the ice to slide for longer horizontal distance in NLFEA analysis.

.

8.2 CONCLUSION POINTERS:

The analysis, results and discussion presented in the chapter are briefly concluded here

- Ice floe collision against passenger vessel resulted in the activation of different failure modes like deformation of outer plates, tripping of web frames, buckling of stiffeners. The regions outside the ice strengthened region resulted in more deformation owing to lesser strength.
- The effect of different steel strengths in accidental collisions have been studied using steel grades S235,S275,S355,S460. The structure with lesser steel grade deformed more in comparison with higher grade. So the possibilities of occurrence of fractures are high in the case of structures with lower steel grades.
- Similar to the FPSO-Ice floe collision, the energy dissipation from passenger vessel-ice floe collision resulted in energy dissipation which is around 37% of that computed from external mechanics. The dissipated energy from NLFEA is denoted as the required energy dissipation and that calculated from simplified external mechanics is termed as the demand for energy dissipation. These results are comparable with the analysis cases of Liu, who developed this external mechanics subroutine, this signifies that the NLFEA results are reasonable.
- Also in coupled analysis, the effect of kinetic energy in accidental collision has been checked by varying the velocity and mass of ice floes. Increase in floe velocities produced maximum deformations in ship structures because of larger kinetic energy. Similarly, collision using 1500 ton ice floe moving with 5m/s resulted in energy dissipation of around 17.5 MJ which is higher than the dissipated energy from platform-supply vessel collision in North Sea. This indicates the damage causing potential of large ice features.
- In coupled approach, the force levels exerted on structures depends on kinetic energy of ice in addition to the strength of ice and structure.
- Sliding of ice has been simulated by orienting the ship structure and the assigning two velocity components to the ice floe. Sliding occurred for a longer extent when brittle ice has been used. Still by using apt collision angles and impact velocities, the ice can be made to slide for longer distance.

CHAPTER 9

9.1 Simplified analytical method for estimating crushing of ice

Simplified methods for force-deformation relationship in ice:

In chapter **5,** ice mechanics has been extensively studied by simulating ice-rigid structure interaction. In that case, ice is the only object that had been crushed. So, here some efforts are dedicated to form force-crushing distance relationship for ice based on simplified methods.

Crushing strength of ice follows the relation,

$$P \propto \frac{1}{\sqrt{A}} \tag{43}$$

Where P is the pressure and A is the nominal contact area

By removing the proportionality in the above equation, it can be written

$$P = \frac{C_R}{\sqrt{A}}$$

Where constant C_R can be regarded as the ice strength coefficient. (Polojarvi 2017)

According to ISO, the ice strength coefficient for ice found in Arctic areas is 2.8 MPa and for ice present in other regions is 1.8 MPa (Tukhuri, Ice Mechanics - Ice failure against structures 2016)

Force due to ice crushing can be developed from the Pressure-Area relation through a simplified formula and is given by the relation.

$$\text{Crushing Force, } F = P.\ A \tag{44}$$

Where A is the nominal contact area of the cylindrical ice floe. There is no predetermined procedure for calculating the nominal surface contact area of a cylinder. So, here it is computed using the simple formula $A = (2\pi r - 2\pi(r - x(t)))H = 2\pi x(t)H$

$$A = 2\pi x(t)H, \tag{45}$$

is taken as the nominal contact area of a cylinder

Where x(t) is the crushing distance which is a function of time(t) since it varies with t, and H is the height of the cylindrical ice feature and r is the radius of ice.

On applying the nominal contact area and pressure in equation **45,** the crushing force can be derived as

$$F = \frac{C_R}{\sqrt{2\pi x(t)H}} * 2\pi x(t)H$$

$$F = \boldsymbol{C_R}\sqrt{\mathbf{2\pi x(t)H}} \quad (46)$$

is the equation derived for crushing force.

In order to solve for the crushing force, there is a need to develop an equation to solve the crushing distance x(t).

Here, the principle of momentum approach has been applied. Based on this, the external work can be equated with the internal work. As a result, it follows that the change in kinetic energy is equal to the work done.

$$E_{Initial}^{Kin} - E_{Final}^{Kin} = \int_0^x F\ dx \quad (47)$$

Assuming that the collision is plastic and the ice is completely stopped after the impact. It follows that the final kinetic energy is zero, so the above equation becomes.

$$E_{Initial}^{Kin} = \int_0^x F\ dx$$

$$\frac{1}{2}mV^2 = \int_0^x C_R\sqrt{2\pi x(t)H}\ dx$$

Solving the terms on the right hand side, the following relation is attained.

$$\frac{1}{2}mV^2 = \frac{2}{3}C_R\sqrt{2\pi H}\,x(t)^{\frac{3}{2}}$$

On rearranging the terms, the equation for x(t) is derived and is given by

$$\text{Crushing distance } x(t) = \left(\frac{3mV^2}{4C_R\sqrt{2\pi H}}\right)^{\frac{2}{3}} \quad (48)$$

Using the above relation, crushing distance can be solved which represents the maximum ice penetration distance. And when this maximum crushing distance (x(t)) is applied in equation **47,** the maximum force can be derived.

$$\mathbf{F} = \boldsymbol{C_R}\left(\frac{\mathbf{3mV^2H}}{\mathbf{4C_R\sqrt{2\pi}}}\right)^{\frac{1}{3}} \quad (49)$$

is the simplified formula which can be used to compute maximum force in ice-rigid structure interaction

9.1.1 Validation of the proposed simplified formula for ice crushing

In chapter **5,** section **5.3.3.6,** one simulation was performed based on coupled approach. Using the results from the simulation, the proposed analytical model for ice crushing is validated.

The maximum crushing distance can be calculated using the following formula

$$\text{Crushing distance } x(t) = \left(\frac{3mV^2}{4C_R\sqrt{2\pi \mathrm{H}}}\right)^{\frac{2}{3}}$$

The values for ice strength coefficient corresponding to different regions is given in the previous section. For this computation, $C_R = 1.8\ MPa$ is chosen.

The ice strength coefficient along with other parameters are entered into the above equation and the crushing distance is calculated as

Maximum Crushing Distance x(t) = 0.14 m

Max. Crushing Distance from Proposed Analytical formula	Max.Crushing distance from Simulation in chapter **5,** section **5.3.3.6**
x(t) = 0.12 m	x(t) = 0.16 m

From the above comparison between the proposed analytical formula and the simulation, the maximum crushing distance from simulation is marginally higher. The analytical formula seems to produce a value for maximum penetration distance 25% lower than that from the simulation. Since the difference is not really significant, this proposed analytical formula can very well be used for initial estimates for the maximum ice penetration.

9.2 Simplified analytical method for computing global structural deformation

In this section, a simplified analytical formula has been proposed for calculating the global ship deformation subjected to ice impacts.

From the energy balance, it can be stated that

$$\text{External Mechanics} = \text{Internal Mechanics} \tag{50}$$

It has already been mentioned that the total energy dissipated due to structural deformation comprises strain (E_{st}), sliding (E_{fn})and damping (E_{dm}) energy components. Considering this, the external mechanics can be equated as

$$\text{External Mechanics (E.M)} = E_{st} + E_{fn} + E_{dm} \tag{51}$$

Strain energy dissipation can be computed from E_{st} = F. dl

Where F is the Force, dl is the deformation/displacement

Ice, naturally has some inherent friction, so there will always be energy dissipation due to sliding, both for the direct and oblique/sliding impact cases. However, the magnitude of sliding energy dissipation will be higher in the case of oblique/sliding impacts in comparison with direct impacts. Sliding energy dissipation can be calculated as

$$E_{fn} = \frac{1}{2} T_{fn}(\omega_1 - \omega_2) t_{dn}$$

Where T_{fn} is the frictional torque in N.m, ω_1, ω_2 ($\frac{rad}{s}$) are the speed at the start of deceleration and end of deceleration respectively and t_{dn} is the time of deceleration.

The damping here can be due to material damping. So, Damping energy dissipation can be computed using, $E_{dm} = \pi C \omega X^2$

Where, C is the damping constant, ω is the frequency and X is the structural response

External Mechanics (EM) deals with the kinetic energy of the ice feature, as a result the kinetic energy can be written as

Kinetic Energy (Ice) = $\frac{1}{2} mV^2$,where m is the mass(kg) of the ice feature and V is its velocity (m/s). Here, it considered that the ice is stopped after the impact.

Substituting these formulas for energy components in Equation **52.** The following equation system can be achieved

$$\frac{1}{2} mV^2 = \text{F. dl} + \frac{1}{2} T_{fn}(\omega_1 - \omega_2) t_{dn} + \pi C \omega X^2 \tag{52}$$

Using the simplified Equation **53.** the global ship deformation and corresponding force levels due to ice impacts can be computed.

In Equation **53,** it is cumbersome to compute the parameters related to sliding and damping energy and in addition the share of these dissipated energies are relatively minor in comparison with the strain energy dissipation. So, equation **53** is simplified based on some assumptions

which are listed below

Assumptions:

- From the simulations, it has been noticed that the dissipated frictional energy is roughly around 10% of the dissipated strain energy and the damping energy dissipation is close to 3% of the dissipated strain energy. These values are considered in the simplified formula.
- Sliding of ice has been simulated by imparting two velocity components to the ice. The sliding energy dissipated from sliding/oblique impacts is twice higher than the dissipated sliding energy in direct impacts with one velocity component.

Direct Impact Case:

Applying the first assumption in equation **52,** the following simplified form can be developed

$$\text{E.M} = E_{st} + 0.1E_{st} + 0.03\ E_{st} = 1.13E_{st}$$

$$\frac{1}{2}mV^2 = 1.13*(\text{F.dl}),$$

Force, F = Stress/Cross sectional area = $\frac{\sigma}{A}$

Stress,σ = Eε, E is the modulus of steel in N/m^2 and ε is the strain.

$$\text{dl} = \frac{\boldsymbol{mV^2A}}{\mathbf{2.26\ E\varepsilon}} \tag{53}$$

which can be used to estimate the global structural deformation for direct ice impacts.

Oblique/Sliding Impacts:

For oblique/sliding impact case, in addition to the first simplification, the second assumption is also incorporated. Applying them in equation **52**, the following equation is derived

$$\text{E.M} = E_{st} + 0.1E_{st} + 0.06\ E_{st} = 1.16E_{st}$$

$$\frac{1}{2}mV_R^2 = 1.16*(\text{F.dl})$$

$\mathbf{dl} = \frac{\boldsymbol{mV_R^2A}}{\mathbf{2.32\ E\varepsilon}}$ can be used for estimating global deformation of ship side structure subjected to oblique/sliding impacts. Here, resultant velocity, V_R is used since sliding of ice had been achieved using two velocity components (lateral and sideway components)

9.2.1 Validation of the proposed simplified methods:

Here, the equation proposed for analysing the structural deformation for the direct ice impact case have been calculated and compared with the simulation data corresponding to the ice floe impacting FPSO side at 2m/s (coupled approach)

$$dl = \frac{mV^2A}{2.26\ E\varepsilon}$$

As a far as strain is concerned, for large deformations green's strain has to be used, whereas for small deformations nominal strains must be used. Here, the calculation is related to the ice floe colliding with the FPSO at an impact velocity of 2m/s. This impact caused only minor deformations on ship side, so it is sufficient to use the nominal/engineering strain.

However, if one wants to evaluate the case of ice floe hitting the passenger vessel at 5m/s, it becomes mandatory to use the greens strain, since this impact is associated with large deformations in ship side.

So, nominal or engineering strain$(\varepsilon) = \frac{\text{deformed length(dl)}}{\text{Original length(L)}}$

Original length is taken as the distance between the two far ends of the panel which is 9.6 m

Cross sectional area is considered as the rectangular strip = (L)* w , where L is the original length and w =1.65m is the vertical distance between two girder plates between which lies the impact location

Applying all these formulas in the proposed equation, the following value is derived.

$$dl = 0.0195 \sim 0.02\ m$$

Comparison has been made between the deformation calculated from simplified formula and that from the simulation corresponding to ice floe hitting the FPSO with an initial velocity of 2 m/s (Coupled Approach)and shown below.

Deformation (Proposed Analytical Formula)	Deformation (Direct impact NLFEA)
0.02 m	0.028 m

From the comparison, it can be seen that the NLFEA produced higher deformation. The global structural deformation computed from the proposed simplified analytical model seems to lag behind the NLFEA by almost 28.6 %. However, difference of 28.6% between the NLFEA and analytical model is acceptable and this formula can be used for some initial estimates.

9.3 Simplified analytical method computing deformation of local structural components

In the previous section, simple analytical models have been put forth for global structural deformation. Here, simple models for analysing the deformation of local structural components have been presented. The proposed analytical models are mostly based on the works of Zhaolong Yu et al(2014) and Hong et al.(2008), in addition some simplifications have been introduced to suit the collision cases presented in this thesis.

For the case of ice floe collision with FPSO at a velocity of 2 m/s (coupled approach), small amount of deformation occurred in the outer plates and frames. However, for the case of ice colliding with passenger vessel at a velocity of 5 m/s (coupled approach), extensive deformations of structural members were noticed. For this case, there occurred many deformation modes in outer plates, frames, stiffeners, and girder plates. As a consequence, there could be energy dissipation associated with each of these deformation modes.

In this section, only the deformation of the outer plate has been considered. The force-deformation relationship for the outer plates have been established based on energy considerations. (Zhaolong Yu 2014).

The internal mechanics can be equated using the formula

$$\boldsymbol{F_P.dl = E_{Int}} \tag{54}$$

Where F_P is the plastic force, Δ is the deformation and E_{Int} is the internal energy

In outer plate, dominant part of the energy is dissipated due to membrane stretching. The membrane energy dissipation is represented using the formula

$$\text{Membrane Energy} = \boldsymbol{E_m} = \int_V \boldsymbol{\sigma_o \varepsilon_{eq} dV} = \boldsymbol{N_o u dt} \tag{55}$$

Where σ_o is the flow stress, ε_{eq} is the equivalent strain , $N_o$is the plastic membrane force and u is the strain rate.

$$\boldsymbol{E_m = N_0}\ \text{dl} \tag{56}$$

Membrane Force, $N_0 = \sigma_0 lt$

Where l, t is the length, thickness of the outer plate.

The above equation **57** after substituting the value of N_0, becomes

$E_m = \sigma_0 lt$ dl which can be regarded as the membrane energy due to membrane force.

The total internal energy becomes,

$$\text{So,}\quad \boldsymbol{E_{Int} = \sigma_0 lt}\ \text{dl} \tag{57}$$

A formula for 'dl' should be developed based on an idealised deformed geometry. On account of time constraints, no idealised deformed geometry has been proposed and the 'dl' is left as it

is. Since the equation for analysing the deformation of outer plate is incomplete, it is not validated.

9.4 CONCLUSION POINTERS:

- The analytical formula proposed for estimating the ice penetration depth during rigid structure-small ice interaction produced value 25 % lesser than that from the simulation data and the equations proposed for predicting the global deformation of ship side in FPSO-Ice floe collision gave value 28.6% lesser than that from the simulation. Since these ranges are under acceptable limit, the proposed equations can be used for initial estimates.

CHAPTER 10

10.1 ADVANCED ANALYSIS METHODS

An important fact that should be noted is that the ice behaves as a continuum material only before failure. After failure, a continuous block of ice is converted into pile of ice pieces which behave as discrete materials. Figure **108** gives a pictorial representation of this fact, the ice behaves as a continuum material before the limit event and after that it becomes discrete materials. The limit event could be shear fractures, flexural failure etc caused due to ice-structure interaction. As far as numerical analysis is concerned, modelling the failed pieces of ice is as important as developing the continuum model. The reason being that the ice pieces contribute to separate loading cycles on structures that need to be accounted in order to have a safe design of structure.

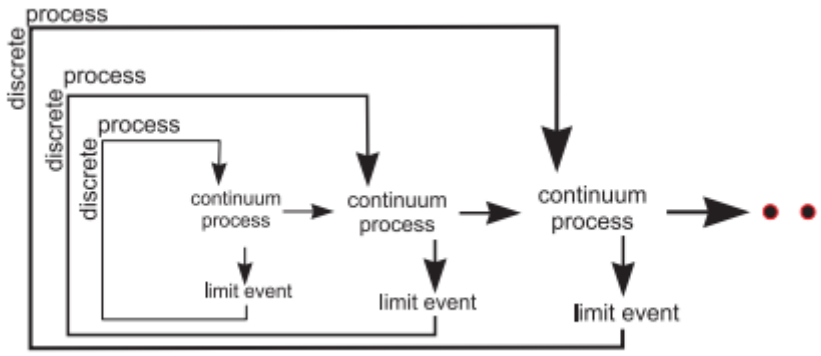

Figure 108 Picture illustrates the failure cycles of ice (Tukhuri, Ice Mechanics-Ridges and Rubble piles 2016)

10.1.1 FEM-DEM approach

Before discussing the concept of FEM-DEM approach, the concept of Discrete element technique should be known. DEM is used to model the discontinuous system with large number of discrete particles. Through this technique, the interaction between the particles and the resulting deformation of the system can be effectively studied.

The DEM procedure for simulating the action of discrete particles includes the following

- Finding pairs of contacting blocks
  The first part deals with detecting the geometry of particles that come into contact with each other.

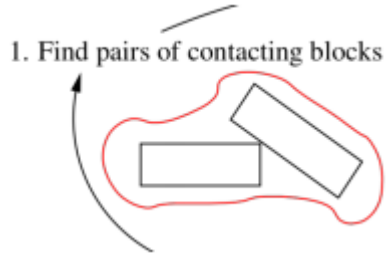

Figure 109 depicts the first step in DEM process in which the blocks that come into contact are found (A. Polojarvi, Ice Rubble and Ridging 2017)

- Solving the contact phenomenon
  The interaction process may give rise to forces, friction, plasticity, damping etc, which are modelled using dynamic equation of motions

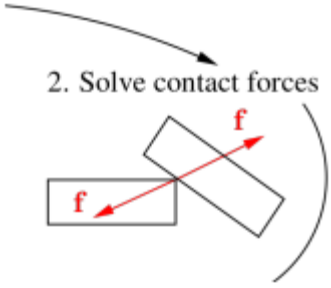

Figure 110 shows the second step in DEM where the forces that arise due to the contact between the particles are solved

- Explicit time stepping:
  The solution to the equation of motion is derived using an explicit time stepping algorithm.

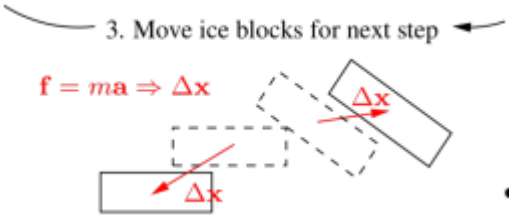

Figure 111 illustrates the final step where the solution is derived for each time step

The main reason for applying DEM to modelling ice is that the failed ice block after impact behaves like a granular material, thus they interact with each other, deform and transmit more force to the structure and these effects can be captured through DEM. On the other hand, the continuum approach is a better approach for modelling the ice floe before failure (impact). Based on the considerations, it can be concluded that a hybrid method (FEM-DEM) combining both continuum and discrete modelling could be an efficient technique for numerical ice modelling.

In this thesis, combined FEM-DEM approach has been created. LS DYNA introduced a newest

keyword called ADAPTIVE_SOLID_TO_DES, wherein the solid elements after reaching their failure strain gets converted to discrete element spheres, similar to that of FEM-SPH.

10.1.2 Modelling:

FEM-DEM simulation has been conducted based on strength design analysis (Rigid Structure-Ice interaction). The same small ice floe of 2m diameter which was used in

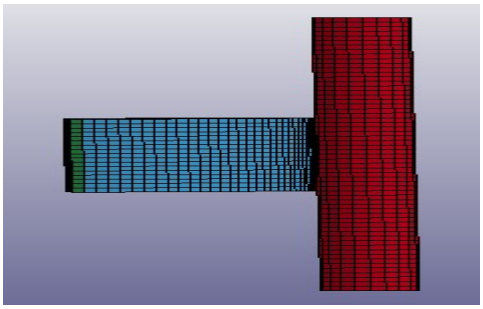

Figure 112 Model setup for the analysis

Chapter **5** is also used here. The ice floe is collided with a cylindrical rigid structure of 0.4 m diameter and 3m height. Cylindrical rigid structures are representatives of the offshore structures found in the Arctic region. The model set up is shown in Figure **112.** FEM-DEM coupled approach can be simulated only using the latest LS DYNA solver and kim's ice model is not yet implemented into the latest LS DYNA solver. So for this simulation the ice had been modelled using a MAT card called PLASTIC_KINEMATIC in LS DYNA. Using this keyword, elastic-plastic behaviour of ice can be modelled by specifying the suitable failure strain of ice. In this simulation low failure strain of 0.15 had been used in order to simulate brittle behaviour of ice.

The ice properties entered into the MAT card is listed below

Density	900kg/m3
Modulus	9500 MPa
Poisson's ratio	0.3
Failure strain	0.15

Furthermore, various parameters need to be defined for the generation of discrete element spheres. The most important attributes of discrete element particles are their bond strength and contact stiffness. These parameters along with other vital parameters for ice discrete particles are referred from (Shaocheng Di 2017), (Shunyung Ji 2014) and (Jani Paavilainen 2006) and they are listed below. These parameters are specified inside ADAPTIVE_SOLID_TO_DES keyword.

Normal Bond Strength, σ_b^n	0.5 MPa
Shear Bond Strength, σ_b^τ	0.5 Mpa
Normal Stiffness, k_{ne}	30 MPa
Tangential Stiffness, k_{te}	20 Mpa
Bond Stiffness Ratio	0.67
Bond Modulus	10 MPa

10.1.3 Results and Discussion:

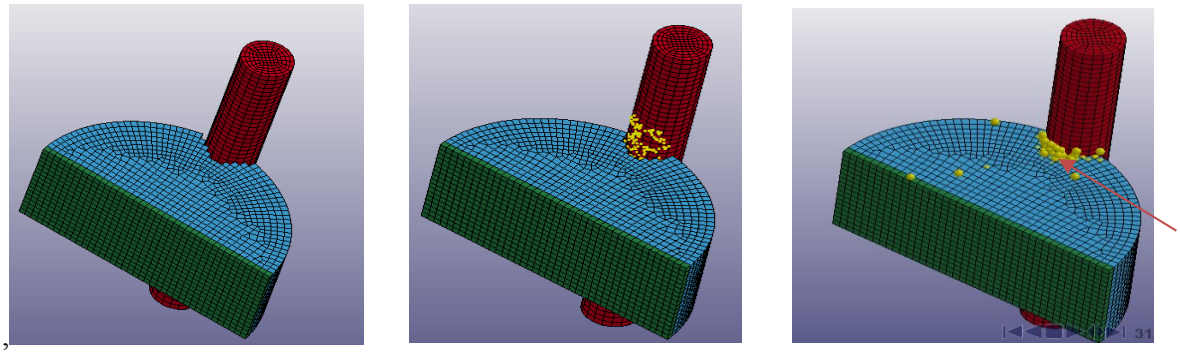

(a) FEM (b) FEM-SPH (c) FEM-DEM

Figure 113 shows animation pictures corresponding to a) FEM ice model b)FEM-SPH ice model c) FEM-DEM ice model

Using the above parameters related to the discrete element particles and the PLASTIC_KINEMATIC keyword, the FEM-DEM simulation has been conducted and compared with the FEM and FEM-SPH techniques which are also modelled using the same plastic kinematic material. The simulation pictures are shown in Figure **113.** The animations corresponding to the FEM-DEM simulation is presented in Figure **113 c** and it could be clearly seen that the discrete element particles are generated after the failure of ice elements. Here FEM-DEM NQ1 option has been used, thus after the failure of one ice element, one discrete element particle is generated, which possess the same properties as that of the ice.

10.1.3.1 Spatial Pressure Patterns

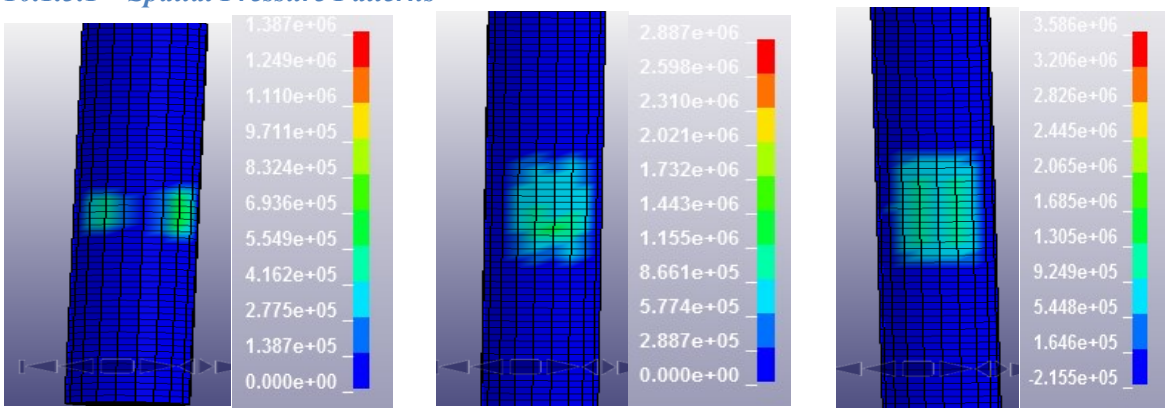

(a) FEM (b) FEM-SPH (c) FEM-DEM

Figure 114 Interface pressure patterns corresponding to a) FEM ice model b) FEM-SPH ice model c)FEM-DEM ice model

The spatial pressure patterns corresponding to FEM, FEM-SPH and FEM-DEM at 0.05 s are presented in Figure **114 a,b,c** As usual the FEM model produced unrealistic zero pressure circles in the middle. The FEM-SPH and FEM-DEM produced continuous distribution of spatial pressures across the contact surface. More importantly, it could be noted that the FEM-DEM model produced high quality pressure distribution, in other words, at the contact surface the spatial pressures are distributed symmetrically.

FEM-DEM modelling can be considered superior to FEM-SPH in many respects. For instance,

in natural ice crushing scenarios, the continuous ice feature is broken into many discrete particles which possess the same properties as that of the ice from which it is broken. In addition, the broken ice particles contribute to some forces on the structure, fails the incoming ice and interact with each other as well. The discrete element particles seem to replicate certain such behaviours like that they have same properties as that of the continuous ice, contribute to some forces on the structure and discrete spheres are interacting with each other. Considering these, it might be inferred that FEM-DEM hybrid ice modelling resembles the ice crushing to a very good extent.

10.2 CONCLUSION POINTERS

- In this chapter, the state of the art FEM-DEM technique had been applied for ice modelling using the newly developed keyword ADAPTIVE_SOLID_TO_DES in LS DYNA.
- Using plastic kinematic mat card, the ice is modelled and the crushing behaviour of FEM-DEM seems to represent the natural ice crushing to a considerable extent, with the only exception that in natural ice discrete particles are randomly shaped and are generated based on fracture mechanics whereas in this model fracturing is not accounted for and it generates uniform discrete spheres.
- FEM-DEM ice model produced a more symmetric spatial pressure pattern.
- On account of time constraints, the force-deformation and process P-A curves of this model could not be studied and still further improvements are required when it comes to ice modelling using this keyword in LS DYNA.

CHAPTER 11

11.1 CONCLUSION

This thesis began with addressing the problems related to the ice-structure interaction, some key issues have been addressed in this part regarding the hydrodynamic effects in the interaction scenario and the lack of stochastic models representing the ice loads. Analysis of the external dynamics using various analytical approaches have been presented. Review on the design of ice strengthened vessels clearly shows the variation between the normal and ice going vessels from structural design point of view. Furthermore, one can clearly understand how much a vessel should be strengthened with respect to its level of exposure to ice conditions.

The ice berg properties are elaborately detailed and it was startling to know that the research on studying the fracture toughness properties of ice bergs has not been undertaken till now. In addition, various material models for capturing the ice failure has been presented along with detailed explanation on the user defined material model used in this thesis. Moreover, some theories related to state of the art technique(SPH) that can be used to model ice was given. From this, the reader can clearly understand about the existing models using which the ice can be modelled. This discussion on the different theories related to the P-A curves provided the basic knowledge on how to represent the loading scenario in terms of P-A curves.

In chapter 5, numerically efficient techniques for modelling different ice features had been presented, followed with the crushing simulations of growler and a small ice floe against rigid plates. Both FEM and FEM-SPH ice model were taken into account. FEM-SPH model seemed to be conservative, in the sense that it produced higher force levels, almost 1.7 times higher than that of the FEM model. More importantly, FEM-SPH model yielded local pressure patterns closer to what can be observed in real ice crushing scenarios. The information on local pressures are necessary for design of local structural components, so for the analysis related to such design cases, FEM-SPH ice models can be used.

Furthermore, envelope of spatial curves were plotted for randomly chosen five different instances. Still some improvements are required in terms of coding an algorithm that could find the time steps at which high pressure peaks may occur and plotting spatial curves for those time instances.

From the shared energy analysis carried out using stiffened panel-growler impact, it was found that the ice model was not strong enough to make significant impact on the structure.

In the analysis performed using rigid plate and stiffened panel, the response of ice had been effectively studied using f-d curves, process P-A curves, spatial P-A patterns and envelope of spatial curves. Whereas in the analysis using FPSO and passenger vessel, more emphasis had been laid on the structural response of the ships subjected to accidental loads. Ice had been modelled intentionally hard and it turned out that the process P-A curves corresponding to the hard ice surpassed the conservative ISO pressure curves. Collision analysis in FPSO were conducted based on the principles of both coupled and decoupled approach. Simplified external mechanics had been computed using Liu's subroutines coupled with the input files generated in this thesis. The required energy dissipation from coupled approach was just around 37% of the energy dissipated from fully plastic impact (decoupled approach limited using external mechanics output). The thickness of the structural components plays a vital part, in that the structure with reduced thickness experienced more deformation than the structure with default thickness, One advantageous fact with weaker panel is that lesser force levels recorded in ice-

structure interaction, since only less quantity of ice had been crushed, but it possessed the risk of development of early fractures. Increasing the frictional coefficient of this ice model is not suggested as it weakened the ice model. And more importantly, the sliding of ice from oblique impacts simulated from NLFEA cannot be compared with simplified external mechanics approach, since the external mechanics assumes that the significant amount of energy is dissipated as sliding, whereas, in NLFEA major part of the energy is dissipated as strain energy as the ice did not slide with one velocity component. However, the sliding of ice to a certain extent had been achieved by imparting the ice with two velocity components.

Since the FPSO side model and passenger vessel are almost similar, few analysis were similar in both cases, but certain other analysis were differed in the sense that the effect of different shape of ice features, thickness effect, frictional coefficient effect were studied in FPSO collision case. On the other hand, the effect of strength of steel grades, floe velocities effect and effect of ice mass were analysed in the passenger vessel case. In accidental ice impacts, structures with lower steel grades experienced considerable deformation and consequently possessed more risk of attaining fractures. From the analysis corresponding to the different floe velocities and masses, it was concluded that larger the kinetic energy, more extensive the damage on both the ice and the structure. The force on the structure directly depends on the strength and kinetic energy of the ice feature.

The proposed analytical model for estimating the ice deformation and ship deformation gave reasonable results and it was concluded that they can be used for initial estimates.

From the discussions in chapter 10, it can be inferred that the FEM-DEM ice model in LS DYNA appears to be an effective technique for representing ice-structure interaction scenarios, but still the model needs considerable refinement.

11.2 RECOMMENDATIONS

This section suggests some recommendations/improvements on the works carried out in this thesis.

- For the case of envelope of spatial curves, an accurate and powerful procedure to find the time instance at which the worst pressure peaks may occur is performing a Monte Carlo simulation. Then the spatial curves corresponding to those time steps can be plotted as an envelope.
- Three different ice features were used in the decoupled collision analysis of FPSO. Out of the three, simplified external mechanics computation were carried out for the cylindrical ice floe and spherical ice growler. However, the external mechanics could not be used for the case of collision with tabular bergy pit, since suitable added mass coefficients and gyration radius formulas could not be found for a rectangular shaped object. As a result, some improvements are needed in the simplified external mechanics codes in order to include ice berg shapes other than circular.
- For the analysis concerned with impacts outside the ice strengthened region due to wave induced motion, the ice was just aligned to hit the non ice-strengthened region. Realistic impacts due to wave induced motion can be conducted only by modelling waves. The waves in LS DYNA can be modelled in two ways, either by using ALE or ICFD technique. In ALE approach, waves cannot be generated, so a piston must also have to be modelled at the far end of the fluid domain and pushed in order to generate waves. Modelling waves using ALE technique is quite complicated. On the other hand,

in ICFD technique, regular waves can be generated without modelling any pistons, however this technique is computationally much more demanding than the ALE technique. Suitable techniques can be chosen based on the resources available.

- There is an approach called FEM-CEM, finite element method coupled with cohesive element method which takes into account the fracturing of ice. This approach must be investigated for ice modelling.

References

Amdahl, Jorgen. 2017. *Accidental Limit State Analysis of Abnormal Ice Actions.* Conference Presentation, Lisbon, Portugal: MARSTRUCT 2017.

Andrew Palmer, Ken Croasdale. 2012. *Arctic Offshore Engineering.* World Scientific Publishing.

Bai, Yong. 2003. *Marine Structural Design.* Kidiington, Oxford: Elsevier.

Bohlerengen, Simen. 2013. *Probabilistic material modelling of iceberg for analysis of accidental impacts with ships and offshore structures.* Master Thesis, Trondheim: Norwegian University of Science and Technology.

Britannica. 2017. *Iceberg structure, Encyclopaedia Brittanica.* Accessed October 16, 2017. https://www.britannica.com/science/iceberg/.

C.Horvat, E.Tziperman. 2015. "A Prognostic model of the sea-ice floe and thickness distribution." *Cryosphere* 2120-2134.

D.Diemand. 2001. *Ice Bergs.* Periodical, VT, USA: Academic Press.

Daley, Claude. 2004. *A study of the Process-Spatial link in Ice Pressure-Area Relationships.* Research report, St.Johns: Memorial University of Newfoundland.

Daley, Claude. 1999. "Energy based ice collision forces." *POAC 99, 15th International conference on Port and Ocean Engineering under Arctic Conditions.* Helsinki: POAC. 1-20.

Designing Buildings Wiki. 2017. *Limit State design, Designing Buildings Wiki.* 24 July. Accessed September 28, 2017. http://www.designingbuildings.co.uk.

Emayavaramban E, Milan Chhetri, Akash Dan, Sonu Yadav. 2015. *A study of material non-linearity during deformation using FEM software.* Bachelor Thesis, Punjab: Lovely Professional University.

Garry Timco, R.Frederking. 1983. "Flexural Strength and Fracture toughness of sea ice." *Cold Region Sciemce and Technology* 34-41.

Hamid Daiyan, Bjornar Sand. 2011. "Numerical Simulation of Ice-Structure Interaction in LS-DYNA." *8th European LS DYNA users conference* 1-8.

Hong, Lin. 2008. *Simplified Analysis and Design of Ships subjected to Collision and Grounding.* PhD Thesis, Trondheim: Norwegian University of Science and Technology.

Hyunwook Kim, Christopher Ulan-Kvitberg, Claude Daley. 2014. "Evaluation of spatial pressure distributionduring ice-structure interaction using pressure indicating film." *IJNAOE* 578-597.

International association of Classification Societies. 2016. "Structural Requirements of Polar Class Ships." In *POLAR CLASS RULES*.

Jani Paavilainen, Jukka tukhuri, Artu Polojarvi. 2006. "Discrete element simulation of ice pileup against an inclined structure." *Research Gate.*

Kelly S. Carney, David J. Benson, Paul DuBois, Ryan Lee. 2006. “A phenomenological high strain rate model with failure of ice.” *Science Direct* 3-10.

Kim, Ekaterina. 2014. *Experimental and numerical studies related to the coupled behaviour of ice mass and steel structures during accidental collisions.* PhD Thesis, Trondheim: Department of Marine Technology, NTNU.

Konuk, Ibrahim. 2011. “Computational Methods for Solving Dynamic Ice Structure Interaction Problems.” *ASME 2011 30th International Conference on Ocean, Offshore and Arctic Engineering.*

Kujala, Pentti. 2017. *Winter Navigation - Ice Induced Loads.* Lectures, Espoo: Department of Mechanical Engineering, Aalto University.

Kujala, Pentti. 2017. *Winter Navigation-Ice Strengthening Rules.* Lectures, Espoo: Department of Marine Technology, Aalto University.

Kujala, Pentti. 2017. *Winter Navigation-Introduction.* Lectures, Espoo: Department of Marine Technology, Aalto University.

Kujala, Pentti. 2017. *Winter Navigation-Ship Design Principles.* Lectures, Espoo: Department of Marine Technology, Aalto University.

Kujala, Pentti. 2016. *Winter Navigation-Ship resistance in ice.* Lectures, Espoo: Department of Marine Technology, Aalto University.

Liu, Zhenhui. 2011. *Analytical and Numerical Analysis of Iceberg collisions with ship structures.* PhD Thesis, Trondheim: Department of Marine Technology, NTNU.

Livermore Software Technology Corporation. 2011. *Lstc.* Accessed December 14, 2017. www.lstc.com.

M.B. Liu, G.R. Liu. 2009. “Smoothed Particle Hydrodynamics(SPH): an overview and recent developments.” *Arch Computational Methods Engineering* 26-76.

Marchenko, Aleksey. 2014. “Influence of added mass effect on rotation of a drifting iceberg in non-stationary current.” *OMAE* 1-7.

Marco Gherardi, Marco Cosentino Lagomarsino. 2015. “Characterizing the size and shape of sea ice floes.” *Scientific Reports.*

Ming Song, Ekaterina kim, Jorgen Amdahl, Jun Ma, Yi Huang. 2016. “A comparative analysis of the fluid-structure interaction method and the constant added mass method for ice-structure collisions.” *Marstruct* 59-74.

Ming Song, Ekaterina kim, Jorgen Amdahl, Marilena Greco. 2016. “Numerical Investigation of Fluid-Ice-Structure interaction during collision by an Arbitrary Lagrangian Eulerian method.” *ASME. 35th International Conference on Ocean, Offshore and Arctic Engineering.*

Moan, Torgeir. 2007. *Development of Accidental Collapse Limit State Criteria for Offshore Structures.* Lectures, Trondheim: Department of Marine Technology, NTNU.

Moan, Torgeir. n.d. "Non Linear Analysis." In *Finite Element methods*, by Torgeir Moan, 118. Trondheim: NTNU.

Patrick, Keirsebilck. 2015. *Pack ice/drift ice/ice floes drifting in the greenland sea.* 8 June.

n.d. "people.brunel.ac.uk." *www.brunel.ac.uk.* Accessed June 18, 2018. people.brunel.ac.uk/~eesrgat/research/pdf_phd/.

Polojarvi. 2017. *Solutions 3-Ice Loads on Structures.* Espoo, Helsinki, 10 March.

Polojarvi, Arttu. 2017. *Ice Loads on Inclined Structures-I.* Lectures, Espoo: Department of Mechanical Engineering, Aalto University.

Polojarvi, Arttu. 2017. *Ice Rubble and Ridging.* Lectures, Espoo: Department of Mechanical Engineering, Aalto University.

R.E Gagnon, P.H Gammon. 1983. "Characterization and Flexural Strength of Iceberg and glacial ice." *Research Gate.*

Riley, Jonas Rinsberg. 2011. "Collision and Grounding of ships." *ASME* 1-8.

Savik, Svein. 2017. *Advanced Structural Analysis-Non linear Analysis.* Lectures, Trondheim: Department of Marine Technology.

Shaocheng Di, Yanzhuo Xue, Qing Wang, Xiaolong bai. 2017. "Discrete element simulation of ice loads on narrow conical structures." *ELSEVIER* 282-297.

Shunyung Ji, Shaocheng di. 2014. "Analysis of ice load on conical structures with discrete element method." *Emerald Insight* 121-1134.

Storheim, Martein. 2016. *Structural Response in Ship-Platform and Ship-Ice Collisions.* PhD Thesis, Trondheim: Department of Marine Technology, NTNU.

Tukhuri, Jukka. 2016. *Ice Mechanics - Bearing Capacity of Ice.* Lectures, Espoo: Department of Mechanical Engineering, Aalto University.

Tukhuri, Jukka. 2016. *Ice Mechanics - Ice failure against structures.* Lectures, Espoo: Department of Mechanical Engineering, Aalto University.

Tukhuri, Jukka. 2016. *Ice Mechanics - Introduction.* Lectures, Espoo: Department of Mechanical Engineering, Aalto University.

Tukhuri, Jukka. 2016. *Ice Mechanics-Crushing and Contact.* Lectures, Espoo: Department of Mechanical Engineering, Aalto University.

Tukhuri, Jukka. 2016. *Ice Mechanics-Occurence of Ice.* Lectures, Espoo: Department of Mechanical Engineering, Aalto University.

Tukhuri, Jukka. 2016. *Ice Mechanics-Ridges and Rubble piles.* Lectures, Espoo: Department of Mechanical Engineering, Aalto University.

2010. *Wikipedia.* 21 November. Accessed June 8, 2018. www.wikipedia.org.

2007. *Wikipedia.* 13 September. Accessed June 11, 2018. www.wikipedia.com.

WikiPedia. 2017. *Limit State Design, WikiPedia.* October. Accessed November 23, 2017. https://en.m.wikipedia.org/wiki/Limit_state_design.

Yu.N.Popov, O.V.Faddeyev, D.Ye.Kheysin, A.A.Yakovlev. 1967. *Strength of ships sailing in ice (US Army translated version).* Leningrad: Sudostroyeniye Publishing House.

Zhaolong Yu, Zhiqiang Hu, Ge Wang. 2014. “Plastic mechanism analysis of structural performances for stiffeners on bottom longitudinal web girders during a shoal grounding accident.” *ELSEVIER* 134-158.

APPENDIX I

SIMPLIFIED EXTERNAL MECHANICS COMPUTATION

```
%           Simplified External Mechanics Computation (input file)

            %FPSO-ICE FLOE & GROWLER COLLISION


   angle = 0;     % Collision angle(deg)
   Vel   = 2;     % Initial impact velocity(m/s)


% FPSO (Object A)
% FPSO cross sectional details
Ha  = 26.6;          % Height(m)
La  = 258.00;         % Length(m)
Ba  = 46.00;          % Breadth(m)
Ta  = 18.04;          % Draft(m)
m_ship = 187100000;     % mass of FPSO(kg)
Cxa = La/2;           % x-CoG
Cya = 0;              % y-CoG
Cza = 12.5;           % z-CoG

Zga = Ta - Cza;       % Vertical distance
Cwp = 0.9;            % Coefficient of Waterplane
Cm  = 0.9;            % Midship coefficient
Cb  = 0.8;            % Block coefficient

% Added Mass factors
Amx = 0.0;                    %  Surge
Amy = 2*Ta/Ba;                %  Sway
Amz = 2/3*Ba*Cwp^2/(Ta*Cb*(1+Cwp)); %  Heave
Am = [Amx,Amy,Amz];
Amrol = 0.25;                 %  Roll
Ampit = Ba/(Ta*(3-2*Cwp)*(3-Cwp));  %  Pitch
Amyaw = 0.3 + 0.05*(La/Ba);       %  Yaw
Amr=[Amrol,Ampit,Amyaw];

% Inertia radius squared:
rxa = (Cwp*Ba^2)/(11.4*Cm)+Ha^2/12;
rya = 0.07*Cwp*La^2;
rza = La^2/16;
Ra = [rxa,rya,rza];


% MULTIYEAR ICE FLOE & ICE GROWLER (Object B)
% ICE FLOE & GROWLER cross sectional details
Hb = 1.00;          % Ice Floe Height(m)
% Hb = 2.0;           % Ice Growler Height(m)
Db = 20.0;          % [m]   Diameter-Ice Floe
% Db = 2.0;           % [m]   Diameter-Growler
Tb = 0.5;          %
% Tb = 1;           %
Cxb = 0;            % [m]   COG x
Cyb = 0;            % [m]   COG y
```

```
Czb = 0.5;          % [m]   COG z - Ice Floe
% Czb = 1;          % [m]   COG z - Growler
Zgb = Tb - Czb;     % [m]   Vertical distance
% m_ice = 3769.9;   % [kg]  Ice growler mass
m_ice = 282743.34;  % [kg]  Ice floe mass

% Assumed added mass factors:
Bmx = 1.00;                 %     Surge-Ice Floe
Bmy = 1.00;                 %     Sway-Ice Floe
Bmz = 1.00;                 %     Heave-Ice Floe
% Bmx = 0.8                 %     Surge-Ice Growler
% Bmy = 0.8                 %     Sway-Ice  Growler
% Bmz = 0.8                 %     Heave-Ice  Growler

Bm = [Bmx,Bmy,Bmz];
Bmrol = 1.00;               %     Roll-Ice Floe
Bmpit = 1.00;               %     Pitch-Ice Floe
Bmyaw = 1.00;               %     Yaw-Ice Floe
% Bmrol = 0.15              %     Roll-Ice Growler
% Bmpit = 0.15              %     Pitch-Ice Growler
% Bmyaw = 0.15              %     Yaw-Ice Growler
Bmr=[Bmrol,Bmpit,Bmyaw];

% Inertia radius squared:

Ixx = (1/12)*m_ice*(3*(20/2)^2 + Hb^2);    % mass moment of inertia

rxb = Ixx/m_ice;            % Ice Floe
ryb = Ixx/m_ice;            % Ice Floe
rzb = 0.5*(20/2)^2;         % Ice Floe
% rxb = 5.4^2               % Ice Growler
% ryb = 4.41^2              % Ice Growler
% rzb = 4.18^2              % Ice Growler
Rb  = [rxb,ryb,rzb];


% Ice
alpha = 90*cosd(angle); % [deg] Waterline angle
gama = 0;           % [deg] Frame angle
betap = 0;          % [deg] Normal frame angle


% Collision point in FPSO:
cp_a = [(La/2 - (Ba/2)*(1 - cosd(angle)))   % x-coordinate
       (Ba/2)*sind(angle)                   % y-coordinate
       -Cza];                               % z-coordinate

% Collision point in ICE:%
cp_b = [-(Db/2)*cosd(angle)                 % x-coordinate
       -(Db/2)*sind(angle)                  % y-coordinate
       -(Czb)];                             % z-coordinate


ve_a = [0 0 0]';
ve_b = [Vel 0 0]';

% Friction
```

```
%   Ice frictional coefficient = 0.15
%   tangential deformation factor = 0.3
miu0 = 0.45;

% Restitution factor
%(0-Plastic)
res = 0;

% Analysis (Liu's subroutine)
[tt,ttm,dvv,ve_af,ve_bf,flag,miu,mass1,mass2] = ...
   stronge3d(m_ice,m_ship,Bm,Am,Bmr,Amr,Rb,Ra,alpha,gama,...
   betap,cp_b,cp_a,res,miu0,ve_b,ve_a);

% RESULTS

E0 = (1/2*mass2(1,1)*ve_a(1,1)^2)/(1+mass2(1,1)/mass1(1,1));   % mass1 - mass matrix for object A, mass2 - mass matrix for object B
E = tt/E0;                                  % tt    - total dissipated energy [J]
ve_af = double(ve_af);                      % ve_af - velocity of object A after the impact
ve_bf = double(ve_bf);                      % ve_bf - velocity of object B after the impact
% Results
fprintf('\n\nRESULTS\n');
fprintf('Total Strain Dissipated Energy:\n');
fprintf('\tE_tot [MJ]  = %6.2f\n', tt*1E-06);
fprintf('\nComponents of issipated energy in each direction(x,y,z)\n');
fprintf('\tEx    [MJ]  = %6.2f\n', ttm(1)*1E-06);
fprintf('\tEy    [MJ]  = %6.2f\n', ttm(2)*1E-06);
fprintf('\tEz    [MJ]  = %6.2f\n\n', ttm(3)*1E-06);
fprintf('\nParallel to impact surface\n');
fprintf('\tEr    [MJ]  = %6.2f  \n', ...
   sqrt(ttm(1)^2 + ttm(2)^2)*1E-06);
fprintf('\nPerpendicular to impact surface\n')
fprintf('\tEz    [MJ]  = %6.2f  \n', ...
   ttm(3)*1E-06);
fprintf('\nType of Impact:\n');
fprintf('\tCase: %s\n', flag);
fprintf('\tNormal frictional coefficient: %f (static friction factor?)\n', miu);
```

APPENDIX II

MATLAB CODE FRO PRESSURE PEAKS PLOT

```
%% Output
Output = table;
Output.Data = cell2mat(raw(:, 1));
Output.Xcoord = cell2mat(raw(:, 2));
Output.Ycoord = cell2mat(raw(:, 3));
Output.Zcoord = cell2mat(raw(:, 4));
Output.pressure = cell2mat(raw(:, 5));

%% Temp
clearvars filename formatSpec fileID dataArray ans raw col numericData rawData row regexstr result numbers
invalidThousandsSeparator thousandsRegExp R;

%% Reading the data for plotting
[Output1] = Output(4412:4852,1:5);
[Output2] = Output(8822:9262,1:5);
[Output3] = Output(17642:18082,1:5);
[Output4] = Output(25139:25579,1:5);
[Output5] = Output(35723:36163,1:5);
[Output6] = Output(44102:44542,1:5);

[X1] = vec2mat(Output1.Xcoord,21);
[Y1] = vec2mat(Output1.Ycoord,21);
[Z1] = vec2mat(Output1.Zcoord,21);
[P1] = vec2mat(Output1.pressure,21);

[X2] = vec2mat(Output2.Xcoord,21);
[Y2] = vec2mat(Output2.Ycoord,21);
[Z2] = vec2mat(Output2.Zcoord,21);
[P2] = vec2mat(Output2.pressure,21);

[X3] = vec2mat(Output3.Xcoord,21);
[Y3] = vec2mat(Output3.Ycoord,21);
[Z3] = vec2mat(Output3.Zcoord,21);
[P3] = vec2mat(Output3.pressure,21);

[X4] = vec2mat(Output4.Xcoord,21);
[Y4] = vec2mat(Output4.Ycoord,21);
[Z4] = vec2mat(Output4.Zcoord,21);
[P4] = vec2mat(Output4.pressure,21);

[X5] = vec2mat(Output5.Xcoord,21);
[Y5] = vec2mat(Output5.Ycoord,21);
[Z5] = vec2mat(Output5.Zcoord,21);
[P5] = vec2mat(Output5.pressure,21);

[X6] = vec2mat(Output6.Xcoord,21);
[Y6] = vec2mat(Output6.Ycoord,21);
[Z6] = vec2mat(Output6.Zcoord,21);
[P6] = vec2mat(Output6.pressure,21);

% Contour Plots
figure(1)
```

```
%surf(X1,Y1,Z1,P1)
surf(Y1,Z1,P1)
title('Interface Pressure t=0.05s')
% xlabel('X-coordinate')
% ylabel('Y-coordinate')
% zlabel('Z-coordinate')
% clabel('Pressure in Pa')

figure(2)
%surf(X2,Y2,Z2,P2)
surf(Y2,Z2,P2)
title('Interface Pressure t=0.1s')

figure(3)
%surf(X3,Y3,Z3,P3)
surf(Y3,Z3,P3)
title('Interface Pressure t=0.3s')

figure(4)
%surf(X4,Y4,Z4,P4)
surf(Y4,Z4,P4)
title('Interface Pressure t=0.3s')


figure(5)
%surf(X5,Y5,Z5,P5)
surf(Y5,Z5,P5)
title('Interface Pressure t=0.4s')
xlabel('Distance(m)')
ylabel('Distance(m)')
zlabel('Pressure(Pa)')


figure(6)
% surf(X6,Y6,Z6,P6)
surf(Y6,Z6,P6)
title('Interface Pressure t=0.5s')
```

APPENDIX III

MISCELLANEOUS – MATLAB CODES USED FOR PLOTTING

1)

```
figure(1)
hold on
plot(PanelIcebergs.X1iU, PanelIcebergs.Yi1U,'b-','LineWidth',1.5)
plot(PanelIcebergs.X11sU, PanelIcebergs.Yi1U,'b-','LineWidth',1.5)

plot(PanelIcebergs.X2iU, PanelIcebergs.Y2iU,'g-','LineWidth',1.5)
plot(PanelIcebergs.X22sU, PanelIcebergs.Y2iU,'g-','LineWidth',1.5)
plot(PanelIcebergs.X3iU, PanelIcebergs.Y3iU,'r-','LineWidth',1.5)
plot(PanelIcebergs.X33sU, PanelIcebergs.Y3iU,'r-','LineWidth',1.5)
plot(PanelIcebergs.X4iU, PanelIcebergs.Y4iU,'y-','LineWidth',1.5)
plot(PanelIcebergs.Y44sU, PanelIcebergs.Y4iU,'y-','LineWidth',1.5)
plot(lineX,lineY)
title('Force-Deformation Curves')
xlabel('Deformation(m)')
ylabel('Force(MN)')
legend('Ice Floe impact(Ship)','Ice Floe impact(Ice)', 'Growler impact(Ship)','Growler Impact(Ice)', 'Bergy Pit
impact(Ship)','Bergy Pit Impact(Ice)', 'Ice Floe-Oblique impact(Ship)','Ice Floe-Oblique impact(Ice)')
grid on
hold off
```

2)

```
figure(1)
hold on
plot(SteelstrengthIceberg1.X1iU, SteelstrengthIceberg1.Y1iU,'b-','LineWidth',1.5)
plot(SteelstrengthIceberg1.X11sU, SteelstrengthIceberg1.Y1iU,'b-','LineWidth',1.5)
plot(SteelstrengthIceberg1.X2iU, SteelstrengthIceberg1.Y2iU,'y-','LineWidth',1.5)
plot(SteelstrengthIceberg1.X22sU, SteelstrengthIceberg1.Y2iU,'y-','LineWidth',1.5)
plot(SteelstrengthIceberg1.X3iU, SteelstrengthIceberg1.Y3iU,'r-','LineWidth',1.5)
plot(SteelstrengthIceberg1.X33sU, SteelstrengthIceberg1.Y3iU,'r-','LineWidth',1.5)
plot(SteelstrengthIceberg1.X4iU, SteelstrengthIceberg1.Y4iU,'m-','LineWidth',1.5)
plot(SteelstrengthIceberg1.X44sU, SteelstrengthIceberg1.Y4iU,'m-','LineWidth',1.5)
legend('Run 1(Ship)','Run 1(Ice)','Run 2(Ship)','Run 2(Ice)','Run 3(Ship)','Run 3(Ice)','Run 4(Ship)','Run 4(Ice)')
title('Force-Deformation Curves')
xlabel('Deformation(m)')
ylabel('Force(MN)')
grid on
hold off
```

3)

```
figure(1)
hold on
plot(SideModelISvsNIS.X1iU, SideModelISvsNIS.Y1iU,'b-','LineWidth',1.5)
plot(SideModelISvsNIS.X11sU, SideModelISvsNIS.Y1iU,'b-','LineWidth',1.5)
plot(SideModelISvsNIS.X2iU, SideModelISvsNIS.Y2iU,'c-','LineWidth',1.5)
plot(SideModelISvsNIS.X22sU, SideModelISvsNIS.Y2iU,'c-','LineWidth',1.5)
x1=[0.287,0.287];
y1=[0,23];
x11=[-0.915,-0.915];
y11=[0,23];
```

```
plot(x1,y1,'b-')
plot(x11,y11,'b-')
x2=[0.392,0.392];
y2=[0,23];
x22=[-0.879,-0.879];
y22=[0,23];
plot(x2,y2,'c-')
plot(x22,y22,'c-')
title('Force-Deformation Curves')
xlabel('Deformation(m)')
ylabel('Force(MN)')
legend('Case 1(Ship)','Case 1(Ice)','Case 2(Ship)','Case 2(Ice)')
grid on
hold off
```

4)

```
figure(1)
hold on
plot(PanelIcebergs.X1iU, PanelIcebergs.Yi1U,'b-','LineWidth',1.5)
plot(PanelIcebergs.X11sU, PanelIcebergs.Yi1U,'b-','LineWidth',1.5)
plot(PanelIcebergs.X5iU, PanelIcebergs.Y5iU,'b--','LineWidth',1.5)
plot(PanelIcebergs.X55sU, PanelIcebergs.Y5iU,'b--','LineWidth',1.5)
title('Force-Deformation Curves')
xlabel('Deformation(m)')
ylabel('Force(MN)')
legend('Case 1 (Ship)','Case 1 (Ice)','Case 2 (Ship)','Case 2 (Ice)')
grid on
hold off

figure(2)
hold on
plot(PanelIcebergs.X2iU, PanelIcebergs.Y2iU,'c-','LineWidth',1.5)
plot(PanelIcebergs.X22sU, PanelIcebergs.Y2iU,'c-','LineWidth',1.5)
plot(PanelIcebergs.X6iU, PanelIcebergs.Y6iU,'c--','LineWidth',1.5)
plot(PanelIcebergs.X66sU, PanelIcebergs.Y6iU,'c--','LineWidth',1.5)
title('Force-Deformation Curves')
xlabel('Deformation(m)')
ylabel('Force(MN)')
legend('Case 3 (Ship)','Case 3 (Ice)','Case 4 (Ship)','Case 4 (Ice)')
grid on
hold off

figure(3)
hold on
plot(PanelIcebergs.X3iU, PanelIcebergs.Y3iU,'r-','LineWidth',1.5)
plot(PanelIcebergs.X33sU, PanelIcebergs.Y3iU,'r-','LineWidth',1.5)
plot(PanelIcebergs.X7iU, PanelIcebergs.Y7iU,'r--','LineWidth',1.5)
plot(PanelIcebergs.X77sU, PanelIcebergs.Y7iU,'r--','LineWidth',1.5)
title('Force-Deformation Curves')
xlabel('Deformation(m)')
ylabel('Force(MN)')
legend('Case 5 (Ship)','Case 5 (Ice)','Case 6 (Ship)','Case 6 (Ice)')
grid on
hold of
```

APPENDIX IV

EXTERNAL MECHANICS COMPUTATION PERFORMED IN PROJECT THESIS

Main Dimensions

Since in this project, an ice berg colliding with a FPSO is considered. A model calculation has been performed considering a head on impact between the ice and the structure. The dimensions and angles of both the FPSO and ice bergs are assumed.

Length between perpendiculars , L= 258

Beam, B= 45.4 m

Depth to main deck , D= 21 m

Draft T = 15 m

Displacement (Seawater Density 1.025) = 148283 metric tonnes

Hull Coefficients

Block Coefficient C_B=0.88

Water plane area coefficient C_{wp} =0.95

Mid ship Coefficient, $C_M = 0.99$

Waterline entrance angle,$\alpha = 36°$

Stem angle from vertical,$\varphi = 35°$

Stem angle from horizontal, $\gamma = 55°$

Frame angle,$\beta = 46.06°$

Normal Frame angle, $\beta' = 40.01°$

Pressure, $P_o = 2500\ Kpa$ (assumed)

Exponent, ex = -0.5 (Considered from P-A curves)

Initial Kinetic energy of the ice berg, KE = $\frac{1}{2} \times M_{e,ice} \times V^2 = 4.5$ MJ

.Kinetic Energy, $KE_e = \frac{1}{2} \times M_e \times V_n^2 = IE$

Where M_e is effective mass = $M_e = \frac{1}{\frac{1}{M_{e\ ship}} + \frac{1}{M_{e\ Ice}}}$

M is the displacement

Mass reduction Coeffiecient Co= Co1+Co2+Co3+C04+Co5+Co6

COG of the ship:

X= 129 m (Half of water line)

Y=0 m (Centreline)

Z=11.5 m (from base line)

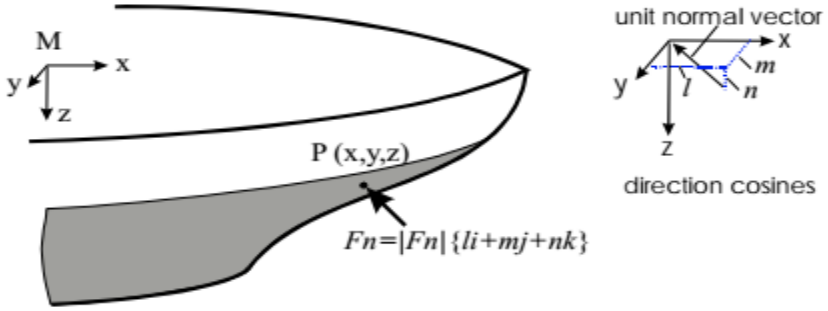

Figure 115 Colliison Point geometry (Daley, Energy based ice collision forces 1999)

The collision point and the direction at which the resultant force is acting is pictorially represented in Figure **23**

There are no existing procedures to follow for this kind of problem, so the calculation has been carried out according to Daley's literature on Ice based collision forces, Popov's literature on Strength design of ships in ice and the solution procedures given to the author of this project by Professor Claude Daley.

Distance of impact from COG of ship:

It is considered that the impact point will be at the bow part. The exact point of impact is assumed in this case. The x,y,z distance from the contact point to the centre of gravity is given by

x_i = 120 m

y_i= 0 m

z_i = -1m

Directional Cosines for collisions (Ship):

For a central head on impact collision, the directional cosines of ships.

l=sinα cosβ' = 0.45

m = cosα cosβ' = 0.62

n=sin$\beta' = 0.64$

Directional Cosines of Ice berg:

The considered case is a head on impact, the ice berg moves with a velocity of 2 m/s and collides with the FPSO. Reference coordinate system X,Y, and Z axis are established in the ice berg system and the local axis x,y,z at the contact point is defined. The directional angles α, β and γ correspond to the orientation of the local axes at the contact point of the ice berg. It has also been assumed that the direction of velocity of ice berg is aligned along the horizontal axis, so the only component that contributes to the velocity is Vx.

The directional angles at the point of contact will remain same before and after the impact. This is due to the fact that Popov formulated the impact theory considering the collision is quick and the movements are very small. Based on these assumptions, the directional cosines of the ice berg are defined for the angles ($\alpha = 0, \beta = 90, \gamma = 90$)

Directional cosines of ice berg:

l_2= cos α = 1

$m_2 = cos\beta$ = 0

n_2=cos $\gamma = 0$

Added Mass terms for the Ship:

In order to find the effective mass of the ships to use in the calculations, the mass reduction coefficients for all degrees of freedom need to be found. The mass reduction coefficients in turn depend on the added mass coefficients of ships. The analytical expressions of added mass coefficients of ships are taken from Popov's literature.

Surge Motion: A$M_x = 0$

Sway Motion :A$M_y = \frac{2T}{B} = 0.66$

Heave Motion :AM_z =2(B.C_{wp}^2)/(3T(C_B(1 + C_{WP})) =1.06

Roll Motion :AM_{roll} = 0.25

Pitch Motion: AM_{pitch}= B/((T(3-2C_{wp})(3 − C_{wp})) = 1.34

Yaw Motion: AM_{yaw} = 0.3+0.05L/B = 0.58

Moment Arms for the ship:

λ_1= n.yi - m.zi = 0.62 m

μ_1 = l.zi –n.xi = - 77.603 m

η_1 = m.xi – l.yi = 74.36 m

Mass Radii of Gyration (squared) for the ship:

$rx^2 = C_{wp}.B^2/(11.4\times C_M) + D^2/12$ = 210.25 m2

$ry^2 = 0.07\times C_{wp} \times L^2$ = 4426.51 m2

$rz^2 = \frac{L^2}{16}$ = 4160.25 m2

Mass Reduction Coefficients of ship:

$Co = Co1+Co2+Co3+Co4+Co5+Co6 = \frac{l^2}{(1+Am_x)} + \frac{m^2}{(1+Am_y)} + \frac{n^2}{(1+Am_z)} + \frac{\lambda l^2}{(r_x^2(1+Am_{roll})} + \frac{\mu l^2}{(r_y^2(1+Am_{Pitch})} + \frac{\eta l^2}{(r_z^2(1+Am_{Yaw})} = 2.0556$

$M_{e,ship}$ is effective mass for ship = M_1 /Co

= 9116.563 tonnes

Added Mass Coefficients for Ice:

Popov, based on experimental results conducted on a ellipsoidal body, proposed the added mass coefficients in surge, heave and pitch motion as

Surge Motion: $AM_x(Ice) = 0$

Heave Motion :$AM_z(Ice)$ = 1

Pitch Motion: $AM_{pitch}(Ice)$ = 1

Mass Reduction Coefficients of Ice:

In addition, Popov also proposed the mass reduction coefficient contributions from the heave and pitch motions of ice berg as 2 ($Co_{ice} = Co_{3,ice} + Co_{5,ice}$)

Effective Mass of Ice Floe:

$M_{e\ ice}$ is effective mass for ice = M_2 /Co

The total effective mass contribution from both the FPSO and Ice is given as $M_e = \frac{1}{\frac{1}{M_{e\ ship}}+\frac{1}{M_{e\ Ice}}}$

The velocity here refers to the effective velocity (V_e) of berg after the impact. In this problem, it has been assumed that the size of FPSO is massive in comparison to the ice berg size, so it is deduced that FPSO would not attain any velocity after the impact, furthermore the movement of the ice berg will be completely stopped so its final velocity will be zero. The effective velocity in kinetic energy calculations can be taken as difference between the initial and final velocity of the ice berg, and it would be 2 m/s.

Kinetic Energy, $KE_e = \frac{1}{2} \times M_e \times V_e^2$ = 2.106 MJ

The kinetic energy dissipation have been estimated and it is around 2.106 MJ. Here, in this case, the ice berg moves with a velocity of 2 m/s and collides head on with FPSO. It is postulated that FPSO intakes this amount of kinetic energy as strain energy after the impact and the bow undergoes ductile deformation. The low value of kinetic energy confirms the fact that the ice berg size is smaller than that of the FPSO dimensions, thus validating the assumptions.

The difference between the initial kinetic energy of ice and the kinetic energy which is absorbed as strain energy by the FPSO is 4.5 – 2.106 = 2.394 MJ. It is assumed that remaining 2.394 MJ of kinetic energy might be dissipated due to hydrodynamic damping and the ice berg is completely stopped.

There are some uncertainties involved in this calculation due to the simplifications made. The considered problem is a head on – symmetrical collision between the ice berg and structure. A lot of simplifications have been considered like the circular shape of ice berg and considered the added mass and mass reduction coefficients of ice bergs based on the experimental results in Popov's literature (Strength of ships in Ice). However, in reality, the shape of the ice berg will be irregular which introduces further complexity in determining the coefficients. These coefficients must be estimated by performing model scale experiments on ice berg samples.

Secondly, the beaching, friction and sliding effects are ignored. However, in real collision scenarios, these phenomena contribute to significant forces which must be estimated.

Thirdly, the effects due to interaction from the surrounding water are completely neglected. Besides, these shortcomings, this estimation provides a reasonable value that can be compared with simulations.